GEOLOGIC EVALUATION OF CRITICAL PRODUCTION PARAMETERS FOR COALBED METHANE RESOURCES

PART I, SAN JUAN BASIN

FINAL REPORT
(August 1988 - July 1989)

Prepared by

W. B. Ayers, Jr., W. R. Kaiser, W. A. Ambrose,
T. E. Swartz, and S. E. Laubach
Bureau of Economic Geology
W. L. Fisher, Director
The University of Texas at Austin
Austin, Texas 78713

C. M. Tremain
Colorado Geological Survey

N. H. Whitehead III
New Mexico Bureau of Mines and Mineral Resources

For

GAS RESEARCH INSTITUTE
Contract No. 5087-214-1544
Richard A. McBane, Manager
Methane from Coal Deposits

January 1990

DISCLAIMER

LEGAL NOTICE This report was prepared by the Bureau of Economic Geology as an account of work sponsored by the Gas Research Institute (GRI). Neither GRI, members of GRI, nor any person acting on behalf of either:

a. Makes any warranty or representation, expressed or implied, with respect to the accuracy, completeness, or usefulness of the information contained in this report, or that the use of any apparatus, method, or process disclosed in this report may not infringe privately owned rights; or

b. Assumes any liability with respect to the use of, or for damages resulting from the use of, any information, apparatus, method, or process disclosed in this report.

50272-101

REPORT DOCUMENTATION PAGE	1. REPORT NO. GRI-90/0014.1	2.	3. Recipient's Accession No.

4. Title and Subtitle
Geologic Evaluation of Critical Production Parameters for Coalbed Methane Resources: Part I, San Juan Basin

5. Report Date
January 1990

6.

7. Author(s) W. B. Ayers, Jr., W. R. Kaiser, W. A. Ambrose, T. E. Swartz, S. E. Laubach, C. M. Tremain, and N. H. Whitehead III

8. Performing Organization Rept. No.

9. Performing Organization Name and Address
Bureau of Economic Geology
The University of Texas at Austin
University Station, Box X
Austin, TX 78713-7508

10. Project/Task/Work Unit No.

11. Contract(C) or Grant(G) No.
(C) 5087-214-1544
(G)

12. Sponsoring Organization Name and Address
Gas Research Institute
8600 West Bryn Mawr Avenue
Chicago, IL 60631
Project Manager: Richard McBane

13. Type of Report & Period Covered
Annual; August 1, 1988 - July 31, 1989

14.

15. Supplementary Notes

16. Abstract (Limit: 200 words)

The Fruitland Formation in the San Juan Basin is the major producer of coalbed methane in the Western U.S. Forty-three to forty-nine Tcf of methane occur in 245 billion short tons of Fruitland coal at depths between 400 and 4,200 ft. Thickest Fruitland coal seams trend northwest and occur in the northern part of the basin, northeast of a syndepositional, structural hingeline; they occur in coastal plain facies southwest of Pictured Cliffs barrier/strandplain sandstones. South of the hingeline, northeast-trending coal seams occur in floodplain facies between northeast-trending Fruitland fluvial systems. Face cleat trends in Fruitland coal seams are predominantly northeast in the southern two-thirds of the basin and northwest, but variable in the northern third. Suggested targets for enhanced coalbed permeability are tectonic fractures and fractures associated with subtle folds.

Fruitland Formation waters are evolved meteoric waters; water composition reflects hydrologic setting. Waters in the north-central San Juan Basin have high alkalinities and low chlorinities; waters in the southern part are Na-Cl type. Distribution of low-chloride ground water in the Fruitland Formation in the north-central basin coincides with the overpressured area and with flow patterns inferred from the head map. The Fruitland Formation acts regionally as a single hydrologic unit or homogeneous aquifer, but large pressure gradients locally indicate that Fruitland strata may be hydraulically disconnected and behave at the field scale as compartmentalized aquifers. Hydrologic studies defined reservoir characteristics and permeability boundaries in the Fruitland Formation. Geologic and hydrologic parameters were used to divide the San Juan Basin into areas in which coal beds have similar reservoir characteristics. Coalbed wells have negative declines early in their production history followed by exponential decline rates at less than 5 percent/year. Sandstone wells that exhibit coal-decline behavior probably are producing coalbed methane indirectly from coal seams.

17. Document Analysis a. Descriptors
Coalbed methane; Fruitland Formation; Pictured Cliffs Sandstone; sedimentology; structural geology; coal occurrence; coal resource; gas in place; coalbed-methane production; hydrology; hydrochemistry; pressure regime; San Juan Basin; Colorado; New Mexico

b. Identifiers/Open-Ended Terms
Methane from coal seams; occurrence and producibility

c. COSATI Field/Group

18. Availability Statement	19. Security Class (This Report)	21. No. of Pages 175
	20. Security Class (This Page)	22. Price

(See ANSI-Z39.18) See Instructions on Reverse

OPTIONAL FORM 272 (4-77)
(Formerly NTIS-35)
Department of Commerce

RESEARCH SUMMARY

Title	Geologic Evaluation of Critical Production Parameters for Coalbed Methane Resources: Part 1, San Juan Basin
Contractor	Bureau of Economic Geology, The University of Texas at Austin; Colorado Geological Survey; New Mexico Bureau of Mines and Mineral Resources. GRI Contract No. 5087-214-1544.
Principal Investigator	W. B. Ayers, Jr.
Report Period	August 1, 1988 - July 31, 1989
Objectives	To identify sedimentologic controls on the occurrence of coalbed methane in the Fruitland Formation; to document the distribution and continuity of Fruitland coal seams; to delineate structures that may form conventional traps and enhance coalbed permeability; to identify cleat and fracture trends and the regional stress regime; to define the regional hydrodynamics of the Fruitland Formation and Pictured Cliffs Sandstone; to relate these geologic and hydrologic factors to the producibility of coalbed methane; and to estimate the resources of coalbed methane in the Fruitland Formation.
Technical Perspective	Coalbed-methane resources in the United States are estimated to be 400 trillion cubic feet (Tcf). The San Juan Basin, which has more than 500 coalbed-methane wells, is one of the most productive basins in the United States. The technology required to exploit this resource is in the developmental stage; there is a need for studies that relate coalbed methane occurrence and producibility to geologic and hydrologic settings, leading to models for exploration and production. These models should reduce the cost of exploration, optimize production of this under-utilized resource, and ensure a supply of natural gas at reasonable cost.
Results	Regional studies of coalbed methane in the Fruitland Formation were divided into geologic, fracture, hydrologic, and production studies. The geologic study showed that the thickest coal seams (individual seams thicker than 20 ft and net-coal thickness more than 50 ft) occur in the northern part of the basin, landward of

the northwest-trending Pictured Cliffs barrier/strandplain sandstones; locally in the southern part of the basin, anomalously thick coal seams trend northeast and formed in a floodplain setting. Fruitland coal seams commonly are extensive, overriding sandstones. Folds may be sites of fracture-enhanced coalbed permeability, and they may form conventional traps. Fracturing is inferred to occur in the Hogback Monocline, the Ignacio and Bondad Anticlines, and in other minor tectonic folds at the periphery of the basin floor. Compaction-induced folds and fractures may occur where coal seams override sandstones. Gas in place in Fruitland Formation coalbeds was calculated to be 43 Tcf to 49 Tcf at depths between 400 and 4,200 ft; coal resources in the same interval are 245 billion short tons.

Cleats and joints in the Upper Cretaceous and Tertiary rocks are extensional fractures. Face and butt cleats in Fruitland coal seams are well developed and orthogonal. Face cleats at the north and northwest margins of the basin, although highly variable, trend northwest to north-northwest. At outcrop in the southern San Juan Basin, the face cleat is nearly parallel to structural dip (north-northeast) and is subparallel to the first-formed joint set; the butt cleat is weakly to moderately aligned with the second-formed joint set. Joints caused by rock relaxation are pervasive at outcrop and prominent in aerial photographs; fracture predictions based on remote-sensing data should be used with caution in the San Juan Basin.

Permeability is the most critical parameter for the producibility of coalbed methane. Hydraulic head, pressure regime, and hydrochemistry define an aquifer's ability to accept and transmit fluid; hence, they are indicators of permeability. In the north-central part of the basin the coal seams are the major aquifers in the Fruitland Formation. These coal seams are overpressured due to artesian conditions. Potentiometric-surface and chloride maps show that recharge occurs primarily at the elevated northwest margin of the basin; the aquifer coal seams pinch out to the southwest. In the southern part of the basin, the Fruitland Formation is underpressured and hydrologically less active than in the northern part of the basin, and coalbed methane wells produce little or no water. Waters produced from Fruitland coal seams have high alkalinities and low chlorinities. Stimulation of coalbed wells and disposal (injection) of these waters will require knowledge of their chemical compatibility with completion fluids and host formation waters, respectively. The Fruitland Formation behaves regionally as a hydrologic unit, but some wells have large

pressure gradients and produce anomalously large or small volumes of water, indicating reservoir compartmentalization.

Production of coalbed methane is favored at hydrologic and geologic transitions (potentiometric, pressure, flow direction, chemical, and depositional) and from a single thick overpressured coal seam rather than several thin overpressured seams. The north-central part of the San Juan Basin is the most productive coalbed-methane area in the basin, but the west-central part of the basin has substantial production either directly or indirectly from underpressured coal seams.

Coalbed-methane production is log-normally distributed. Decline behavior of coalbed wells differs from that of sandstone wells. Coalbed wells show negative decline early in their production history and exponential decline late, at less than 5 percent per year. Numerous sandstone wells exhibit coal-decline behavior and probably are producing coalbed methane indirectly from interbedded coal seams.

Technical Approach

As many as 2,500 geophysical well logs were used in the geologic study of the San Juan Basin, which covers approximately 6,695 mi^2. A grid of interlocking cross sections was made with closely spaced well logs, and the remaining logs were correlated with the cross sections. Stratigraphic units defined by 18 marker beds in the Upper Cretaceous and lower Tertiary section were correlated in these cross sections. Structure, isopach, lithofacies, and coal-occurrence maps were made. Cross sections and maps were evaluated individually and were compared one to another to interpret geologic controls on the occurrence and producibility of coalbed methane. To evaluate fractures systems in the San Juan Basin, cleats and joints were described in cores and at outcrops. A study was conducted to evaluate the utility of lineament studies in predicting fractures in the Fruitland Formation.

Fruitland hydrodynamics were evaluated on the basis of hydraulic head, pressure gradients, and hydrochemistry. More than 350 fresh-water equivalent heads were calculated. BHP's were plotted against elevation (msl) to calculate vertical pressure gradients for determination of vertical flow direction. A chlorinity map and Stiff ionic-ratio diagrams were made to help characterize ground-water circulation and hydrochemical facies. Production data from 400 Fruitland wells were analyzed. Initial potential (IP) and maximum-annual production (MAP) were mapped to compare productivity among wells with long and short production

histories. Decline curves and Q plots were used to evaluate decline behavior of Fruitland coalbed and sandstone reservoirs. Maps of IP and MAP were compared with potentiometric-surface, pressure-gradient, hydrochemical, structure, and coal-occurrence maps to establish correlations between hydrogeology and the producibility of coalbed methane.

Implications

This report describes the geologic framework and hydrologic regime of coalbed methane in the Fruitland Formation in the San Juan Basin. This research effort has significantly improved understanding of the relationships of geologic and hydrologic factors to gas occurrence and producibility. The preliminary models developed in this study will be further investigated and confirmed by coordinated research that focuses on areas in the San Juan Basin with contrasting reservoir and production properties. In addition, these models will be used to select sites for cooperative wells that will advance coalbed-methane technology in the San Juan Basin and to test the transfer of coalbed-methane technology from the San Juan Basin to other western coal basins.

CONTENTS

Figures

Tables

GEOLOGIC EVALUATION OF CRITICAL PRODUCTION PARAMETERS FOR COALBED METHANE RESOURCES:

PART 1, SAN JUAN BASIN

In the San Juan Basin, Fruitland Formation coal seams contain an estimated 43 to 49 Tcf of methane. With more than 500 producing coalbed methane wells and approximately 1,000 wells scheduled for drilling in 1990, this basin is one of the most active areas of coalbed methane exploration and production in the United States.

Among the most important geologic factors affecting the occurrence and producibility of coalbed methane are (1) depositional setting, (2) structural attitude and fracturing of the coal, and (3) regional hydraulic setting. In the second year of this study, the Bureau of Economic Geology evaluated the depositional setting and structure of Fruitland coal seams, which are both source rocks and reservoirs for coalbed methane, throughout the basin. This report, which builds on last year's research (Ayers and others, 1988), is divided into five sections. In the first section, we summarize the regional tectonic setting of the San Juan Basin. Next, we describe the Cretaceous stratigraphy, structure, and basin evolution, and we relate these factors to Fruitland coal and coalbed methane occurrence. The third section describes studies of lineaments, fractures, and cleats. Section four presents hydrodynamic controls on the producibility of coalbed methane from the Fruitland Formation. Finally, in section five we summarize production from the Fruitland Formation, and we evaluate geologic and hydrologic controls on coalbed methane producibility.

REGIONAL TECTONIC SETTING OF THE SAN JUAN BASIN

C. M. Tremain, N. H. Whitehead, III, and S. E. Laubach

INTRODUCTION

Tectonic history influenced Mesozoic and Cenozoic depositional patterns, coal occurrence, and gas generation in the San Juan Basin of New Mexico and Colorado. Tectonic events also affected or controlled the distribution and orientation of folds and fractures in coals and adjacent rocks. This section reviews basin origin and evolution in order to provide a framework for studies of depositional patterns and fracture occurrence in Cretaceous and Tertiary rocks in the San Juan Basin. An understanding of the overall tectonic setting of this basin, combined with the studies in the following chapters, provides a basis for predicting coalbed methane occurrence and producibility in this and other western coal basins.

LOCATION AND STRUCTURE OF THE BASIN

The San Juan Basin occupies the east-central part of the Colorado Plateau in northwestern New Mexico and southwestern Colorado. It is a roughly circular, asymmetrical, structural basin of Late Cretaceous to early Tertiary age (fig. 1). The structures that bound the basin include the Hogback Monocline on the west and northwest, the San Juan–Archuleta Uplift on the north, the Nacimiento Uplift to the southeast, and the Chaco Slope and Zuni Uplift to the south and southwest. The depocenter and the synclinal axis of the basin on Upper Cretaceous strata occurs near, and parallels, the north and the northeast margin of the basin.

Rocks in the basin range in age from Precambrian through Cenozoic. In the deepest part of the basin, Precambrian crystalline basement rocks are more than 14,000 ft beneath the

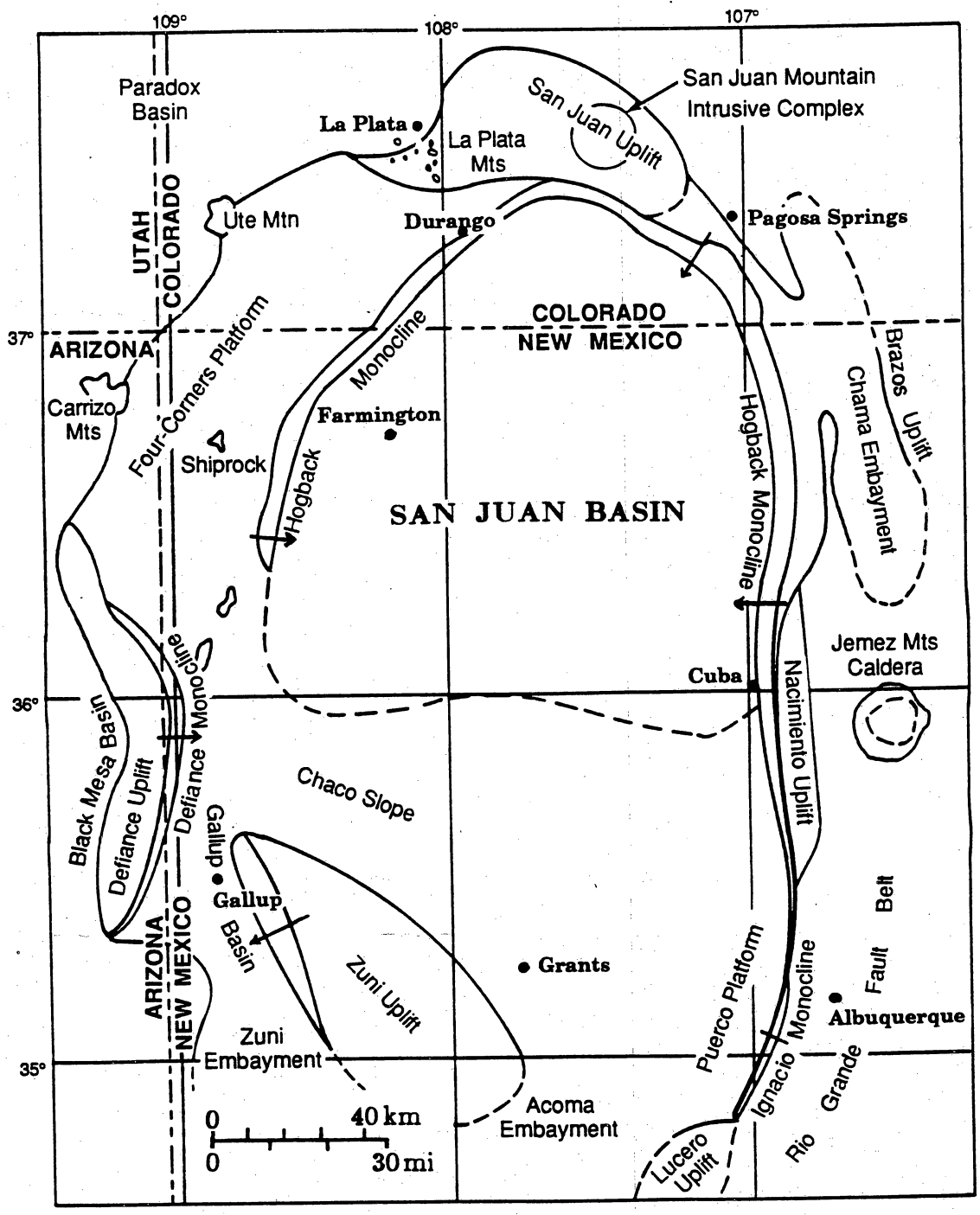

Figure 1. Regional tectonic setting of the San Juan Basin. Steeply dipping strata form the Hogback Monocline that rims the northern half of the basin. Modified from Fassett and Hinds (1971), after Kelley (1951, p. 125).

surface. Coal is present throughout the Cretaceous System, but the largest coal and coalbed methane resources are in the Fruitland Formation, which is the focus of this study. The Fruitland Formation outcrop encompasses approximately 6,700 mi^2. Fruitland coal seams occur from outcrop to depths as great as 4,200 ft.

EVOLUTION OF THE BASIN

During the Cretaceous, the area of the present San Juan Basin was on the western margin of the Western Interior Basin, which was a rapidly subsiding, elongate, asymmetric trough. At that time, the basin was occupied by a shallow sea (fig. 2) that extended from north to south across much of the Midcontinent (Kauffman, 1977; Merewether and Cobban, 1986; Weimer, 1986). The Western Interior Basin was bounded on the west by the Cordilleran orogenic belt, a fold and thrust belt that is exposed west of the San Juan Basin in Utah and Nevada (Armstrong, 1968; Burchfiel and Davis, 1975; Royse and others, 1975) and southwest of the Colorado Plateau in western Arizona and southeastern California (Burchfiel and Davis, 1975; Laubach and others, 1989). The western margin of the Western Interior Basin was the site of the greatest subsidence, which was controlled by tectonism in the orogenic belt. The eastern part of the basin was shallow and adjacent to a broad, stable platform (Hattin, 1965; Kauffman, 1977).

A major episode of subsidence in the Western Interior Basin during mid-Cretaceous (Aptian–Cenomanian) time is interpreted as recording the initiation of thrust-loading deformation in the adjacent overthrust belt (Heller and others, 1986). The correlation of transgressions and regressions of the Upper Cretaceous shoreline with episodic thrust faulting and uplift of the orogenic belt shows that basin subsidence was accelerated by thrust-loading deformation (Jordan, 1981). The structure of the Western Interior Basin is complicated by spatial and temporal variability of thrusting and subsidence, intermittent uplift of broad, gentle arches in the foreland as a result of flexure, and eustacy.

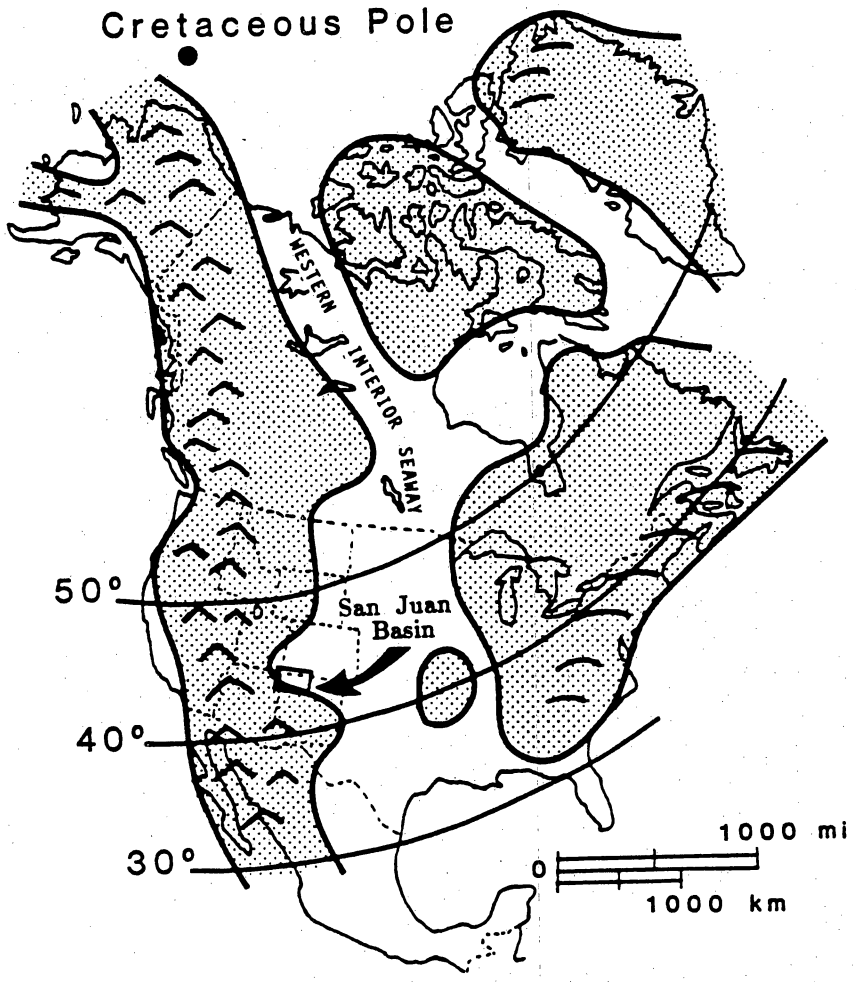

Figure 2. Location of the San Juan Basin relative to the Western Interior Seaway. Modified from Palmer and Scott (1984) after Williams and Stelck (1975) and Irving (1979).

The San Juan structural basin formed as a result of Laramide orogeny, which began in the Late Cretaceous, peaked in the Paleocene, and waned in the Eocene (approximately 80 to 40 mya). The Colorado Plateau was translated east-northeast to northeast relative to the North American craton (Hamilton, 1978). The San Juan Basin and other Rocky Mountain intermontane basins and Precambrian-cored uplifts formed in this compressional regime (Chapin and Cather, 1981; Dickinson and others, 1988). The San Jose Formation (Eocene) is the oldest rock unit for which isopachs clearly indicate a depocenter for the San Juan Basin (Stone and others, 1983, figs. 18, 21, and 27). Reactivation of basement anisotropy (Cordell and Grauch, 1985) and Paleozoic structures (Kluth and Coney, 1981; Ross and Ross, 1986) may have localized Mesozoic and Cenozoic deformation or controlled structural trends.

The Colorado Plateau is a coherent, uplifted crustal block surrounded by the extended terrain of the Basin and Range and Rio Grande Rift provinces (Thompson and Zoback, 1979). It began to decouple from the Basin and Range province and the Rio Grande Rift about 32 mya (Aldrich and others, 1986, fig. 3). The plateau has not had major crustal deformation since the Laramide orogeny, but it was affected by mild Cenozoic extension and volcanism. The eruption of voluminous Oligocene volcanic rocks to form the San Juan Volcanic field and the emplacement of igneous intrusives beneath the volcanic pile along the north side of the San Juan Basin marked this time of extensional stress (Steven, 1975; Lipman and others, 1978). This late Oligocene thermal event was a heat source for hydrocarbon generation in the San Juan Basin (Choate and Rightmire, 1982; Bond, 1984; Meissner, 1984; Clarkson and Reiter, 1988). In the northeastern San Juan Basin, the north-trending Dulce dike swarm gives radiometric ages of 28 to 22 mya. These dikes indicate east-west least principal horizontal stress. They were emplaced when the Rio Grande Rift–Colorado Plateau boundary was still being delineated (Aldrich and others, 1986). The Dulce dikes had only a local heating effect on the basin, as indicated by the lack of deflection of coal rank contours across the dike swarm (Meissner, 1984, his figure 18; Kelso and others, 1988, their figure 19).

Regional uplift of the Colorado Plateau began in the Miocene and has continued to the present (Epis and Chapin, 1975). Erosion of basin fill from the San Juan Basin has contributed to the post-Oligocene cooling of the basin (Meissner, 1984). Especially important from the standpoint of this report is the erosion of Oligocene volcanic and volcaniclastic rocks over the upturned outcrop of the Fruitland Formation along the northern flank of the basin, which allowed meteoric recharge of elevated sandstones and coal seams to cause artesian conditions and overpressuring in the Fruitland Formation in the northwestern part of the basin (Kaiser and Swartz, 1988; 1989).

MINOR STRUCTURES AND STRESS REGIME

A structural map of the San Juan Basin shows only minor anticlinal and synclinal noses superimposed on large areas of homoclinal dip (Ayers and Ambrose, this report, p. 22). These minor folds, which may cause fracture-enhanced permeability in coal seams, have structural relief of less than 200 ft.

Natural fractures (joints and cleats) are widespread in Cretaceous and Tertiary rocks in the San Juan Basin. Within the Fruitland Formation and adjacent rocks, all are extensional fractures rather than shear fractures (Tremain and Whitehead, this report). Face and butt cleats that intersect at approximately 90 degrees are well developed within the Fruitland coal seams. Two joint sets in brittle sandstones adjacent to the coal seams commonly have similar strike and dip to the face and butt cleats.

The present stress regime of the Colorado Plateau is extensional, the minimum horizontal stress being oriented east-northeast. This stress direction is rotated approximately 70 degrees counterclockwise from the west-northwest direction of the surrounding Rio Grande Rift–Basin and Range extensional province (Wong and Humphrey, 1989; Zoback and Zoback, in press).

GEOLOGIC CONTROLS ON THE OCCURRENCE OF COALBED METHANE, FRUITLAND FORMATION, SAN JUAN BASIN

W. B. Ayers, Jr., and W. A. Ambrose,

assisted by Joseph Yeh, J. D. Beckman, P. S. Reiss, G. A. Warren,

W. J. Garey, D. R. Grote, and J. N. Ashton

INTRODUCTION

Many geologic factors act in concert to determine the occurrence and producibility of coalbed methane, but the sedimentary depositional system that hosts the coal seams and the fractures and faults within the coal are the primary determinants of resources and recoverability, respectively. The sedimentary depositional system controls the occurrence, geometry, and thickness of coal seams by building platforms for peat (coal) accumulation and by bounding the seams. Additionally, the coarse-grained sandstones of sedimentary depositional systems commonly act as conduits for fluid flow. Regionally, Fruitland sandstones and associated coal seams perform as a single aquifer in the San Juan Basin (Kaiser and Swartz, 1988). Locally, however, fluid migration within coal seams and, hence, producibility of coalbed methane, is enhanced by faults and fractures. Thus, the focus of this geologic report is on sedimentology, coal occurrence, and structure.

Regional Geologic Setting and Stratigraphy

During the Late Cretaceous, the region of the present San Juan Basin was on the west margin of the Western Interior Seaway (fig. 2). In the Late Cretaceous (Campanian), the coastline migrated to the northeast, depositing a vertical succession of shelf through coal-

bearing continental sediments. The marine Lewis Shale (figs. 3 through 5), deposited in the Western Interior Seaway, contains several bentonite beds that are excellent marker beds for correlation. However, only the Huerfanito Bentonite Bed has been correlated throughout the San Juan Basin (Fassett and Hinds, 1971).

The Pictured Cliffs Sandstone is a coastal facies that was deposited as the Late Cretaceous shoreline prograded northeastward into the Western Interior Seaway. No regional lithofacies maps of the Pictured Cliffs Sandstone have been published. In geophysical well logs (fig. 3) and at outcrop, the Pictured Cliffs is divisible into genetically related upper and lower units. The lower unit is composed of a series of upward-coarsening subunits and is interpreted as shelf and shoreface mudstone and sandstone interbeds (fig. 3). The upper unit has a blocky well-log signature and is composed of amalgamated sandstone bodies having a composite thickness of 40 to 120 ft, representing the framework facies of an inferred prograding barrier/strandplain depositional system. These sandstones are well sorted and crossbedded (figs. 6 and 7). Grain size increases slightly upward, but the upper 2 to 4 ft of the unit is fine grained. This upper part of the unit contains planar and contorted laminae; plant fragments are common, and the interval is organic stained.

Conventionally, the base of the Pictured Cliffs Sandstone is placed at the base of the upward-coarsening units (fig. 3). However, that boundary is time-transgressive because the Pictured Cliffs Sandstone intertongues with the Lewis Shale (figs. 4 and 5). Contemporaneity of the coastal (blocky) and shoreface and shelf (upward-coarsening) units is documented by marker beds representing time lines that cross the proximal shelf and shoreface to intersect and terminate in the Pictured Cliffs coastal sandstones (fig. 4). The Pictured Cliffs Sandstone and equivalent marine units thicken basinward above the Huerfanito Bentonite Bed of the Lewis Shale because of progradation into a subsiding basin, resulting in basinward offlap of these marker beds.

In subsurface studies, the contact between the Pictured Cliffs Sandstone and the Fruitland Formation (fig. 3) is "placed at the top of the massive sandstone below the lowermost coal of

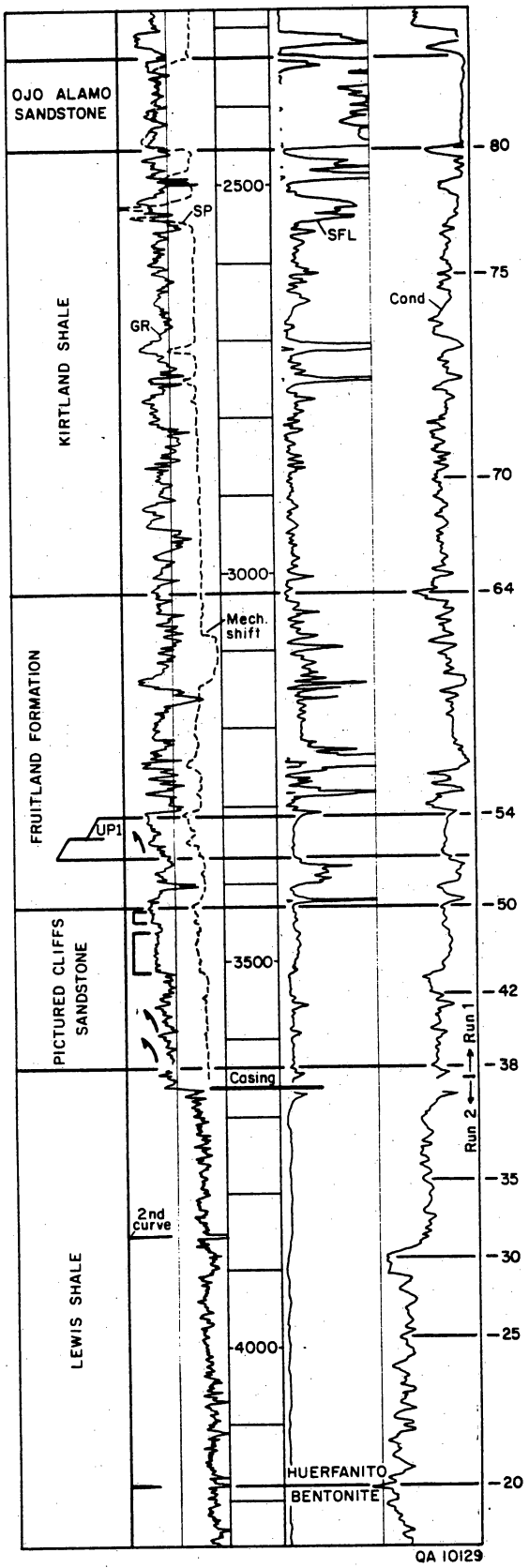

Figure 3. Type log showing Upper Cretaceous stratigraphy in the San Juan Basin. See figure 9 for well location and figure 23 for identification of Fruitland coal seams. Two-digit numbers on the right margin of the conductivity curve refer to marker beds used in this study.

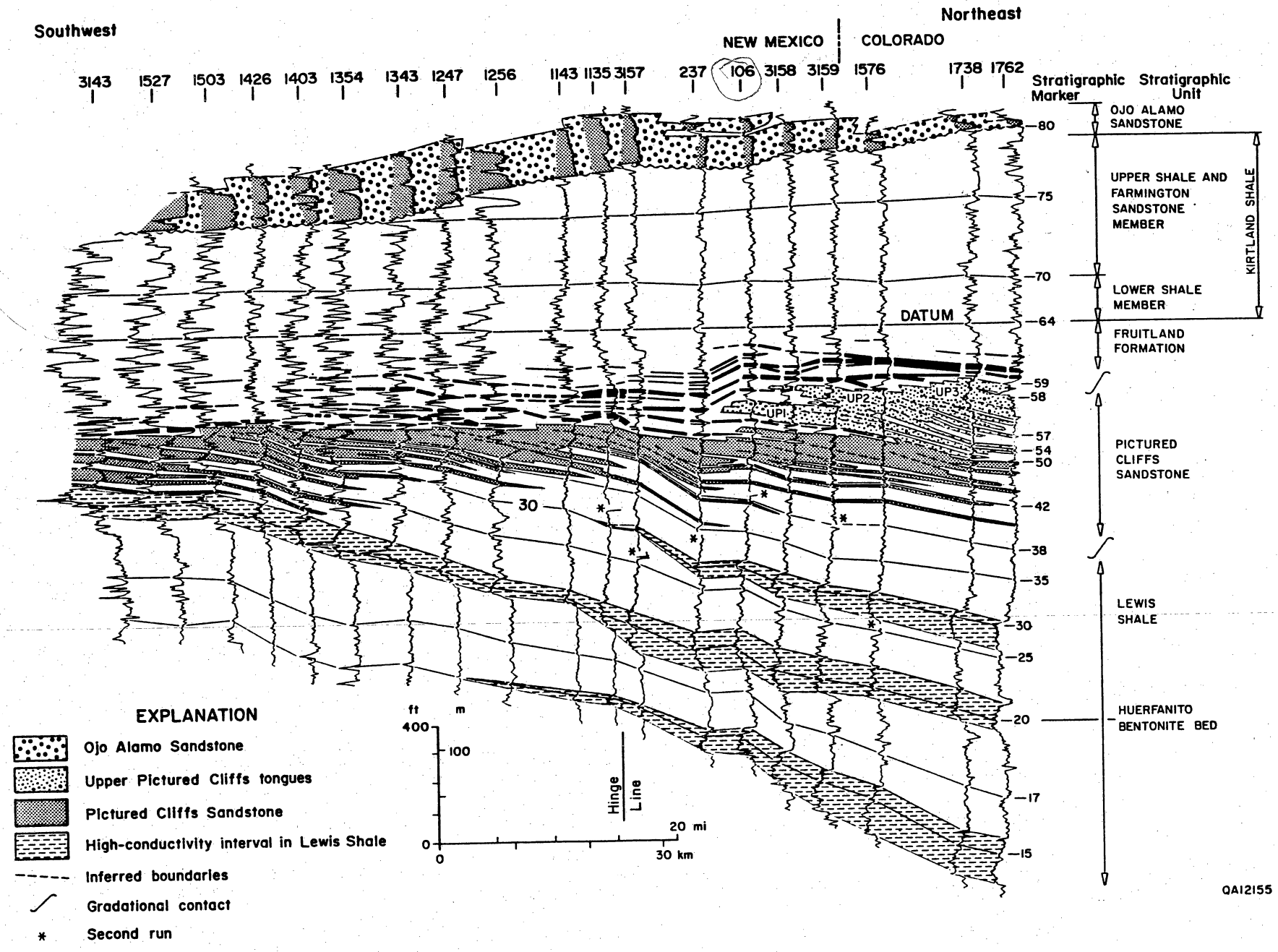

Figure 4. Stratigraphic dip section D20, located in figure 13. Traces of conductivity curves are shown for wells in this section; datum is the base of the Kirtland Shale, defined as a high-conductivity zone at the top of an upward-fining sequence in the upper Fruitland Formation. Log 106 ties with cross section S10 (fig. 5).

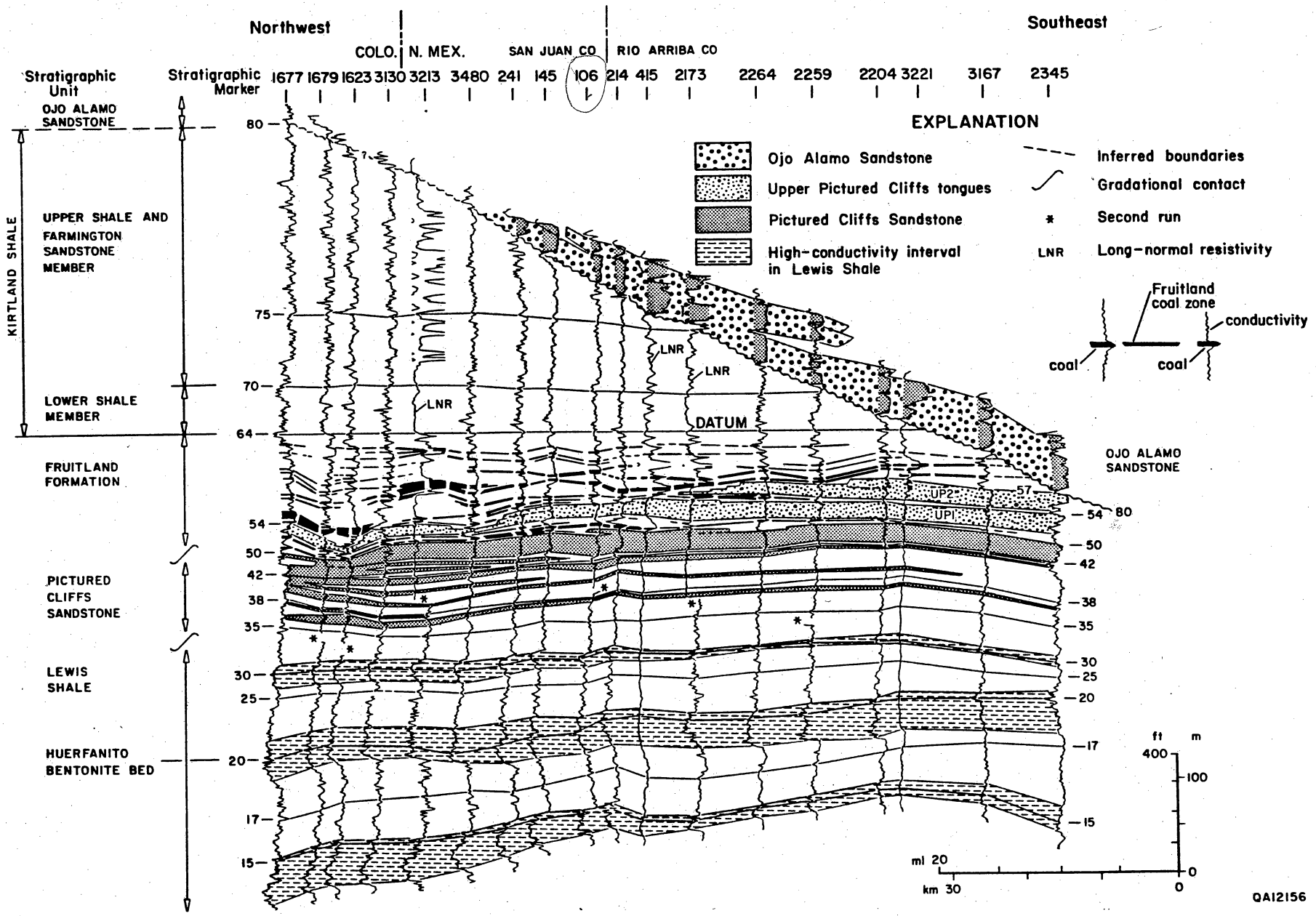

Figure 5. Stratigraphic strike section S10, located in figure 13. Log traces not labeled as long-normal resistivity are traces of conductivity logs. Datum is the high-conductivity, low-resistivity marker also used in cross section D20 (fig. 4). Log 106 ties with cross section D20 (fig. 4).

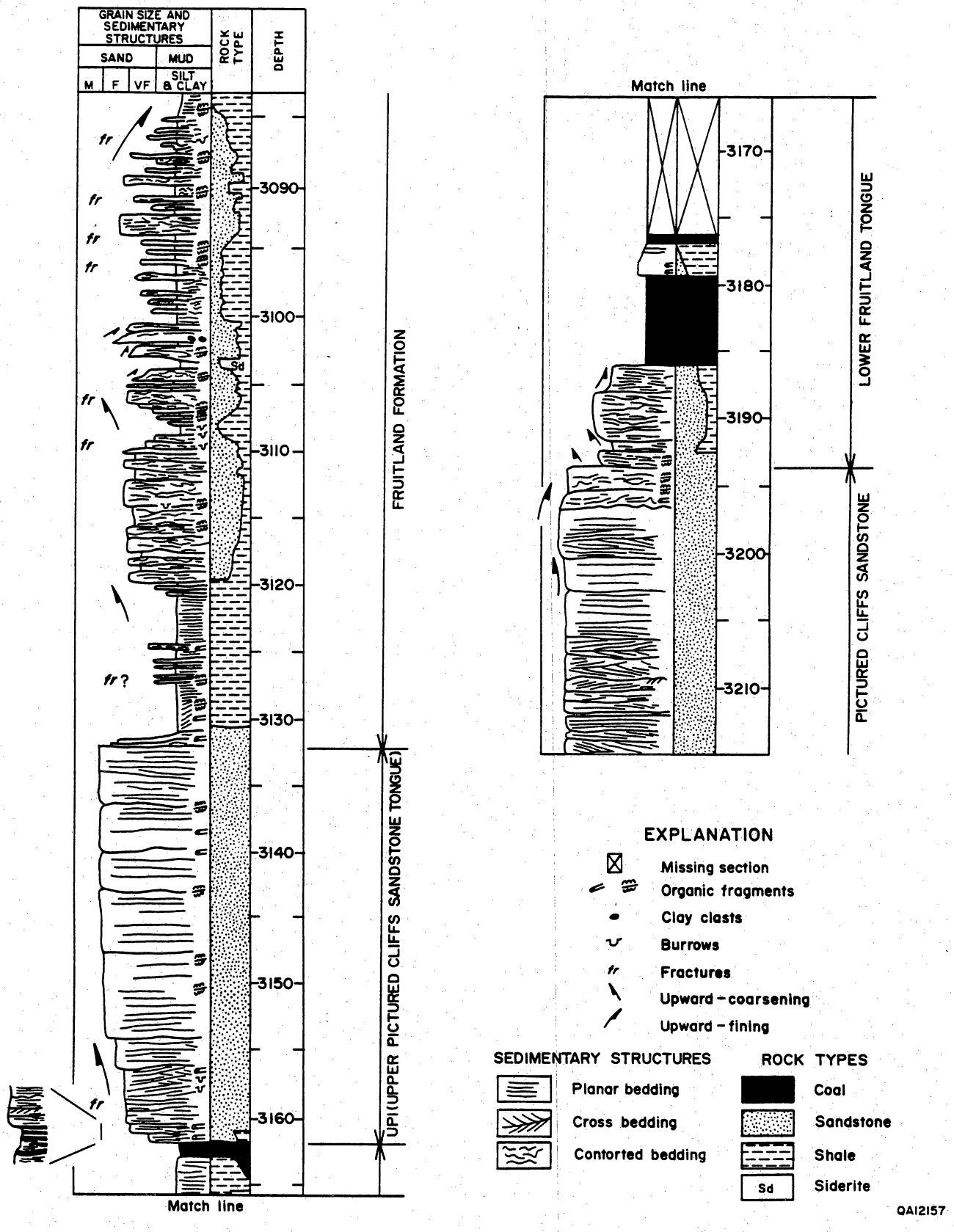

Figure 6. Core description of Pictured Cliffs Sandstone, lower Fruitland tongue, upper Pictured Cliffs tongue (UP1), and Fruitland Formation in Blackwood and Nichols NEBU No. 403 in Northeast Blanco field. Footage of this described interval is indicated on the geophysical log of this well (fig. 7).

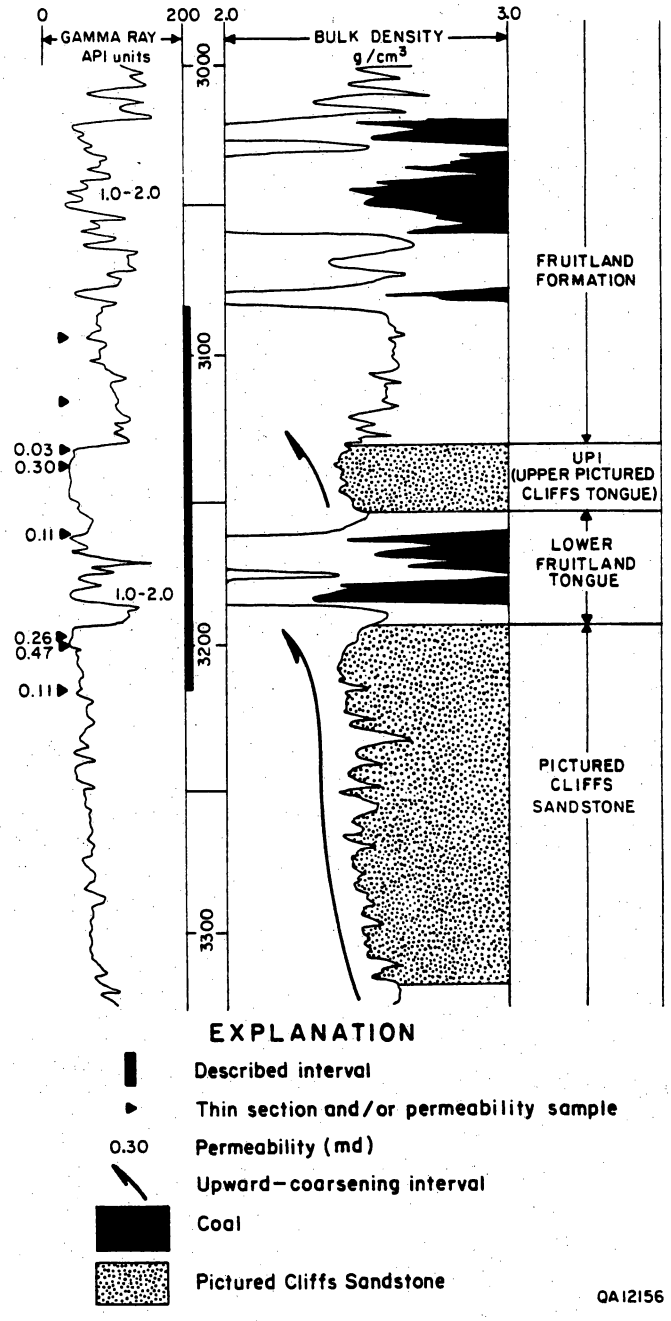

Figure 7. Gamma-density log of Blackwood and Nichols NEBU No. 403, located in figure 9. Core description of interval from 3,084 ft to 3,213 ft is in figure 6. Permeabilities are from core plugs in sandstone beds and well tests in coal seams.

the Fruitland except in those in those areas where the Fruitland and Pictured Cliffs intertongue" (Fassett and Hinds, 1971, p. 8). Pictured Cliffs sandstones are the depositional platforms upon which Fruitland peats (coals) accumulated, and ultimately, Pictured Cliffs shoreline sandstones bound coal seams in the basinward direction. Progradation of the Pictured Cliffs shoreline, dependent on complex interactions of sediment supply, basin subsidence, and eustacy, was intermittent, resulting in shoreline stillstands. Intertonguing of the Pictured Cliffs and the Fruitland Formation resulted from temporary landward shifts of the shoreline during overall regression of the Late Cretaceous shoreline. In this study, the Pictured Cliffs sandstones that intertongue with the Fruitland Formation are called "upper Pictured Cliffs sandstones," or "Pictured Cliffs tongues." There are three upper Pictured Cliffs tongues in the basin; individually, they are called "UP1," "UP2," or "UP3" in this report (fig. 4). Together, UP1, UP2, and UP3 account for approximately 270 ft of stratigraphic rise of the Pictured Cliffs over a 25-mi distance in the northern third of the San Juan Basin (fig. 4). The upper Pictured Cliffs tongues overlie upward-coarsening sequences on geophysical logs (fig. 3), and each is composed of northwest-trending, amalgamated barrier-strandplain sandstones up to 100 ft thick. These upper Pictured Cliffs tongues typically consist of crossbedded, fine-grained, burrowed sandstone that overlies a coal-bearing lower Fruitland tongue (fig. 6). These crossbedded sandstones grade upward into medium-grained, planar-bedded sandstones that make up the upper two-thirds of the Pictured Cliffs tongue.

The Fruitland Formation (fig. 3), the primary coal-bearing formation in the San Juan Basin and the focus of this study, is the continental facies deposited landward of the barrier/ strandplain facies of the Pictured Cliffs Sandstone and is composed of sandstone, mudstone, and coal interbeds. Fruitland sandstones typically are thin, ranging from a few inches to less than 15 ft thick (fig. 6). These sandstones are fine grained, rich in plant fragments, and commonly interbedded with silty mudstone. They contain poorly defined sedimentary structures that have been distorted by soft-sediment deformation, microfaults, and burrowing. Individual

Fruitland sandstone beds are arranged in poorly defined, upward-coarsening sequences 3 to 6 ft thick, and amalgamated or upward-fining sequences that are as much as 15 ft thick.

In past regional subsurface studies, the contact between the Fruitland Formation (Campanian) and the overlying Kirtland Shale (Campanian and Maestrichtian) was placed at the top of the highest coal bed or carbonaceous shale bed; for the most part, the Kirtland lacks coal and carbonaceous shale (Fassett and Hinds, 1971). However, because coal and carbonaceous shale occur locally in the Kirtland, that boundary is erratic. Therefore, in this study the Fruitland/Kirtland contact was placed at a high-conductivity peak that occurs at the top of an upward-fining sequence (figs. 3 through 5). This high-conductivity peak corresponds to the base of a regionally extensive shale (lower Kirtland shale) that may have formed as a consequence of a short-lived marine transgression over the Fruitland coastal plain. Fusulinids have been reported in this interval (Dilworth, 1960). This marker is at approximately the same stratigraphic position as the boundary chosen by earlier workers (Fassett and Hinds, 1971; Molenaar and Baird, 1989), and it has more genetic significance and less variability than the previously selected boundary.

The Kirtland Shale, which conformably overlies the Fruitland Formation, is composed of the lower shale member, the Farmington sandstone, and the upper shale member (fig. 3). The basal contact of the Paleocene Ojo Alamo Sandstone (fig. 3) is unconformable with the Kirtland Shale and Fruitland Formation (figs. 4 and 5); a hiatus of approximately 11 million years (m.y.) is reported at the southern margin of the basin (Fassett, 1985), but this hiatus diminishes in magnitude northwestward. Near the eastern margin of the basin, the fluvial Ojo Alamo Sandstone truncates the Kirtland Shale and Fruitland Formation, and in the southeast part of the basin, the present study documents truncation of the Kirtland Shale and Fruitland Formation by a pre-Ojo Alamo unconformity that merges westward with the Ojo Alamo Unconformity (fig. 8). This pre-Ojo Alamo unconformity is at the base of an upward-fining unit inferred to be a fluvial sandstone, and it beveled a planar, tilted surface, as is apparent from the relation between this unconformity and the Huerfanito Bentonite in figure 8. Although some

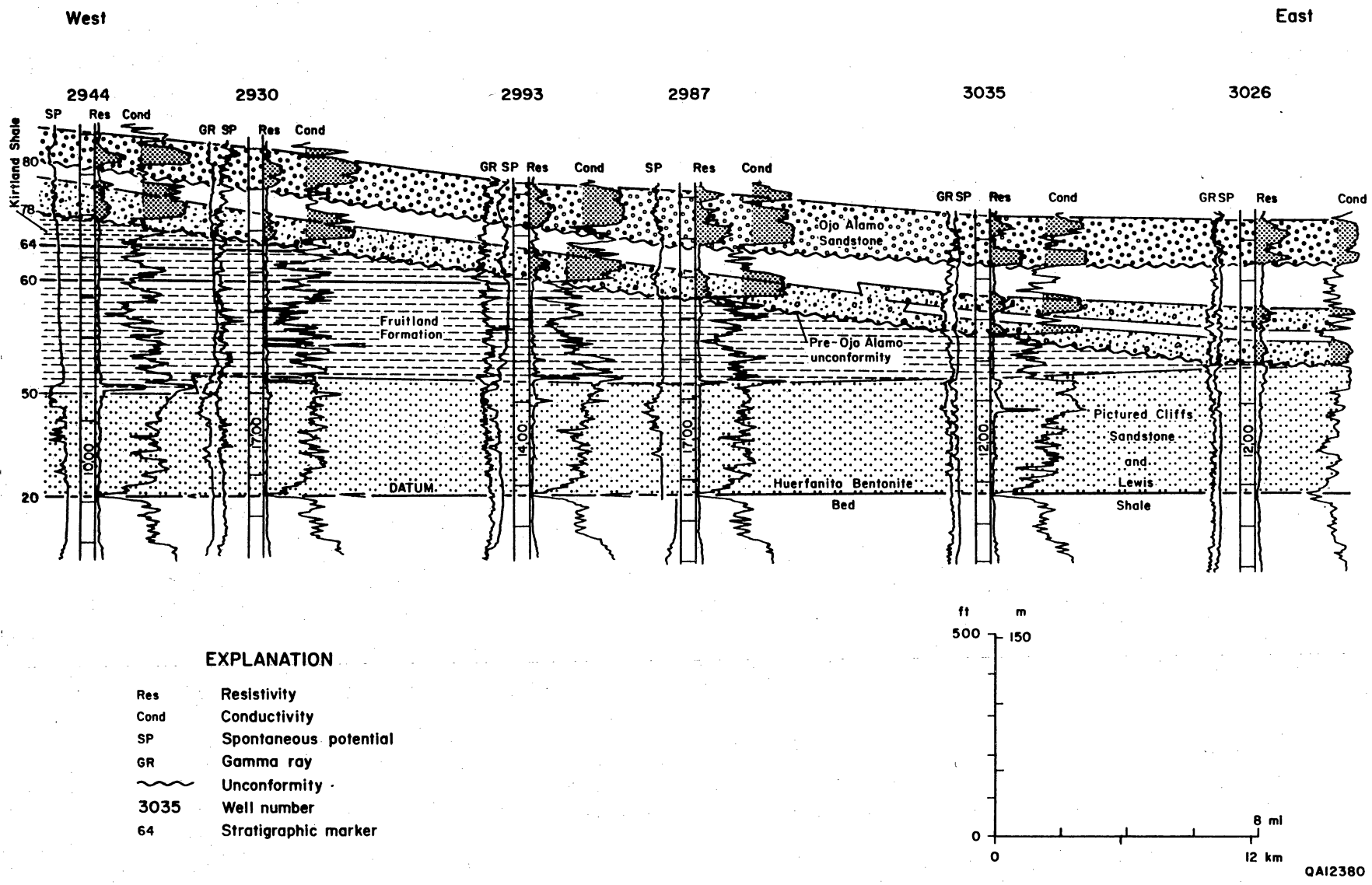

Figure 8. Stratigraphic strike section in the southeast part of the San Juan Basin, illustrating truncation of the Kirtland Shale, Fruitland Formation, and Pictured Cliffs Sandstone by a pre-Ojo Alamo unconformity. Cross section is located in figures 18, 19, and 21.

earlier workers recognized that this sandstone differed in character from adjacent sandstones, they generally assumed that it was a facies variation of either the Fruitland sandstone (Fassett and Hinds, 1971, p. 17) or the Ojo Alamo Sandstone (Sikkink, 1987, p. 89–90). However, a pre-Ojo Alamo unconformity at the southeast margin of the basin was suggested from an earlier outcrop study, on the basis of thickness variations in the Fruitland Formation and Kirtland Shale and lithologic differences in pre-Ojo Alamo and Ojo Alamo sandstones (Baltz, 1967, p. 34).

Previous Studies

Fassett and Hinds (1971) described the regional geology and energy resources of the Fruitland Formation in the San Juan Basin. They used measured sections and data from approximately 325 well logs to calculate 200 billion short tons of Fruitland coal in the basin, but they did not report coalbed methane resources. Choate and others (1984) summarized previous work in which TRW, Inc., working under contracts with the Department of Energy, estimated 31 Tcf of methane in Fruitland coal seams. This estimate was made by multiplying Fassett and Hinds' (1971) coal-tonnage estimate by gas-content values for Fruitland coal seams. The gas-content estimates were based on limited data. Most recently, Kelso and others (1988) reevaluated coal and coalbed methane resources in the Fruitland Formation. For their estimate, they used coal-thickness data from 549 geophysical well logs to calculate coal volume and desorbed-gas values from 28 coal samples to calculate gas content; Kelso and others (1988) estimated 219 billion short tons of coal and 50 Tcf of coalbed methane in Fruitland coal seams thicker than 2 ft. Although the previous regional studies defined regional coalbed methane resources of the Fruitland Formation, they did not address geologic and hydrologic controls on the occurrence and producibility of the methane.

In a pilot geologic study in the north-central San Juan Basin, Ayers and Zellers (1988) used closely spaced well control (approximately 400 well logs in a 215-mi^2 area) to show that geologic conditions that affect the occurrence and producibility of coalbed methane are more complex

than inferred from previous regional studies with sparse data. Using a datum above rather than below the coal-bearing Fruitland Formation, as had been done by previous researchers (Fassett and Hinds, 1971; Fassett, 1985), they concluded that basin subsidence indirectly controlled the occurrence of thick coal seams by causing reversals in the direction of shoreline migration and deposition of interfingering upper Pictured Cliffs sandstones. They also concluded that, although lower Fruitland coal seams pinch out behind Pictured Cliffs shoreline sandstones, upper Fruitland seams may override abandoned-shoreline sandstones, thereby forming extensive coalbed methane reservoirs. Additionally, Ayers and Zellers (1988) demonstrated that 12 to 15 wells/township are necessary to delineate coal-seam-thickness variations and minor structures.

OBJECTIVES

Goals of this study were to (1) evaluate the structural evolution of the San Juan Basin as it applies to the distribution and maturation of Fruitland coal, (2) define depositional systems, (3) delineate the occurrence and continuity of coal seams and evaluate geologic controls on coal occurrence, geometry, and trends, and (4) identify structural features that may enhance coal permeability or affect coalbed continuity.

METHODS

In the San Juan Basin, which covers approximately 6,700 mi^2 encompassed by the Fruitland Formation outcrop, more than 17,000 oil and gas wells have been drilled and logged, providing an excellent data base for a subsurface study of Fruitland coalbed methane. In this study we used 2,500 of these geophysical logs. Geophysical well logs were used to make interlocking cross sections, and stratigraphic units defined by 18 marker beds in the Upper Cretaceous and lower Tertiary section were correlated in these cross sections. All remaining logs

were correlated to these sections. Structure, isopach, lithofacies, and coal data from the logs were tabulated in computer files; these data were used to make computer-contoured maps, or they were posted by the computer for hand contouring. The cross sections and maps were then evaluated individually and compared one to another to interpret evolution of the San Juan Basin and geologic controls on the occurrence and producibility of coalbed methane.

Structural Evolution of the San Juan Basin

Structure affects the availability and producibility of coalbed methane in three ways. First, the timing of structural development of the San Juan Basin affected the burial depth and, hence, thermal maturity of Fruitland coal seams. Second, structural deformation caused fractures that may offset the coal reservoirs and/or enhance coalbed permeability. Finally, structural folding of Fruitland strata uplifted and exposed them at the basin margin, which has greatly affected the water movement by exposing truncated beds for recharge or expulsion of fluids and by providing potential energy for fluid movement.

Structure of Huerfanito Bentonite Bed

The structure map of the Huerfanito Bentonite Bed of the Lewis Shale was made using data from approximately 2,500 well logs (fig. 9). Structural relief on the Huerfanito Bentonite exceeds 4,500 ft. The steeply dipping Hogback monocline is apparent around the north, northwest, and east margins of the basin. In the south half of the basin, dip is 1 degree (92 ft/mi) to the northeast. The structural axis of the basin is complex and is strongly displaced to the northeastern side of the basin. The floor of the basin is the conspicuously flat area below 2,600 ft (fig. 9) that trends northwest and measures about 20×30 mi^2. Dip on the floor is approximately 0.1 degree (10 ft/mi). An inferred structural hingeline coincides with the 2,400-ft contour at the southwest margin of the basin floor; the significance of this hingeline to

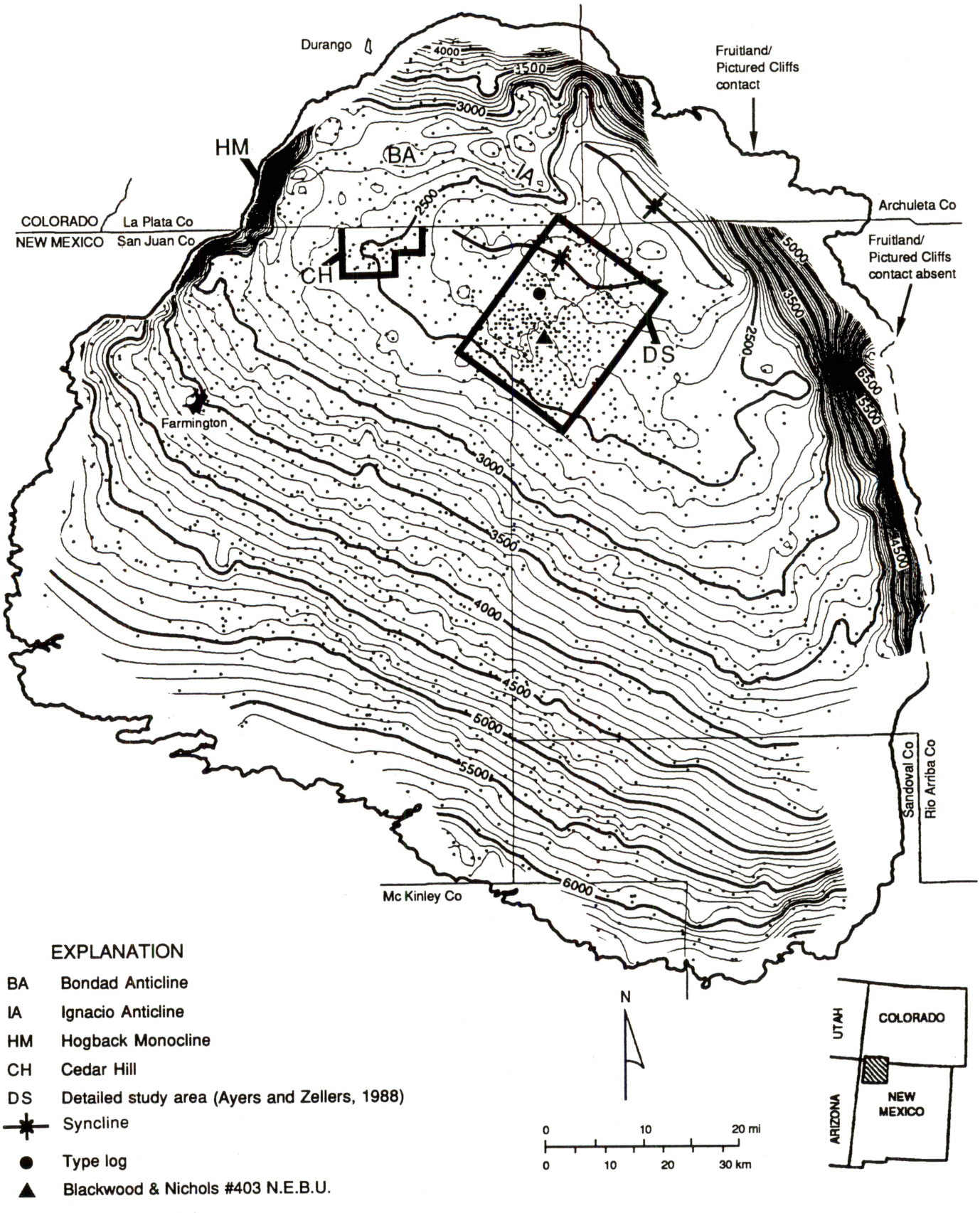

Figure 9. Structure map of the San Juan Basin, contoured on the Huerfanito Bentonite, and location of type log (fig. 3) and Blackwood and Nichols NEBU No. 403 (fig. 7). The basin displays gentle dips on the southern margin and steep dips on the north margin along the Hogback Monocline.

Pictured Cliffs shoreline trends and Fruitland coal occurrence will be developed further in subsequent discussions.

Coal seams may have fracture-enhanced permeability in major folds like the Hogback Monocline and Ignacio Anticline (fig. 9). From the north margin of the basin, a complex structural promontory consisting of several folds extends southward approximately 25 mi. The most prominent of these folds is the Ignacio Anticline in Colorado that plunges southeastward. In New Mexico, the distal nose of the Ignacio Anticline turns eastward. Maximum structural relief on the anticline is approximately 250 ft.

Minor folds with structural relief less than 100 ft may also form structural traps and contribute fracture-enhanced permeability to coal seams. These minor folds occur throughout the basin and are especially apparent where the regional dip changes, such as near the Hogback Monocline and at the periphery of the basin floor. Northwest-plunging folds occur in the detailed study area, and a tightly folded, east-plunging syncline bisects Cedar Hill field (fig. 9). These minor folds were not apparent in an earlier regional structural map of the Huerfanito Bentonite Bed that was made using a data density of one to two well logs per township and a contour interval of 400 ft (Fassett and Hinds, 1971; fig. 15); this map showed only one structural feature within the basin, the Ignacio Anticline.

Elevation of Pictured Cliffs Sandstone

The elevation of the top of the Pictured Cliffs Sandstone (fig. 10) was mapped because it is subjacent to the coal-bearing Fruitland Formation in the southern two-thirds of the basin, whereas the Huerfanito Bentonite Bed is as much as 700 ft below the Fruitland in that area. This is not a true structure map because the Pictured Cliffs Sandstone is time-transgressive (fig. 4). Relief on top of the Pictured Cliff Sandstone is approximately 3,500 ft, which is considerably less than structural relief on the Huerfanito Bentonite Bed (more than 4,500 ft); this difference is due to northward thickening of the Huerfanito to Pictured Cliffs interval (see

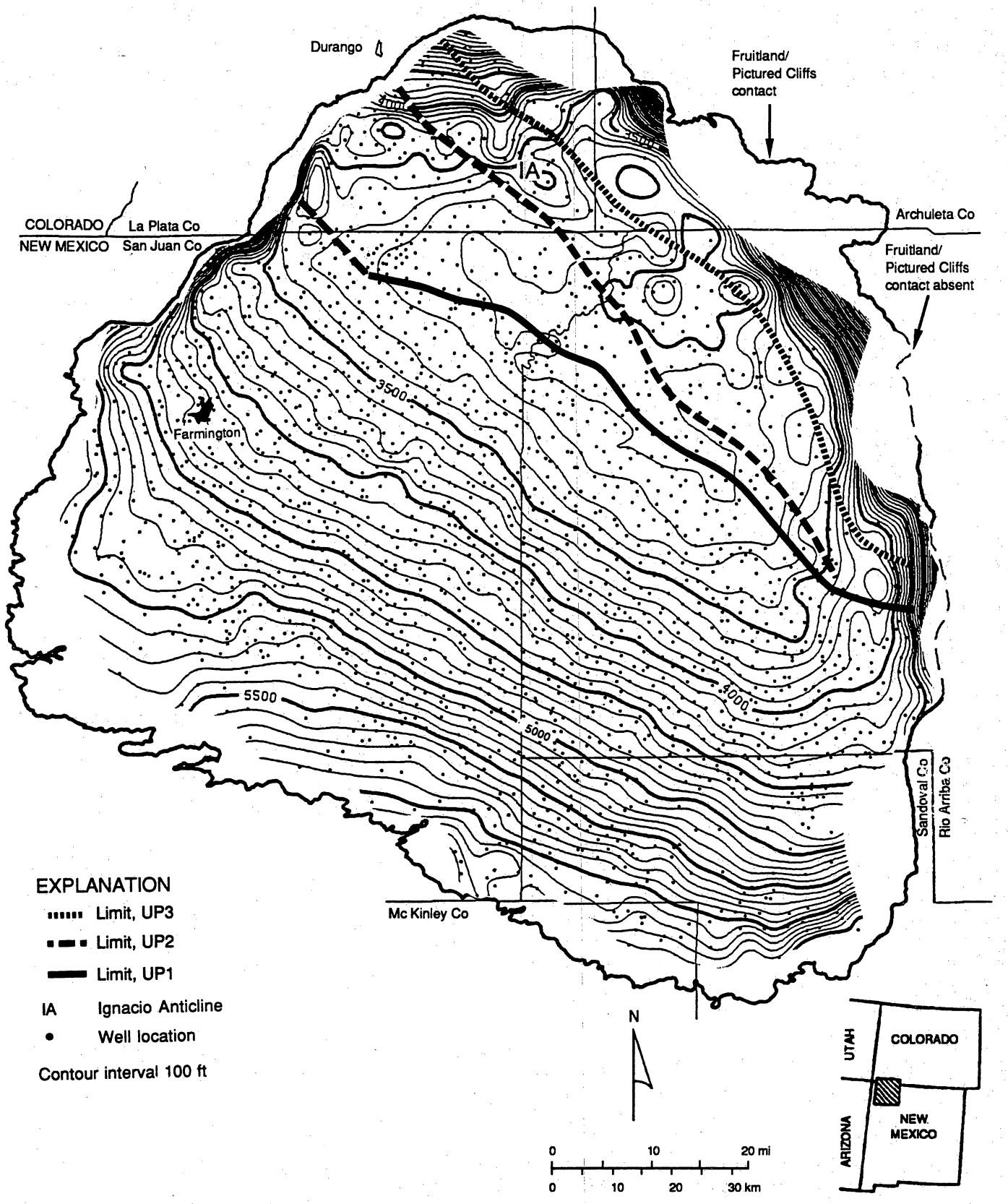

Figure 10. Elevation of the top of the Pictured Cliffs Sandstone, showing structural features similar to those in the structure map contoured on the Huerfanito Bentonite (see fig. 9).

"Huerfanito to Top of Pictured Cliffs Sandstone" section). The map shows, with minor differences, the structural features delineated on the Huerfanito Bentonite map (fig. 9), confirming that formation of the structural basin mostly postdates deposition of the Pictured Cliffs Sandstone. Structural axes on the Pictured Cliff Sandstone are displaced 5 to 10 mi southwest of those mapped on the Huerfanito Bentonite.

Elevation of Ojo Alamo Sandstone

Having demonstrated that most basin structure postdates Pictured Cliffs deposition, we mapped the elevation of the base of the Ojo Alamo Sandstone (fig. 11) to constrain the timing of deformation. This map also is not a structure map because the basal Ojo Alamo contact is unconformable and significant basin tilting predated Ojo Alamo deposition. However, post-Ojo Alamo deformation is evidenced in the map by presence a structural axis that trends north-northwestward in the east-central part of the basin. Structural relief on the base of the Ojo Alamo Sandstone is 1,500 ft in the northwest-southeast direction compared to only 1,000 ft of relief on Huerfanito Bentonite and 500 ft on the Pictured Cliffs Sandstone (fig. 10) across the same region, as a result of the southeast-dipping unconformity at the base of the Ojo Alamo Sandstone (fig. 5).

DEPOSITIONAL FRAMEWORK OF THE PICTURED CLIFFS SANDSTONE AND THE FRUITLAND FORMATION

The thickness, continuity, and extent of Fruitland coal seams are controlled by their depositional setting, which in turn was controlled by syndepositional tectonic activity. To interpret the tectonic and depositional controls on coal seam occurrence, we made cross sections and isopach and coal-occurrence maps. Formation-thickness, or isopach, maps are useful in defining the regional paleoslope, basin evolution, and local syndepositional structural

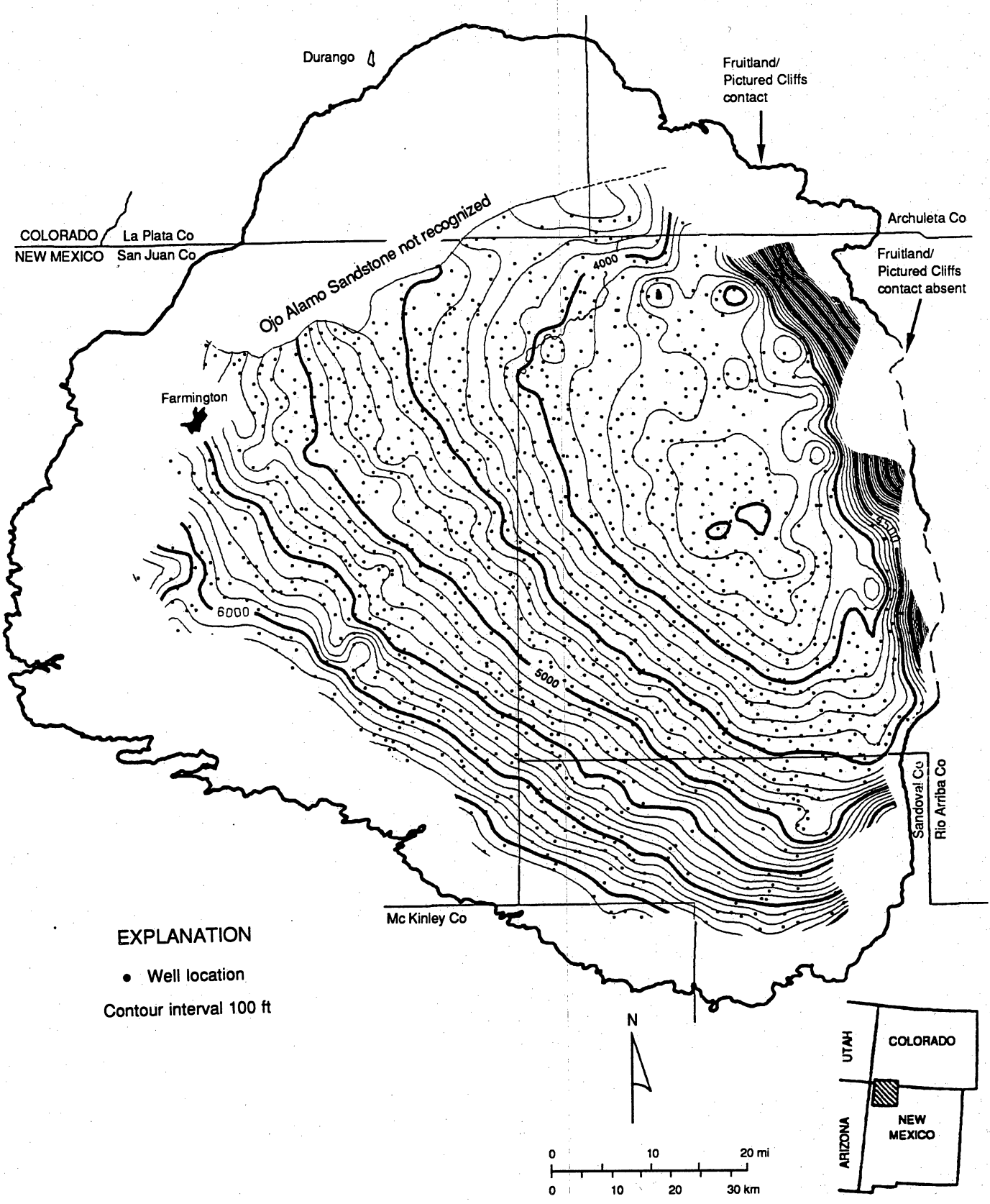

Figure 11. Elevation of the base of the Ojo Alamo Sandstone, which is an erosional surface.

features. The intervals mapped in this study are shown in figures 4 and 5. They are identified either by stratigraphic name or by bounding marker beds that were numbered consecutively, beginning with the lowest (oldest) marker bed. These two-digit numbers were used to facilitate computer manipulation of data in this study and are not suggested as official names or as replacements for existing stratigraphic nomenclature. Intervals mapped in this study are the (1) top of the Huerfanito Bentonite to the top of the Pictured Cliffs Sandstone (marker 20 to 50), (2) Huerfanito Bentonite Bed to top of upper Pictured Cliffs sandstone (marker 20 to 58), (3) Pictured Cliffs Sandstone to top of the Fruitland Formation (marker 50 to 64), (4) Huerfanito Bentonite Bed to base of Ojo Alamo (marker 20 to 80), and (5) top of Fruitland to base of Ojo Alamo Sandstone (Kirtland Shale; marker 64 to 80). Other isopach maps included in this report are of upper Pictured Cliffs tongues, including (6) top of the Pictured Cliffs Sandstone to top of UP1 (marker 50 to 80), (7) top of UP1 to top of UP2 (marker 54 to 57) and (8) top of UP2 to top of UP3 (marker 57 to 58).

Huerfanito to Top of Pictured Cliffs Sandstone (Marker 20 to 50)

This interval, which does not include the Pictured Cliffs tongues, thickens from less than 100 ft on the south to more than 950 ft in the north (fig. 12), consistent with a paleoslope to the north or northeast; basinward thickening of the interval (900 ft over 90 mi) averages 10 ft/mi but is less in the northern third of the basin, north of the 750-ft isopach. This area north of the 750-ft isopach nearly coincides with the basin floor described in the Huerfanito structure map (fig. 9). Throughout the basin, isopach trends are oblique to updip (southwest) pinch-out lines of marker beds in Lewis Shale. This demonstrates that, although isopach trends are useful tools in evaluating paleoslope, they do not necessarily parallel depositional strike.

The 500 to 750-ft isopachs cut across structural axis (fig. 9) on the east side of the basin, indicating that basin axis was not subsiding during deposition. Furthermore, there is no

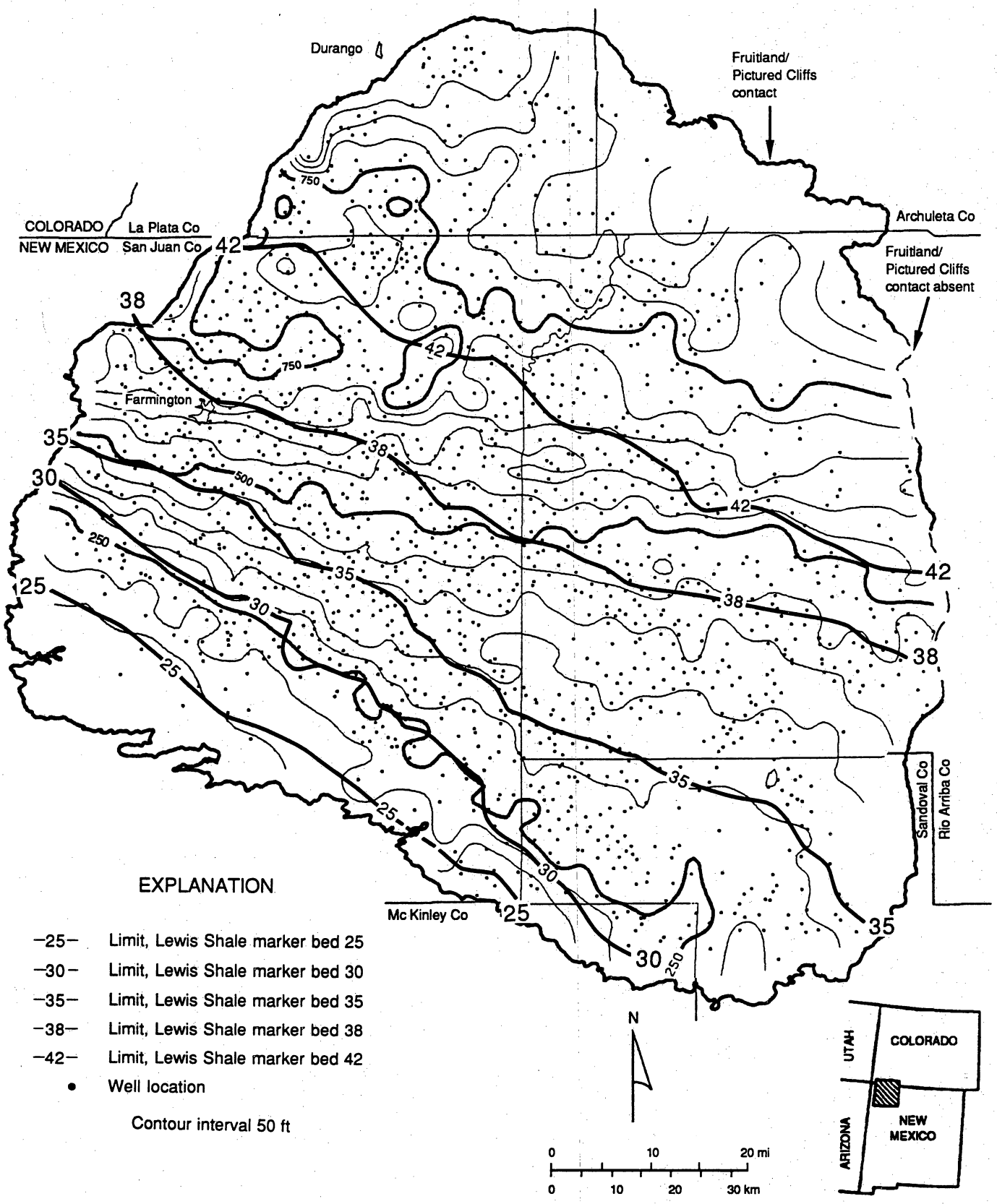

Figure 12. Isopach map from the Huerfanito Bentonite to the top of the Pictured Cliffs Sandstone. The interval thickens basinward from less than 100 ft to more than 900 ft near the north rim of the basin. Greatest thickening, or stratigraphic rise, occurs near the western rim of the basin.

evidence of thinning over the Ignacio Anticline or Bondad Anticline (fig. 9). However, the northern 750-ft isopach is subparallel to many of the fold axes in the basin floor.

Huerfanito Bentonite Bed to Top of Upper Pictured Cliffs Sandstone (Marker 20 to 58)

This map (fig. 13) is equivalent to the Huerfanito to Pictured Cliffs Sandstone isopach of Fassett and Hinds (1971, fig. 7); the interval includes lower Fruitland tongues and is bounded by the top of the uppermost Pictured Cliffs tongue. Southwest of the updip pinch-out line of UP1, the map is identical to the isopach map of the Huerfanito Bentonite Bed to the Pictured Cliff Sandstone interval (fig. 12).

This interval thickens from less than 100 ft on the southwest to more than 1,200 ft on the north. The rate of thickening northeast of the 800-ft isopach is approximately 15 ft/mile. The 800-ft contour nearly coincides with the UP1 pinch-out line and the southernmost structural axis in the basin floor (fig. 13). In the northern part of the basin, isopach trends are discordant (rotated about 30° clockwise) with the underlying Huerfanito/Pictured Cliff Sandstone (marker 20 to 50) isopach trends (fig. 12), suggesting initiation of differential subsidence across the hinge line at the southwest floor of the basin and realignment of the upper Pictured Cliffs shoreline parallel to that hinge. Contours are closely spaced north of the 800-ft contour (for example, 900 to 1,000-ft) where UP2 and UP3 pinch out, particularly in the northwest.

Isopachous thickening of the interval occurs in the syncline at Cedar Hill field, and thinning is apparent at minor anticlines in northwest Rio Arriba County and at Bondad Anticline, suggesting that these structures were active during deposition of upper Pictured Cliffs tongues. Thinning across the Ignacio Anticline indicates minor syndepositional structural activity, as suggested by Sandberg (1988).

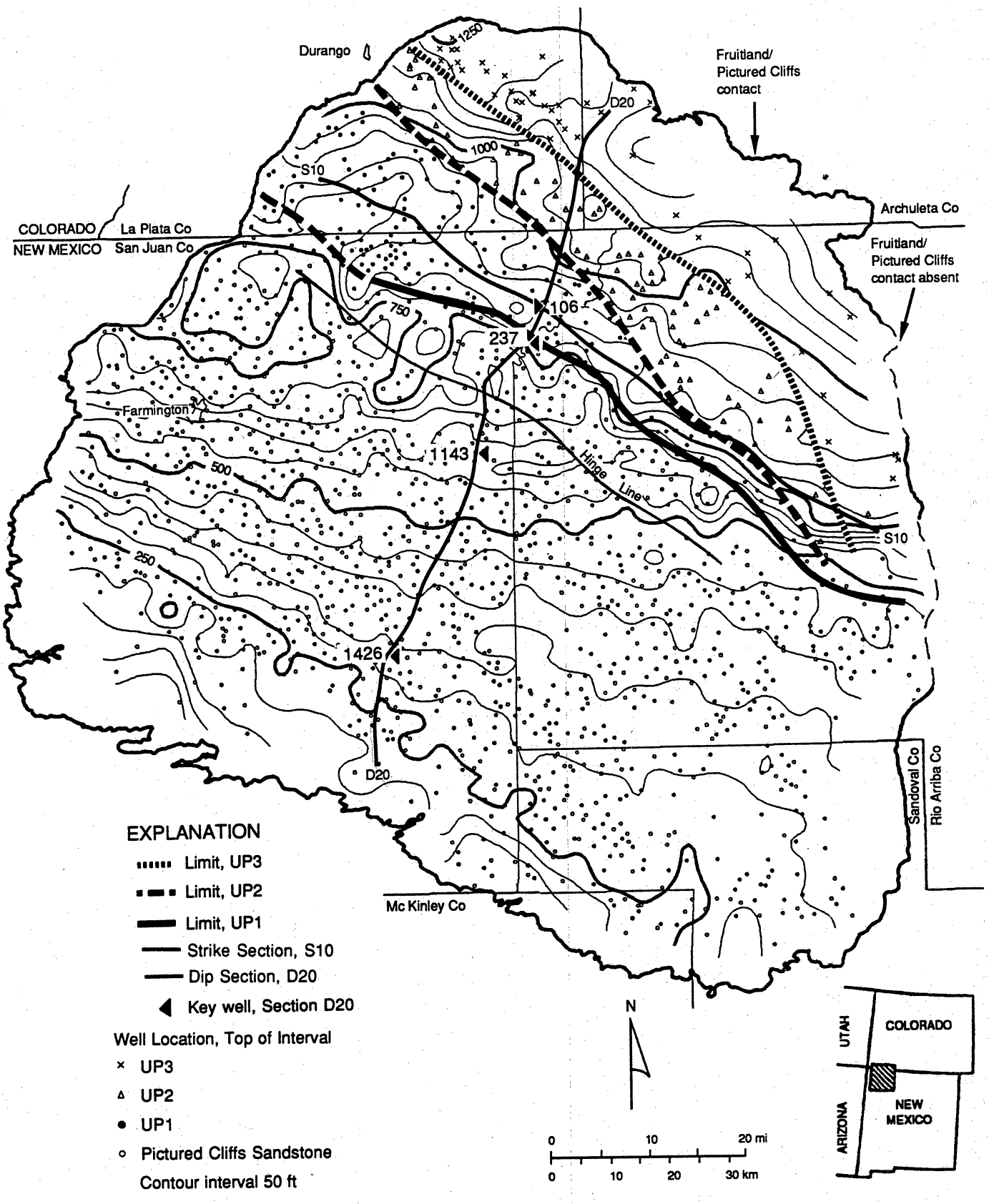

Figure 13. Isopach map from the Huerfanito Bentonite to the uppermost upper Pictured Cliffs sandstone. Closely spaced contours show abrupt thickening across the updip (southwest) limit of UP1, UP2, and UP3. Cross sections D20 and S10 are shown on figures 4 and 5, respectively.

Upper Pictured Cliffs Tongues

In the northeast half of the basin, transgressive shoreline deposits of the upper Pictured Cliffs tongues bound thick, lower Fruitland coal seams in the basinward (northeast) direction. The updip boundaries of the isopach maps of the upper Pictured Cliffs tongues are placed at the pinch-out lines of the Pictured Cliffs tongues. Because each map includes both upper Pictured Cliffs sandstone and the underlying Fruitland tongue, thicknesses of the intervals commonly exceed 100 ft along the pinch-out lines, where the underlying Fruitland tongue comprises most of the interval. Also, due to inclusion of Fruitland tongues, geometries in these isopach maps may not precisely reflect the geometries of the Pictured Cliffs depositional framework elements (sandstones); these framework elements will be mapped as this study continues. In the interim, these isopach maps will be used, in conjunction with coal-occurrence maps and cross sections, to show geologic controls on coal occurrence and geometry.

UP1 Interval (Marker 50 to 54)

The northwest-trending pinch-out line of UP1 (fig. 14) parallels the southern margin of the structural floor (hinge line) and nearly coincides with structural axes of the basin as mapped on the Pictured Cliffs Sandstone (fig. 10), suggesting that transgression was initiated by subsidence of the basin floor and that landward pinch-out of UP1 was against a hingeline. Geometry of the UP1 interval is lobate to dip-elongate, suggesting a deltaic rather than a barrier shoreline. Four depocenters, designated 1, 2, 3, and 4 (fig. 14), are defined by areas where the interval thickness exceeds 100 ft. In these depocenters, dip-elongate pods, defined by the 100-ft contour, extend 12 to 19 mi basinward. Interval thickness is greatest in depocenter 2 in Cedar Hill field (fig. 14).

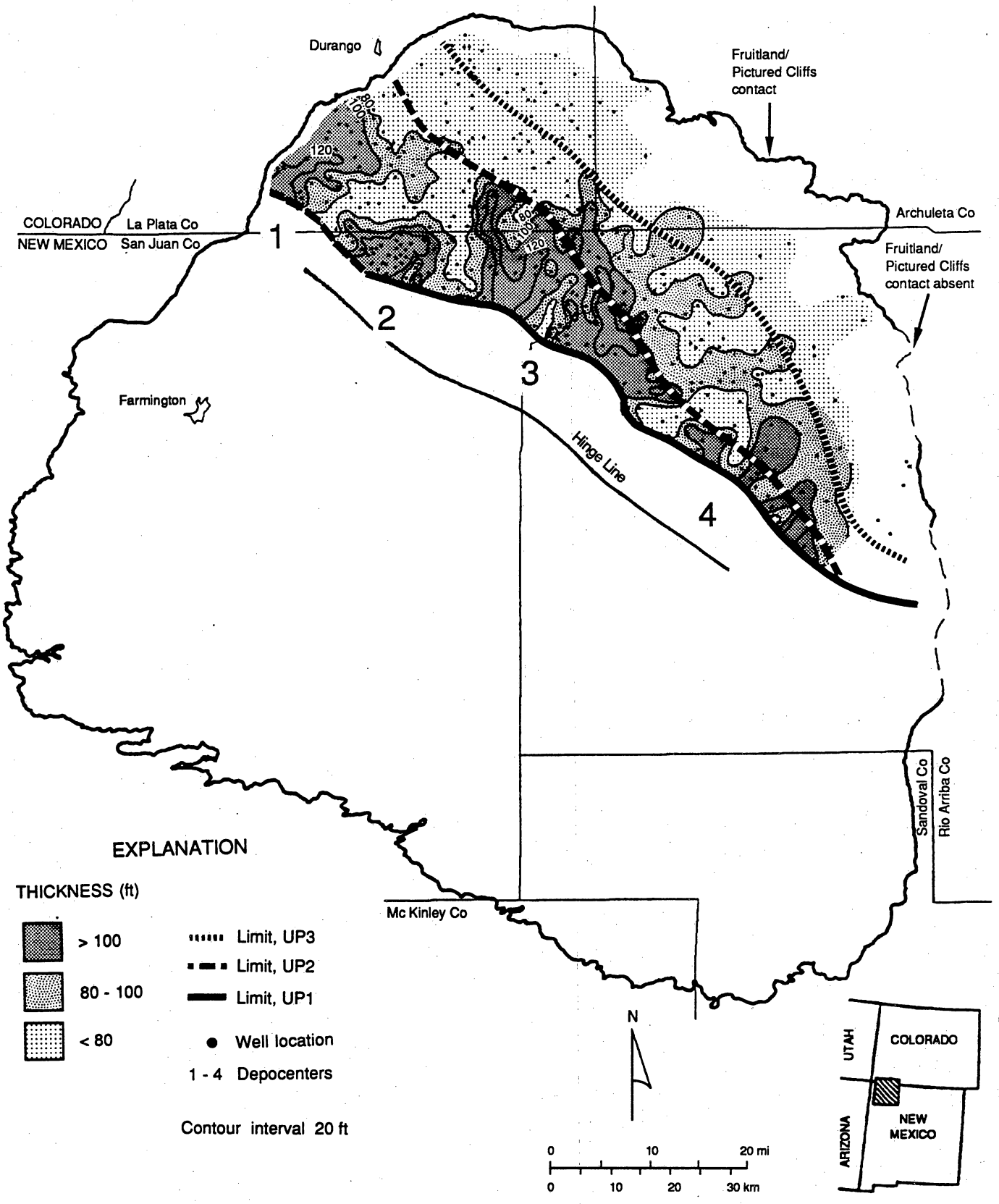

Figure 14. Isopach map from the top of the Pictured Cliffs Sandstone to the top of UP1. Lobate and dip-elongate thickness trends indicate an irregular shoreline with four main depocenters.

UP2 Interval (Marker 54 to 57)

Geometry of UP2 (fig. 15, which overlies UP1 (fig. 4), is strike elongate, consistent with deposition in a wave-dominated shoreline setting. The interval is 50 to 140 ft thick, and the depositional axis, defined by the 100-ft contour interval, is 1 to 12 mi wide. The only break in the depositional axis is a minor, dip-elongate trend in the eastern third of the area, where thicknesses are as low as 60 ft. Dip-elongate trends on updip (southwest) margin in this area suggest a back-barrier environment and fluvial or tidal channel-fill sandstones. From the strike-elongate depositional axis, UP2 thins gradually basinward to the north. The Ignacio Anticline crosses the depocenter in the center of the trend and appears to have been inactive during UP2 sedimentation.

The pinch-out line of the UP2 interval is nearly parallel to the structural grain of the basin, occurring along a line that bisects the structurally lowest part of the basin (fig. 10). This pinch-out line terminates (laps out) against the basinward side of UP1, resulting in a shingled or imbricated relation of the units (fig. 4). In the eastern part of the basin, the UP2 pinch-out line converges toward the UP1 pinch-out line.

UP3 Interval (Marker 57 to 58)

UP3, the third upper Pictured Cliffs tongue, was deposited in a wave-dominated shoreline setting; geometry of the UP3 interval (fig. 16), like that of UP2, appears to be strike-elongate, but the UP3 shoreline prograded to the north margin of basin, so that the sequence was incompletely preserved. The depositional axis of UP3, which is parallel to UP2, is 3 to 16 mi downdip (northeast) of the UP2 depositional axis. Thickness of the UP3 interval is 50 to 150 ft thick and is inversely related to thickness of the underlying UP2 interval. Dip-elongate fluvial

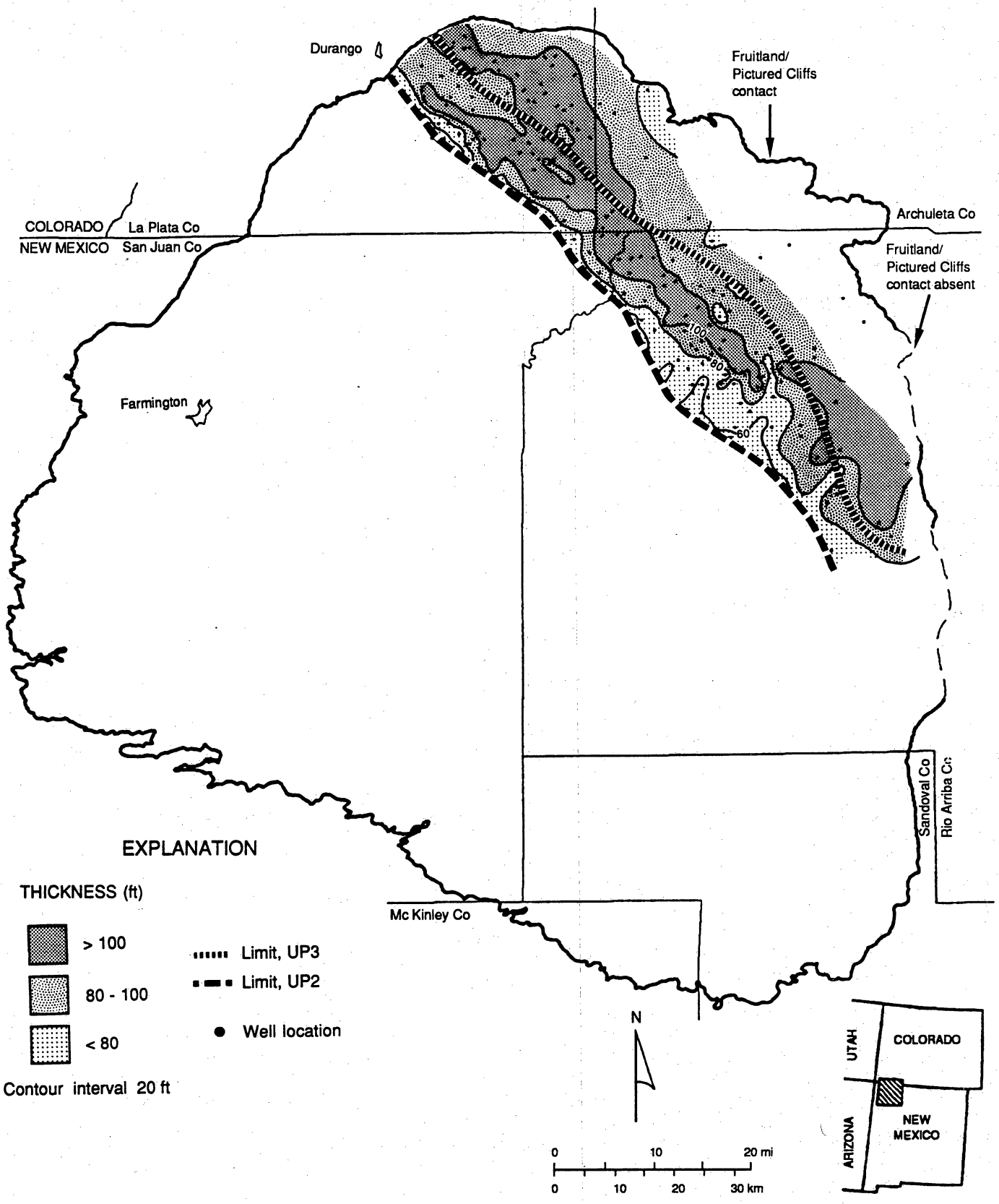

Figure 15. Isopach map from top of UP1 to top of UP2. In contrast to the isopach of UP1 (fig. 14), the isopach of UP2 shows prominent strike-elongate (northwest) trends.

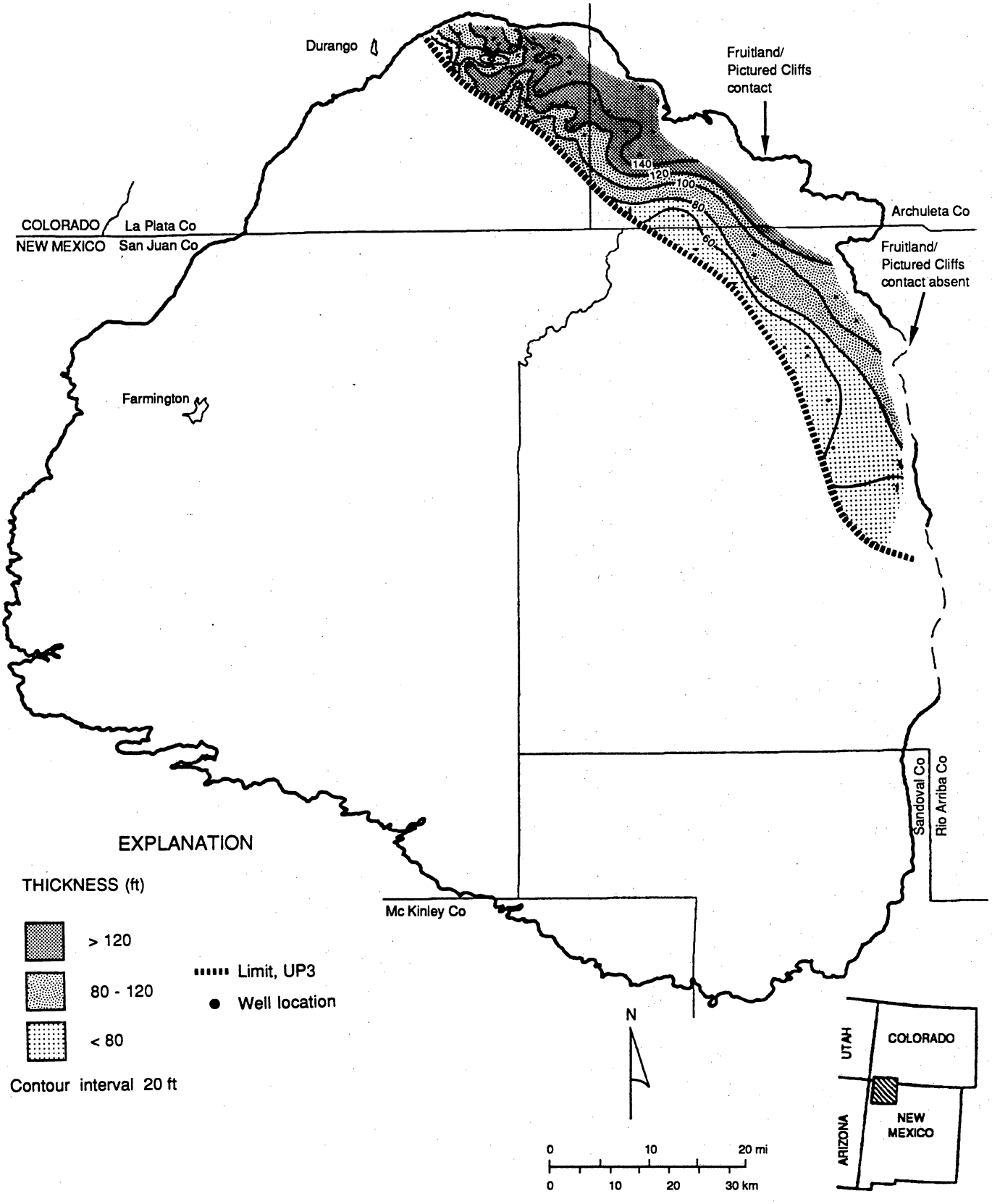

Figure 16. Isopach map from top of UP2 to top of UP3, exhibiting prominent strike elongation similar to the UP2 interval (see fig. 15). A local depocenter in the northwestern part of the basin is indicated by dip elongation of the contour lines.

feeders are inferred on the updip (southwest) side of the depositional axis at the northwest end of the trend.

Structural influence of the Ignacio Anticline was not a factor in deposition of UP3, because the UP3 pinch-out line is just basinward of the anticline. However, the northwest-trending pinch-out line of UP3 is influenced by the structural trough on the east side of the basin (fig. 16). In the vicinity of the trough, it swings southward to nearly intersect the UP2 pinch-out line.

Pictured Cliffs Sandstone to Top of the Pictured Cliffs Tongues (Marker 50 to 58)

The isopach map (fig. 17) of the combined upper Pictured Cliffs tongues and the intervening Fruitland tongues shows a strike-elongate (northwest) trend that is parallel to the structural grain of the basin. The depositional axis is near the northeast margin of basin and nearly coincides with the UP3 depositional axis. In contrast with the downdip (northern) part of this composite upper Pictured Cliff interval, the updip (southern) part is irregular, containing lobate and dip-elongate isopach trends that reflect the geometry of UP1, the only upper Pictured Cliffs tongue in the updip area. Thickness of the composite interval is 60 to 350 ft, which is less than the sum of the maximum thicknesses of component intervals (UP1 through UP3) because of a shingle effect and basinward offset of successive depocenters. Rates of thickening are greatest north of pinch-out lines of individual Pictured Cliffs tongues. For example, the greatest rate of thickening (30 to 60 ft/mi) is north of the UP3 pinch-out line.

Pictured Cliffs Sandstone–Fruitland Formation Interval (Marker 50 to 64)

The interval from the top of the Pictured Cliffs Sandstone to the top of the Fruitland Formation (marker 50 to 64) includes the coal-bearing Fruitland Formation as well as the Pictured Cliffs tongues that occur only in the northeastern third of the basin (fig. 4). Two

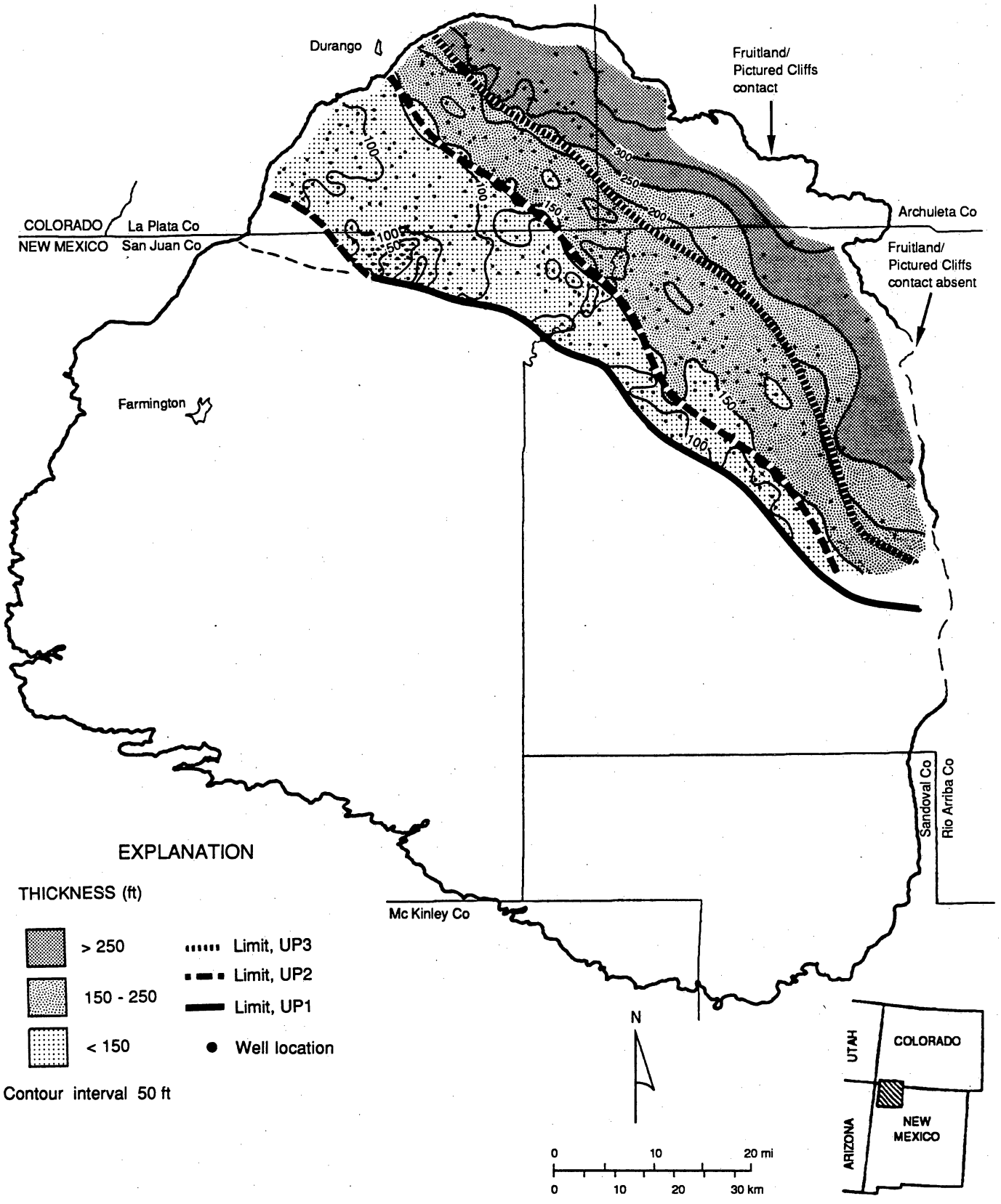

Figure 17. Isopach map from the top of the Pictured Cliffs Sandstone to the top of UP3, illustrating combined thickness of UP1, UP2, and UP3.

isopach maps of this interval were made: one that includes the Pictured Cliffs tongues (fig. 18) and one without the tongues (fig. 19) that is a true isopach map of only the Fruitland Formation. Marked eastward thinning at the eastern side of basin (figs. 18 and 19) results from erosional beveling of the Fruitland Formation; the Fruitland Formation is truncated along the extreme eastern margin of the basin (fig. 5).

The isopach map of the combined Fruitland and Pictured Cliffs tongues (fig. 18) shows that this interval thickens to more than 650 ft in the northern third of the basin from a rather uniform thickness of 300 to 350 ft in the southern part of the basin. By contrast, the isopach map of the coal-bearing Fruitland only (fig. 19) indicates a basinward-thinning trend in the northeast and north-central parts of the basin. Both of these maps show local thickening in the northwest part of San Juan Basin near the Colorado/New Mexico state line. This area may be the Fruitland depocenter described for the Fruitland Formation by earlier workers (Silver, 1951; 1957). If so, then southeastward thinning of the Huerfanito–Ojo Alamo interval (fig. 20) may not be entirely due to postdepositional erosion of the Kirtland Shale as concluded by Fassett and Hinds (1971), and uplift of the southeast rim of the basin may have started during Pictured Cliffs–Fruitland deposition.

Eastward and southeastward thinning of the Kirtland Shale in the south and southeast part of the basin also was attributed to deposition rather than exclusively to the effects of erosion (Dane, 1936, p. 120–121). During deposition of the Fruitland Formation and Kirtland Shale, local uplift occurred at the southeastern margin of the basin (Baltz, 1967, p. 34). Therefore, lower subsidence rates and reduced basin accommodation (thus, more oxidizing conditions) may have existed along the east margin even before Kirtland time and may partly explain the absence of thick coal seams in the eastern part of the basin.

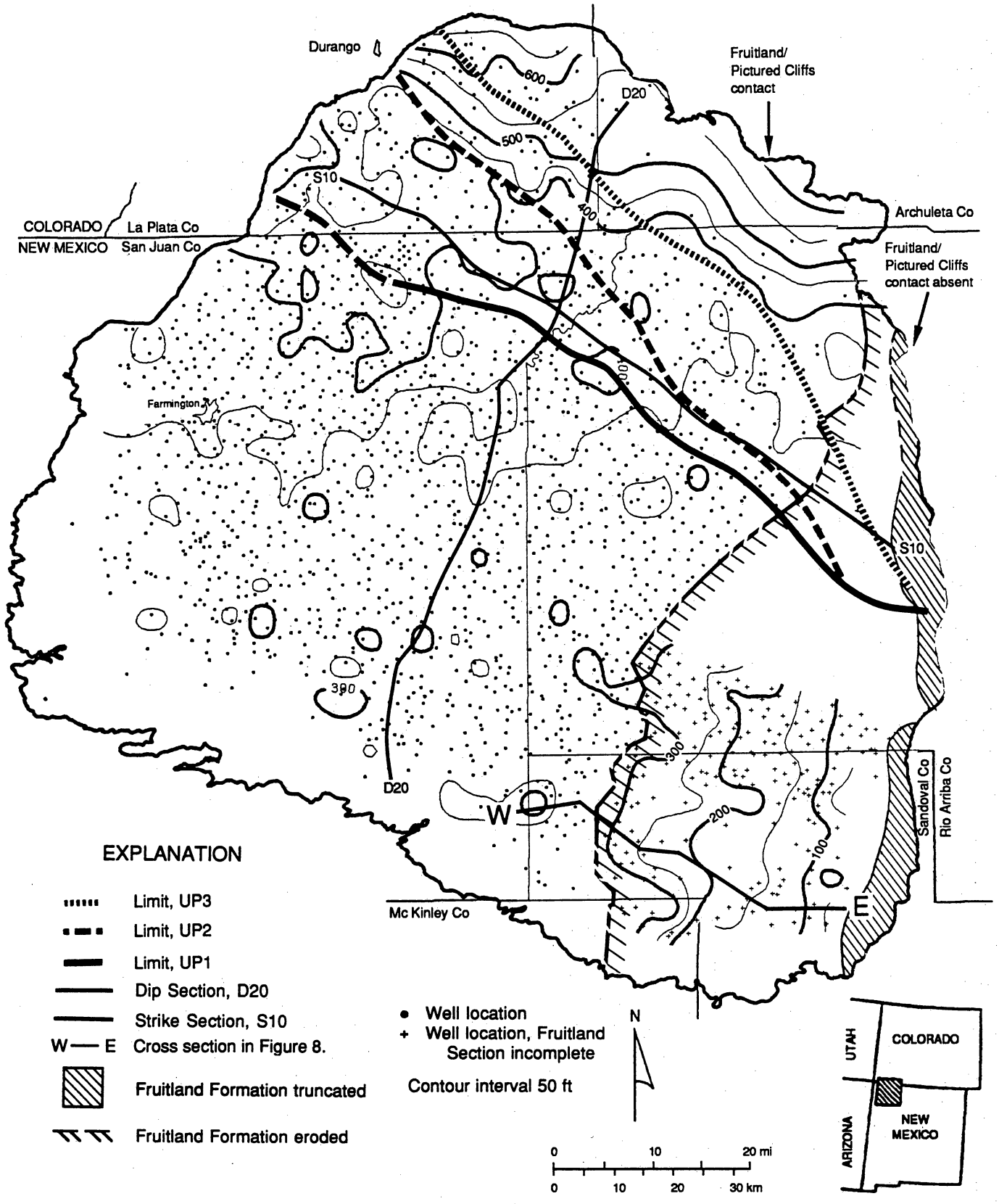

Figure 18. Isopach map of the Fruitland Formation, including the upper Pictured Cliffs tongues UP1, UP2, and UP3. Inclusion of these tongues causes a basinward-thickening trend in the northern third of the basin. Cross sections D20 and S10 are shown in figures 4 and 5, respectively.

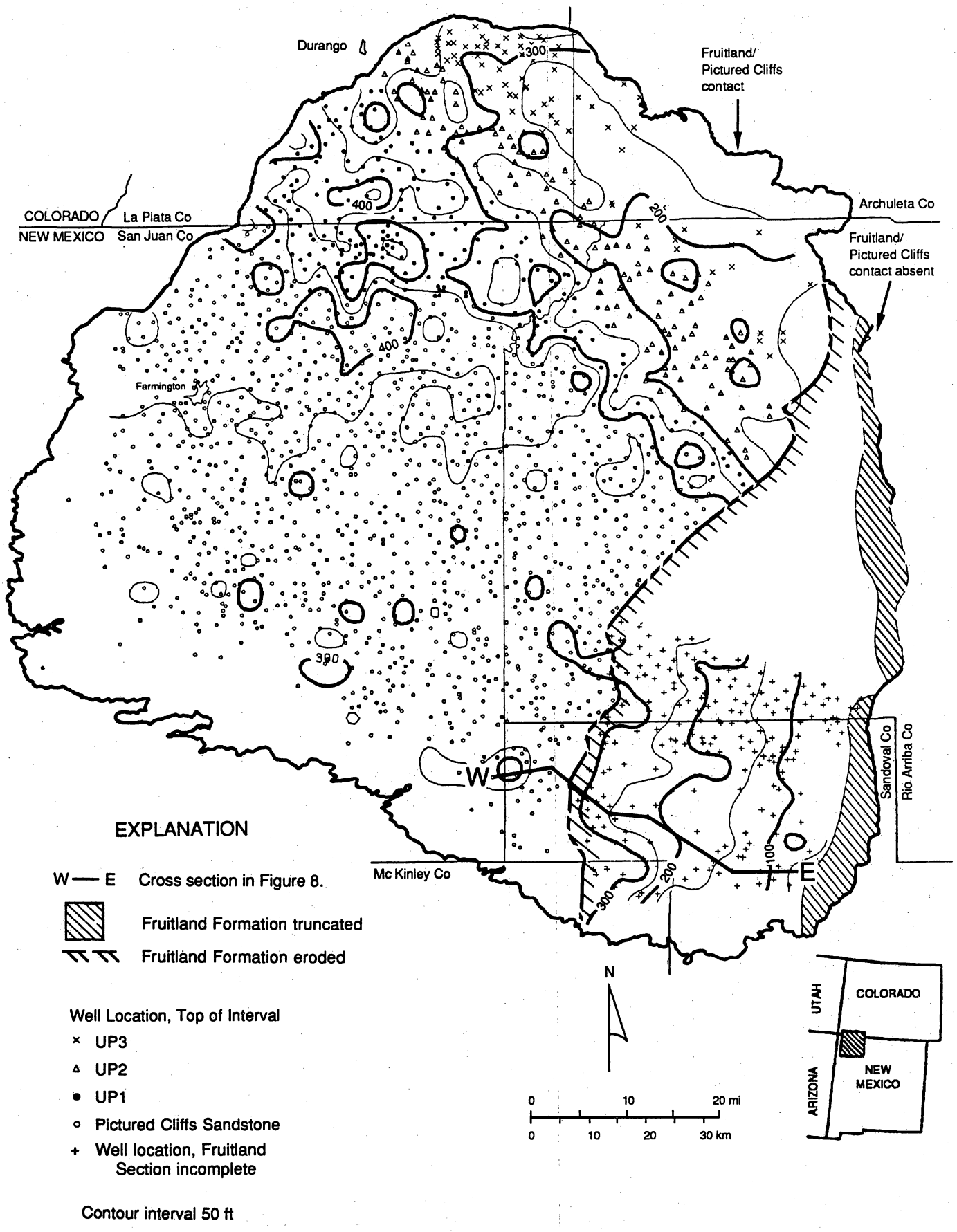

Figure 19. Isopach map of the Fruitland Formation, without upper Pictured Cliffs tongues. The Fruitland Formation thins basinward toward the northeast but maintains thickness toward the northwest.

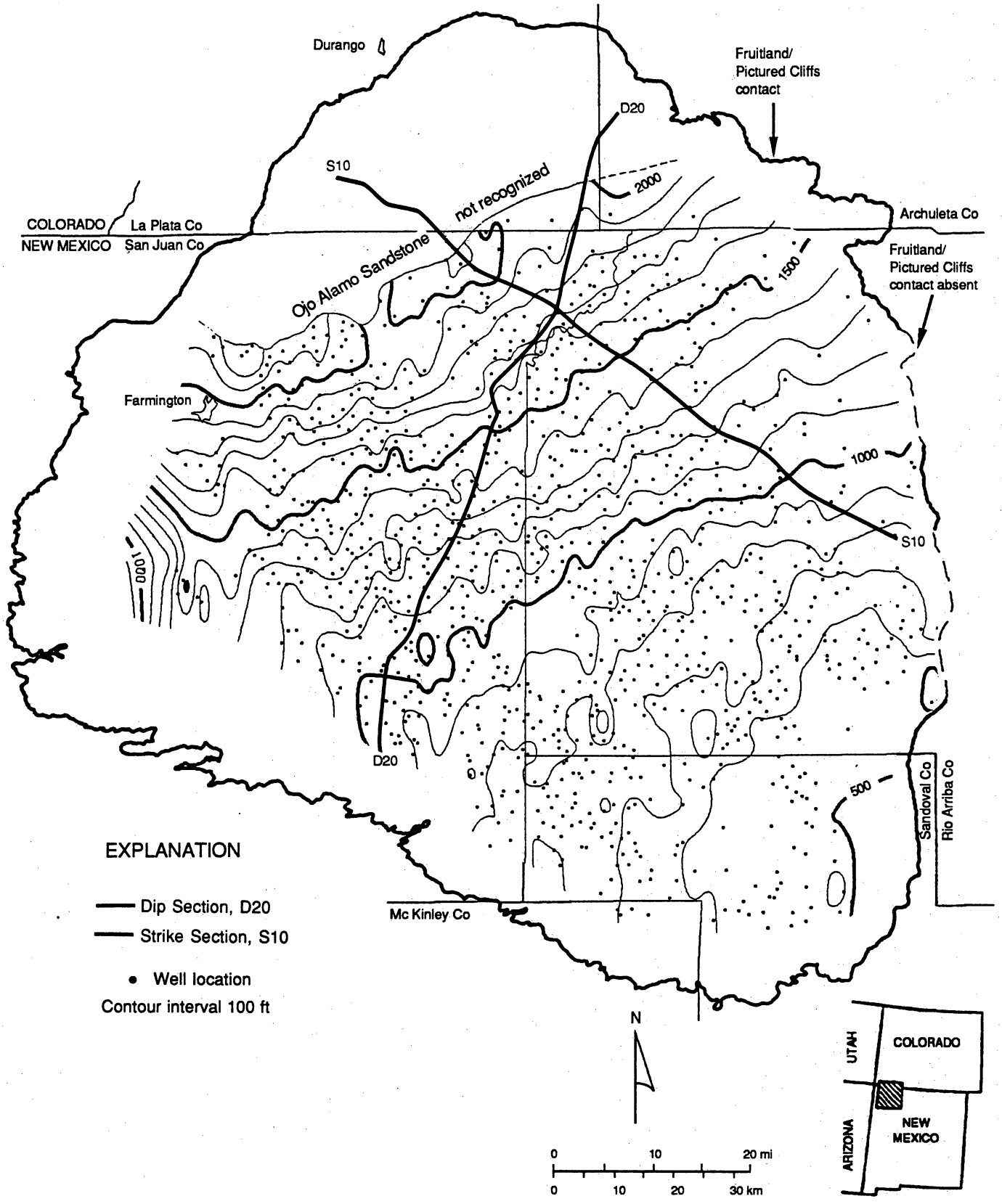

Figure 20. Isopach map from the Huerfanito Bentonite to base of the Ojo Alamo Sandstone. East-northeast orientation of contours results from combination of eastward-dipping erosional surface of the Ojo Alamo unconformity and basinward thickening of the Pictured Cliffs Sandstone. Cross sections D20 and S10 are shown in figures 4 and 5, respectively.

Huerfanito Bentonite Bed to Base of Ojo Alamo Sandstone (Marker 20 to 80)

Northeast-trending contours on the isopach map of this interval (fig. 20) are the result of truncation of Upper Cretaceous strata by the southeastward-dipping unconformity at the base of the Ojo Alamo Sandstone. This interval is not mapped in the northwest part of the basin where the Ojo Alamo Sandstone is unrecognized, due either to facies change or to erosional truncation of the Ojo Alamo. Fassett (1985) suggested that the pre-Ojo Alamo strata were eroded by a northwestward-flowing fluvial system that predated the southward-flowing Ojo Alamo fluvial system that was deposited above the unconformity. The second-order, northwest-trending bands of isopach thinning were present in an earlier map and were inferred to be paleovalleys (Fassett and Hinds, 1971; Fassett, 1985). However, we have identified and mapped an unconformable surface 50 to 200 ft below and discordant with the Ojo Alamo Unconformity in the southeastern part of the basin (fig. 8).

Because of erosional truncation, Upper Cretaceous strata thin southeastward from more than 2,200 ft thick in the northwest to less than 500 ft thick in the southeast part of the basin (figs. 5 and 20). Closer spacing of contours in the northwest part of the basin indicates that the surface of the unconformity is steeper there, suggesting that there was little tilting in the southeast; this area was uplifted as a platform and was bounded to the northwest by a poorly defined, northeast-trending hingeline. Rate of thinning is 35 ft/mile northwest of the 1,000-ft contour and 15 ft/mi southeast of the 1,000-ft contour, in the platform area. Near the south margin of the basin, the isopachous strike is oriented north-northeast, reflecting the Ojo Alamo Unconformity.

Kirtland Shale Isopach (Marker 64 to 80)

The Kirtland Shale thins southeastward because it has been beveled by erosion (figs. 5 and 21). In the southeast part of the basin, the pre-Ojo Alamo unconformity (fig. 8) truncates the Kirtland Shale east of the zero contour (fig. 21) in Rio Arriba and Sandoval Counties.

Tertiary Fill of the San Juan Basin (Depth to Base Ojo Alamo Sandstone)

The map of Tertiary fill of the San Juan Basin, or depth to base of the Ojo Alamo Sandstone (fig. 22), indicates post-Cretaceous basin fill. This map reflects several factors including (1) slope of the unconformable surface, (2) basin structure, and (3) topography. More than 3,500 ft of Tertiary sediments occur in the east-central part of the basin, where the base of the Ojo Alamo Sandstone is lowest structurally (fig. 11). To date, no regional marker bed has been recognized in the Tertiary strata that will allow further analysis of the structural development of the basin.

FRUITLAND COAL

In the San Juan Basin, Fruitland coal rank is subbituminous B to high-volatile A bituminous around much of the south and west margins of the basin; rank increases into the basin to low-volatile bituminous in T34N, R8W (Campbell, 1985; Kelso and others, 1988). The area of highest coal rank does not coincide with present depth of burial or basin structure (Kaiser and Swartz, 1988). Ash content ranges from 10 to 30 percent and commonly is greater than 20 percent; sulfur averages less than 1 percent, and moisture averages 10 percent in New Mexico and approximately 2 percent in Colorado (Keystone, 1986; Fassett, 1987).

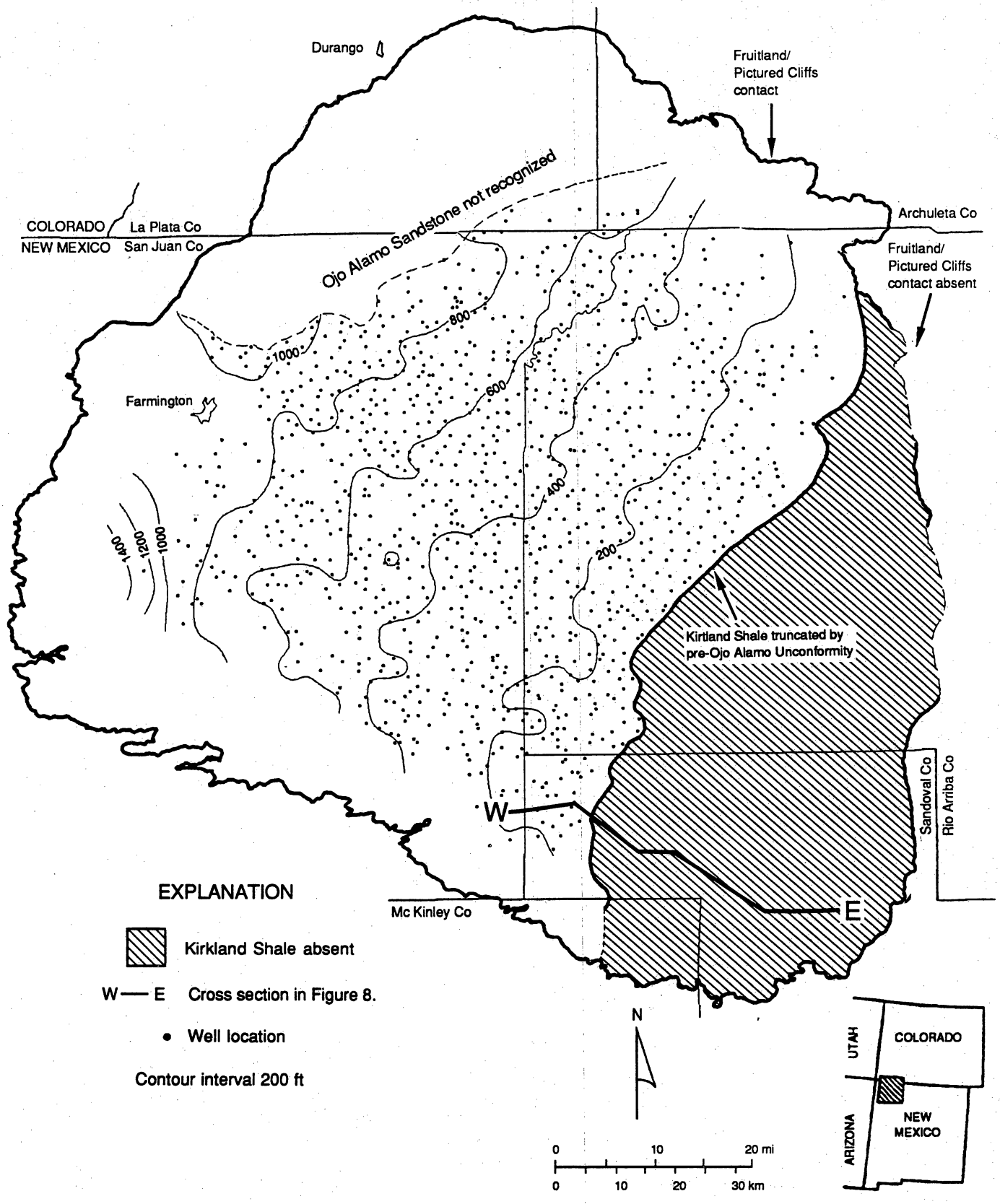

Figure 21. Isopach map of the Kirtland Shale. North-northeast-oriented contours reflect gradual eastward beveling of the Kirtland Shale below the Ojo Alamo Unconformity. The Kirtland Shale is absent east of the zero line.

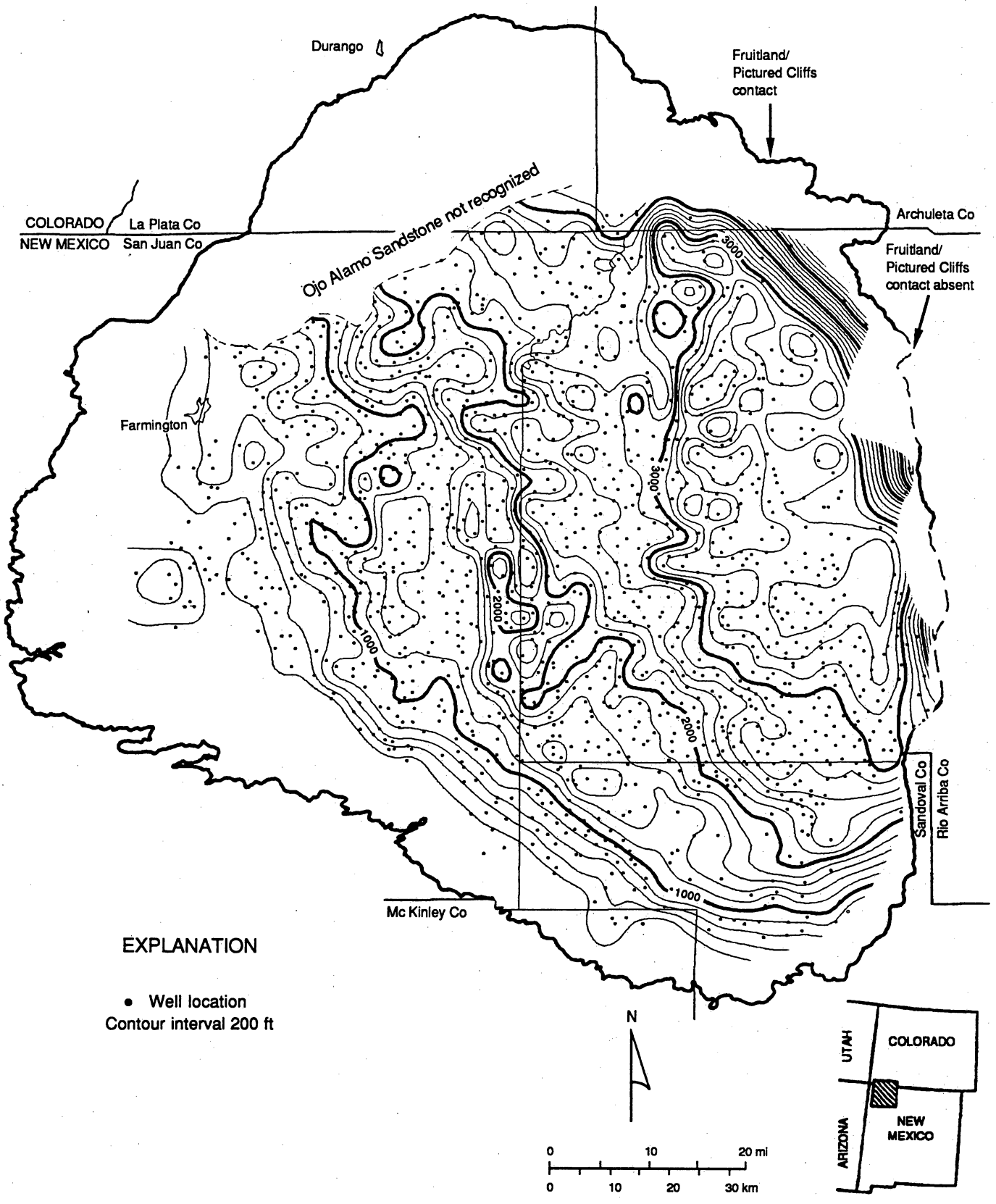

Figure 22. Isopach map of Tertiary fill in the San Juan Basin, defined as depth to the base of the Ojo Alamo Sandstone.

Coal Identification

On geophysical well logs, coal was identified by its low density, high neutron and density porosities, low sonic velocity, and/or low neutron count (fig. 23; Ayers and Zellers, 1988). Low natural gamma response can be used to reliably identify coal seams in some basins. However, gamma response in Fruitland coal seams is variable, probably because of high and variable ash content of the coal. In figure 23, the thick coal at 3,225 to 3,255 ft is split by a parting at 3,240 ft. Coal above the parting is more radioactive (higher gamma count) than coal below the parting; response in the upper coal is similar to that in the overlying sandstone (3,180 to 3,215 ft). The upper coal has a higher bulk density than coal below the parting, implying greater ash content in the upper coal. The gamma-ray curve is useful for correlation locally; high-gamma counts (peaks) in coal seams and associated Fruitland deposits (fig. 23) can be correlated for several miles. These natural gamma peaks are attributed to thin clastic beds that are interpreted as volcanic ash layers (tonsteins) in the coal or attributed to organically bound radioactive elements in adjacent sediments. Volcanic ash beds are described in Fruitland coal seams from the south margin of the basin (Fassett and Hinds, 1971), and bentonite beds are common in the Lewis Shale. The abundant tonstein layers most likely contribute to the high-ash content of Fruitland coal seams. Formation resistivity is of limited use for coal identification in the northern part of the San Juan Basin. However, it can be used to reliably identify coal in the southern part of the basin because there are no other highly resistive beds in the Fruitland Formation in this area (Fassett and Hinds, 1971).

On geophysical logs, the thickness of a bed is commonly measured halfway between the shale baseline and the peak corresponding to that bed. On the bulk density log (fig. 23), coal-seam thickness was measured at a density of approximately 1.80 g/cm^3, which is a slightly conservative measurement. We recorded the thickness of coal seams thicker than 2 ft; partings thinner than 2 ft within thick coal seams were included as coal because of the limits of

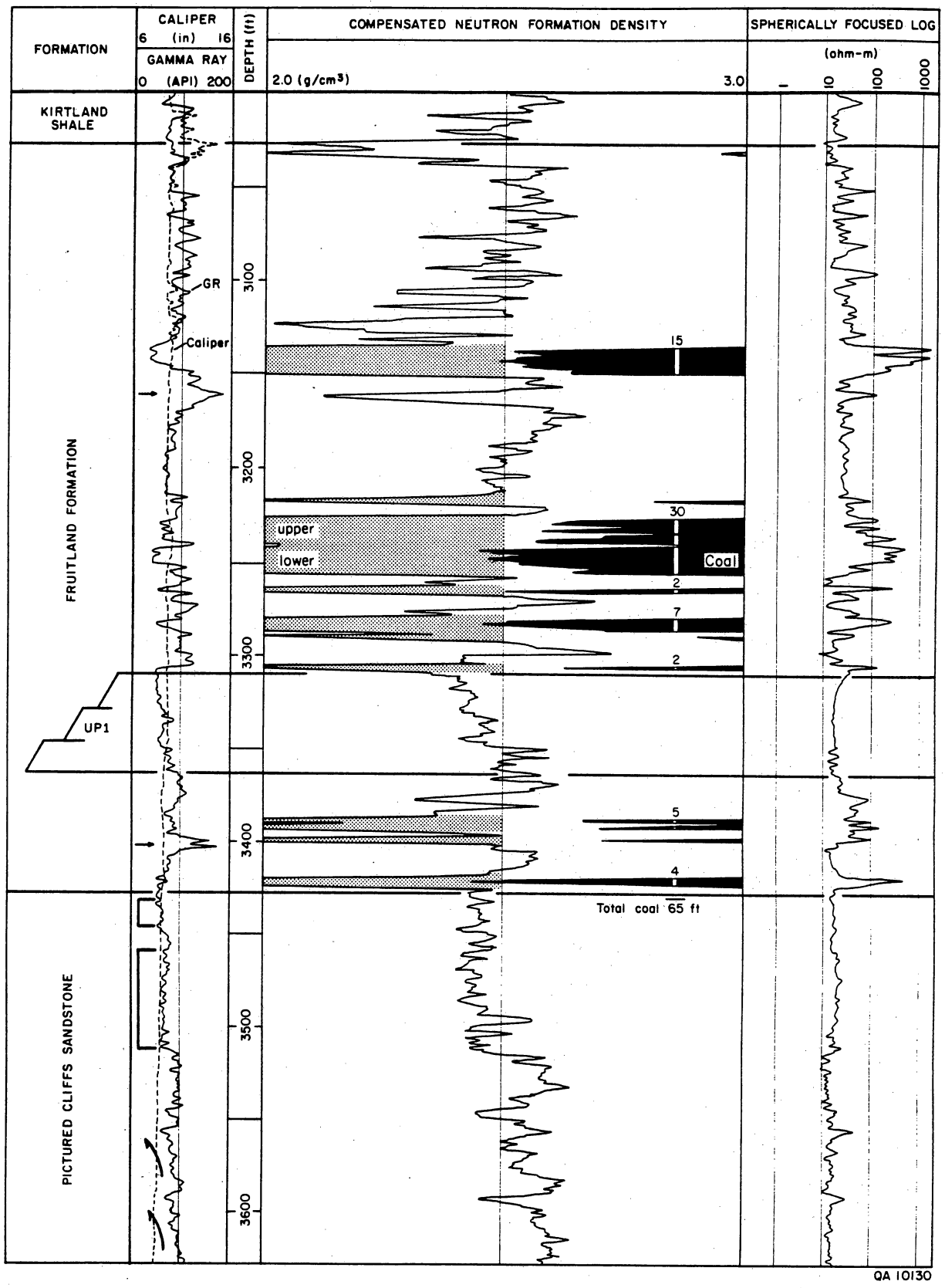

Figure 23. Identification and measurement of Fruitland coal in type log in figure 3. High natural gamma-ray responses, indicated by arrows, are attributed to volcanic ash beds and to organically bound radioactive elements in coal seams.

resolution of the geophysical logs. High-ash coal also is a source and reservoir rock for coalbed methane, and inclusion of minor thicknesses of high-ash coal does not conflict with our goals of delineating the distribution and depositional setting of the coal seams. A 3-ft parting cutoff in thick coal seams was used by Fassett and Hinds (1971) in mapping the thickest individual (maximum) coal in the Fruitland Formation. However, Fassett and Hinds (1971) excluded partings thicker than 1 ft when mapping total coal thickness. Kelso and others (1987, 1988) do not state the maximum thickness of partings included in coal seam measurements for their resource calculations.

Coal Stratigraphy

In the southern part of the San Juan Basin, thick coal seams occur in the lower half (150 to 200 ft) of the Fruitland Formation; seams in the upper Fruitland Formation are thin (fig. 4). In the northern part of the basin, thick lower Fruitland coals pinch out against the Pictured Cliffs Sandstone, and the thickest coal seams are stratigraphically equivalent to other seams in the upper Fruitland in the south; the lower Fruitland Formation and coal seams of the south part of the basin are absent in the north due to pinching out between Pictured Cliffs tongues UP1, UP2, and UP3 (fig. 4). Thick coal seams in the north either pinch out against or override upper Pictured Cliffs tongues. However, because they are immediately above UP1, UP2, or UP3, these coal seams commonly are referred to as lower Fruitland seams, even though they are stratigraphically higher than thick coal seams in the south. As pointed out by Fassett (1987), the terms "upper and lower" Fruitland have little validity in regional discussions.

Coal Overburden

The depth to Pictured Cliffs Sandstone or the uppermost Pictured Cliffs tongue, where present (fig. 24; overburden map), indicates thickness of the overburden for sealing the coal

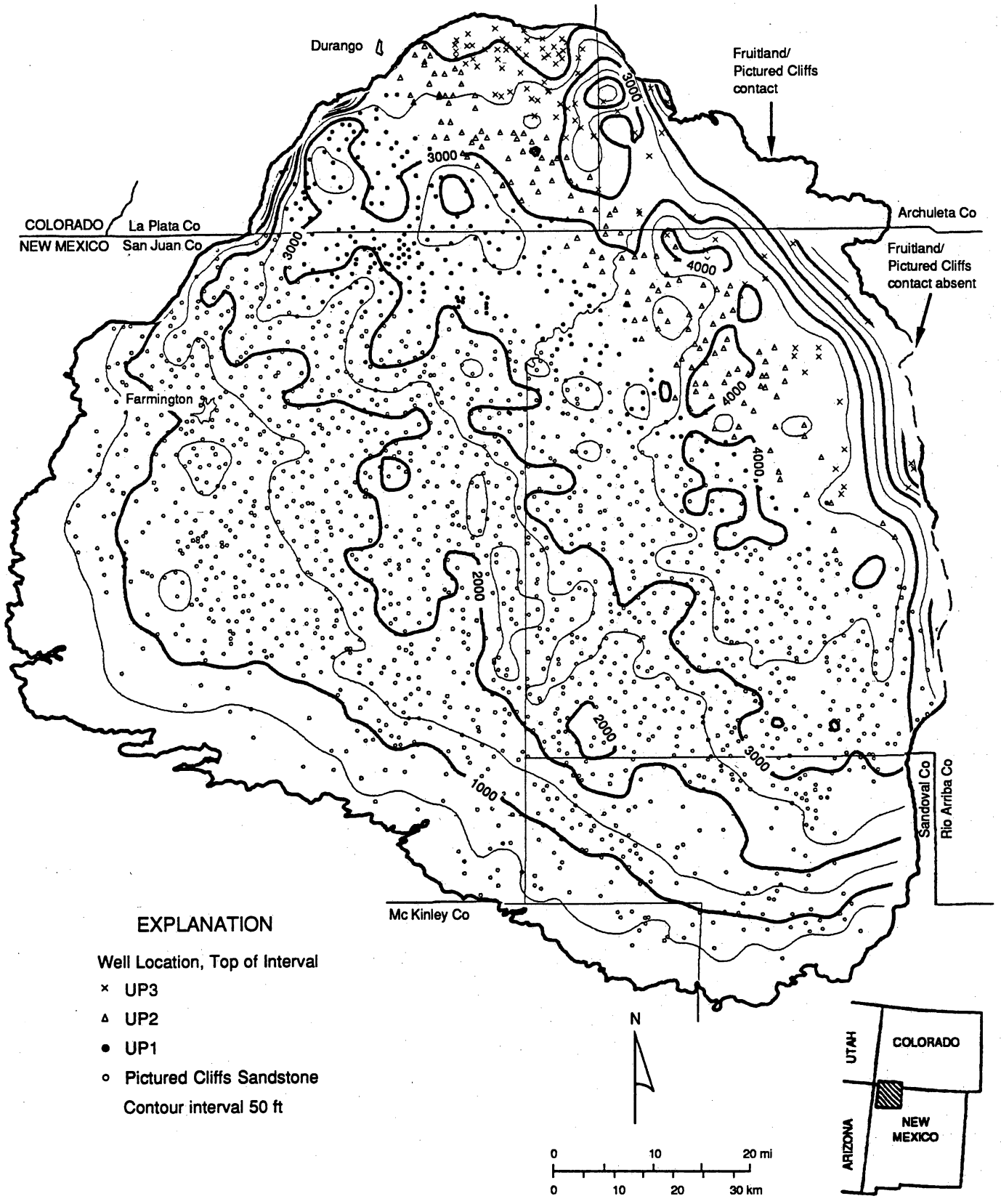

Figure 24. Coal-overburden map, defined as the depth to the top of the Pictured Cliffs Sandstone or the uppermost Pictured Cliffs tongue.

seams and the drilling depth required to evaluate all Fruitland coal seams. Depth to the top of the Pictured Cliffs reflects present topographic relief, basin structure, and stratigraphic rise of Pictured Cliffs tongues. Overburden is thickest in the east part of the basin, in a north-northwest trending area. Fruitland coal seams in the San Juan Basin are as deep as 4,200 ft. However, overburden thickness (present burial depth) does not relate to greatest coal rank (Kelso and others, 1988). Eastward thinning of the Huerfanito Bentonite–Ojo Alamo Sandstone interval (fig. 20) suggests lesser burial depths in the eastern part of the basin. Therefore, Fruitland coal seams on the east side of the basin are inferred to be lower rank. Coal seams are absent near the east margin of the basin because the Fruitland Formation is truncated.

Coal Distribution

Coal data from geophysical well logs were used to make a series of coal maps. Our goals were to determine the distribution, thickness, and trends of Fruitland coal seams, which are both source rocks and reservoirs for coalbed methane in the San Juan Basin.

To evaluate the occurrence of coal and coalbed methane, we mapped net-, maximum-, and average-coal thickness, and number of coal seams in the Fruitland Formation. These maps were compared to identify trends of persistent coal occurrence. These trends are summarized in figure 25. Thick Fruitland coal seams occur in several major northwest-trending, strike-parallel belts (fig. 25, belts A through G) and in minor northeast-trending, dip-elongate belts (fig. 25, belts 1 through 3). Fruitland coal and coalbed methane are concentrated northeast of the hinge line, as is discussed in a later section (Geologic Controls on Coal Occurrence).

Net-Coal Thickness

Net thickness of Fruitland coal seams in the San Juan Basin is as much as 110 ft. The greatest net-coal thickness occurs in a northwest-trending belt in the northeastern half of the

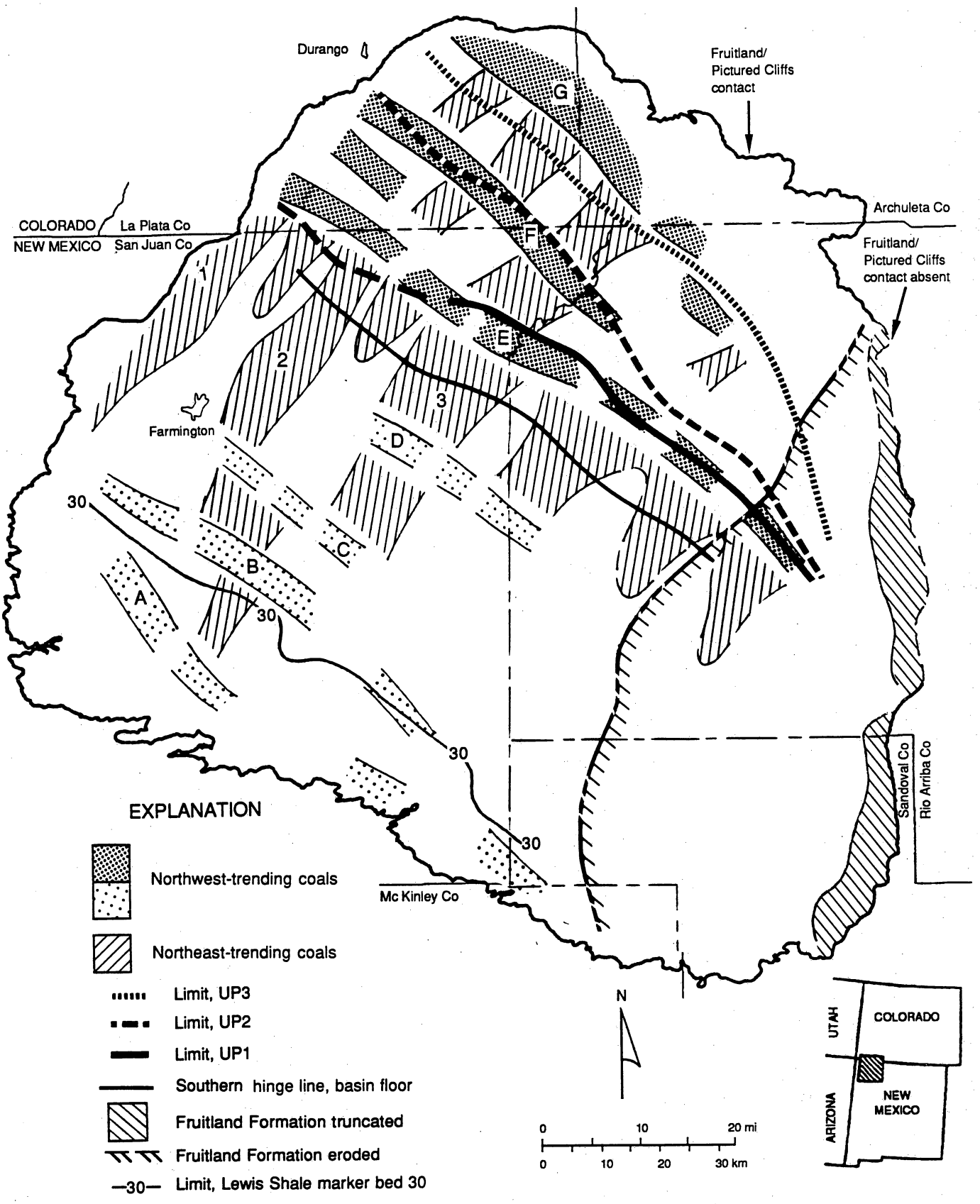

Figure 25. Major coal-occurrence trends in the Fruitland Formation, summarizing figs. 26 through 29. Thickest coal seams occur northeast of the structural hingeline, and they parallel northwest-trending upper Pictured Cliffs tongues, UP1, UP2, and UP3. Southwest of the hinge line, anomalously thick coal either strikes northwest and parallels minor Pictured Cliffs shorelines buildups (such as indicated by Lewis Shale marker bed 30, which is shown in fig. 5), or it trends northeast and lies between Fruitland fluvial systems.

basin where net-coal thickness exceeds 50 ft (fig. 26); this complex belt, which encompasses belts E and F in figure 25, is about 50 mi wide in the northwest and narrows southeastward, terminating about 12 mi from the eastern margin of the basin. This boundary is partly due to erosional beveling of the Fruitland Formation and truncation of coal seams (figs. 5 and 26) by the post-Cretaceous unconformity.

The major northwest-trending region of thick coal was described in earlier regional maps (Fassett and Hinds, 1971; Kelso and others, 1987). However these earlier studies used less data and showed fewer secondary coal trends. For example, these studies did not show the presence of numerous dip-elongate belts of coal 1 to 8 mi wide and 30 to 70 ft thick that extend southwestward from the main northwest-trending belt of 50 to 100 ft of net coal to the Fruitland outcrop at the southwest margin of the basin (fig. 26).

Maximum-Coal Thickness

The maximum-coal map (fig. 27) was made by contouring the thickest Fruitland coal seam recorded in each well, regardless of its stratigraphic position. Therefore, it does not record an individual seam across the basin. However, individual thick seams are mapped locally.

Maximum Fruitland coal-seam thickness is as much as 40 ft. Coal seams greater than 20 ft thick occur primarily in northwest-trending belts (fig. 27) that coincide with trends of greatest net-coal thickness (fig. 26). Within these strike-elongate belts, the thickest individual coal seams (1) are more than 30 ft thick, (2) have podlike geometries, and (3) are 2 to 8 mi across. A northwest-trending belt of coal more than 30 ft thick occurs in the northern third of the basin (fig. 27; belts E and F in fig. 25). A second northwest-trending belt of thick coal occurs near the northeast margin of the basin (fig. 27; belt G in fig. 25). Less prominent northwest-trending belts of thick coal occur at the southwest margin of the basin (fig. 27; belts A and B in fig. 25). Northeast-trending, dip-elongate belts, in which the maximum-coal is greater than 10 ft thick, intersect the northwest-trending coal belts (fig. 27; belts 1, 2, and 3 in fig. 25). An earlier

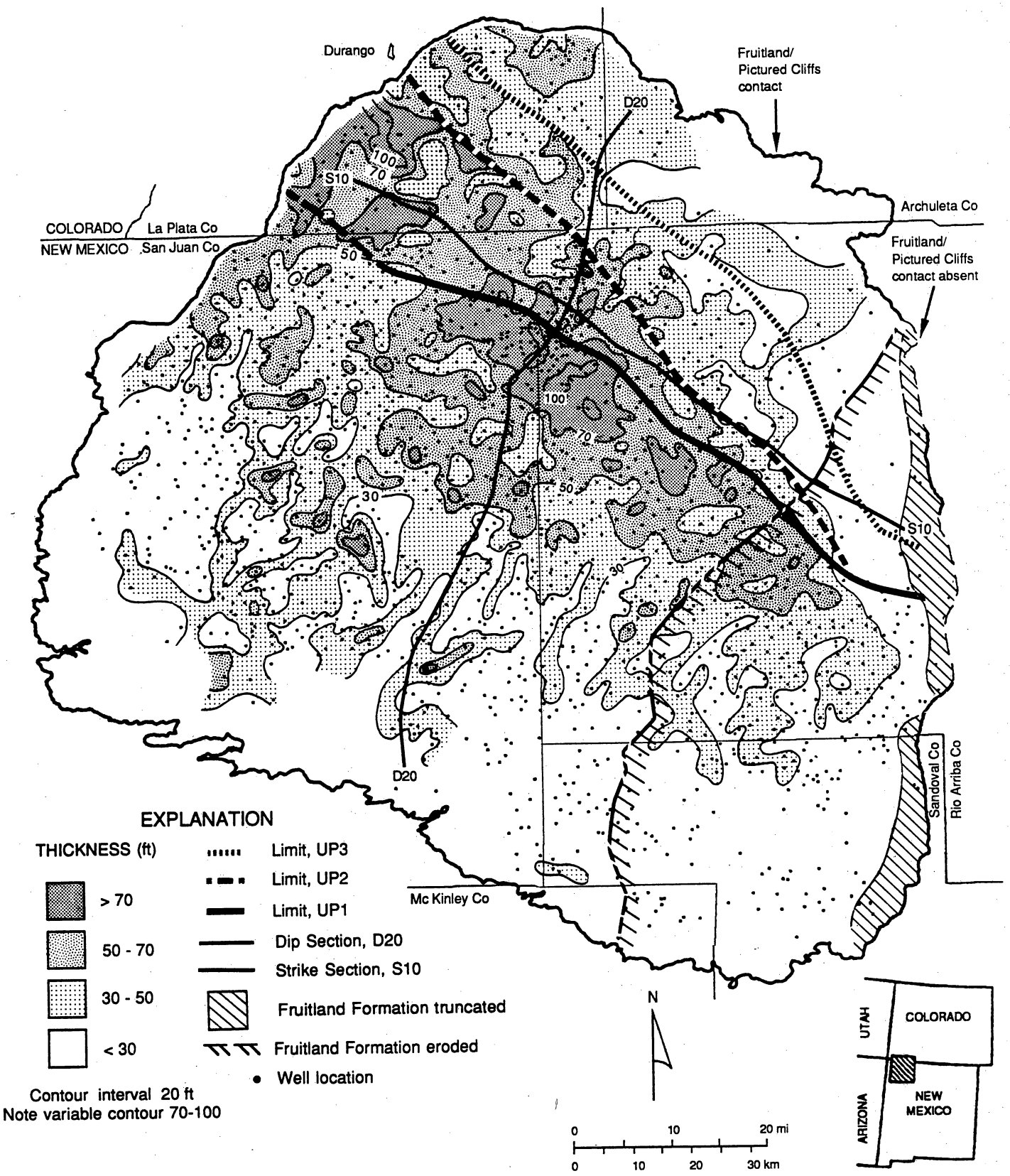

Figure 26. Fruitland net-coal map. Greatest net-coal thickness occurs in a northwest-trending belt in the north-central part of the basin. From this belt, complex dip-oriented net-coal patterns trend southwestward and are inferred to be associated with Fruitland floodplain deposits. Cross sections D20 and S10 are shown in figures 4 and 5, respectively.

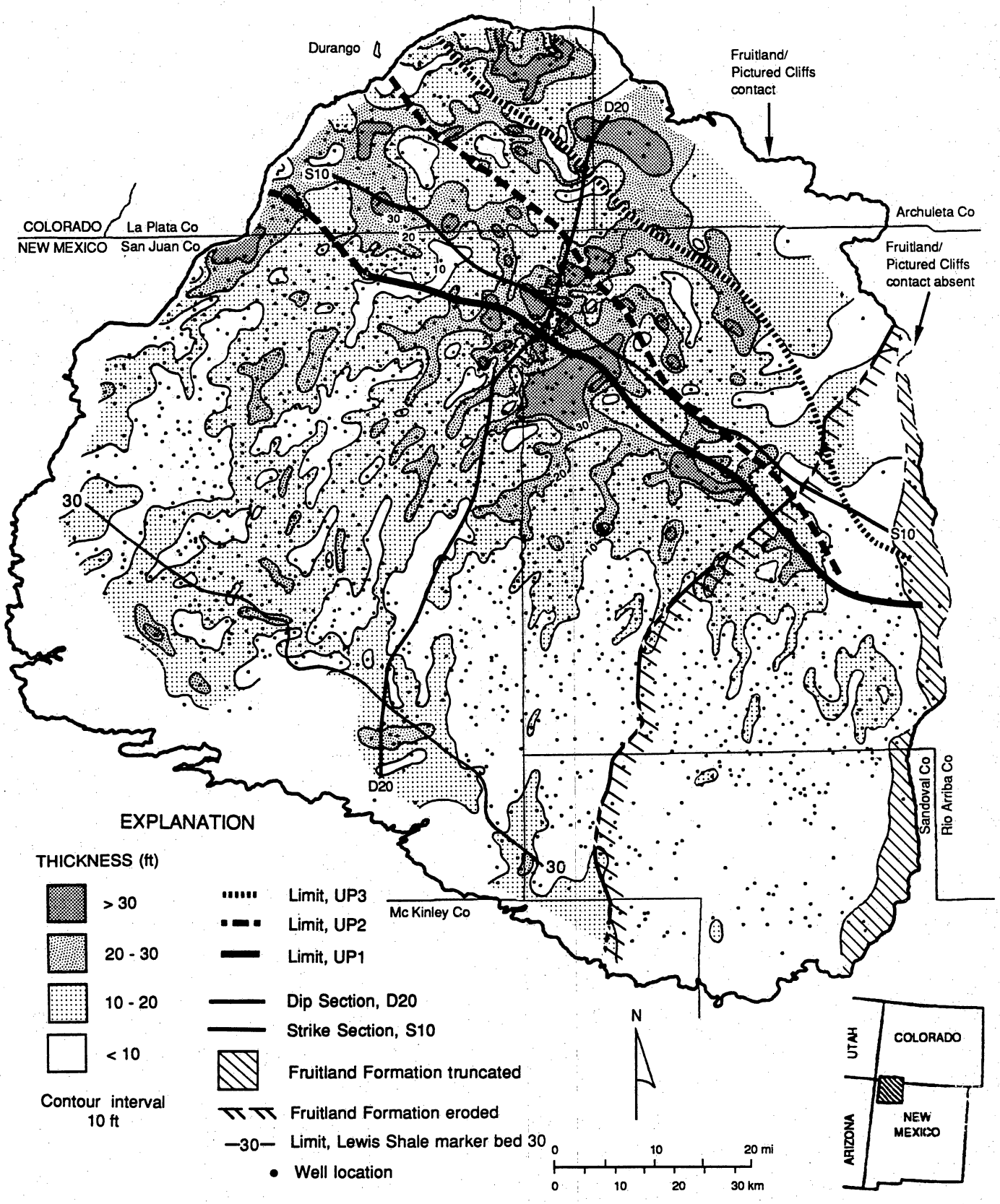

Figure 27. Fruitland maximum-coal map. The strike-elongate trend of thick maximum coal in the extreme southwest part of the basin is genetically related to the 30 marker bed (see figs. 3 through 5). Regional trends of maximum-coal thickness are correlated with coalbed methane productivity (fig. 66). Cross sections D20 and S10 are shown in figures 4 and 5, respectively.

regional maximum-coal map (Fassett and Hinds, 1971, their fig. 22), which was made with fewer data, shows the major northwest-trending belts of maximum coal but little evidence of the secondary northeast-trending coal deposits.

Number of Coal Seams

Fruitland coal occurs in 16 seams in the San Juan Basin (fig. 28). Coal seams are most abundant in a 40-mi-wide, northwest-trending belt of six or more coal seams that bisects the basin; seams are most numerous in the northwestern half of this trend. Generally, areas with the greatest numbers of coal seams (more than nine) coincide with areas of greatest net-coal thickness (more than 70 ft, fig. 26) and with the thickest individual seams (those more than 30 ft thick, fig. 27).

Average-Coal Thickness

The map of average coal thickness (fig. 29) clearly delineates coal occurrences and geometries. In the northern half of the San Juan Basin, three distinct belts of northwest-trending, thick coal are defined by areas where average coal thickness exceeds 9 ft (fig. 29; belts E, F, and G in fig. 25). The northernmost belt (fig. 25, belt G) of thick coal is better defined in this map than in other coal maps; although there are few coal seams in this area (fig. 29), individual seams commonly are greater than 30 ft thick (fig. 28). Belts A and B coincide with the northeast-trending belts of high values of net-coal thickness (fig. 26). In the southwest part of the basin, there are three strike-elongate belts in which the average coal seam is more than 6 ft thick (fig. 29; belts A, B, and C in fig. 25). Several dip-oriented belts occur in which the coal seam thickness is greater than 6 ft (fig. 29; belts 1, 2, and 3 in fig. 25). These northeast-trending belts are common in the southwestern part of the basin.

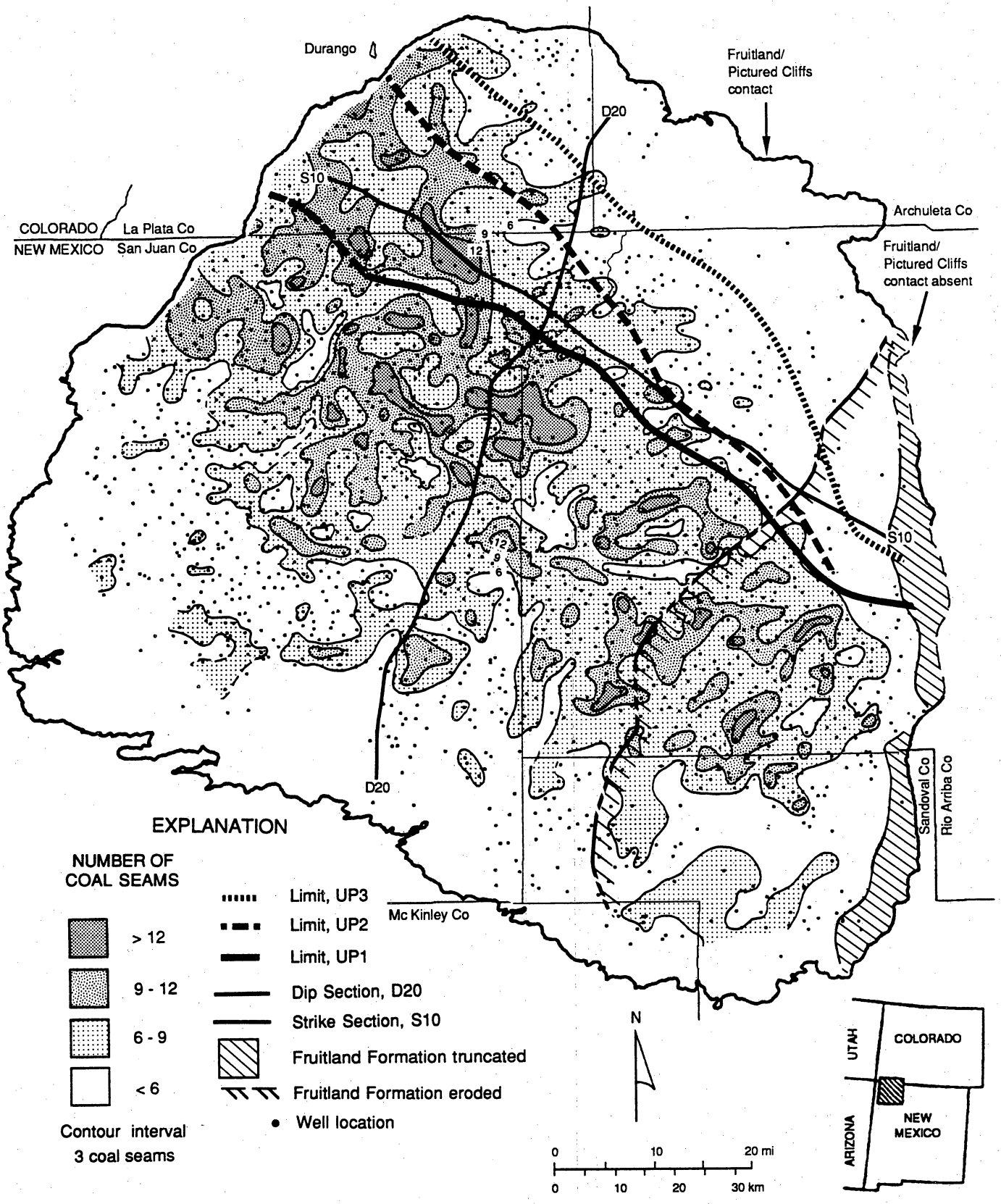

Figure 28. Fruitland coal-isopleth map. Coal seams are most numerous in a broad, strike-elongate belt in the central part of the basin; this belt is landward (southwest) of UP1, UP2, and UP3 shorelines. Cross sections D20 and S10 are shown in figures 4 and 5, respectively.

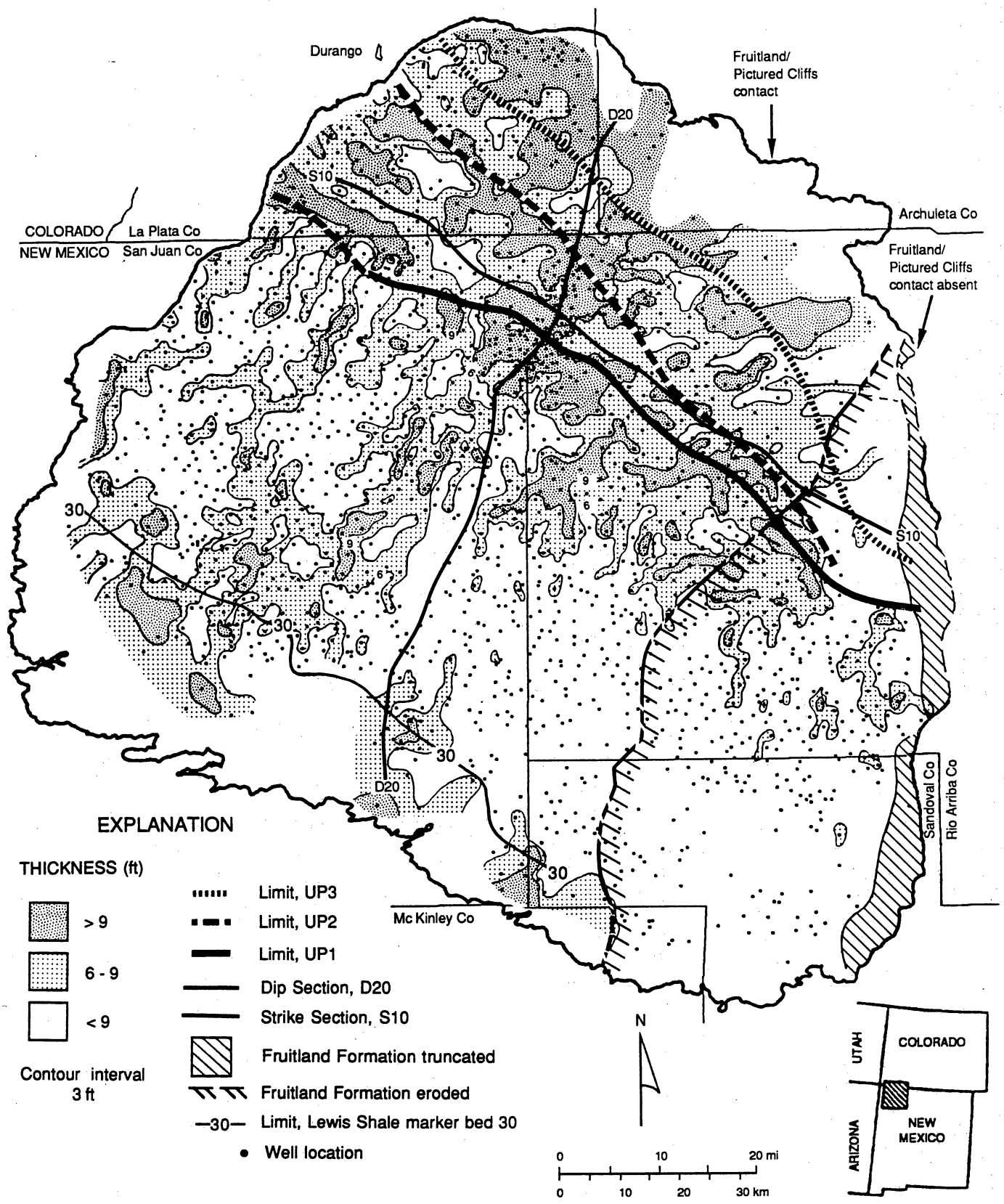

Figure 29. Fruitland average-coal-thickness map. Trends of coal occurrence are similar to those in other Fruitland-coal maps. Strike-elongate trends are well developed landward (southwest) of UP1, UP2, and UP3. Cross sections D20 and S10 are shown in figures 4 and 5, respectively.

GEOLOGIC CONTROLS ON OCCURRENCE OF COAL SEAMS

Previous Studies

Coal seams are facies or subsets of genetically related sedimentary units called depositional systems (Fisher and others, 1969). The depositional system controls the occurrence, trend, and thickness and greatly influences the quality of coal (McGowen, 1968; Horne and others, 1978; Kaiser and others, 1978; Donaldson and others, 1979; Houseknecht and Iannacchione, 1982). Therefore, the relations between depositional systems and coal occurrence, determined from maps and cross sections, are predictive and are a useful tool in coalbed methane exploration.

Pictured Cliffs and Fruitland sandstones are the depositional framework facies that control the occurrence, trend, and thickness of Fruitland coal seams. Previous studies of the depositional setting the Pictured Cliff Sandstone and Fruitland Formation and other coal-bearing and coal-bounding strata in the San Juan Basin (Sears and others, 1941; Scruton, 1961; Fassett and Hinds, 1971; Erpenbeck, 1979; Flores and Erpenbeck, 1981; Devine, 1980; Kelso and others, 1980; Cumella, 1981; Palmer and Scott, 1984; Wright, 1986) were reviewed in Ayers and Zellers (1988). Wave-dominated coastal processes and resulting wave-dominated deltas and barrier/strandplain systems have long been suggested for the Pictured Cliffs and earlier coastal units in the basin. However, "fluvial-influenced" deltas flanked by barrier-strandplains were described for the Pictured Cliffs in the southwestern quarter of the basin by Flores and Erpenbeck (1981, p. 33) and Erpenbeck (1979, p. 67), who suggested that Fruitland coal seams occur in two depositional settings. The thickest coal seams are in the lower Fruitland, and they are dip-elongate seams flanked by distributary channel-fill sandstones. They concluded that Fruitland back-barrier coal seams are thinner and contain abundant carbonaceous shale.

The thinness of Fruitland fluvial sandstone complexes and their poor definition on lithofacies maps (Ayers and Zellers, 1988) suggest that fluvial systems within the north-central

part of the basin were minor and of insufficient size to form fluvially dominated deltas where they debouched into the Western Interior Seaway. This conclusion is supported by linear geometry of the Pictured Cliffs shoreline sandstone tongues that suggest a wave-dominated coastline.

The depositional setting of Fruitland coal seams in the pilot study (Ayers and Zellers, 1988) of an area in the north-central San Juan Basin was established from coal-seam geometry and distribution and from the relations between the coal seams and the Pictured Cliffs and Fruitland depositional framework facies, as defined in cross sections and net-sandstone maps. Coal is thickest and seams are most numerous landward of upper Pictured Cliffs tongues (fig. 30). These relationships suggest that thick coal formed in persistent and recurring swamp environments landward of the upper Pictured Cliffs barrier shorelines. Palynologic studies (Manfrino, 1984) and the low sulfur content of Fruitland coal seams indicate peat accumulation in a fresh-water setting that was isolated from marine influence, suggesting that peat accumulation occurred inland behind abandoned and foundering shoreline deposits. From cross sections and maps made in this regional study and the previous detailed study we conclude that syndepositional tectonic activity controlled the depositional system and, indirectly, the occurrence of thick Fruitland coal (fig. 30). Pulsatory differential subsidence across the hinge-line at the southwest margin of the basin floor (figs. 4 and 13) caused a relative sea-level rise, which resulted in stillstands of the Pictured Cliffs shoreline (UP1, UP2, and UP3). These stillstands allowed ample time for peat (coal) to aggrade and to overspread abandoned shoreline- and fluvial-sandstone complexes. Hence, the greatest concentrations of coal resources occur in northwest-trending belts, north of the hingeline.

Relations between Depositional Systems and Coal Occurrence

Northwest-trending belts of thick Fruitland coal (figs. 25 through 29) are related to Pictured Cliffs shoreline positions. Coal in belts A and B (fig. 25) is the oldest Fruitland coal in

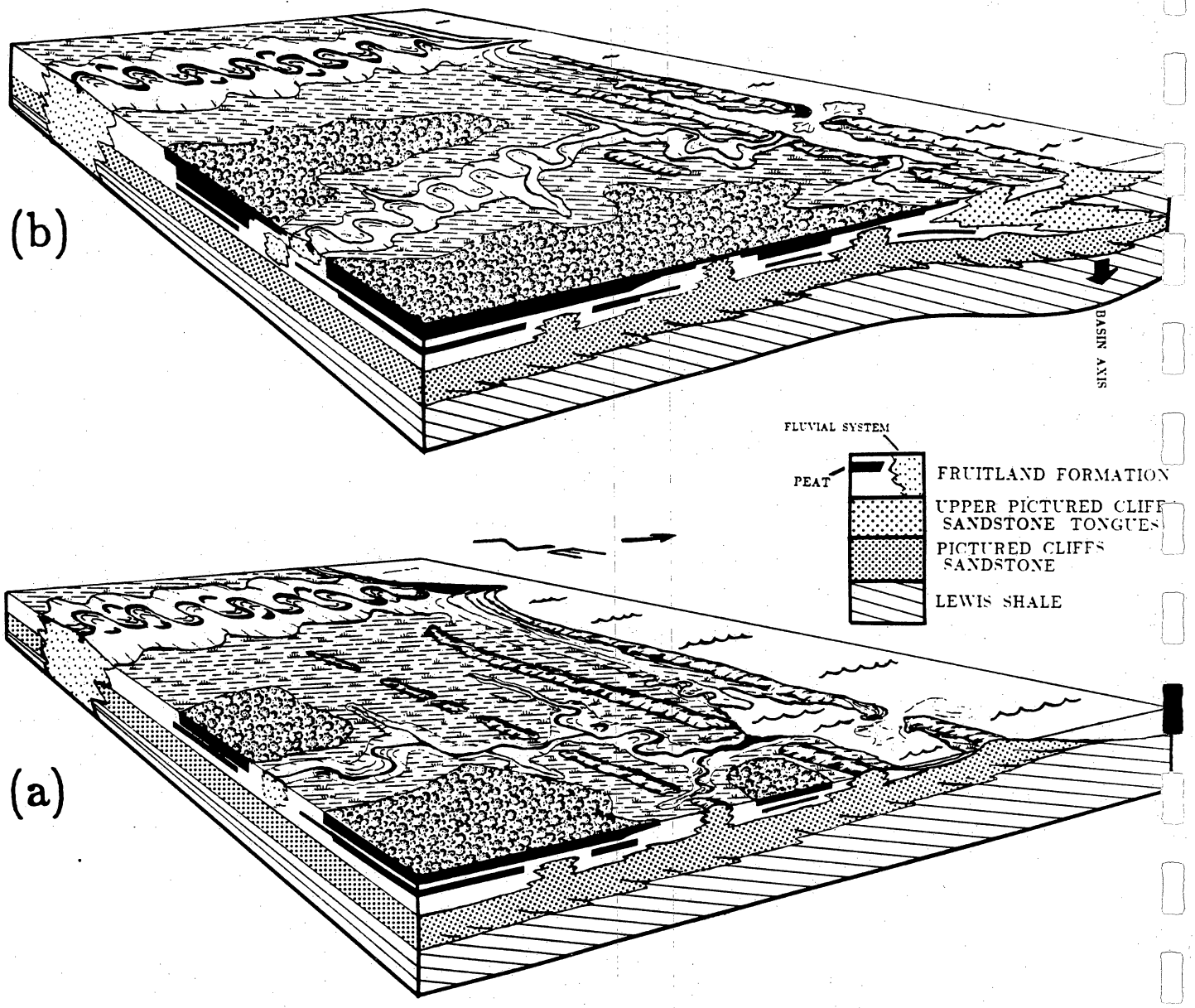

Figure 30. Depositional model of Fruitland coal seams in the detailed study area. (a) Peat is deposited behind, and overrides, abandoned and foundered Pictured Cliffs shoreline sandstones that occur inland and downdrift of a postulated wave-dominated delta. Area is crossed only by minor fluvial feeders that shift periodically. (b) Intermittent subsidence along basin axis temporarily halts regression, causing a shoreline stillstand and allowing accumulation of thick, extensive peat deposits. Not to scale. From Ayers and Zellers (1988).

the basin and formed behind a shoreline associated with initial Pictured Cliffs shoreline progradation; in contrast, belt G contains the youngest Fruitland coal, formed as the Pictured Cliffs shoreline prograded beyond the northern margin of the present San Juan Basin.

The initial Pictured Cliffs shoreline progradation reached a limit in the southern part of the basin marked by the updip pinch-out of the 30 marker bed (figs. 4 and 25). The 30 marker occurs in a high-conductivity shale that was deposited during a minor transgression over an early Pictured Cliffs progradational wedge. Individual coal seams as much as 30 ft thick and net coal as much as 50 ft thick locally occur along the retrogradational Pictured Cliffs shoreline defined by the updip limit of the 30 marker (figs. 26 and 27). Following the transgression associated with the 30 marker, the Pictured Cliffs shoreline prograded rapidly to the north-central third of the San Juan Basin. As the Pictured Cliffs shoreline advanced basinward, relatively thin peats (coal seams less than 20 ft thick; fig. 27) formed in floodplains between northeast-flowing Fruitland rivers that supplied sediment to the prograding Pictured Cliffs shoreline. This northeast-trending system of interfluvial coal seams was superimposed on the northwest-trending belts of shoreline-related coal seams as the Pictured Cliffs shoreline prograded toward the northeast. Areas that were occupied by inferred Fruitland rivers correspond to areas of low values of net, and maximum, and average coal-seam thickness (figs. 26, 27, and 29); in contrast, interfluvial areas correspond to narrow (1- to 8-mi-wide), dip-elongate pods of relatively thick coal. In the southwest part of the basin, a wide band of thick coal (figs. 26, 27, and 29; belts 1, 2, and 3, fig. 25) formed in a relatively stable part of the coastal plain that was not occupied by major Fruitland fluvial systems.

The thickest and most laterally continuous Fruitland coal seams were deposited in back-barrier settings corresponding to the northwest-trending belts, E, F, and G (fig. 25). These belts of thick coal are landward (southwest) of pinch-out lines of upper Pictured Cliffs tongues that were deposited during during periods of shoreline stillstand and/or marine transgression (retrogradation). Two minor, discontinuous belts of northwest-trending coal (fig. 25, belts C and

D) also were deposited during short-lived Pictured Cliffs shoreline stillstands associated with deposition of transgressive shales represented by the 35 and 38 marker beds (figs. 4 and 5).

As much as 100 ft of coal locally occurs landward of UP1, the oldest upper Pictured Cliffs tongue (fig. 26). This is the thickest belt (fig. 25, belt E) of Fruitland coal in the basin, which suggests a long period of stability of the Pictured Cliffs shoreline. This belt of thick coal encompasses Cedar Hill (fig. 9) and "Meridian" 400 (fig. 9, southern part of detailed study area) areas, two of the most productive Fruitland coalbed methane areas in the basin.

Downdip (southeast) of coal belt E, the number of coal seams (fig. 28) and the net-coal thickness (fig. 26) decrease as the Fruitland Formation thins at the expense of the Pictured Cliffs tongues, UP1 and UP2 (figs. 4 and 19); commonly, net-coal thickness is less than 70 ft landward of UP2 and 50 ft thick landward of UP3. However, net-coal thickness locally exceeds 70 ft near the northern margin of the basin near the Ignacio Anticline (located in fig. 9). These areas of great coal thickness are related to a fourth Pictured Cliffs tongue that prograded beyond the northern limit of the San Juan Basin (fig. 4).

Geologic Controls on Producibility of Coalbed Methane

Locally in the San Juan Basin, Fruitland coal seams are folded due to tectonic activity, and structure maps can indicate areas of fracture-enhanced permeability. In other areas, coal seams may be folded over or under Fruitland channel-fill sandstones or Pictured Cliffs shoreline sandstones because of differential compaction. Such compactional folding of brittle coal beds may cause fractures (Donaldson, 1979; Houseknecht and Iannacchione, 1982) that enhance coalbed permeability. If fracture systems of differential-compaction origin are sufficiently developed, areas of interbedded sandstones and coal seams would be good targets for coalbed methane exploration (fig. 31).

Earlier workers concluded that Fruitland coal seams have limited extent and that they are bounded on their basinward (northeast) margins by Pictured Cliffs shoreline sandstone and

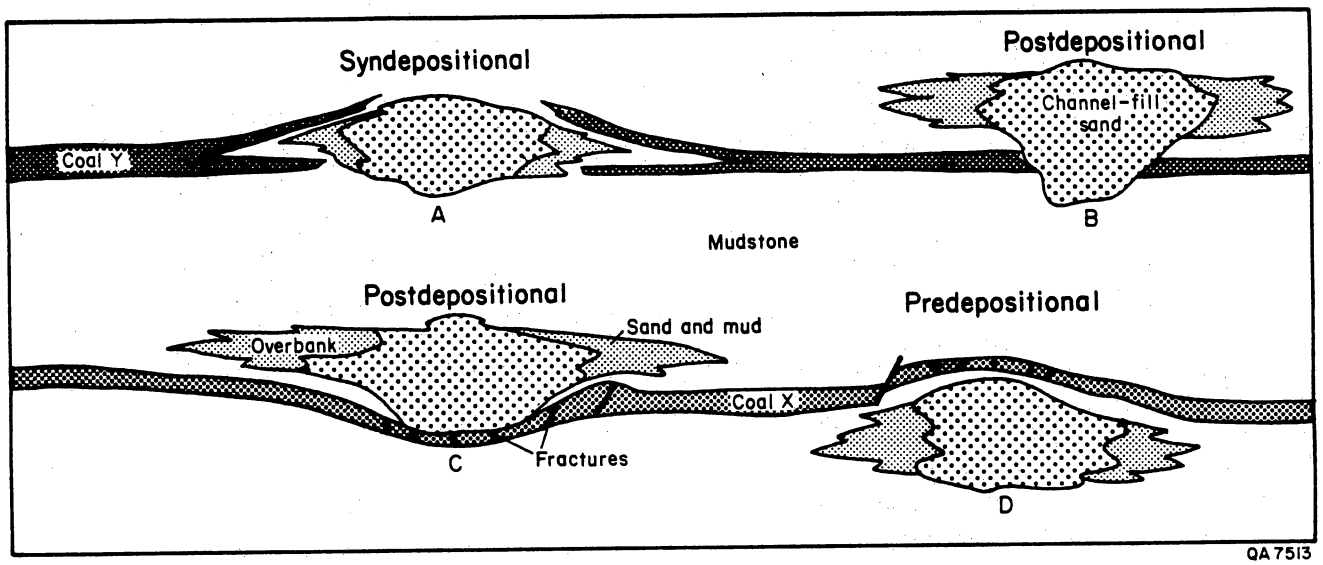

Figure 31. Relations between sedimentary depositional facies and coal seams. Coal seam Y splits and pinches out at interface with channel-fill sandstone, A; seam Y was removed postdepositionally by channel B. Coal seam X is folded and fractured under postdepositional channel-fill sandstone, C, and over channel-fill sandstone, D (from Ayers and Zellers, 1989; concepts from Donaldson, 1979).

along paleostrike (northwest-southeast) by Fruitland fluvial sandstones (Fassett and Hinds, 1971; Fassett, 1986). However, some Fruitland coal seams may be regionally continuous, overriding and thinning over the top of the Pictured Cliffs Sandstone and Pictured Cliffs tongues with continued progradation. This implies that many Fruitland coal seams may be time-transgressive, and it conflicts with the previous interpretation that Fruitland coal beds are "...essentially time-equivalent throughout their extent," (Fassett, 1988, p. 35). Results of this study suggest that, at least in one area of the San Juan Basin (fig. 32), some thick Fruitland coal seams override an upper Pictured Cliffs tongue (UP1, figs. 4 and 33) in the paleodip direction. Updip pinch-out lines of upper Pictured Cliffs tongues may be areas where Fruitland coal seams drape over shoreline sandstones and have compaction-induced fractures. Along paleostrike, coal seams split and interfinger with fluvial channel-fill sandstone complexes (fig. 34), and many of these splits, rather than terminating against the channel sandstones, override or underlie them, forming zig-zag splits much like those described in coal-bearing strata in other basins (Britten and others, 1975; Ayers and Kaiser, 1984). The significance of this complex coal-seam geometry is three-fold: first, coal seams, and hence coalbed methane reservoirs, are more extensive than previous workers suggested; second, compaction-induced fractures and therefore enhanced coalbed permeability may occur in areas where coal seams drape over shoreline sandstones or form zig-zag splits with channel-fill sandstone complexes; finally, the greater lateral extent of coal seams, inferred from this research, is critical to the interpretation of ground-water flow and abnormal pressure in the Fruitland Formation (Kaiser and Swartz, 1988, 1989).

The significance of tectonic and compaction-induced fractures to enhanced permeability in coal seams is uncertain. However, the abundance of folds and their potential contribution to enhanced production justify further study. Evaluations of compaction and tectonic folds, in both subsurface and outcrop studies, will be required for clarification of the relations between folding and fracturing.

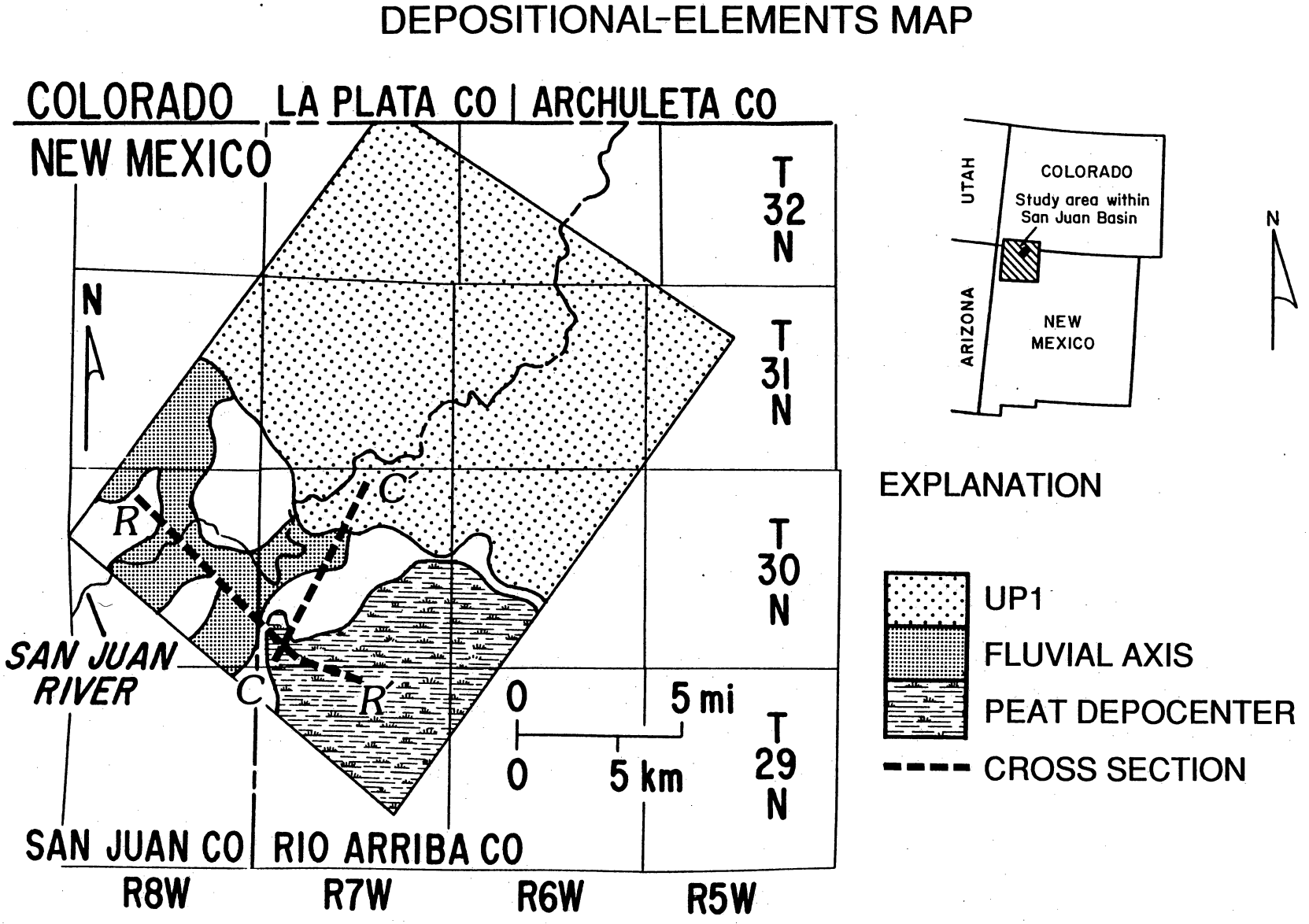

Figure 32. Depositional elements of Fruitland Formation and upper Pictured Cliffs sandstone (UP1) in detailed study area in the northern part of the San Juan Basin. Peat depocenter was developed lateral to Fruitland fluvial depositional axis and landward of the UP1 transgressive shoreline. Detailed study area located in figure 9. Cross sections C-C′ and R-R′ shown in figures 33 and 34, respectively.

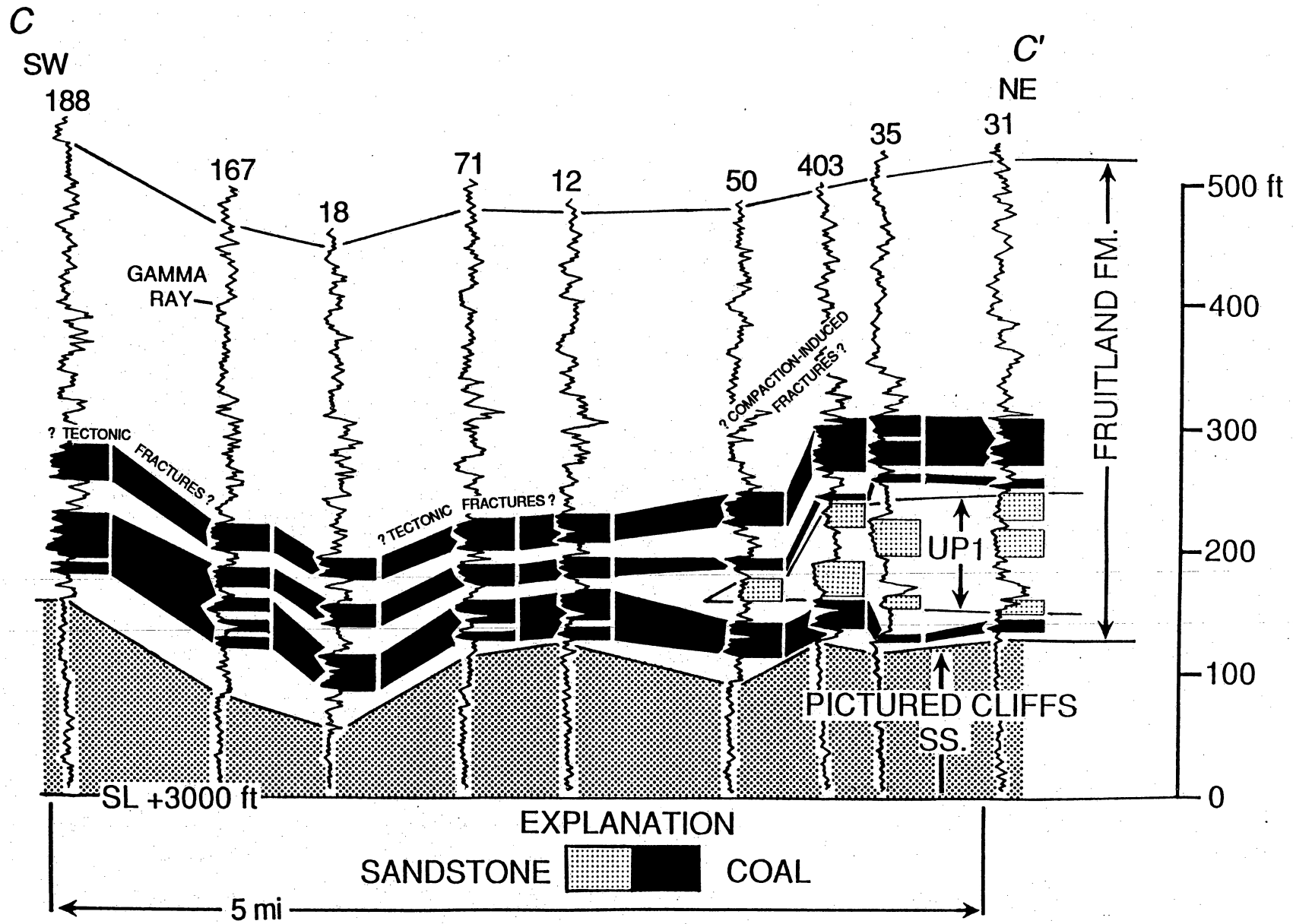

Figure 33. Structural cross section C-C'. Although lower Fruitland coal seams pinch out landward of Pictured Cliffs shoreline sandstones, a thick upper Fruitland coal seam overrides UP1. Fractures may occur in areas of tectonic folding, such as between wells 188 and 71, and in area of compaction-induced folding where coal seams override shoreline sandstones, such as the upper coal, between wells 50 and 403. See figure 32 for location.

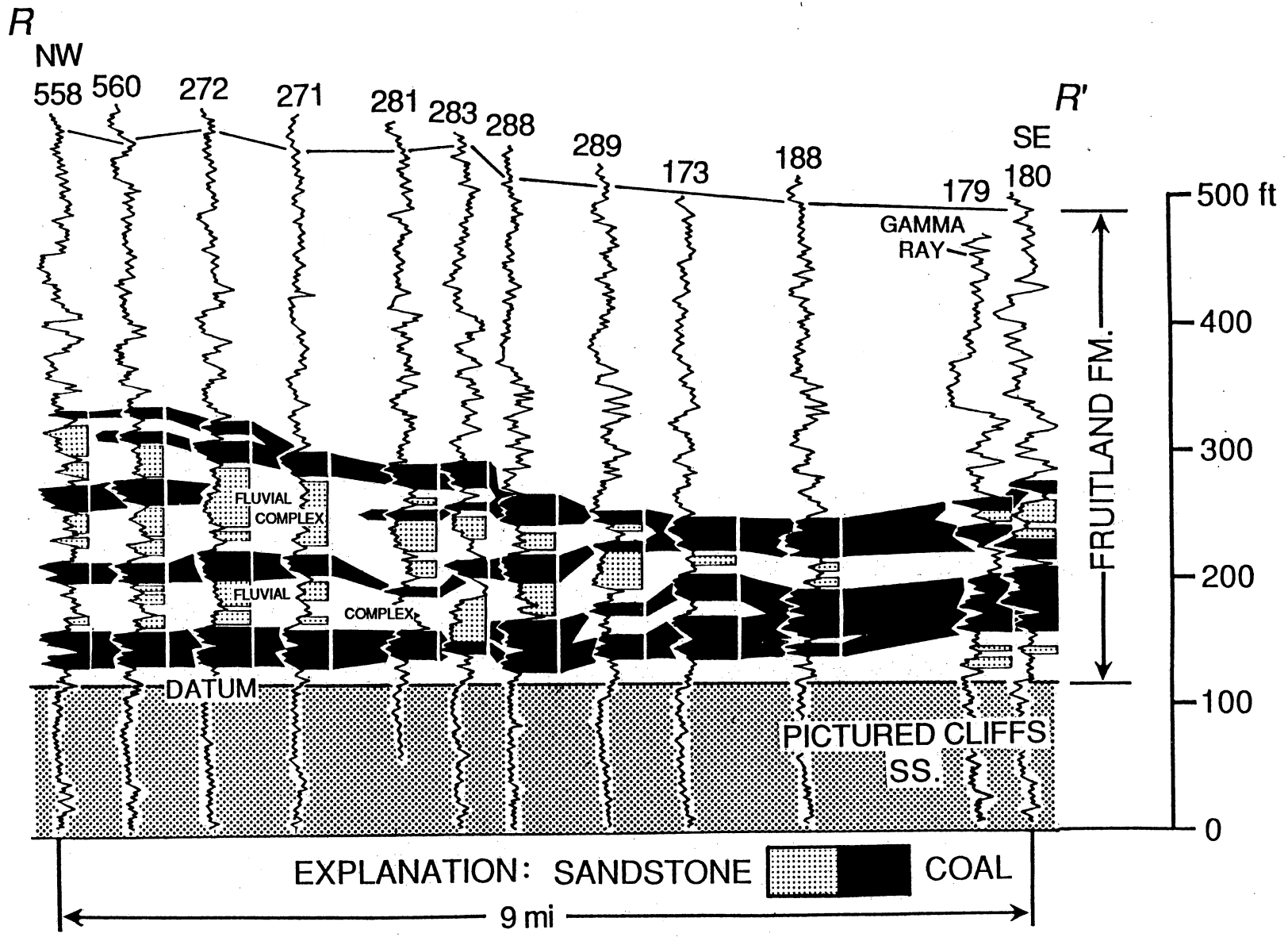

Figure 34. Stratigraphic cross section R-R'. Thick Fruitland coal in well 188 forms zig-zag splits to the southeast and northwest where more compactable peat (coal) interfingers with fluvial complexes (sandstones and mudstones) along paleostrike. These folds may cause fracture-enhanced permeability. Because datum is the top of the Pictured Cliffs Sandstone, structural folding is masked. See figure 32 for location of cross section.

COAL AND COALBED METHANE RESOURCES

In this study, we calculated coal and coalbed methane resources only in Fruitland coal seams deeper than 400 ft deep. Coal resources in the Fruitland Formation were calculated to be 245 billion short tons. This estimate is 11 percent greater than that of Kelso and others (1988; 219 billion short tons), and it is 23 percent greater than that of Fassett and Hinds (1971; 200 billion short tons). Coalbed methane in place was calculated to be 43 to 49 Tcf, which is 2 to 14 percent less than reported by Kelso and others (1988; 50 Tcf) but is 39 to 58 percent greater than the estimate by Choate and others (1984; 31 Tcf).

The large data base (1,731 well logs) used in the present study resulted in better definition of coal occurrences and trends and in a larger coal resource estimate than in previous studies. Fassett and Hinds (1971) used data from approximately 325 well logs to calculate Fruitland coal resources; the coalbed-methane-resource estimate of Choate and others (1984) was based on Fassett and Hinds' (1971) coal-resource estimate. Kelso and others (1988) used 549 well logs to calculate coal and coalbed methane resources.

Although coal resources estimated in this study are 11 percent greater than those estimated by Kelso and others (1988), the in-place gas in Fruitland coal seams estimated in this study is 2 to 14 percent less than that of Kelso and others (1988). Differences between the coalbed methane estimates stem from differences in the methods of calculation and assumed ash content of coal seams. Kelso and others (1988) calculated coalbed methane resources on the basis of average coalbed thickness, rank, depth, and gas content in each township; the total resource is the sum of the resources in individual townships. To account for the reduced gas content of the coal due to presence of inorganic material (commonly referred to as ash) in coal seams, Kelso and others assumed that the ash values (10 to 36 percent) mapped by Fassett and Hinds (1971, their fig. 24) reflected regional trends common in all Fruitland coal seams (B. Kelso, personal communication, 1989). In the present study, resources were computer-

calculated on a well-by-well basis using coal thickness and depth data recorded from well logs. Values for gas content and coal density were those used by Kelso and others (1988). Rather than assume that the ash content of one coal sample was representative of all Fruitland coal seams at that locality, in this study we used average ash contents of 20 percent and 30 percent to calculate 49 Tcf and 43 Tcf, respectively, of methane in Fruitland coal seams.

Gas-in-place in Fruitland coal seams locally exceeds 35 Bcf/mi^2 in the north-central part of the basin (fig. 35). In-place gas, although influenced by coal rank and present depth, predominantly is controlled by coal thickness. Gas contents greater than 35 Bcf/mi^2 (fig. 35) generally coincide with northwest-trending areas where net-coal thickness exceeds 70 ft (fig. 26) and maximum-coal thickness exceeds 20 ft (fig. 27); the 10-Bcf/mi^2 contour (fig. 35) generally coincides with the 50-ft net-coal thickness contour (fig. 26).

CONCLUSIONS

1. Geologic factors that affected the occurrence and producibility of coalbed methane in the San Juan Basin were tectonic controls on sedimentation, depositional controls on coal occurrence and geometry, and structural controls on the permeability of coal seams.

2. Pictured Cliffs shoreline sandstones accumulated in northwest-trending barrier/strandplains. The retrogradations recorded in upper Pictured Cliffs tongues were partly due to differential basin subsidence; UP1 pinches out northeast of, and parallel to, a structural hingeline that separates the northeast-dipping monocline of the southern half of the basin from the low-relief basin floor.

3. The thickest and most continuous coal seams in the Fruitland Formation occur in the northwestern part of the basin and are associated with these retrogradational upper Pictured Cliffs tongues. These coal deposits occur in three northwest-trending belts that are updip (southwest) of and parallel to these upper Pictured Cliffs shoreline sandstones. Other

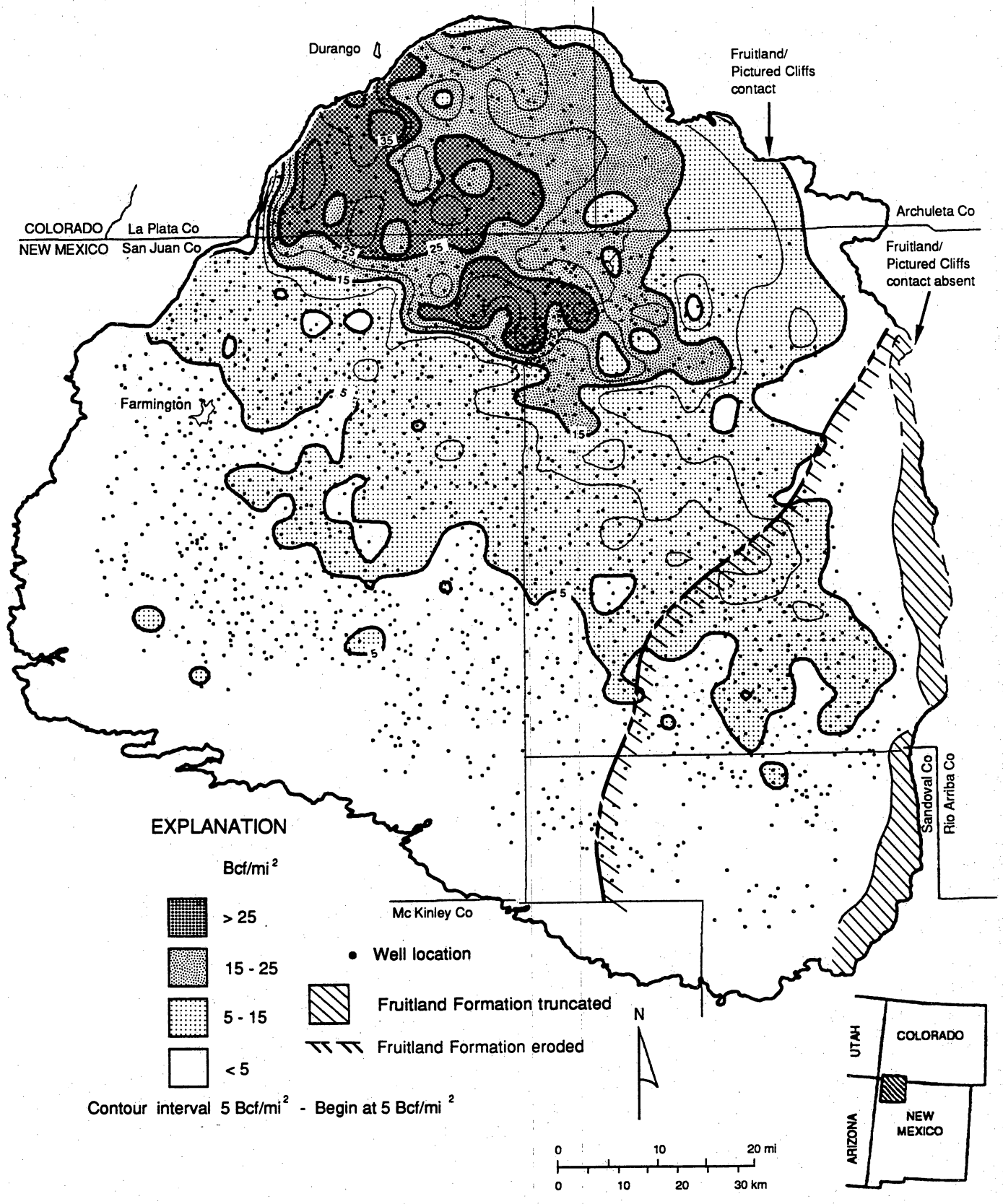

Figure 35. Gas-in-place map for Fruitland Formation coal seams, calculated on the basis of 20 percent average ash content in coal. High values of in-place gas occur in the west-central part of the San Juan Basin and reflect the presence of thick coal seams, high coal rank, and high formation pressure.

northwest-trending belts of thick Fruitland coal seams in the southern part of the basin are genetically related to older, minor Pictured Cliffs transgressions.

4. Coal seams commonly override sandstones to extend tens of miles in either the paleodip or the paleostrike direction.

5. Dip-elongate belts of thick Fruitland coal seams project landward (southwestward) from the northwest-trending belts of thick coal and are inferred to have formed in a floodplain setting.

6. The northeast-trending belts of Fruitland coal were identified and the geometry of the northwest-trending belts of thick coal were better defined in this study because regional maps were made using more data (12 to 15 well logs per township) than were used in earlier studies (2 to 5 wells per township).

7. The northwest-trending belts of thick coal crop out along the northwest margin of the basin where they may receive or discharge fluids; hydrologic maps suggest that these Fruitland coal seams are major aquifers that are regionally overpressured due to the elevated recharge area and coal-seam pinch-out (Kaiser and Swartz, 1988, 1989). The dip-elongate coal seams that extend southwestward are poorly connected to the overpressured coal seams.

8. Coal and coalbed methane resources in the Fruitland Formation are 245 billion short tons and 43 to 49 Tcf, respectively, at depths of 400 ft or more. These resources are most abundant in the northwestern part of the basin, where Fruitland gas-in-place may exceed 35 Bcf/mi^2.

9. Targets for increased coalbed methane production due to fracture-enhanced permeability may exist along minor tectonic folds such as those developed along the Hogback Monocline or at the margin of the basin floor. Potential targets for enhanced permeability due to compaction-induced fractures occur where Fruitland coal seams drape Pictured Cliffs and Fruitland sandstones.

10. The Fruitland Formation thins eastward in the southeastern part of the San Juan Basin due to syndepositional uplift. Coal seams are thinner and fewer in that area. Postdepositional

uplift of the southeastern part of the basin caused pre-Ojo Alamo erosion that beveled the Fruitland Formation, truncating coal seams near the eastern margin of the basin.

NATURAL FRACTURE (CLEAT AND JOINT) CHARACTERISTICS AND PATTERNS IN UPPER CRETACEOUS AND TERTIARY ROCKS OF THE SAN JUAN BASIN, NEW MEXICO AND COLORADO

C. M. Tremain and N. H. Whitehead III

INTRODUCTION

This report presents observations of natural fractures (joints and cleats) in coal and sandstone of the Fruitland Formation (Upper Cretaceous) and in adjacent Cretaceous and Tertiary rocks in the San Juan Basin. New data presented here include measurements of cleat and joint orientations from core and outcrop and lineaments from aerial photographs. Cleat is a coal miner's term for closely spaced joints in coal seams. The main or first-formed cleat, based on cross-cutting relationships, is the face cleat. The second-formed and less continuous cleat, which terminates against the face cleat, is the butt cleat. In Fruitland Formation coal beds, there are generally two orthogonal cleat sets.

Successful development of Fruitland coalbed methane reservoirs depends on an understanding of their fracture patterns, as fractures enhance permeability and affect engineering operations. The results of this study also may be applicable to coalbed methane exploration in the Menefee Formation, and to improved design of in-fill drilling programs in Upper and Lower Cretaceous, gas-bearing sandstones in the San Juan Basin (Crist and others, 1989; Hugman and others, 1989).

FRACTURE OCCURRENCE AND PRODUCTION

Fracture-enhanced and fracture-controlled reservoirs account for a significant percentage of the oil and gas production from the San Juan Basin (e.g., Gorham and others, 1979). Fractured reservoirs in the San Juan Basin can be divided into three types based on the presumed origin of the fractures. The first type is the reservoir in which fractures were induced in predominantly layer-confined horizons by overpressuring during the volume increase associated with the transformation of kerogen to oil and gas (Bond, 1984). This type of fractured reservoir occurs in tight sandstone and in the Mancos Shale (Upper Cretaceous) in areas of homoclinal dip; these reservoirs are no longer overpressured. The second type of fractured reservoir occurs in siltstone and calcareous shale that are interbedded with plastic shale of the Mancos Shale. These reservoirs are believed to be fractures along folds in areas of maximum bed curvature (Mallory, 1977; Gorham and others, 1979). Boulder, Puerto Chiquito, and Verde fields are this type of reservoir (Gorham and others, 1979). Finally, the third type of fractured reservoir is the coal seam. In coal seams, cleats form the primary avenues of permeability. Cleat can result from either of the processes described above, or from compaction and coalification.

DESCRIPTION OF NATURAL FRACTURES

For this study, cleat and joint orientations at 22 stations in Colorado (table 1) and 36 stations in New Mexico were measured (table 2). The "selection approach" (Davis, 1984) to fracture mapping was used in which long, planar, consistently oriented (systematic) fractures were measured. Because of the uniformly high dips of the fractures, orientation data were plotted on rose diagrams (figs. 36 and 37). The cleats or joints seldom have slickenside striations or shear offset; they are extension fractures rather than microfaults.

Table 1. Stratigraphic units, age, and number of stations with cleat or joint orientation measurements in Colorado.

Unit	Age	No. of stations
San Jose Formation	Eocene	2
Fruitland sandstones	Late Cretaceous	7
Fruitland coals	Late Cretaceous	11
Pictured Cliffs Sandstone	Late Cretaceous	2

Table 2. Stratigraphic units, age, and number of stations with cleat or joint orientation measurement in New Mexico.

Unit	Age	No. of stations
Regina Member, San Jose Formation	Eocene	3
Cuba Mesa Member, San Jose Formation	Eocene	3
Fruitland sandstones	Late Cretaceous	4
Fruitland coals	Late Cretaceous	16
Pictured Cliffs Sandstone	Late Cretaceous	3
Cliff House Sandstone (undiff.)	Late Cretaceous	3
Uppermost, calcareous sandstone		3
Calcareous "Lower Sand" of Mytton and Schneider (1987)		1

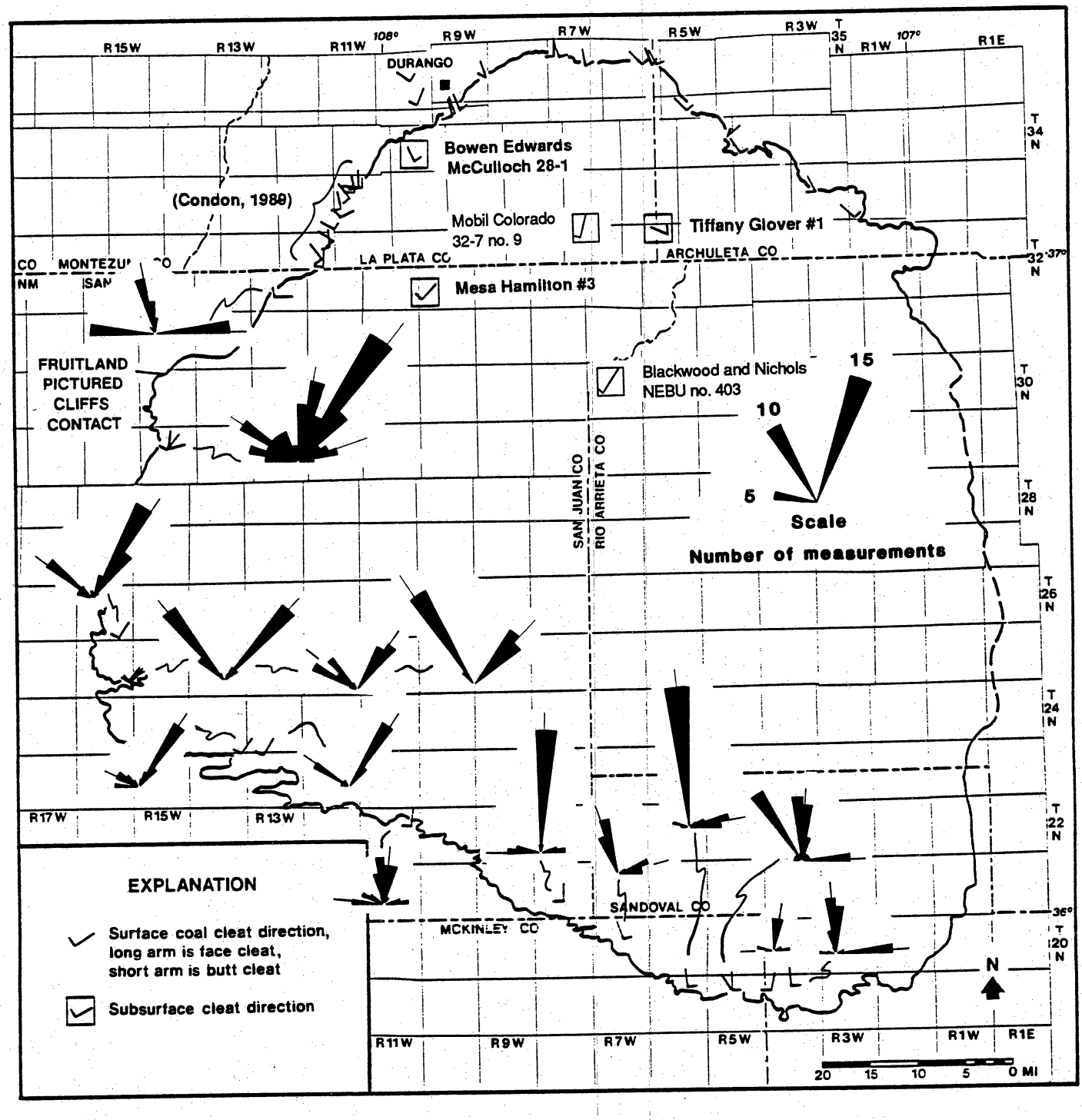

Figure 36. Coal cleat directions and rose diagrams in the San Juan Basin.

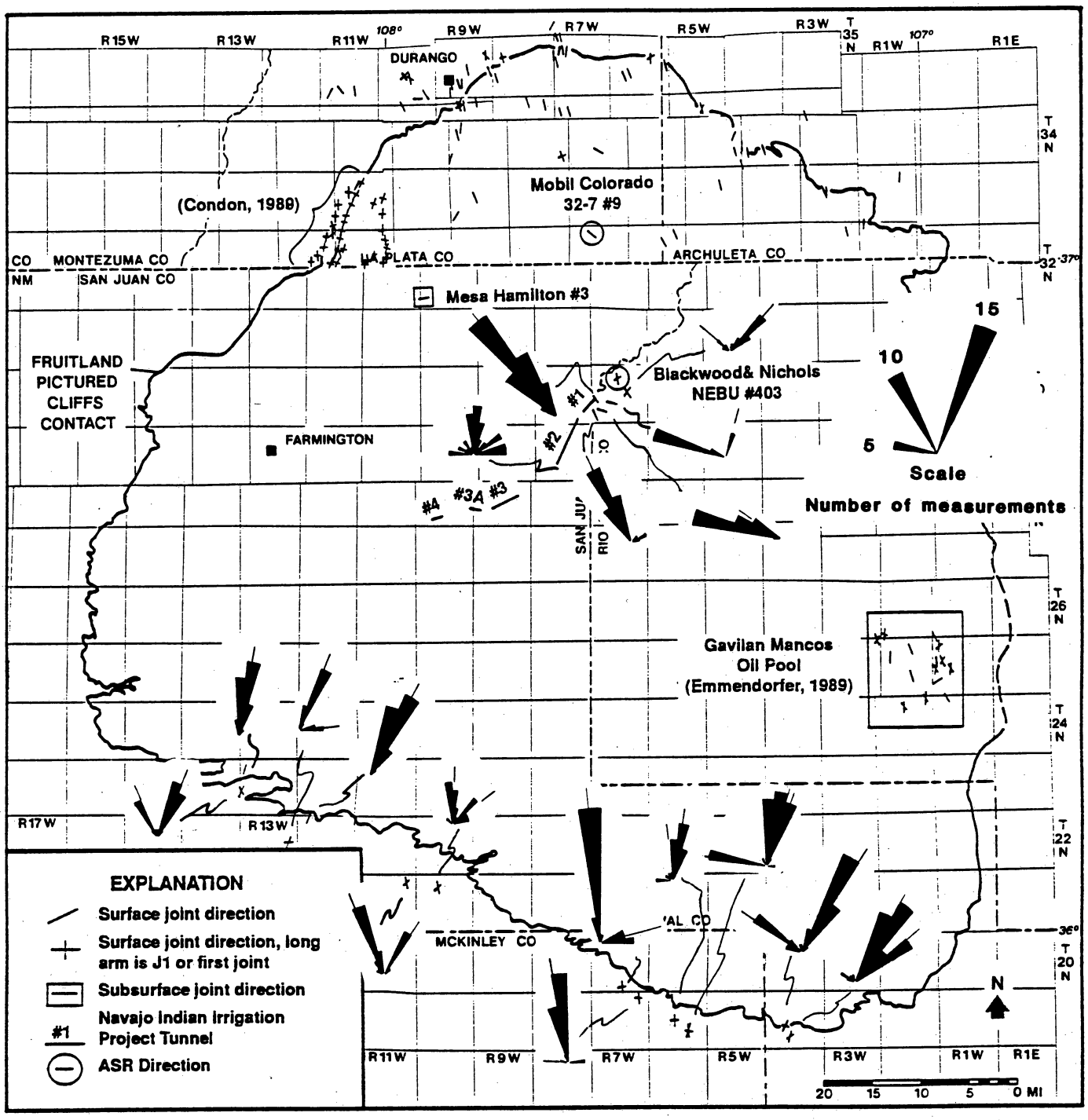

Figure 37. Joint directions and rose diagrams from the Cretaceous and Tertiary in the San Juan Basin.

Newman and McCord (1980, unpublished maps, figs. 3 and 4) measured cleat and "dominant fracture directions" at 70 locations on the north and northeast flank of the San Juan Basin in Colorado. Condon (1988, figs. 3, 5 through 9) measured cleats in coal seams and joints in sandstones from 37 localities on the northwestern flank of the San Juan Basin in Colorado. Cleat and joint data from these two studies are incorporated in figures 38 and 39.

Physical Characteristics of Cleats

Fruitland coal seams at all outcrops in the San Juan Basin have well-developed face and butt cleats. The arithmetic mean of the face-to-butt cleat angle from 14 stations in New Mexico is 90 degrees. In Colorado, the arithmetic mean of the face-to-butt cleat angle at 11 stations around the northern flank of the basin is 88 degrees. Condon (1988) reported that the arithmetic mean at 10 stations from the northwestern flank of the Basin is 69 degrees. Both face and butt cleats are perpendicular to bedding irrespective of bed attitude. At several localities in New Mexico, three or more cleat trends were mapped (figs. 36 and 38).

In New Mexico, face-cleat spacing ranges from 0.3 to 6 inches; typically spacing is 1 to 2.5 inches. Butt-cleat spacing ranges from 1 to 18 inches and typically is 2.5 to 3.5 inches. In Colorado, in the northwestern part of the San Juan Basin, where coals have a greater thermal maturity, face-cleat spacing commonly is 0.25 to 0.50 inches (Condon, 1988). In five Fruitland cores from Colorado (table 3), coal seams have cleat spacings of 0.05 to 0.25 inches. In New Mexico, no systematic changes in cleat spacing are evident, yet cleat is more closely spaced in Colorado than in New Mexico. Because most of the coal outcrops are deeply weathered, the cleat density of unweathered coal in New Mexico was not determined but may differ from that in weathered outcrops. Any relationship between thermal maturity of coal and cleat spacing in fresh rock in the San Juan Basin is therefore still undetermined.

In New Mexico, some coal-seam outcrops have thin (0.05 to 0.1 inch) gypsum and calcite mineralization on cleat faces. Examination with a hand lens shows some of this mineralization

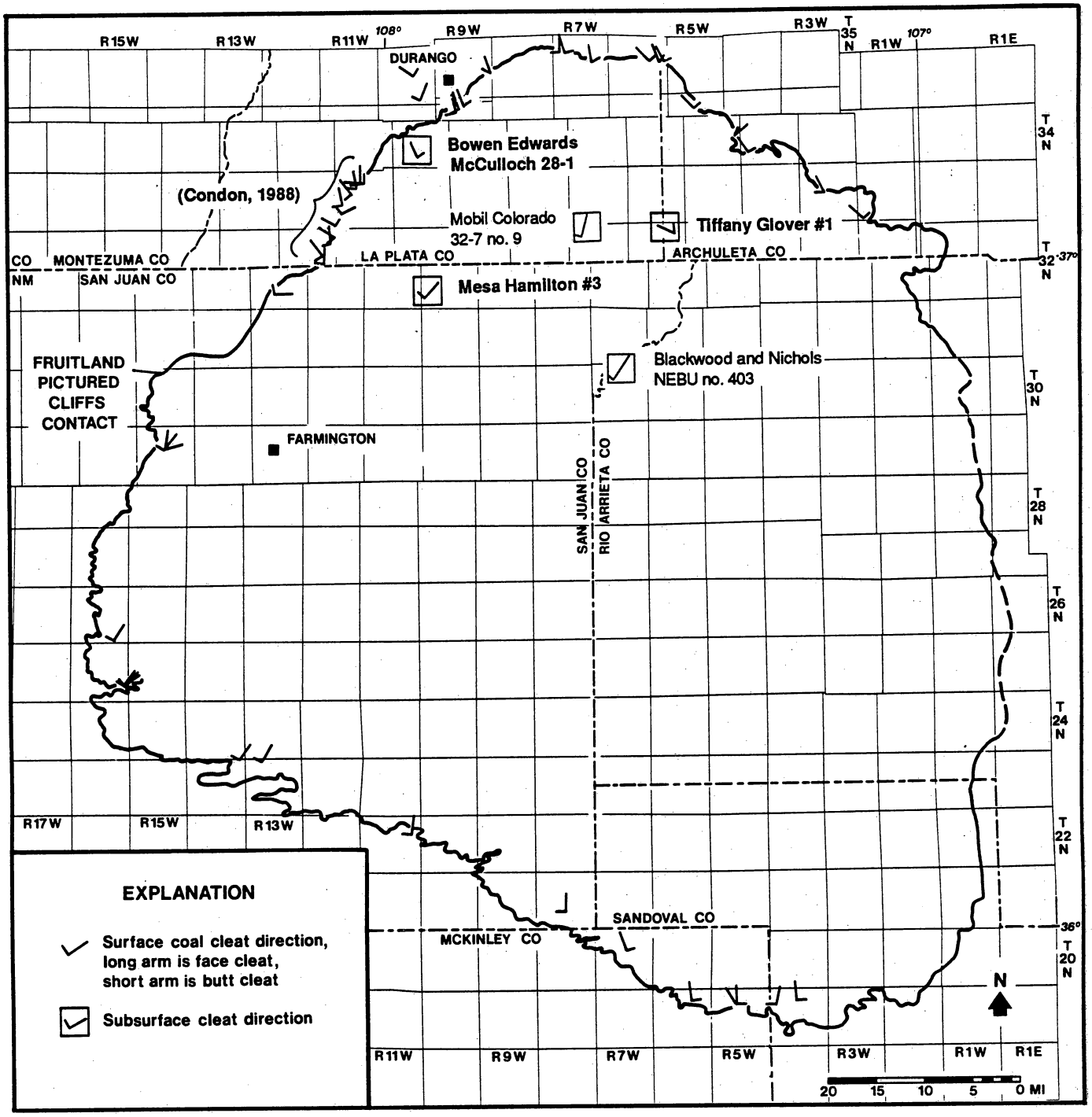

Figure 38. Coal cleat orientations in the San Juan Basin. Cleats in Colorado are from Newman and McCord (1980), Condon (1988), and this study. Cleats in New Mexico are from this study.

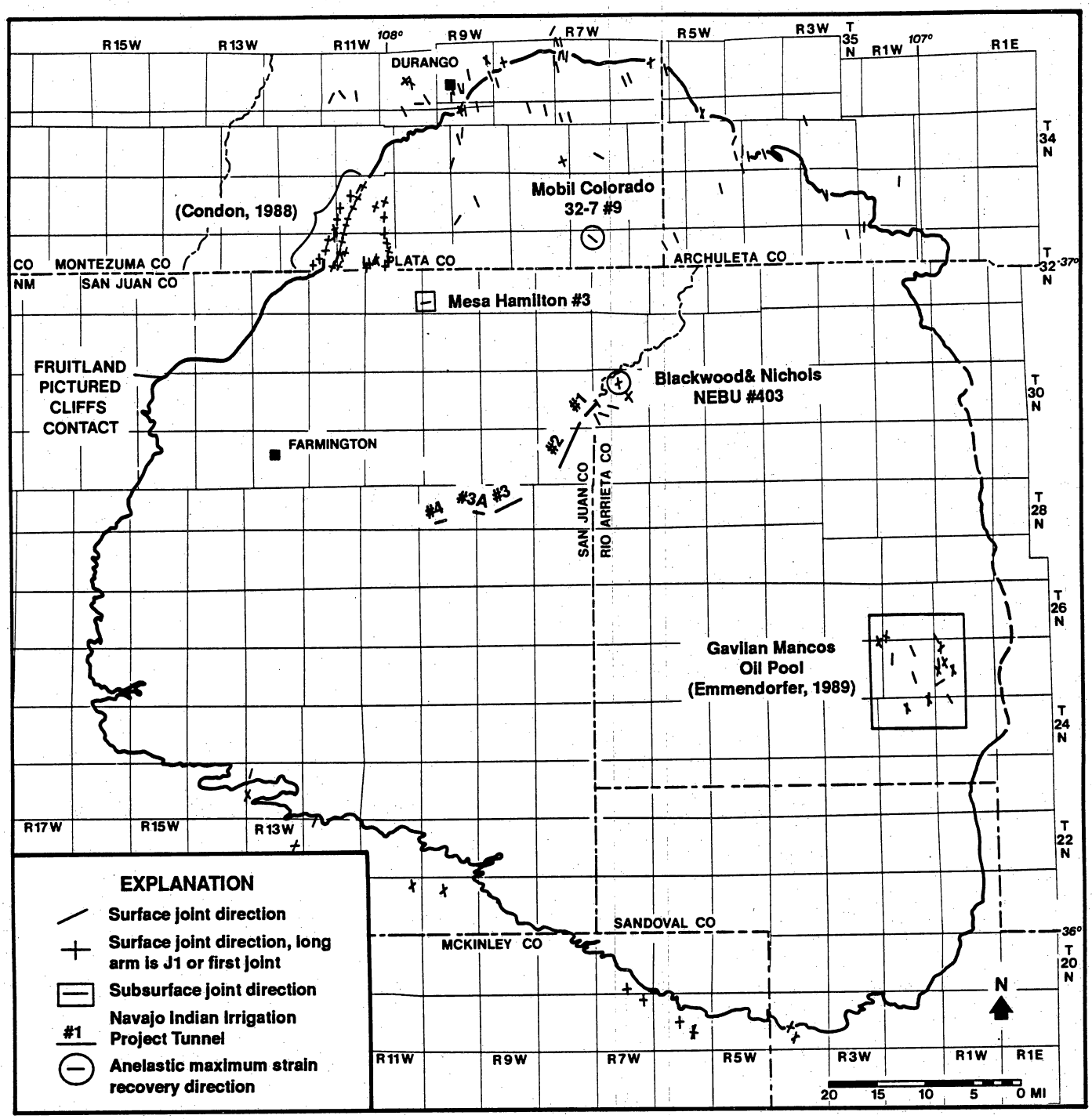

Figure 39. Joint orientations and maximum anelastic strain recovery directions from the Cretaceous and Tertiary rocks in the San Juan Basin. Colorado data from Newman and McCord (1980), Condon (1988), and this study. New Mexico data are from Emmendorfer (1989) and this study.

Table 3. Summary of fractures observed in cores of the Fruitland Formation in Colorado.

Well name	Location	Cored interval (ft)	Slickensides in carbonaceous shale	Mineralized slickensides in carbonaceous shale	Calcite in cleats	Vertical fractures in sandstone or claystone	Mineralized vertical fractures in sandstone or claystone
Ladd 2-3 North Cox Canyon	Sec. 3, T32N, R10W	3089–3114	4	Yes	—	—	—
SUTEC Oxford No. 1	Sec. 25, T34N, R8W	2769–2787	—	—	Yes	Yes	Yes (30"+)
		2804–2822	2	—	—	—	—
SUTEC Oxford No. 2	Sec. 25, T34N, R8W	2832–2850	11	Yes	Yes	—	—
Tenneco Larson 1-12	Sec. 12, T34N, R9W	2991–2297	—	—	—	—	—
		2303–2361	2	—	—	Yes	—
Tenneco Fassett 2-13	Sec. 13, T34N, R9W	2468–2482	2	—	Yes	2	—
		2496–2512	4	—	—	—	—

to be fibrous. At the Chimney Rock Mine (Sec. 30, T34N, R4W), Colorado, joints in one sandstone outcrop have calcite mineralization that continues into the cleats in an underlying coal bed. Coal cleats show calcite or gypsum mineralization in a number of cores from Colorado and New Mexico (tables 3 and 4).

Physical Characteristics of Joints

Like cleat, joints commonly are subvertical to vertical in flatlying sandstone beds (Newman and McCord, 1980; Condon, 1988). Where bedding dips are steep, as along the Hogback Monocline, joints are perpendicular to the local bedding (Condon, 1988). Vertical and subvertical joints invariably terminate at boundaries of sandstone beds. Joint spacing is largely a function of bed thickness and degree of cementation. In thin beds, joints typically are closely spaced, whereas in thick beds they are more widely spaced. Joint spacing commonly is not uniform in thick (greater than 10 ft thick) sandstone beds. Well-cemented (brittle) beds have more closely spaced joints than do poorly cemented beds.

Fractographic features such as arrest lines on joint surfaces can provide evidence of the direction of fracture propagation (Kulander and others, 1979). On joint surfaces in the San Juan Basin, these features are scarce, possibly due to weathering of the joint surfaces (Condon, 1988). On joint surfaces in the San Juan Basin, plumose structure, twist hackle, and arrest lines also are uncommon.

Joints in Fruitland and Pictured Cliffs sandstone are mineralized with calcite at Chimney Rock and Carbon Junction mines and at outcrops at Florida River, Squaw Creek, and Soda Springs in Colorado. In New Mexico, mineralization of joints in noncalcareous sandstone is rare. Calcite veins in joints that cut thin, calcareous sandstone within and at the top of the Upper Cretaceous Cliff House Sandstone are common. These veins have a medial septum and commonly are fibrous. In the Fruitland Formation, at two localities, carbonate beds a few feet above coal seams contain subparallel sets of calcite veins. These veins commonly display

Table 4. Fractures reported in core descriptions on file with the Colorado Oil and Gas Conservation Commission, Denver, Colorado.

Well name	Location	Cored interval (ft)	Formation	Shale slicken-sides	Gypsum or calcite in coal	Other fractures
Tenneco Pritchard No. 9	Sec. 1, T30N, R9W	2467-2491 2626-2639	Fruitland Fruitland	–	Yes	–
Tiffany Glover No. 1	Sec. 2, T32N, R6W	3062-3111	Fruitland	–	–	"mineralized microfractures" in siltstone
Amoco Hott 29-2 No. 2	Sec. 29, T33N, R6W	3021-3031 3103-3113	Fruitland Fruitland	– –	Yes	–
El Paso Natural Gas, Ignacio 33-7 No. 14-20	Sec. 20, T33N, R7W	7616-7772	Dakota	–	–	sandstone w/calc. veins and vert. and horiz. fractures
Amerada No. 1 Harmon	Sec. 17, T33N, R8W	7796-7810	Dakota	–	–	fractures in sandstone
Benson-Montin Greer Ute A-1	Sec. 35, T33N, R12W	3634-3686	Dakota	–	–	Yes
Bowen & Edwards McCulloch Well No. 28-1	Sec. 28, T34N, R10W	3140-3168	Fruitland	Yes	–	–
Bowen & Edwards SE Durango Federal 3-1	Sec. 3, T34N, R9W	1890-1918 2010-2040 2132-2160	Fruitland Fruitland Fruitland	Yes	Yes	–

evidence of several cycles of fracturing and healing. Generally, the calcite veins are completely filled.

Cleat and Joint Orientation

Four joint sets (designated J1 to J4 in order of formation) and a face cleat–butt cleat pair were described by Condon (1988) on the northwest flank of the San Juan Basin in Colorado. The J1 set, first-formed and best developed, contains long planar joints, commonly with exposed lengths of 20 to 30 ft, but at several exposures joints exceed 100 ft long. The J1 joints generally are parallel to the strike of the outcrop along the Hogback Monocline, whereas in areas away from the monocline the trend is more northerly. The J1 set has a mean strike of N15°E (Condon, 1988, figs. 3 and 4a).

The J2 set, similar in style to the J1 set, has joint lengths commonly 2 to 4 ft long, meets the J1 set at approximately right angles, and terminates against the J1 set (Condon, 1988, figs. 4b and 5). The J1 and J2 joint sets form a linked pair of joint sets. The J3 set has a mean orientation of N53°E, with exposed lengths of 3 to 10 ft (Condon, 1988, figs. 4c and 6). The J3 set terminates against J1 and J2 joints where the three sets are present. The J4 set has a mean orientation of N43°W. This joint set is the last formed and least developed. J4 joints are commonly less than 5 ft long and are curved in many exposures. J4 spacings are not consistent, and these joints may be widely scattered in some outcrops (Condon, 1988, figs. 4d and 7). The J1-J2 and J3-J4 joint pairs tend to occur in different areas with only moderate overlap (Condon, 1988).

In the northwestern part of the San Juan Basin in Colorado, the mean of the face-cleat measurements is N21°W, and the mean of the butt-cleat measurements is N48°E; however, there is considerable variability in orientation between stations (Condon, 1988, figs. 8 and 9). The orientation of the face cleats (formed first) suggests a correlation with the J4 joint set, while the trend of the butt cleats (formed second) indicates a correlation with the J3 joint set.

These correlations are the opposite of the age relationships established for the J3 and J4 joint sets. Condon (1988) suggested that either the cleat system in the Fruitland formed prior to the J3 and J4 joints or the butt cleat is younger than the J4 joint and only coincidentally parallel to the J3 set.

On the north and northeast flank of the San Juan Basin in Colorado, the "dominant fracture trend" and face cleats have a strong north-northwest to northwest trend (figs. 38 and 39; Kelso and others, 1988, fig. 8). The arithmetic mean of the dominant joint trend in sandstones in the Eocene San Jose Formation is N23°W. Joints in Fruitland Formation sandstones and face cleats in Fruitland coals at the same locality commonly are subparallel. A general similarity in fracture strike in rocks from the Menefee Formation (Upper Cretaceous) to the San Jose Formation (Eocene) suggests the possibility that these trends may continue into the subsurface (Newman and McCord, 1980).

In New Mexico, joint-measurement stations were divided into (1) outcrops of brittle beds (including coals) where systematic joints are clearly evident and (2) outcrops of ductile beds where systematic joints, if present, are believed to represent local fractures caused by surficial processes.

Two joint sets are recognized in the brittle beds. These sets are referred to herein as the "first-formed" joint set and the "second-formed" joint set. The first-formed joints are planar surfaces and may be 10 to 15 ft long. These joints terminate by tapering to closure on each end. The second-formed joints are more curvilinear in plan view and shorter due to termination against the first-formed joint set. At several localities (fig. 37), the second-formed joint set is weakly developed or absent.

Brittle beds (other than coal seams) containing systematic joint sets were measured in several stratigraphic horizons. Near the west part of the southern outcrop belt of the Fruitland Formation in New Mexico (figs. 37 and 39), two thin, calcareous sandstone beds in the Cliff House Sandstone provided most of the joint orientation measurements. The lower bed occurs at the top of the "lower sand" of Mytton and Schneider (1987) in Chaco Culture National

Historical Park. The upper brittle bed lies at the top of the Cliff House Sandstone immediately beneath the contact with the Lewis Shale. The upper calcareous sandstone extends at least 45 mi along the southwestern part of the Cliff House Sandstone outcrop in New Mexico (T22N, R13W to T20N, R8W). Along the southeastern part of the Fruitland Formation outcrop belt in New Mexico (figs. 37 and 40), joints were described in brittle beds that are thin tongues of Cliff House Sandstone and in thin beds of the Pictured Cliffs Sandstone.

The first-formed and second-formed joint sets in New Mexico may or may not correlate with the J1 to J4 joint sets of Condon (1988) in Colorado. Based upon joint style, not the joint trends, the first-formed joint set may correlate with the J3 joint set of Condon (1988). Joint style also indicates the possibility that the J1 and J2 sets of Condon (1988) were caused by surficial processes.

In New Mexico, face cleats in the Fruitland Formation (figs. 36 and 38) are generally subparallel to parallel to the present dip as defined by the base of the Dakota Sandstone (Thaden and Zech, 1984) and the structure on the Huerfanito Bentonite (fig. 9). Butt cleats (figs. 36 and 38) trend along present-day strike as referenced to the base of the Dakota Sandstone and Huerfanito Bentonite. The first-formed joint set (figs. 37 and 39) tends to be subparallel to the face cleats and thus subparallel to the present-day dip direction of Lower and Upper Cretaceous rocks. The second-formed joint set (figs. 37 and 39) shows a weak to moderate alignment with the local butt-cleat trend.

One example of possible parallelism of cleats and basement faults occurs eastward of R9W (fig. 40). Here butt cleats in the Fruitland coal, the second-formed joint set, and post-Fruitland–pre-Quaternary normal faults are parallel to east-northeast-trending, aeromagnetic isogamma contours as mapped by Cordell (1983). The belt of low magnetic intensity may mark a boundary between metasupracrustal rocks on the north and granitic rocks on the south (Cordell and Grauch, 1985, fig. 12). The Fruitland outcrop belt trends obliquely across the inferred basement rock contact. Face cleats and the first-formed joint set trend at right angles to the faults and isogamma contours.

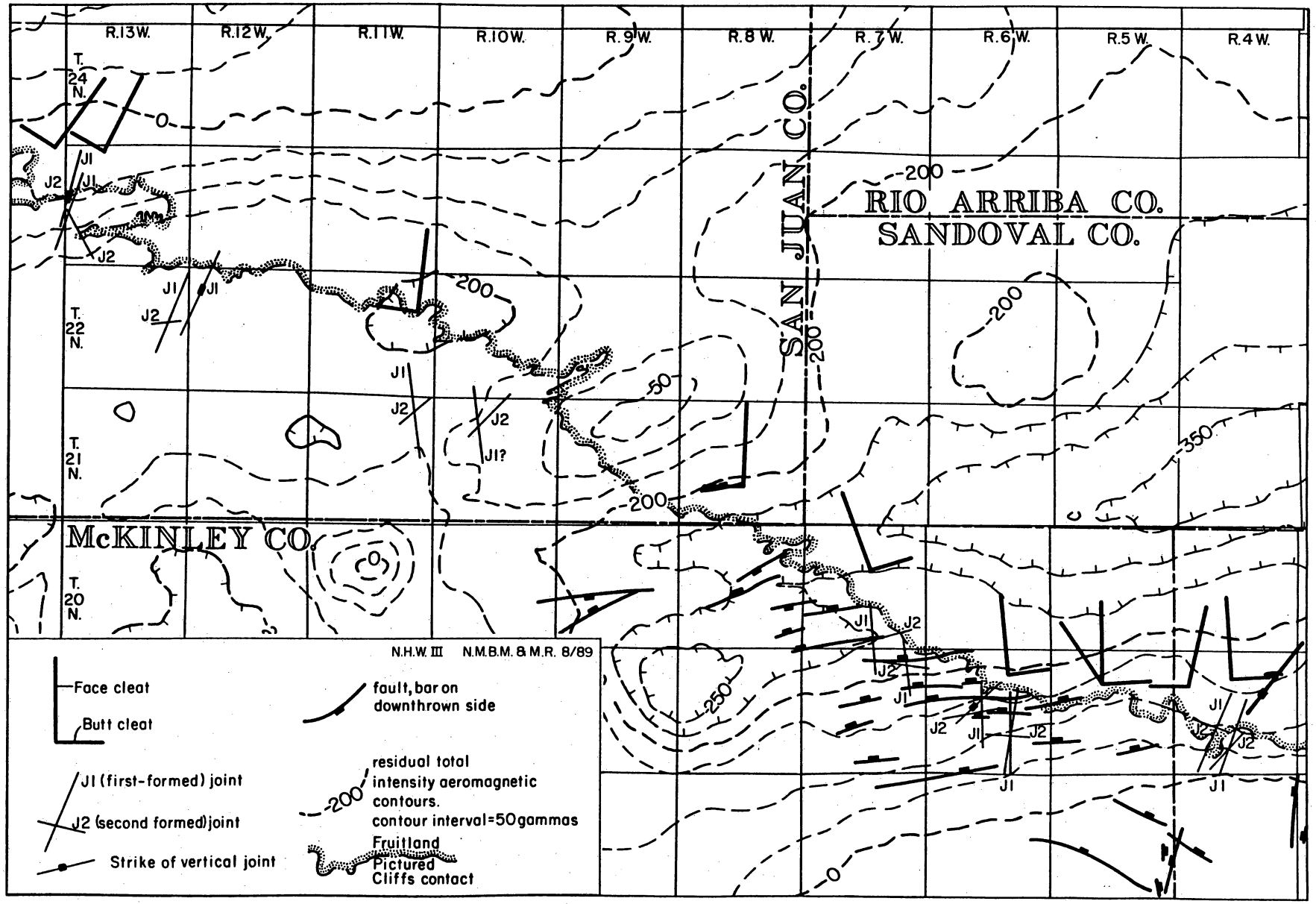

Figure 40. Relationship of joints and coal cleats in Upper Cretaceous rocks, aeromagnetic isogamma contours (Cordell, 1983), and post-Fruitland to pre-Quaternary age normal faults (Thaden and Zech, 1984).

Dike trends in the San Juan Basin area (fig. 41) seldom correlate with coal cleat directions. The dikes in the San Juan Basin area are post-Laramide and thus were emplaced after the formation of the basin. A northwest-trending dike from Table Mesa (T27N, R17W) has the same trend as butt cleats in T25N, R16W. The north-northeast trending Dulce dikes (fig. 41), if projected south-southwest to the outcrop area of the Fruitland, show no correlation with measured cleat trends (figs. 36 and 38).

FRACTURES IN CORES

Cores permit the inspection of fractures that exist in the subsurface. Subsurface fracture patterns may differ from those in outcrop (e.g., Engelder, 1985). At the U.S. Geological Survey Core Library, Denver, Colorado, 14 Fruitland and 9 Pictured Cliff cores from the San Juan Basin are available for study. Fractures were observed in all five Fruitland cores that were described during this study (table 3). The most common fracture type is steeply dipping shear fractures (with slickenside striations) in carbonaceous shale, which may result from early diagenetic dewatering of the shales. The shear fractures are mineralized in the Ladd 2-3 North Cox Canyon and the SUTEC No. 2 Oxford, indicating that these fractures were permeable during mineral precipitation. Calcite also was found in cleats of the Tenneco 2-13 Fassett and the SUTEC Oxford No. 1 and No. 2 wells; it also occurs in a 30-inch-long, vertical extension fracture in the sandstone of the SUTEC No. 1 Oxford. The mineralized fracture in the sandstone is parallel to the calcite-filled butt cleats in a coal seam several inches below and is probably physically continuous with them. The Tenneco 1-12 Larson and the Tenneco 2-13 Fassett also contain vertical fractures in sandstone and claystone, although these are not mineralized.

Seven of nine core descriptions of San Juan Basin strata on public record at the Colorado Oil and Gas Conservation Commission, Denver, Colorado, report fractures (four cores in Fruitland coal, shale, and sandstone, and three cores in the Lower Cretaceous Dakota Formation [table 4]). Calcite or gypsum occurs in the cleats of the Fruitland coal in the Tiffany No. 1

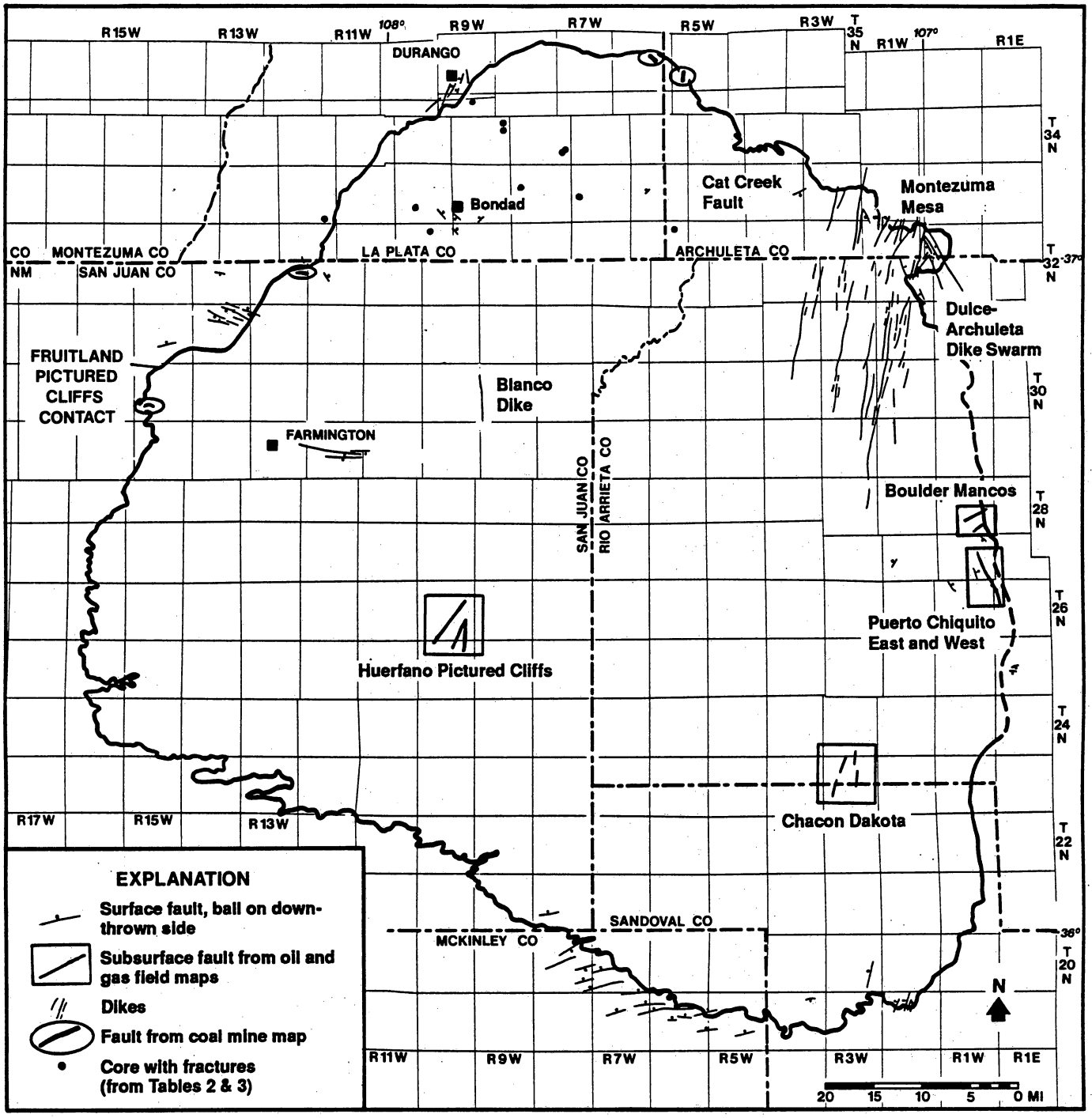

Figure 41. Map of faults, fractures, and dikes in the central San Juan Basin.

Glover, the Amoco 29-2 No. 2 Hott, and the Bowen and Edwards 3-1 SE Durango Federal. A core description of a New Mexico well, the Tenneco No. 9 Pritchard, also reports mineralized cleats. The core description of the Tiffany No. 1 Glover well reports mineralized microfractures in the siltstone, but specific details are unavailable. Slickensides are reported in the shales of the Bowen and Edwards 28-1 McCulloch core and the Bowen and Edwards 3-1 SE Durango core.

TOPOGRAPHIC EXPRESSION OF FRACTURE PATTERNS

Joints Caused by Surficial Processes

Field work in New Mexico indicates that joints caused by surficial processes are a prominent and pervasive fracture type in outcrops of the Cliff House Sandstone at Chaco Canyon Culture National Historical Park and in the Eocene San Jose Formation in the Navajo Reservoir area. Upper Cretaceous and Tertiary sandstone in large outcrops away from valley walls have widely spaced joints or joint zones or lack joints altogether. Near cliff valley walls, joints are plentiful. These joints strike subparallel to the local topographic contours (figs. 42 and 43), suggesting that the joints result from rock relaxation toward a free or unsupported surface with primarily gravitational processes acting to cause failure.

The tendency for joint sets to align parallel to the local topographic slope, along with joint surfaces that break through the entire bed, produces straight cliff segments. In the area of figure 43, extensive joint surfaces are exposed along cliff faces, including one joint surface 20 ft high (bed thickness) and over 150 ft long. In standard-scale aerial photographs (about 1:20,000), these cliff segments are mappable as straight trends, i.e., linears. Thus, a surface phenomenon, topographically induced stress, is forming joint trends that are interpretable as photolinears.

Brief descriptions of fractures in massive sandstones (Bradley, 1963; Nelson, 1985, p. 26) and a mention of "rim joints" (Kelley and Clinton, 1960, p. 16) are the only published

Figure 42. A meander neck-like outcrop (Sec. 3 and Sec. 10, T21N, R11W) formed in the resistant "middle sandstone" (Mytton and Schneider, 1987) of the Cliff House Sandstone. Note the very finely adjusted linking of local topographic slope and contour-parallel joints to form an arcuate pattern. Scale: 1 inch ~ 350 ft.

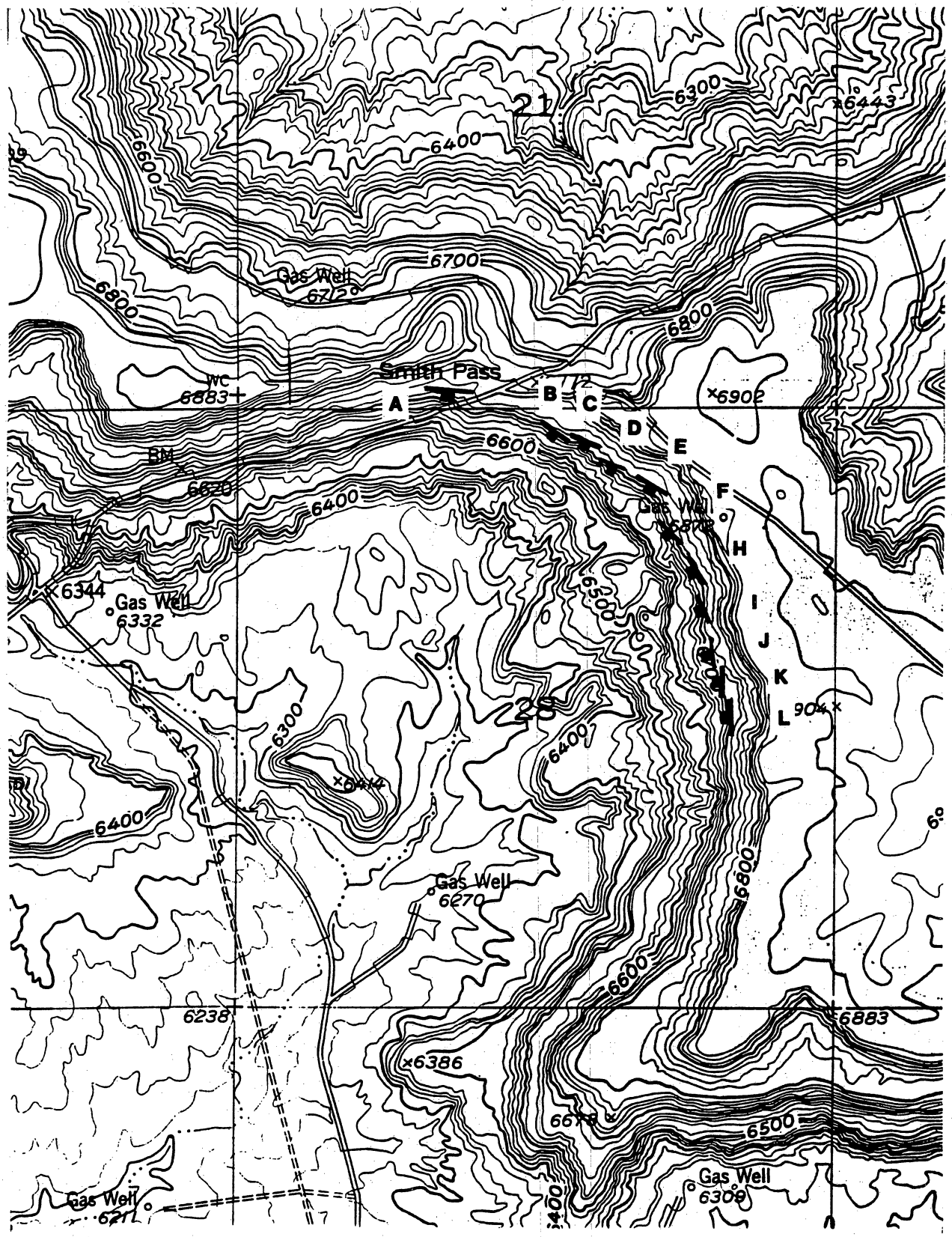

Figure 43. Strike and dip measurements of the first-formed joint set in a continuous sandstone bed in the Regina Member, San Jose Formation (Sec. 21 and 28, T30N, R7W).

references to jointing induced by local topography in the Colorado Plateau. This jointing process may be common in other Rocky Mountain intermontane basins. Our study indicates that joint orientations observed in outcrop and inferred from topography must be used with caution when inferring subsurface fracture patterns. Nevertheless, Decker and others (1989) concluded that many lineaments mapped in Cedar Hill field (T32N, R10W) coincide with fractures and regional tectonic trends.

Relationship of Fractures and Lineaments

Lineaments are linear features on aerial photographs and satellite images that may indicate zones of increased fracture density. Lineaments are defined as simple or composite features of an image or map whose parts are aligned in a rectilinear or slightly curvilinear relationship (O'Leary and others, 1976). Examples of topographic features that may cause lineaments include straight sections of streams, cliffs, ridges, aligned vegetation, and linear tonal differences. Figure 44 shows the locations of previous lineament studies in the San Juan Basin. In general, studies by Kelley and Clinton (1960) and Knepper (1982) show strongly developed northeast-trending lineaments and well-developed, secondary, northwest-trending lineaments in the basin.

The relation of lineaments, which are surface features, to subsurface fracture patterns can be difficult to document. Field work performed during this study has elucidated the relation between fractures and some remotely sensed lineaments. In New Mexico, tunnel exposures offer a way to link a remotely sensed lineament with ground geology. The U.S. Bureau of Reclamation excavated four tunnels for the Navajo Indian Irrigation Project (figs. 37 and 39; table 5). The reports on tunnel geology (Anonymous, 1966, 1967) contain geologic maps of the tunnels at scales of either 1:120 or 1:240. The tunnels were excavated in an area of known gas production, between the Navajo Reservoir and Bloomfield, New Mexico. During construction, tunnels were checked daily for flammable gas. A minor amount of gas was detected only in an

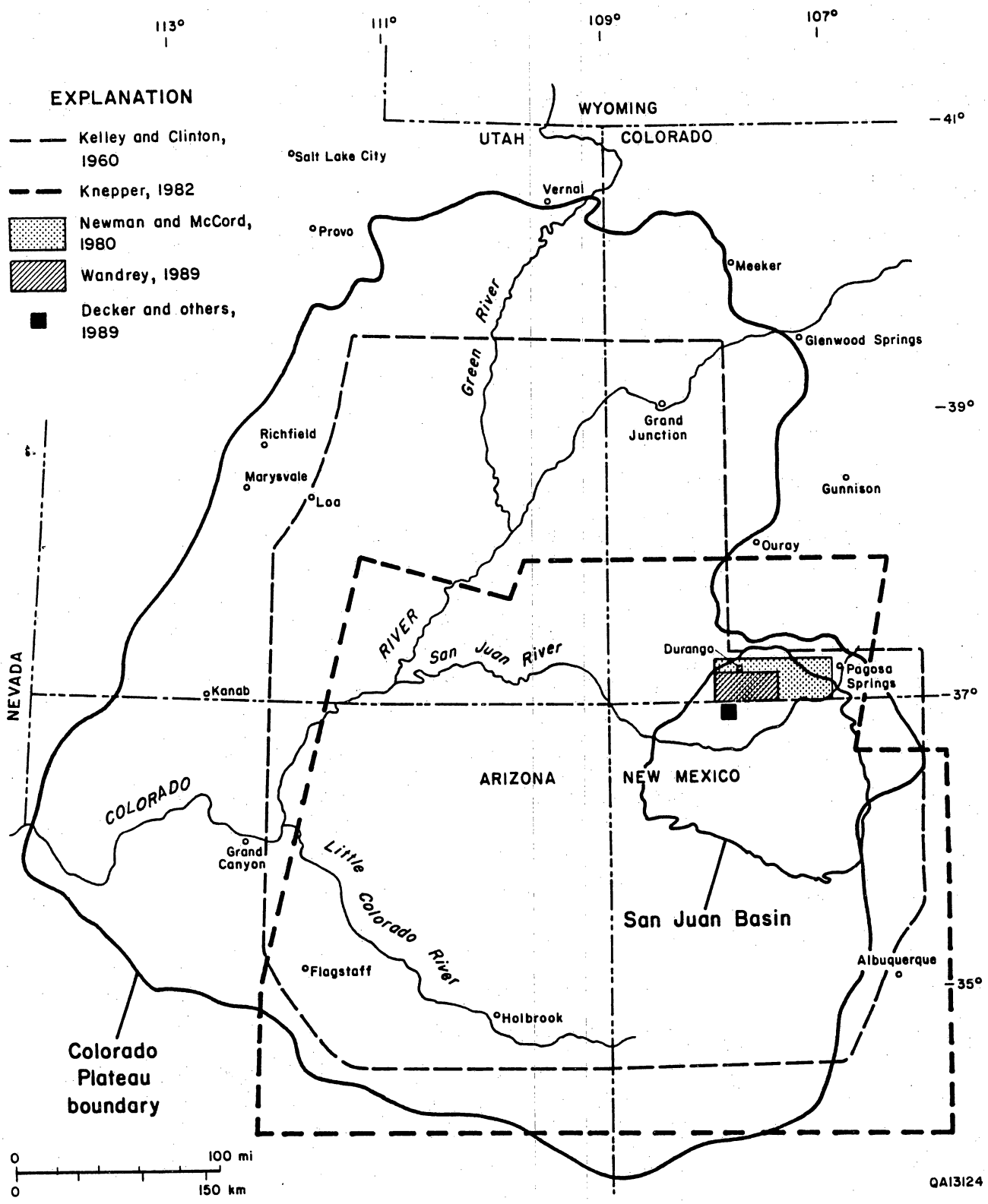

Figure 44. Index map of lineament studies in the San Juan Basin.

Table 5. Tunnel data, U.S. Bureau of Reclamation, Navajo Indian Irrigation Project.

Tunnel	Length (ft)	Formation	Author
Tunnel #1	10,700	San Jose (Eocene)	Anonymous, 1966
Tunnel #2	25,800	San Jose (Eocene)	Anonymous, 1967
Tunnel #3	15,300	Nacimiento (Paleocene)	Cooper, no date
Tunnel #3a	3,200	Nacimiento (Paleocene)	Cooper, no date
Tunnel #4	5,000	Nacimiento (Paleocene)	Cooper, 1975

800-ft section of Tunnel 2, which showed 0.1 to 0.2 percent of flammable gas. The amount of gas influx decreased over several months, as evidenced by the amount of gas bubbles seen in the water on the tunnel floor. Only a minor amount of ground water was encountered during excavation of the tunnels. Most of this water was perched above shale beds, and amounts of water entering the tunnel decreased as these perched bodies were drained.

No fracture zones or faults were reported in these tunnel maps made from 100 percent exposure. Although the tunnels are now inaccessible, tunnel stability was the primary geologic concern in the tunnel reports (see table 5). Lineaments from Knepper (1982, fig. 3) cross Tunnels 2, 3, and 4. Neither significant gas seeps nor ground-water influxes, both of which commonly occur along fractures, were reported in 11.4 mi of tunnels, indicating that linears/lineaments mapped by Knepper (1982, fig. 3) do not represent permeable fractures. However, fractures may be present but sealed.

CONTEMPORARY STRESS

Contemporary stress direction indicators for the Colorado Plateau and vicinity include Pliocene or younger dike trends, cinder-cone alignments, slip directions on young normal faults, earthquake focal mechanisms, anelastic strain recovery (ASR) measurements from cores, hydrofracture azimuths, and borehole breakout trends (Zoback and Zoback, 1980, fig. 1; Aldrich and Laughlin, 1982; Aldrich and Laughlin, 1984, fig. 6; Aldrich and others, 1986, fig. 5; Owen, 1988; Owen, 1989; Wong and Humphrey, 1989; Zoback and Zoback, in press, fig. 1).

The maximum horizontal stress (greatest horizontal compressive stress) within the Colorado Plateau is oriented west-northwest, which is essentially orthogonal to stress direction in the surrounding Rio Grande Rift–Basin and Range extensional stress province. Zoback (1988) and Zoback and Zoback (in press), on the basis of new earthquake focal mechanism data, report that the stress regime of the Colorado Plateau is extensional, not compressional as reported earlier in Zoback and Zoback (1980). Zoback and Zoback (in press) further suggest that the

difficulty in interpreting the stress regime may be due to the small differences between the horizontal stresses. The Colorado Plateau stress province is distinctly smaller than the physiographic boundaries, as the Basin and Range extensional regime has encroached upon the margins of the Plateau (Zoback and Zoback, in press). Recent stress measurements in the San Juan Basin part of the plateau include ASR measurements for two wells. At the Blackwood and Nichols NEBU No. 403 (Sec. 9, T30N, R7W) horizontal strain recovery azimuths are bimodal (fig. 39). The dominant direction (maximum horizontal stress) is in the north-northwest direction (N7°W +13°), with a subsidiary trend to the northeast (N62°E +13°) (Owen, 1988). In the Mobil 32-7 No. 9 Colorado (Sec. 4, T32N, R7W), the maximum horizontal strain recovery is N55°W +20° (Owen, 1989). These northwest quadrant values are similar to the west-northwest direction of maximum horizontal compressive stress reported by Zoback and Zoback (in press).

CONCLUSIONS

1. Cleats and joints in the Upper Cretaceous and Tertiary rocks show no evidence of shear offset; all are extension fractures.

2. Face and butt cleats are well developed in Fruitland coals. The cleats are orthogonal to bedding and intersect at about a 90-degree angle. Face-cleat strikes are predominantly north or northeast in the southern part of the basin and northwest in the northern part of the basin. Face-cleat strike varies abruptly over short (1 to 2 mi) distances.

3. Two joint sets occur in New Mexico. The first-formed set is subparallel to the face cleat. The second-formed joint set has a weak to moderate alignment with the butt-cleat trend. The early-formed set is subparallel to the present strike direction of the Dakota Sandstone and Huerfanito Bentonite.

4. Parallelism of cleats and basement faults is unsubstantiated for the Fruitland Formation. Locally butt cleats in Fruitland coals and the second-formed joint set parallel post-Fruitland pre-Quaternary faults and east-northeast-trending aeromagnetic isogamma contours, but this

relationship may be fortuitous. Dike trends in the San Juan Basin show little correlation to coal cleat trends at the surface. The dikes are post-Laramide and thus were emplaced after the basin had attained its present structural configuration.

5. Joints caused by surficial processes are common in outcrops of the Cliff House Sandstone at Chaco Culture National Historical Park and in the San Jose Formation in the Navajo Reservoir area. These joints resulted from rock relaxation toward a free surface and probably have little significance to subsurface fracture patterns, suggesting that remote-sensing data should be used with caution in the San Juan Basin.

HYDRODYNAMICS OF THE FRUITLAND FORMATION

W. R. Kaiser and T. E. Swartz

INTRODUCTION

The regional hydrologic setting of the Fruitland Formation was established in an earlier study (Kaiser and Swartz, 1988, 1989). This report begins with a summary of key findings about ground-water circulation, pressure regime, hydrochemistry, and hydrostratigraphy, and it focuses on aspects of Fruitland hydrodynamics not fully investigated in the earlier study.

The Fruitland Formation is recharged mainly from the wet, topographically high, north and northwest margins of the basin where numerous thick aquifer coal seams crop out; a potentiometric high dominates the north-central part of the basin. Limited recharge occurs at the eastern, southern, and western margins of the basin. Ground-water flow in the Fruitland Formation converges from the northeast and southeast toward the San Juan River valley in the west-central part of the basin. Discharge is primarily to the San Juan River valley and secondarily, in the southwest part of the basin, to the tributaries of the Chaco River.

The Fruitland Formation is abnormally pressured—an overpressured area in the north-central part of the basin is surrounded by a much larger underpressured area that covers the remainder of the basin. Overpressuring is explained hydrodynamically and is attributed to artesian conditions; it is not a fossil geopressure. Underpressuring is due to late Tertiary basinal uplift, erosion, and cooling and endures because of poor hydraulic connection with the northern recharge area, limited recharge from the southern margin of the basin, and isolation from shallow water-table aquifers.

The diverse composition of Fruitland Formation waters reflects the hydrologic setting rather than the producing lithology. Distinct hydrochemical regions occur in the overpressured

north-central part and the underpressured southern part of the basin. Fresh to brackish Na-HCO_3 type waters from the north-central part of the basin are unique in their very high alkalinities (several thousand mg/L) and low chlorinities (tens to hundreds of mg/L), reflecting, respectively, the presence of organic acids and fresh water. Waters in the southern part of the basin are saline Na-Cl type that closely resemble seawater.

On the basis of hydraulic head, pressure regime, hydrochemistry, and permeability, a Fruitland–Pictured Cliffs aquifer system was defined in the north-central part of the basin to include the Fruitland and the upper Pictured Cliffs sandstone tongues and in the southern part of the basin to include the Fruitland Formation and the Pictured Cliffs Sandstone. Previously, the Fruitland had been combined with the Kirtland Shale to form the Kirtland/Fruitland confining unit (Stone and others, 1983). Recently, McCord (1988) proposed for the north-central part of the basin a major Fruitland aquifer defined by thick, laterally extensive coal seams, which in the northern part of the basin are the most permeable aquifer units. Their permeabilities are orders of magnitude greater than those of associated sandstones.

HYDRODYNAMICS

Details of Fruitland hydrodynamics were established from the potentiometric surface, pressure regime, and hydrochemistry (Kaiser and Swartz, 1988; 1989). Additional observations and reinterpretations of old hydrologic data are presented here. Additional head mapping has better defined sources of recharge to the Fruitland–Pictured Cliffs aquifer, potentiometric anomalies in the aquifer, and head in the Pictured Cliffs Sandstone. A map of bottom-hole pressure was made. Vertical pressure gradients were calculated for individual Fruitland gas-producing areas associated with potentiometric anomalies to evaluate vertical flow direction and pressure anomalies. To further characterize the hydrochemistry and chemical evolution of Fruitland ground waters, we made a chlorinity map and Stiff ionic-ratio diagrams.

Hydraulic Head

The Fruitland potentiometric surface was mapped from fresh-water equivalent heads calculated from approximately 200 bottom-hole pressures (BHP) that were calculated from wellhead shut-in pressures (WHSIP), 50 SIP's recorded in drill-stem tests (DST), and 10 BHP's measured or extrapolated in well tests. Static water levels (approximately 30) along the north and south margins of the basin and 14 outcrop elevations of perennial streams at the north margin were used to map the Fruitland water table.

Analysis of the potentiometric surface shows that recharge is at the elevated north and northwest margins of the basin (fig. 45) in the foothills of the San Juan Mountains, where numerous thick coal seams crop out in the wettest part of the basin (precipitation 20 to 30 inches/yr). Recharge from the eastern margin is limited because (1) the Fruitland is absent along much of the margin (figs. 8 and 18) and where present is dominated by low-permeability, fine-grained rocks, (2) there is less annual precipitation (12 to 20 inches), and (3) the continental divide lies west of the basin margin, diverting potential recharge available through leakage eastward out of the basin. Moreover, much of the recharge is accepted by the overlying high-permeability Ojo Alamo Formation (figs. 3 through 5). Recharge from the south and west margins of the basin also is limited. Annual precipitation in those parts of the basin is lower than on the east, ranging, respectively, from 8 to 12 inches and 4 to 8 inches. Furthermore, the Fruitland–Pictured Cliffs outcrop along the southwest margin of the basin is topographically lower than the basin interior (fig. 45) and lies just east and northeast of the Chaco River. Consequently, potential recharge to the unconfined Fruitland–Pictured Cliffs aquifer is diverted westward out of the basin as discharge to the Chaco River and its tributaries and is thus unavailable as recharge basinward to the confined aquifer system. Widely spaced head contours in the southern part of the basin reflect limited recharge from the southern margin of the

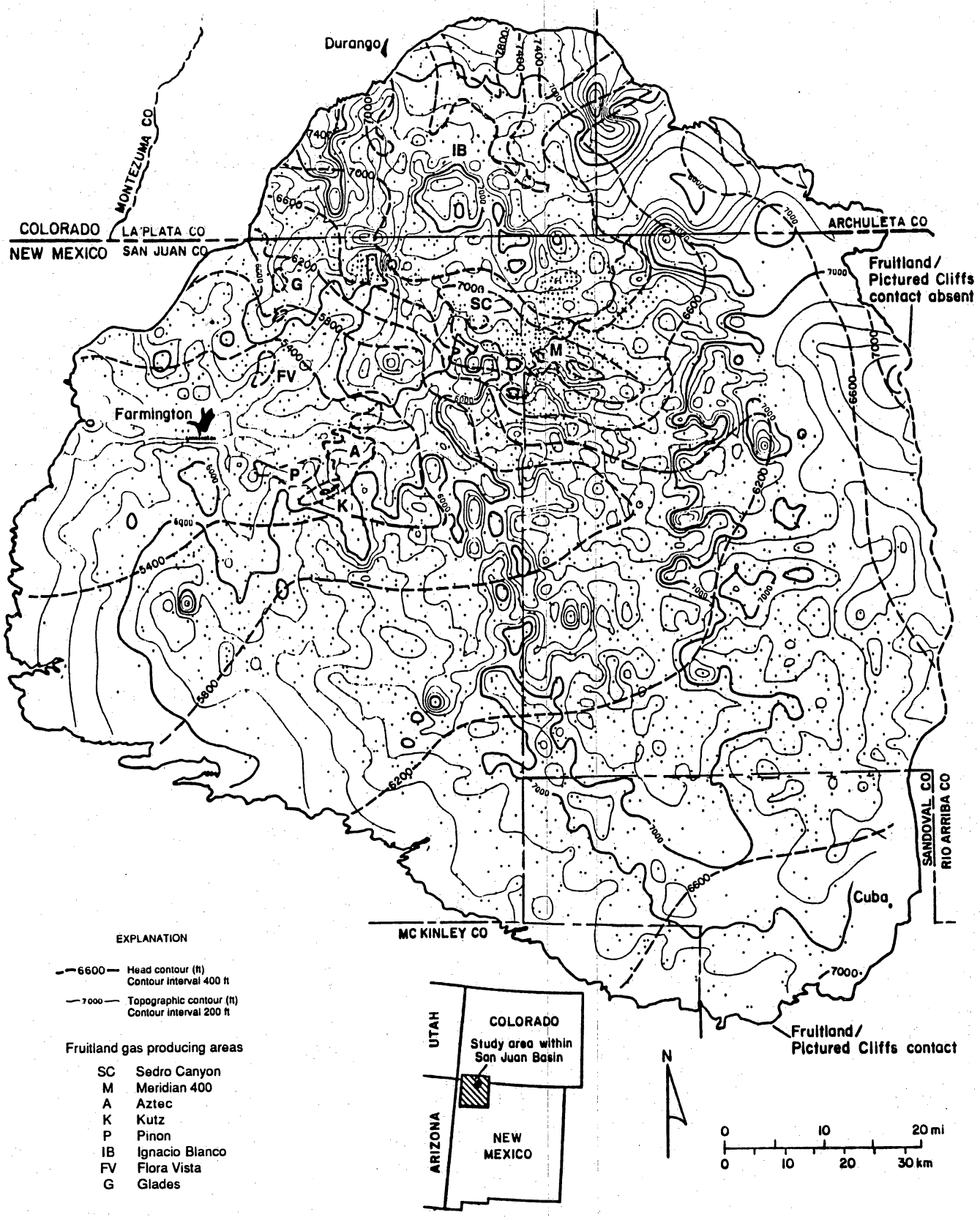

Figure 45. Fruitland Formation potentiometric-surface map and topographic map of land surface, San Juan Basin.

basin, whereas widely spaced contours in the San Juan River valley reflect discharge (upward flow).

Potentiometric mounds at Sedro Canyon, Meridian 400, Aztec, Kutz, Pinon, Flora Vista, and Glades areas are of uncertain origin. The largest of these are in the Sedro Canyon–Meridian 400 area (SC–M) and the Aztec–Kutz–Pinon area (A–K–P) (fig. 45). The mound in the SC–M area trends northwest-southeast as a continuous potentiometric ridge 25 mi long, as defined by the 7,000-ft head contour, and mounds in the A–K–P area trend northeast-southwest for 4 to 8 mi. These mounds probably do not represent recharge mounds (downward flow) because there is no apparent source for the recharge. The SC–M area is well basinward and unassociated with any topographic highs. In fact, topography is higher to the northwest of SC–M and elevations (msl) of test intervals at SC–M are lower than those to the southwest, proving that elevation head cannot explain the high heads at SC–M. On the other hand, A–K–P is located in the San Juan River valley, the regional discharge area where upward flow is expected. Some A–K–P wells are overpressured and located mainly along the San Juan River. Overpressuring in these wells is explained hydrodynamically as evidence for upward flow.

The presence of free gas causes heads to be higher, which may contribute to the potentiometric anomalies, particularly at A–K–P, where gas is conventionally trapped in sandstone reservoirs. However, free gas is not the main contributory factor. Gas columns many times the thickness of sandstone reservoirs at A–K–P would be required to account for the anomalies seen. At SC–M, the presence of gas has a negligible effect on heads as water and gas reservoir pressure are approximately equal.

The alternative explanation for the potentiometric mounds at SC–M and A–K–P, having eliminated recharge, topography, and buoyant force as primary causes, is that they indicate areas of upward flow. Pressure-elevation (msl) plots for SC–M and A–K–P show vertical pressure gradients of approximately 0.80 psi/ft, indicating a very strong potential for upward flow (figs. 46 and 47). The large vertical pressure gradients imply that the Fruitland strata are not well interconnected vertically and that a large driving force is needed to move fluid vertically.

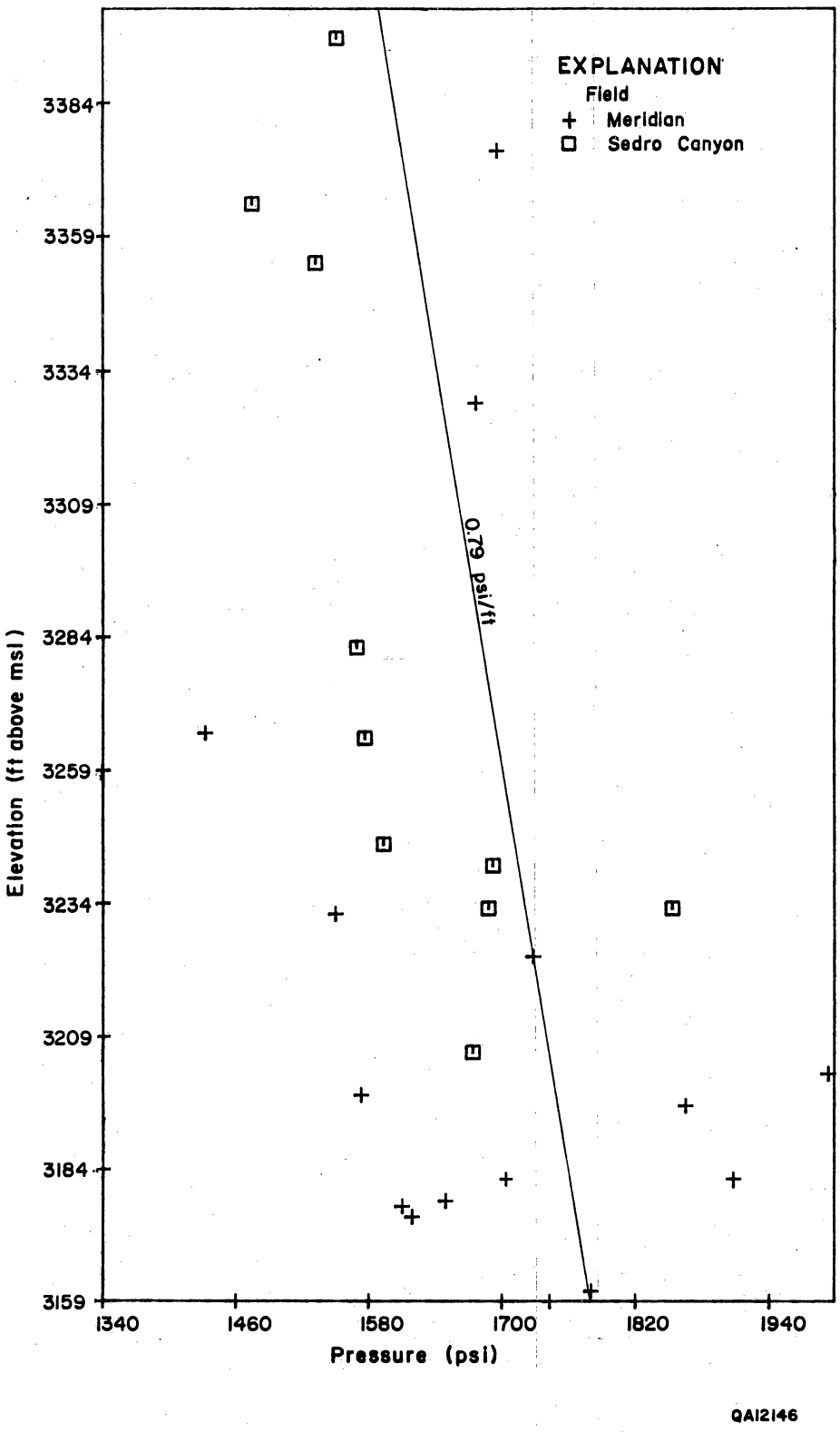

Figure 46. Fruitland Formation pressure-elevation plot, Sedro Canyon–Meridian area. Vertical pressure gradient (~ 0.79 psi/ft) is the slope of the trend line.

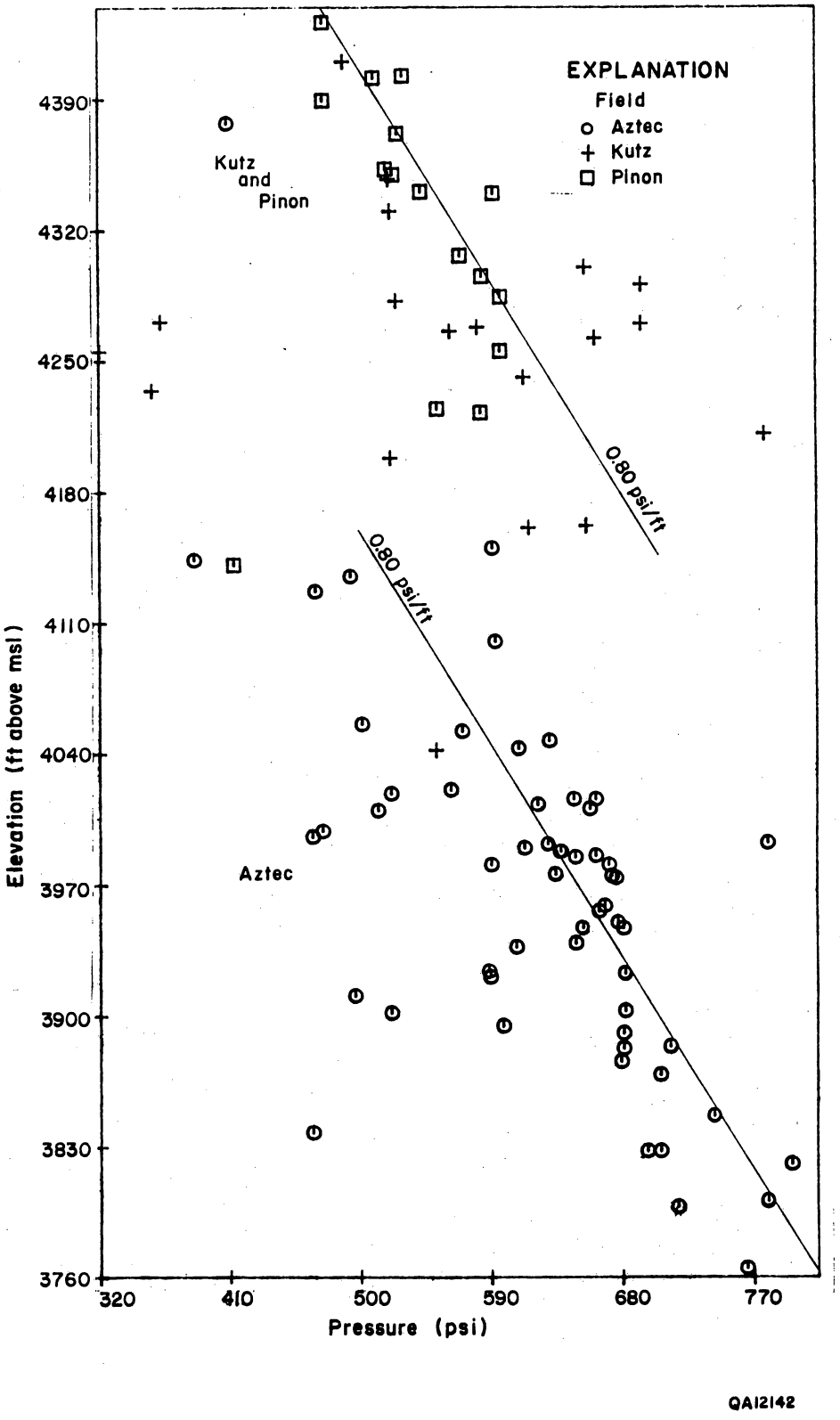

Figure 47. Fruitland Formation pressure-elevation plot, Aztec–Kutz–Pinon area. Vertical pressure gradient (~ 0.80 psi/ft) is the slope of the trend lines.

The SC–M area is thought to represent a pressure ridge coinciding with upward groundwater flow caused by pinch-out of thick, laterally continuous coal seams (aquifers) in the area (figs. 4, 27, and 29). Wells in the SC–M area are overpressured and have the basin's highest reported bottom-hole temperatures (up to 140°F or 60°C). Aquifer coal seams transmit recharge from the north and northwest margins of the basin under high pressure that upon aquifer pinch-out must turn upward. Note that the potentiometric mound is associated with thick coal seams (figs. 27 and 29) and marked steepening of the potentiometric surface (fig. 45), indicative of a facies change or lower permeability. This resistance to horizontal flow would tend to cause a buildup of fluid pressure and, in turn, reversal of the vertical pressure gradient from downward, which is shown regionally for the north-central basin (fig. 48), to upward (fig. 46). Although the vertical pressure gradient at A–K–P (fig. 47) exceeds the regional gradient (~ 0.60 psi/ft), it is consistent with upward vertical flow and available Pictured Cliffs head data.

In the vicinity of A–K–P and within the general area defined by the 5,400-ft head contour (fig. 45), Pictured Cliffs heads are similar to or slightly above those of the Fruitland. Elsewhere, in the west-central part of the basin, Pictured Cliffs heads are somewhat less than Fruitland heads or about equal to them, indicating a single aquifer system in hydraulic communication. However, in the southeast part of the basin, where Pictured Cliffs heads are as much as 700 ft lower than Fruitland heads, the two units are hydraulically separate. This large head difference undoubtedly reflects, in part, failure to attain pressure equilibrium during short-term well testing, and low permeability in the Pictured Cliffs Sandstone is inferred from it.

Pictured Cliffs heads are highest (6,200 to 7,000 ft) in the northwest part of the basin adjacent to the outcrop and decrease southeastward, parallel to the Pictured Cliffs depositional strike, to approximately 6,000 ft. Throughout the north-central part of the basin, Pictured Cliffs heads are lower than those of the Fruitland. Except for the northwest part of the basin, Pictured Cliffs heads in the northern part of the basin are as much as 1,300 ft lower. They are about 800 ft lower in the Sedro Canyon–Meridian 400 area, indicating strong potential for downward flow that is directly opposite to that inferred from the vertical pressure gradient

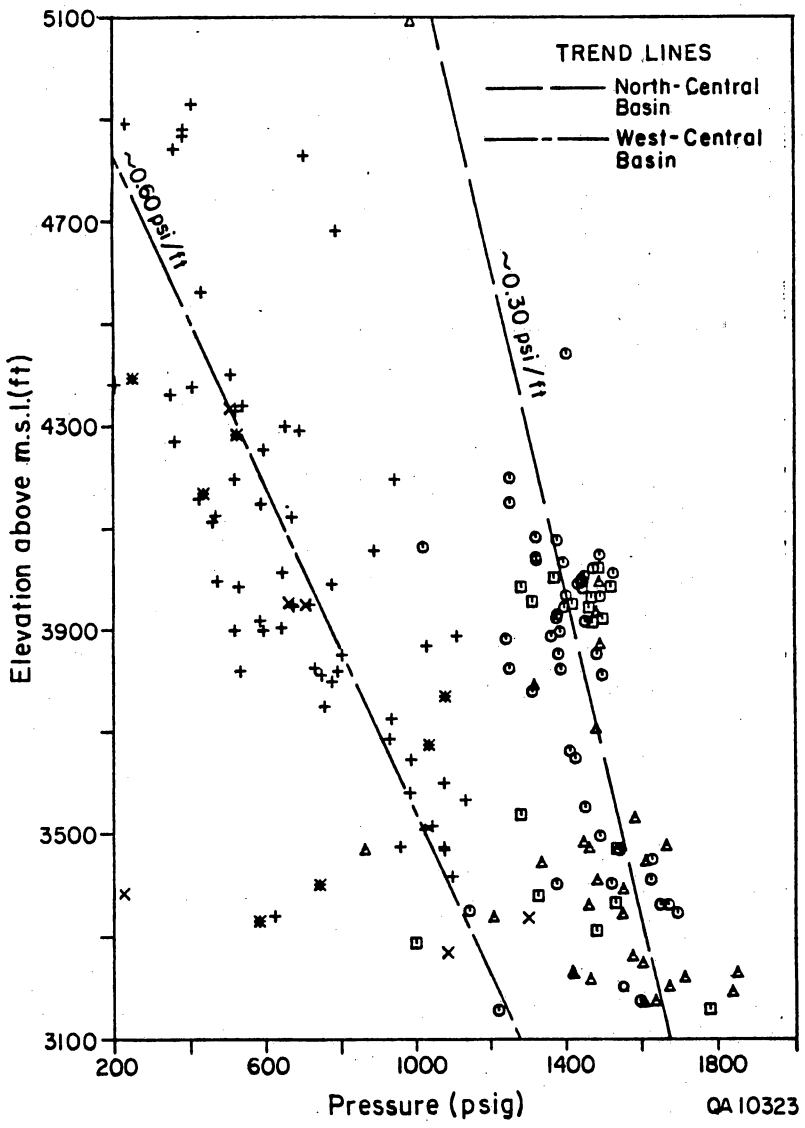

Figure 48. Fruitland Formation pressure-elevation plot, San Juan Basin (from Kaiser and Swartz, 1988). Vertical pressure gradient (~ 0.30 and ~ 0.60 psi/ft) is the slope of the respective trend line. Geometric symbols, north-central basin and stick symbols, west-central basin. Relative to fresh-water hydrostatic gradient, flow is potentially downward in the north-central basin and upward in the west-central basin (regional discharge area).

(fig. 46). This seeming contradiction can be explained in terms of relative permeability. Even though strong potential for downward flow is indicated from the Fruitland to the Pictured Cliffs, this potential is, particularly in low-permeability strata, only a potential and does not mean that significant flow actually occurs. The very large head difference between the Fruitland and Pictured Cliffs indicates separate aquifer units and low permeability in the Pictured Cliffs, which is too tight to receive and transmit much recharge (Kaiser and Swartz, 1988, 1989). Thus, ground-water flow is mainly in the more permeable Fruitland coal seams, which are confined by the low-permeability Pictured Cliffs Sandstone below and the Kirtland Shale above. Consequently, in the northern part of the basin, flow occurs mainly in the Fruitland Formation. If this were not the case, head differentials and vertical pressure gradients would be much less.

Pressure Regime

The Fruitland Formation is abnormally pressured relative to the fresh-water hydrostatic gradient (0.433 psi/ft) and has been divided into an overpressured north-central basin and an underpressured south basin. The overpressured area is surrounded by a much larger underpressured area (simple pressure gradient less than 0.44 psi/ft), and the transition between them is marked by pronounced steepening of the potentiometric surface. Anomalous islands of overpressuring in the regionally underpressured part of the basin occur at Kutz, Pinon, Aztec, Flora Vista, and Glades areas and are explained hydrodynamically by local upward flow of ground water. Flora Vista and Glades areas lie in a dip-elongate belt of thick coal seams (fig. 29) and may thus receive recharge from outcrops to the north contributing to overpressuring. Anomalous underpressuring in the overpressured north-central part of the basin is attributed to pressure decline due to production in the Ignacio Blanco field. A cluster of 17 wells in the vicinity of the Ignacio Anticline (T34N, R7W and T33N, R6W), completed in the early 1980's, are thought to have undergone pressure decline due to long-term production from nearby wells dating from the 1950's.

In the north-central part of the basin, BHP's typically range from 1,400 to 1,900 psi, translating into simple pressure gradients of 0.50 to 0.63 psi/ft, whereas BHP's in the southern part of the basin commonly range from 400 to 1,000 psi (0.30 to 0.40 psi/ft). The 1,200-psi contour (fig. 49) approximately encloses the area of overpressuring defined by a simple pressure gradient of 0.44 psi/ft. The area of highest pressure (BHP's greater than 1,600) is located in New Mexico astride the San Juan River, is elongate northwest-southeast parallel to depositional strike, and is south of the structural axis of the basin as mapped on the Huerfanito Bentonite (fig. 9). The Meridian 400, Northeast Blanco, Sedro Canyon, and Los Pinos fields areas are in this region. To the southwest, between Sedro Canyon and Blanco areas, the pressure drops abruptly from approximately 1,500 psi to 800 psi over a lateral distance of approximately 10 mi. Low permeability is inferred from this steep, lateral pressure gradient, which coincides with the pinch-out of thick coal seams (figs. 4, 27, and 29) and conspicuous steepening of the potentiometric surface (fig. 45). Subsequently, to the southwest, pressure uniformly decreases to approximately 700 psi at Aztec area and to less than 400 psi at Gallegos South area. The lowest reported BHP's (less than 200 psi) occur in the San Juan River valley near the western margin of the basin.

Hydrochemistry

Hydrochemistry reflects rock-water interaction and the prevailing ground-water flow rates and directions. A hydrochemical map indicates ground-water circulation through distribution of mass or dissolved solids, whereas a head map indicates circulation through distribution of potential energy. In other words, chemical composition records actual ground-water movement (mass transfer), whereas hydraulic head shows the direction of force that drives ground-water flow. Because the ground water evolves chemically along its flow path, hydrochemistry can be used to help define recharge and discharge areas. Generally, ground water is freshest at the outcrop in recharge areas and the penetration of this fresh water into a basin marks the most

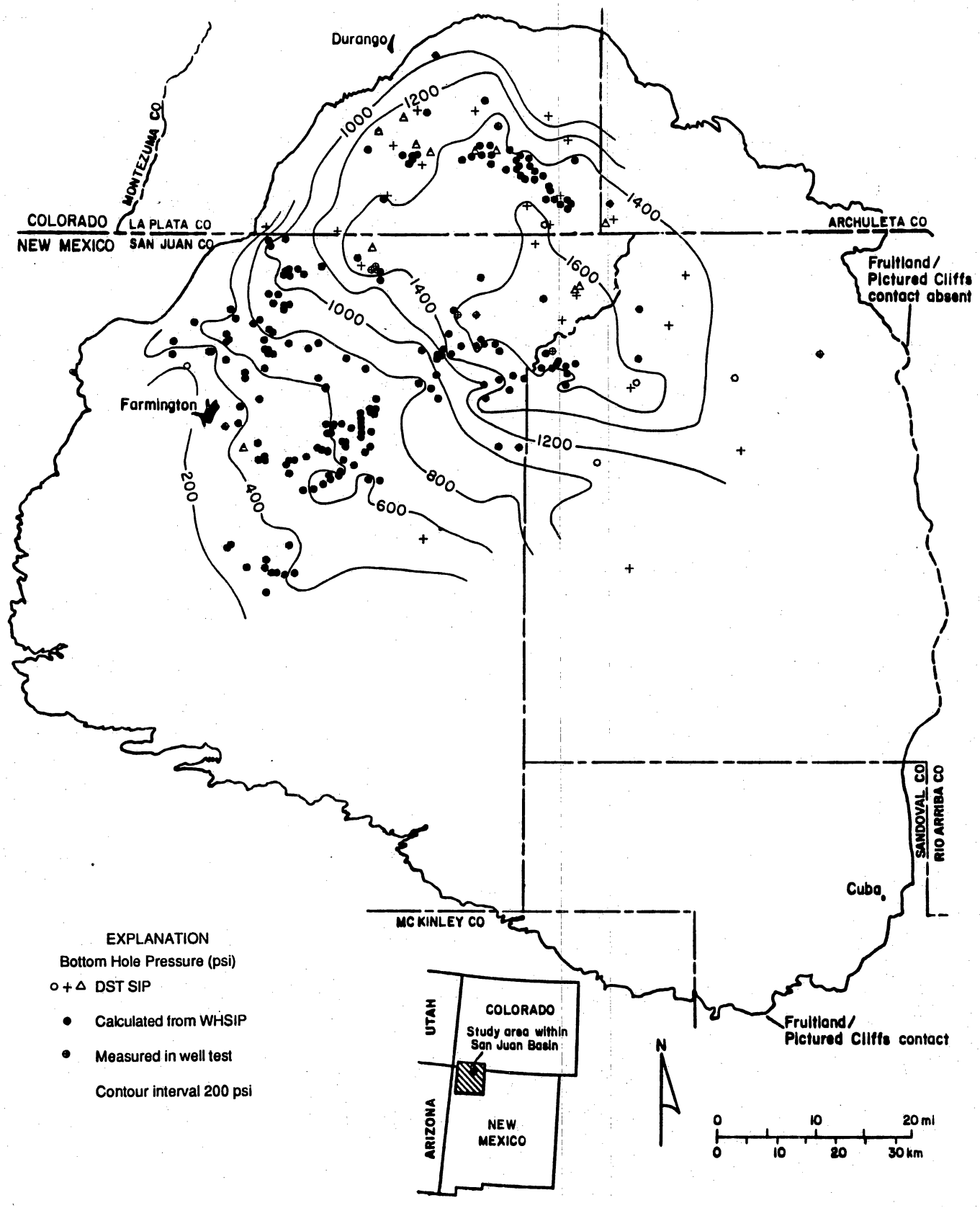

Figure 49. Fruitland Formation bottom-hole-pressure map.

permeable flow paths and implies an active, dynamic flow system. To further evaluate Fruitland hydrochemistry, a chlorinity map and Stiff ionic-ratio diagrams were prepared from approximately 250 chemical analyses disaggregated by geographic region and producing lithology. Most of the analyses are from the north-central part of the basin; a smaller number come from the northern and southern margins of the basin. Few analyses were available from the southern part of the basin, basinward of the margin. Chloride was mapped because it is a conservative chemical species unaffected by rock-water interaction. Ionic ratios allow discrimination among waters of the same type, or hydrochemical facies.

In the north-central part of the basin, the chlorinity map shows a fresh-water plume extending basinward from the north and northwest margins as predicted from the potentiometric-surface, or head, map (fig. 50). The distribution of dissolved solids, or mass, shows that flow is indeed in the directions inferred from the head map. For example, the Southern Ute–Mobil 36-1 well is positioned to receive recharge directly from the northwest margin of the basin. Predictably, its produced waters have a total dissolved solids (TDS) content of approximately 1,500 mg/L and contain 2 mg/L chloride. In contrast, the Southern Ute 1-24 well, although closer to the outcrop, should, as predicted from the chloride and head maps, receive little direct recharge from the outcrop. Indeed, its produced waters have a TDS content of approximately 10,000 mg/L and contain about 600 mg/L chloride.

Tongues of low-chloride water project basinward along generalized flow paths inferred from the head map, defining the configuration of the fresh-water recharge (fig. 50). Major tongues are oriented northwest-southeast, parallel to depositional strike and the orientation of aquifer coal seams. The northerly tongue in eastern La Plata County coincides with thick coal seams that extend to the outcrop (fig. 27), possibly serving as avenues for fresh recharge. A basinward protrusion of low-chloride water from the northwest margin also coincides with thick coals. Secondary tongues are oriented northeast-southwest and may reflect the dominant fracture trend (fig. 36), dip-elongate coal seams (fig. 25), Fruitland channel sandstone belts, or a combination of all three.

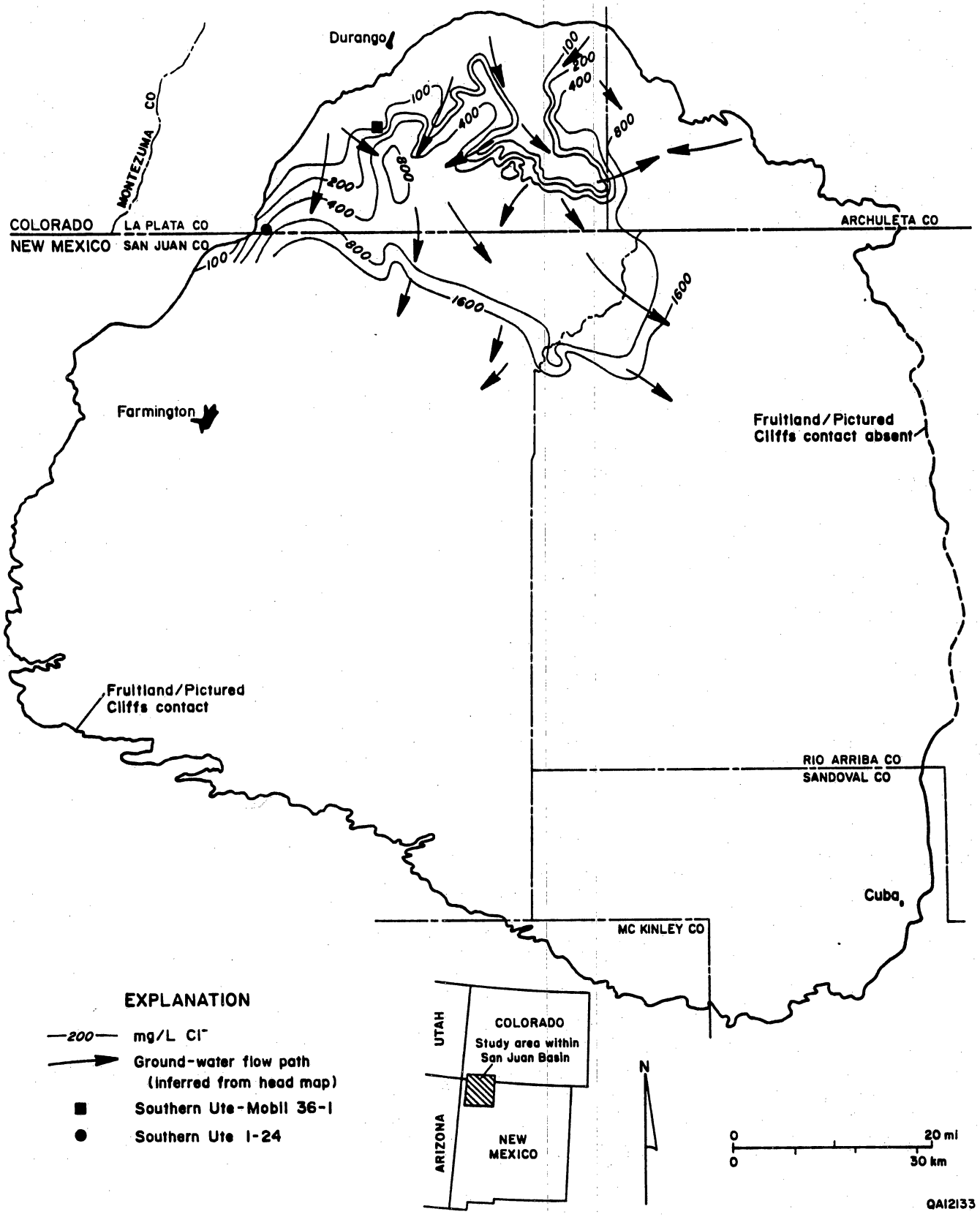

Figure 50. Chlorinity map of Fruitland produced formation waters, north-central part of the San Juan Basin.

Some extremely low-chloride waters are present. For example, waters located in T33N R6W, at the end of a 20-mi flow path, have chloride contents of less than 5 mg/L. Their meaning is ambiguous. Analytical error has been eliminated by the fact that the commonly used technique (AgCl titration) tends to produce results that err on the high side. Possibly, the low chlorinities reflect recharge of fresh Pleistocene waters, which commonly are very low in chloride, and therefore relatively fast ground-water flow rates and short residence times. The age of ground water from the Ojo Alamo Sandstone in the southwest part of the basin, based on ^{14}C dating, ranges from modern to 26,000 yr B.P. (Phillips and others, 1989). Lateral ground-water velocities in the Fruitland Formation, based on heat-flow data (McCord, 1988) and permeability values consistent with the highest aquifer test values (50 md), yield, respectively, rates of 6.1 and 6.4 ft/yr, which translates to travel (residence) times of approximately 17,000 yr (20 mi at 6.1 or 6.4 ft/yr). This age corresponds almost exactly to that of a major recharge event calculated from stable isotopes in San Juan Basin ground water and is close to another event dated at approximately 22,000 yr B.P. (Phillips and others, 1986). When Fruitland aquifer permeabilities typically reported in well tests (10 md or less) are used, relatively long travel times of greater than 80,000 yr are calculated. Because permeability in a fractured reservoir is scale dependent, or increases with sample size (Garven, 1986), high permeabilities (fast ground-water flow times) are predictable from heat-flow data.

Fruitland formation waters are chemically diverse and reflect the hydrologic setting rather than the producing lithology. Their diversity was investigated earlier using Piper (trilinear) diagrams (Kaiser and Swartz, 1988, 1989). However, Piper diagrams cannot be used to differentiate among waters of the same type, whereas ionic ratios can be used to better fingerprint waters of the same hydrochemical facies (Novak and Eckstein, 1988). Thus, to further evaluate Fruitland hydrochemistry, we modified the Stiff diagram, plotting eight ionic ratios: Ca+Mg/Na+K, Mg/Ca, Ca/Na+K, SO_4/Na+K, Na+K/HCO_3, Ca+Mg/HCO_3+CO_3, Cl/Na+K, and SO_4/Cl. A computer program (STIFF4N) was written to calculate ionic ratios in terms of meq/L and to plot the diagrams.

To evaluate chemical characteristics of waters produced from coal and sandstone we plotted by lithology analyses of waters sampled in wells in T33N, R7W. Waters from each lithology are Na-HCO_3 facies and have ionic-ratio diagrams of similar shape and ionic ratios (figs. 51 and 52); that is, the variations seen are common to waters from both lithologies, showing that chemical composition should not be used to identify completion lithology. However, some coal waters have large Mg^{2+}/Ca^{2+} ratios, giving the diagram a distinctive triangular segment, or magnesium triangle. Coal waters from Meridian 400 area have Mg^{2+}/Ca^{2+} ratios as large as 12 (fig. 53), whereas those from Cedar Hill (fig. 54) are not unusually large but are similar to those in T33N, R7W. Note the similarity of coal and sandstone waters at Cedar Hill.

Waters in the north-central part of the basin are unique in their very high HCO^{3-} contents (several 1,000 mg/L up to 25,000 mg/L), low Cl^- contents (tens to hundreds of mg/L), and possible enrichment in Mg^{2+}. Although HCO_3^- is reported in analytical results, total alkalinity titration is the actual analysis performed on the sample. Besides HCO_3^- and CO_3^{2-}, organic acid anions are important contributors to total alkalinity. Most HCO_3^- values (total alkalinity) in excess of several hundred mg/L are probably due to the presence of such organic acids as acetic and propionic (Kharaka and others, 1985, 1986; Morton and Land, 1987). Up to 100 percent of field-determined alkalinities in oil and gas field waters may be contributed by organic species (Carothers and Kharaka, 1978; Lundegard and Land, 1986). Laboratory oxidation of brown coal yields organic acid contents in excess of 16,000 mg/L (Surdam and others, 1989). The high reported HCO_3^- contents and neutral to slightly alkaline pH's (approximately 8) of the produced waters in the north-central part of the basin strongly supports the presence of abundant organic acids. However, we can only speculate about their origin and preservation. The organic acids are thought to have been generated by the late Oligocene thermal (oxidation) event (Bond, 1984). At 70 °C, organics are generated faster than they are destroyed by bacteria and at 100 °C their half life is 20 to 60 m.y. (Y. K. Kharaka, 1989, personal communication, 1989). Although concentration of organics is independent of temperature (Shock, 1988), organics probably are not forming today because present subsurface

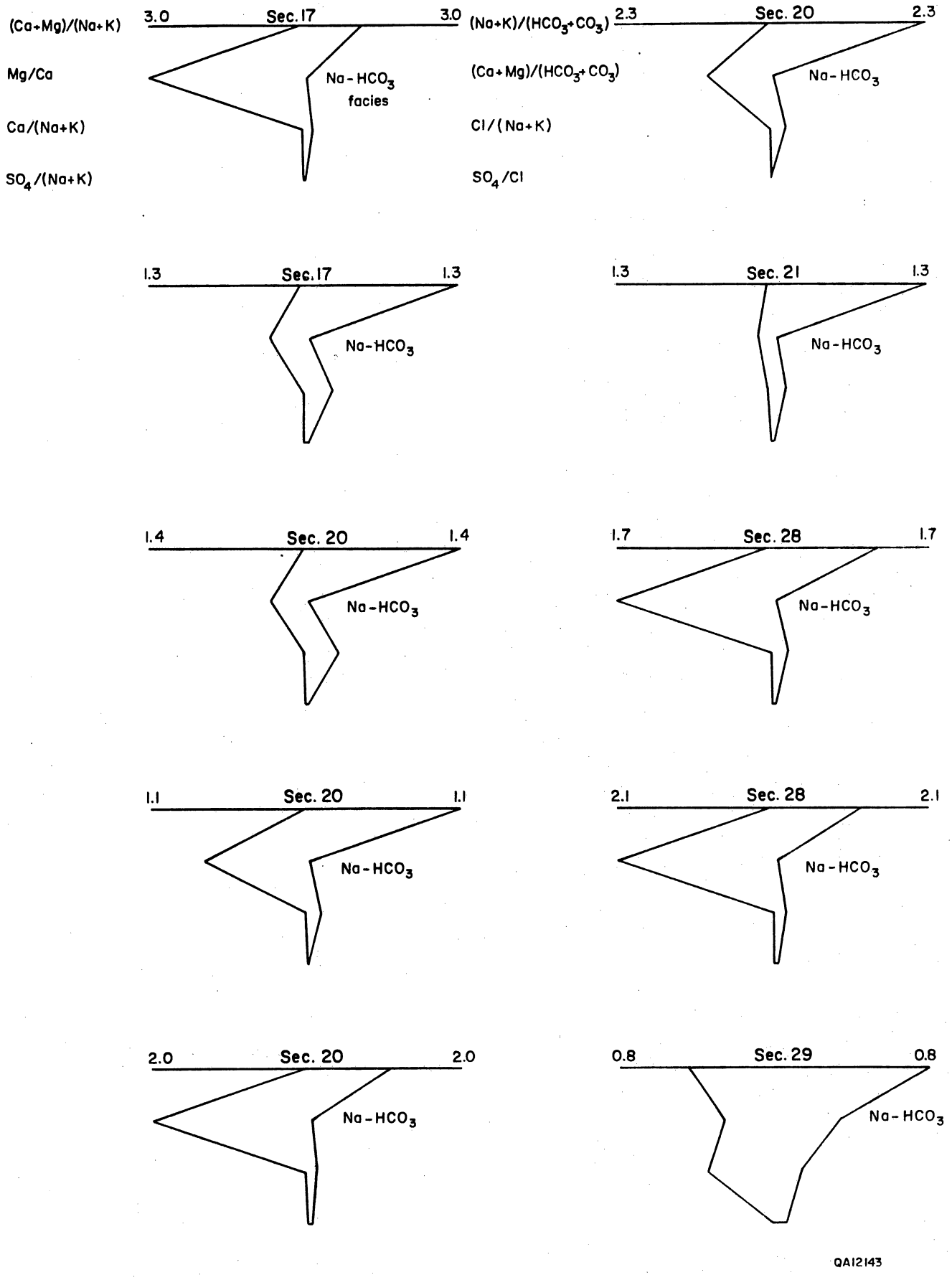

Figure 51. Stiff ionic-ratio diagrams, Fruitland coal waters, T33N, R7W.

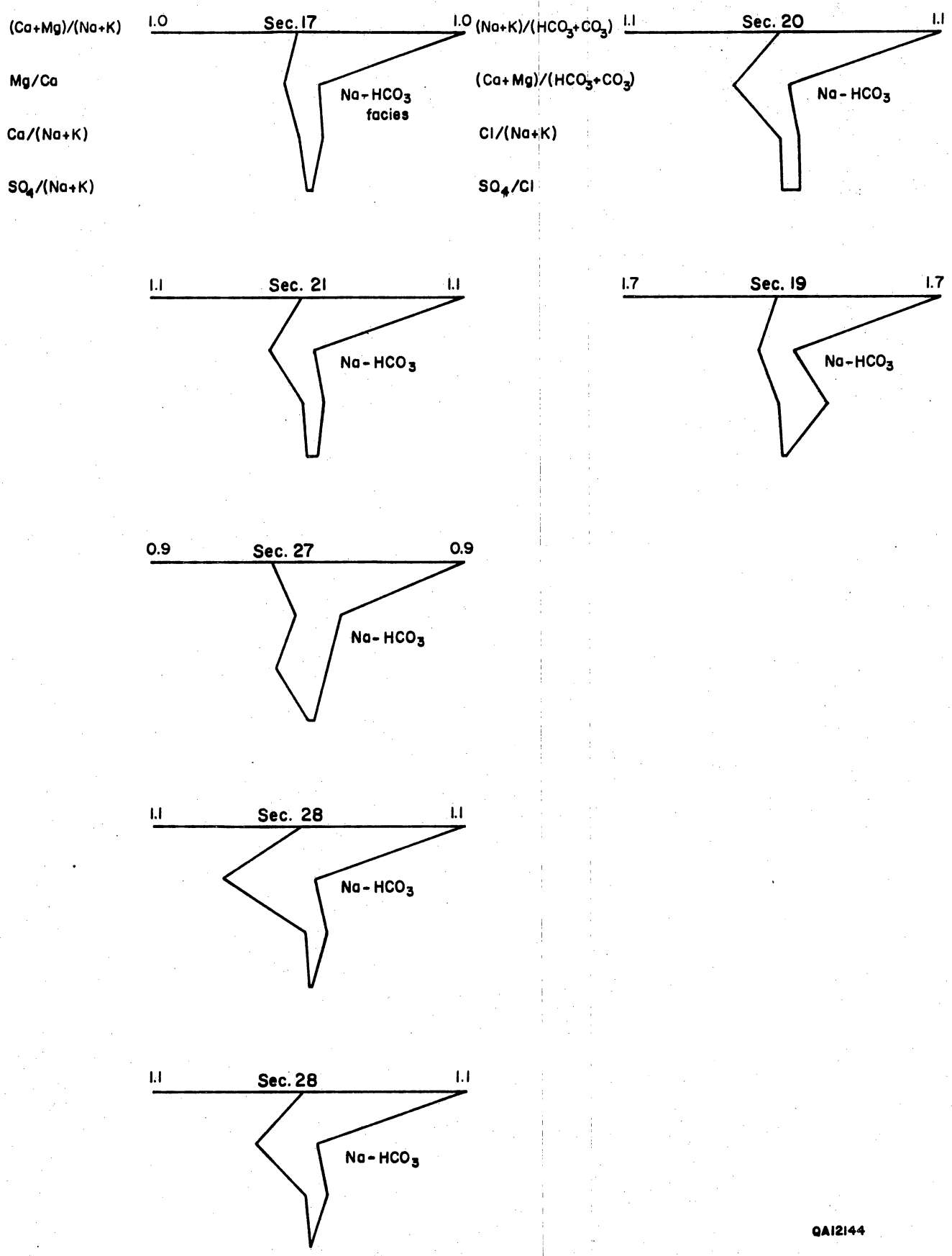

Figure 52. Stiff ionic-ratio diagrams, Fruitland sandstone waters, T33N, R7W.

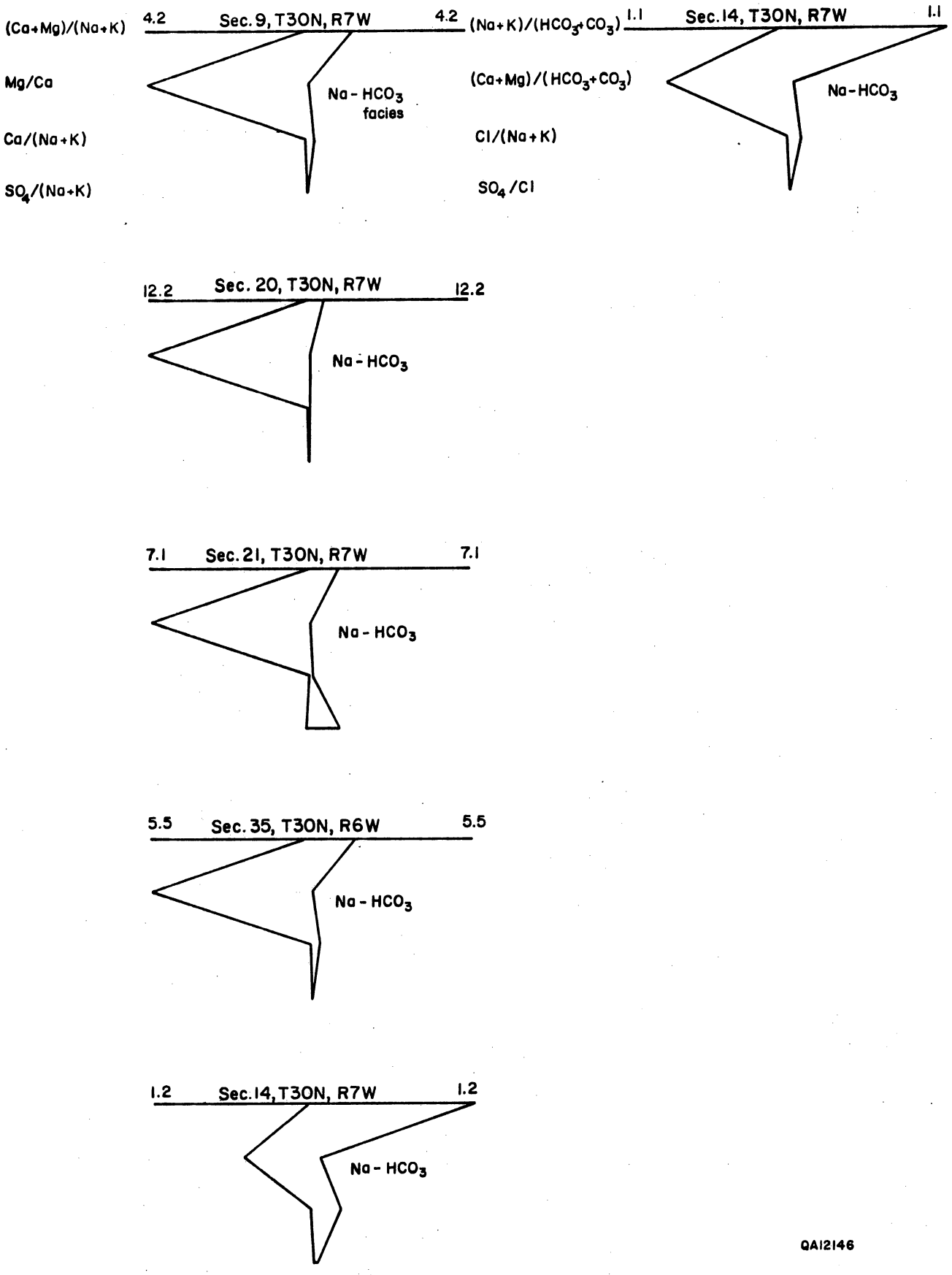

Figure 53. Stiff ionic-ratio diagrams, Fruitland coal waters, Meridian area.

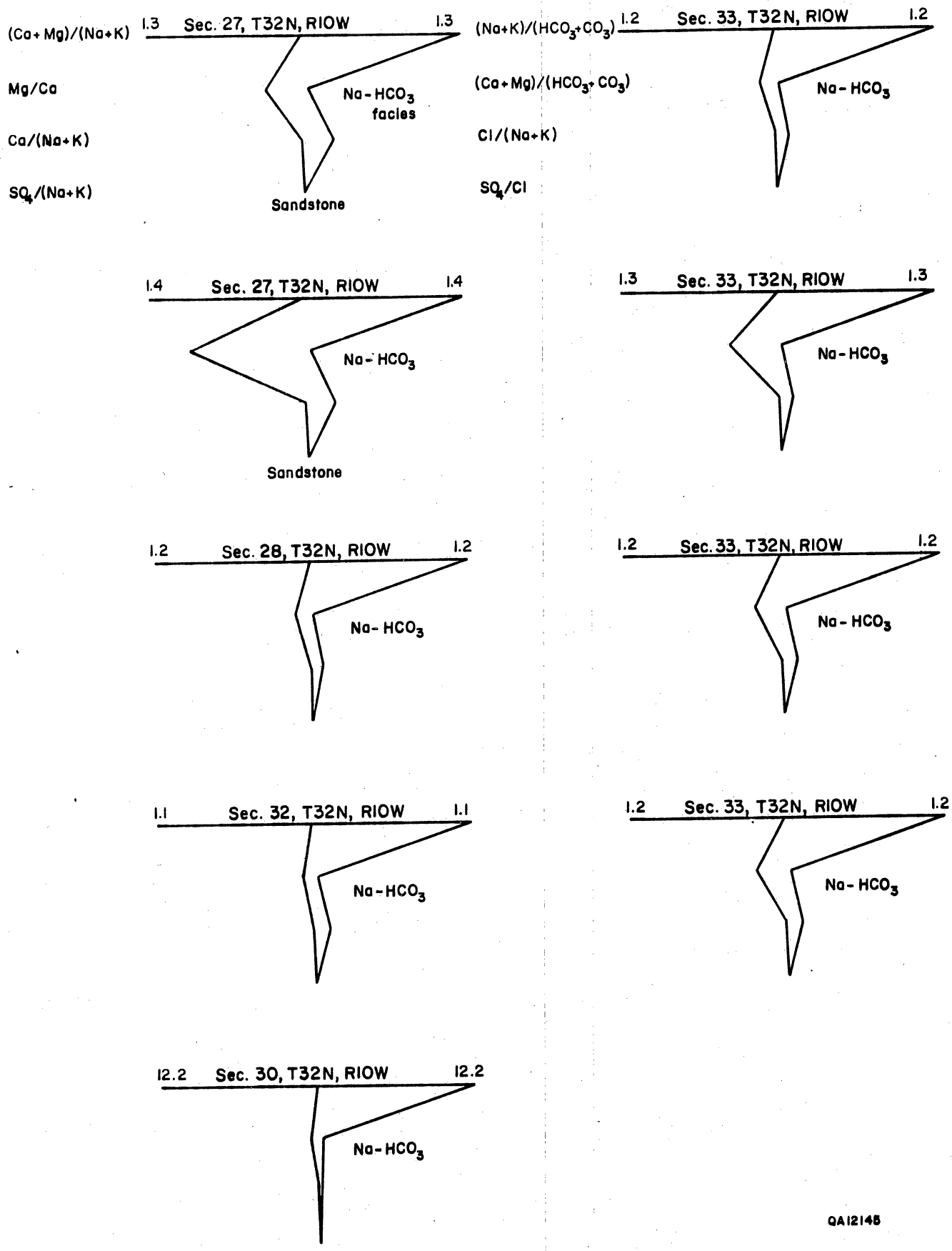

Figure 54. Stiff ionic-ratio diagrams, Fruitland coal and sandstone waters, Cedar Hill area.

temperatures are too cool (~ 50 °C or ~ 125 °F). However, organic acids content (alkalinities) increases basinward, and enrichment from below in areas of upward flow is possible. Preservation of the organics implies an environment toxic to bacteria such as the presence of phenols (R. C. Surdam, 1989, personal communication, 1989) or insufficient nutrients (mainly P and N). Sluggish circulation of meteoric water basinward as well as lack of time since the Oligocene for bacterial degradation of organics may also be factors in their preservation. On the basis of carbon-isotopic data, bacterial activity is inferred to be minimal. Coalbed methane has $\delta^{13}C$ values ranging from -44 to -39 ppt, which is typical of thermogenic gas and isotopically much heavier than values ($\delta^{13}C$ < -55 ppt) for bacterial, or biogenic, methane (Rice and others, 1988).

In reality, waters in the north-central part of the basin may actually be Na-acetate or Na-oxalate waters diluted by fresh, low-chloride meteoric waters (fig. 50), and not Na-HCO_3 waters. Magnesium enrichment is problematical. Calcium analyses are suspect in many waters; some analyses report zero Ca^{2+}, which is highly unlikely. Commonly Ca^{2+} is analyzed by EDTA titration and Mg^{2+} is calculated by difference, based on hardness. If the sample size is too small and the titrant too concentrated, an end point shows immediately and zero Ca^{2+} is reported. This means that Mg^{2+} will be erroneously high. However, it is possible that the large Mg^{2+}/Ca^{2+} ratios in some coal waters have physical meaning. The solubilities of Ca-oxalate and Ca-malonate are very low (Kharaka and others, 1986), and precipitation of these compounds by waters rich in organics could drastically lower Ca^{2+} concentration. Moreover, the solubility of calcite is less than that of magnesite and in ion exchange Ca^{2+} is more strongly adsorbed than Mg^{2+}. Interestingly, the faces of coal cleats observed in cores show calcite and gypsum mineralization (Tremain and Whitehead, this report).

Waters from the north margin of the basin graphically differ from those of the north-central part of the basin. Those of the north margin are Ca-Mg and Na-HCO_3 type waters that have large SO_4^{2-}/Cl^- ratios (up to 116), giving the ionic-ratio diagram a distinctive triangular foot, or sulfate triangle (fig. 55), which allows easy differentiation among Na-HCO_3 type waters from

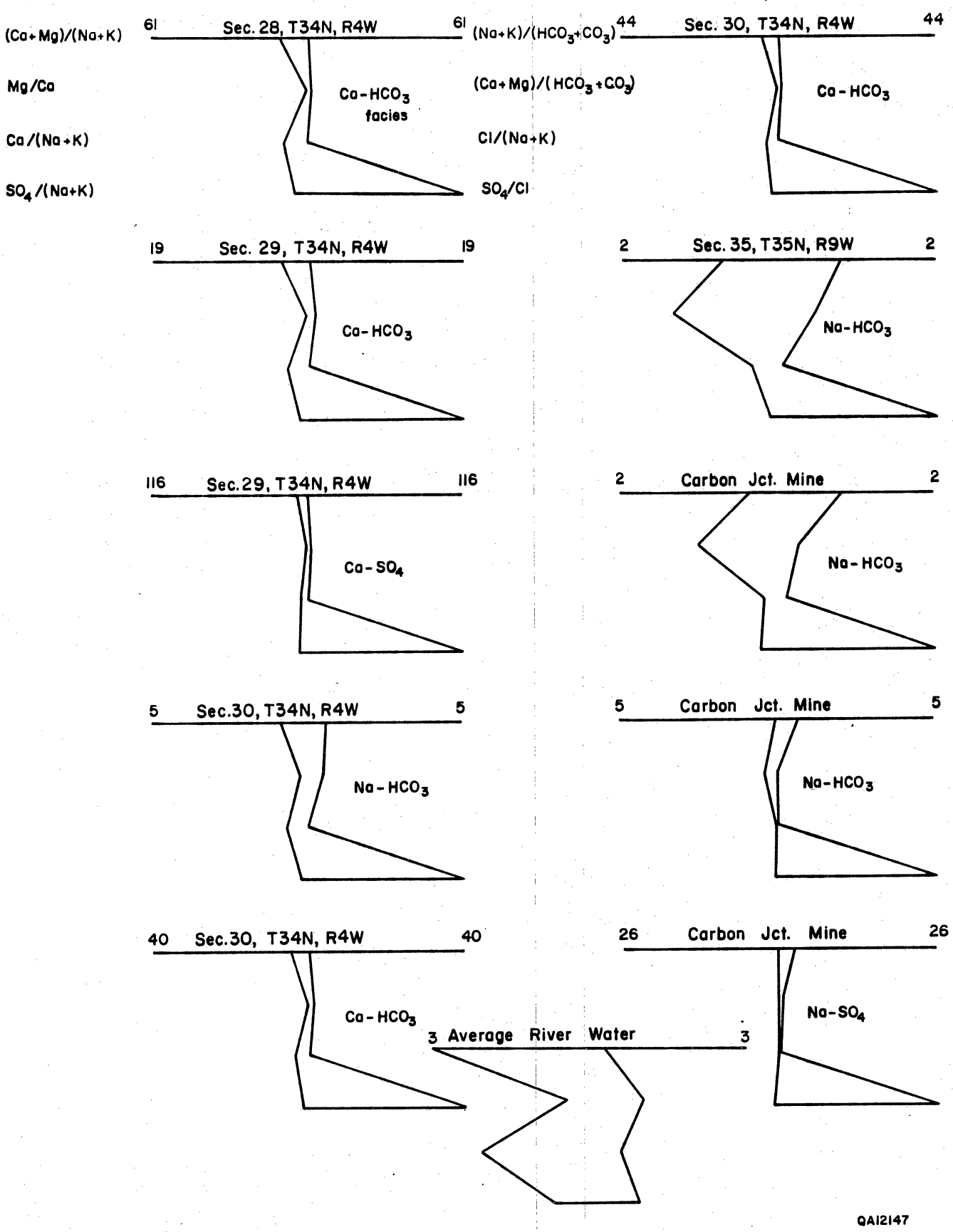

Figure 55. Stiff ionic-ratio diagrams, Fruitland waters, northern margin of San Juan Basin.

the north margin and north-central part of the basin. The pattern for world average river water is shown for comparison (fig. 55). Note the absence of sulfate and magnesium triangles. Apparently, northern meteoric waters evolve by addition of SO_4^{2-} and Mg^{2+}, followed downflow by loss of SO_4^{2-}, addition of Cl^-, Na^+, and HCO_3^- (organics), and possible addition of Mg^{2+} as well as loss or no addition of Ca^{2+}.

Waters from the southern margin of the basin are sodium dominated, with Na-HCO_3, Na-SO_4, and Na-Cl facies or types being present. Consequently, waters display a variety of diagram shapes (figs. 56 and 57), illustrating the diversity of chemical facies in the Fruitland Formation. Na-SO_4 waters are thought to be the chemically evolved shallow ground water because thenardite (Na_2SO_4) is deposited by area spring waters (Stone and others, 1983). Among the 29 analyses plotted from the southern margin of the basin, 19 have a sulfate triangle, 7 a magnesium triangle, and 3 a north-central basin signature (similar facies and diagram shape). All diagrams from the southern margin are dissimilar to those for world average river water and seawater (figs. 55 and 58). Three coal waters located basinward in T24N, R9W have diagrams identical to that for seawater (fig. 58). These waters have TDS contents of 30,000 to 42,000 mg/L and chlorinities of 18,000 to 26,000 mg/L. Their $Na+K/HCO_3+CO_3$ ratios are less than seawater, suggesting some meteoric dilution. Finally, their presence further indicates limited recharge from the southern margin of the basin.

CONCLUSIONS

1. Recharge to the Fruitland–Pictured Cliffs aquifer system is limited from the eastern, southern, and western margins of the basin because the aquifer thins and becomes shalier eastward, there is low annual precipitation along those margins, and the aquifer outcrop is topographically low to the basin interior such that potential Fruitland recharge is diverted out of the basin. The western margin of the basin is driest and probably contributes the least amount of recharge. Fruitland potentiometric mounds represent pressure mounds due to

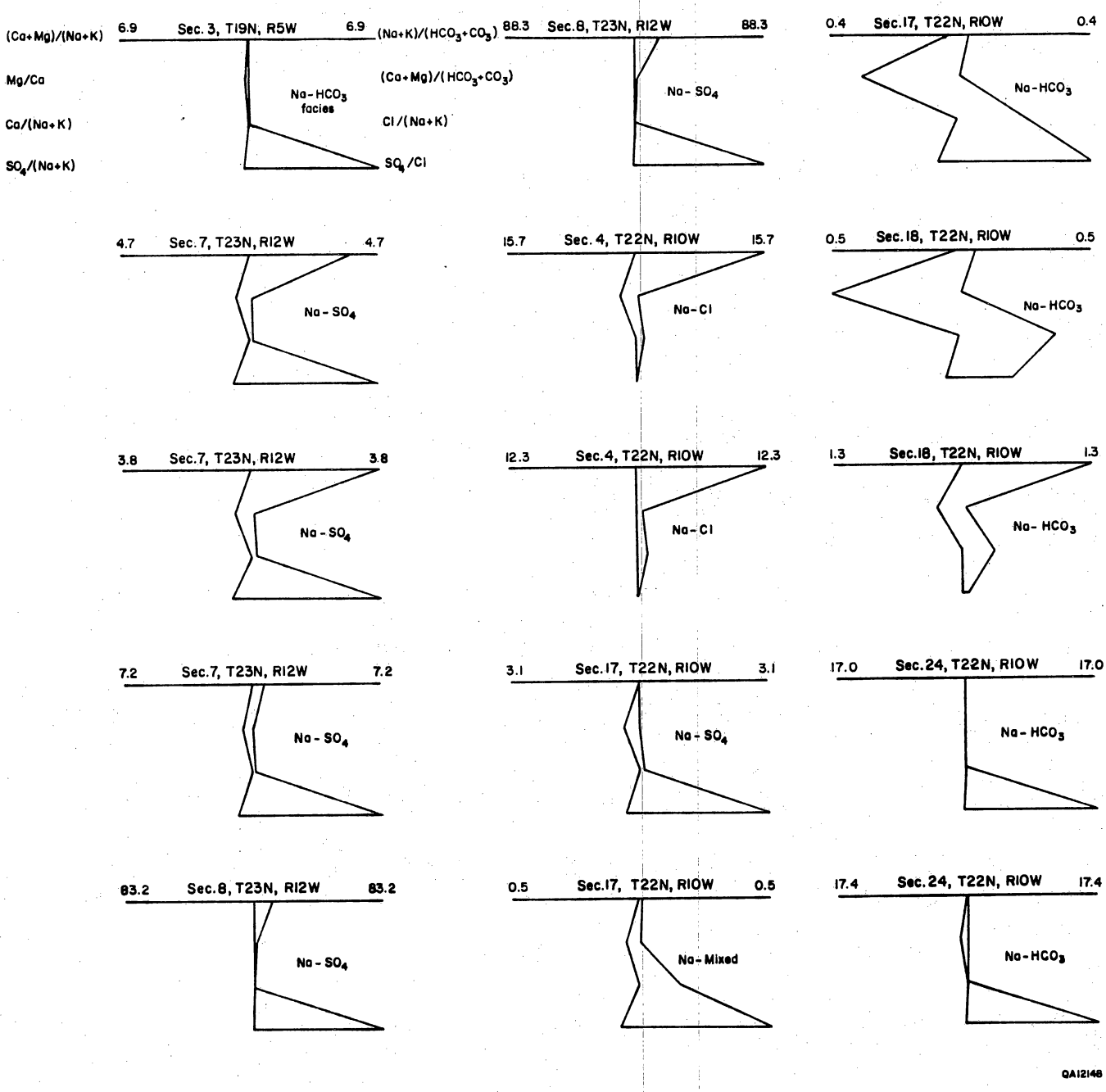

Figure 56. Stiff ionic-ratio diagrams, Fruitland waters, southern margin of San Juan Basin.

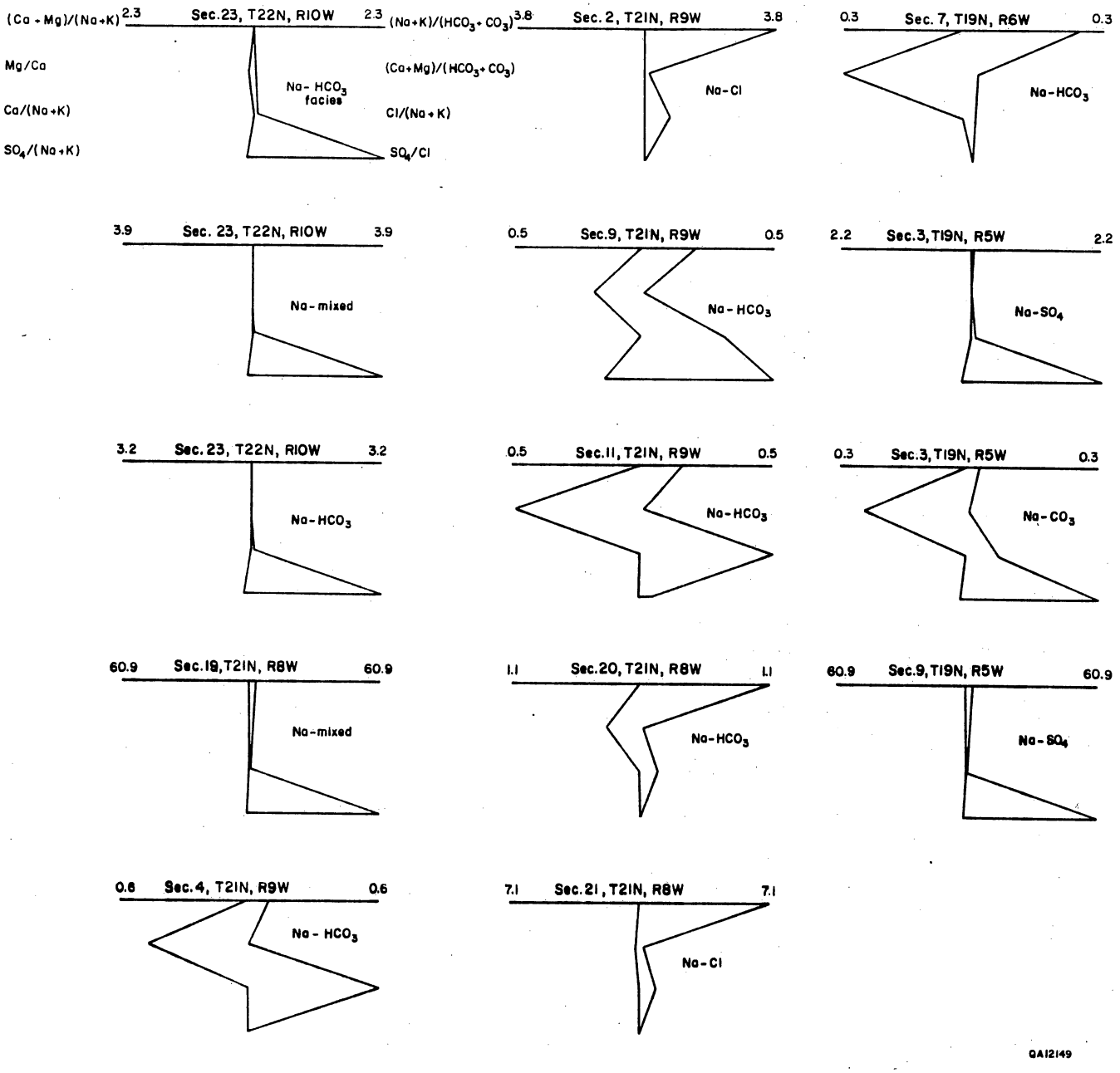

Figure 57. Stiff ionic-ratio diagrams, Fruitland waters, southern margin of San Juan Basin.

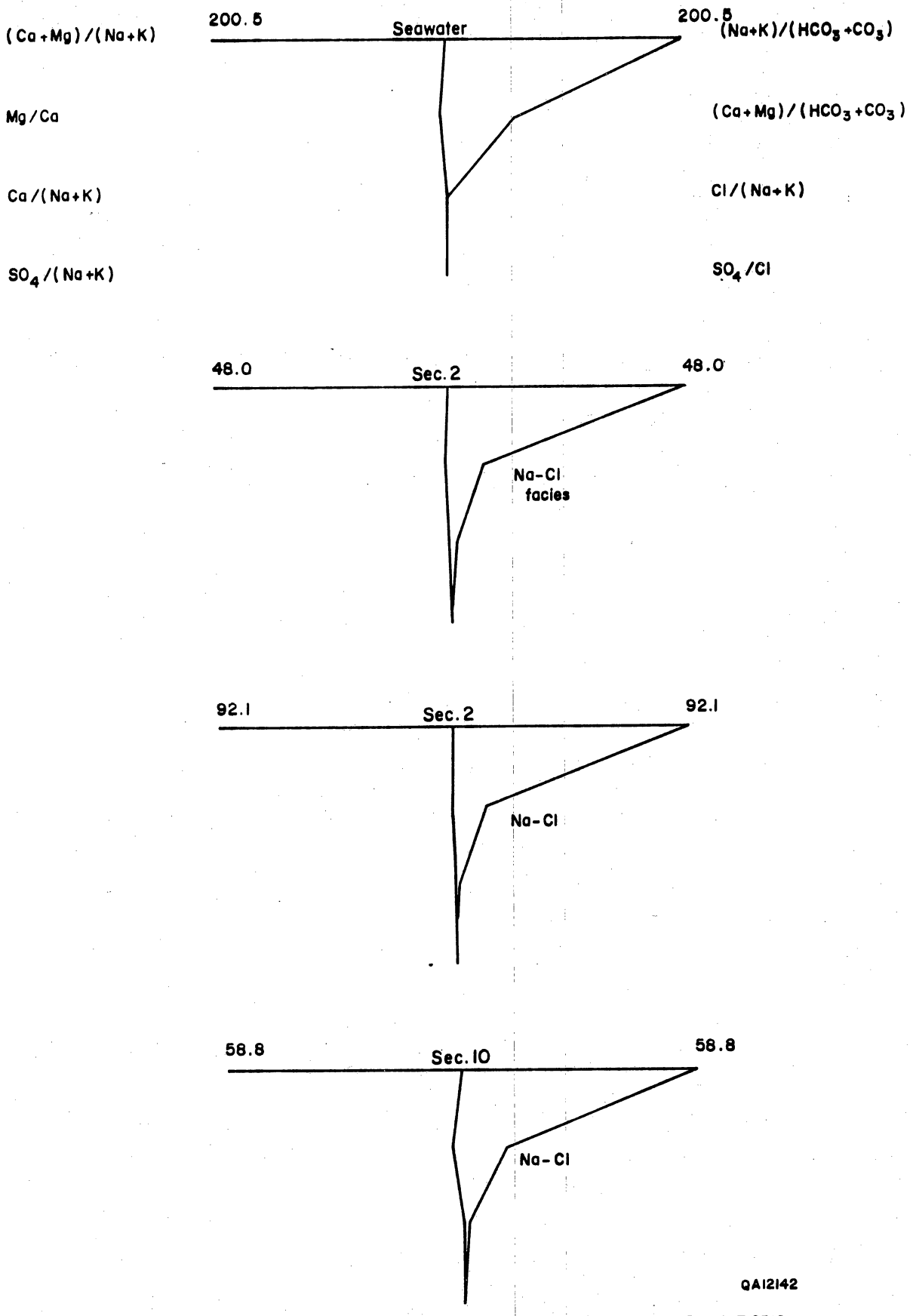

Figure 58. Stiff ionic-ratio diagrams, Fruitland coal waters, T24N, R9W.

upward flow of ground water. Upward flow in the north-central part of the basin is attributed to aquifer pinch-out and confinement basinward, whereas in the west-central part of the basin it is a consequence of regional ground-water discharge to the San Juan River valley. In the west-central part of the basin, Fruitland and Pictured Cliffs heads are about the same, and the two units are in hydraulic communication. In the north-central part of the basin, heads in the Fruitland and Pictured Cliffs differ greatly because of their contrasting permeabilities and lack of hydraulic communication between them. The high-permeability Fruitland Formation is an aquifer and is not part of the Kirtland/Fruitland confining unit. Coal seams are the primary aquifers in the Fruitland Formation.

2. Anomalous areas of overpressuring in the underpressured, west-central part of the basin are explained hydrodynamically (upward flow), whereas anomalously underpressured areas in the overpressured, north-central part of the basin are attributed to pressure decline upon gas production. The 1,200-psi BHP contour approximately encloses the overpressured area. The highest BHP's (1,600 to 1,900 psi) are in the Meridian 400, Northeast Blanco, Sedro Canyon, and Los Pinos areas. Low permeability regionally and locally is inferred from steep lateral pressure gradients. Although the Fruitland Formation behaves regionally as a single hydrologic unit or homogeneous aquifer (Kaiser and Swartz, 1988, 1989), large vertical and lateral pressure gradients locally indicate that Fruitland strata may be hydraulically disconnected and behave at the local, or field, scale as a heterogeneous aquifer. Shale interbeds and abundant tonsteins may limit vertical connectivity between and within coal seams.

3. Permeabilities estimated from heat-flow data are larger than those calculated from well tests, reflecting the fact that permeability in fractured reservoirs is scale dependent, or increases with sample size. Regional aquifer interconnectedness follows from higher permeability regionally, whereas local disconnectedness is inferred from lower permeability locally. Consequently, the Fruitland Formation can behave regionally and locally, respectively, as a homogeneous and heterogeneous aquifer.

4. The distribution of low-chloride ground water in the north-central part of the basin complements flow patterns inferred from the head map and coincides with the overpressured area. The close correlation between chlorinity and the present-day flow system shows conclusively that these low-chloride waters are not fresh connate waters but evolved meteoric waters. Their presence is indicative of an active, dynamic flow system and of permeable pathways. Thus, the distribution of mass (dissolved solids) and potential energy indicates permeability anisotropy and identifies regional, ground-water flow paths.

5. Stiff ionic-ratio diagrams can be used to characterize waters of the same chemical facies. Waters in the north-central part of the basin are unique in their very high alkalinities and low chlorinities. In reality, they may be mixtures of Na-organic acid waters and low-chloride, meteoric waters, rather than Na-HCO_3 waters. Waters in the southern part of the basin are Na-Cl type and are inferred to be marine connate waters. Their presence indicates limited recharge from the southern margin of the basin and low permeability.

6. Coalbed methane wells in the hydrologically less active southern part of the basin should produce gas water free and be inexpensive to operate. Large vertical and lateral pressure gradients are indicative of reservoir compartmentalization, or heterogeneity. Well spacing will have to be established accordingly to maximize recovery of coalbed methane. Produced coalbed waters are compositionally diverse, reflecting their hydrologic setting, and the sources of their high alkalinities are uncertain. Successful disposal (injection) and well stimulation will depend on their chemical compatibility with host formation waters and completion fluids.

HYDROGEOLOGIC PARAMETERS FOR THE PRODUCIBILITY OF COALBED METHANE

W. R. Kaiser, T. E. Swartz, W. A. Ambrose, and W. B. Ayers, Jr.

INTRODUCTION

Little is known about the hydrogeology of coal basins and its relation to the producibility of coalbed methane. The importance of permeability and coalbed thickness is obvious, as is the need to dewater (depressure) some coal seams to stimulate gas desorption. However, lacking knowledge of the structural setting, distribution of coal seams, and sandstone geometry, we can say little, for example, about favorability of production in structurally complex or simple areas, from a single thick coal seam or several thinner seams, or the role of differential compaction in permeability enhancement, respectively. The relative importance of structural/stratigraphic trapping and adsorption remains clouded without an understanding of structure, stratigraphy, and pressure regime. Earlier it was concluded that hydraulic head, pressure regime, and hydrochemistry are indicators of gas producibility because they indicate an aquifer's permeability, or ability to accept and transmit fluid (Kaiser and Swartz, 1988, 1989).

The relative importance of such hydrogeologic parameters as seam thickness, folds, faults, and joints, hydraulic head, and pressure regime as controls or indicators of the producibility of coalbed methane is the focus of this paper. A review of coalbed methane production is followed by a discussion of correlations among these hydrogeologic parameters and the producibility of coalbed methane. Finally, potential for future coalbed methane production is evaluated in a basinwide hydrogeologic characterization of the Fruitland Formation.

PRODUCTION

Our analysis of Fruitland production is based on data collected by the Colorado Geological Survey, which provided gas and water production through 1987 on an annual basis and monthly for the first year of production for all reported Fruitland completions. We evaluated each completion to confirm its Fruitland status and to determine the lithology of the producing interval. Through 1987, the basinwide tally is 396 definite Fruitland completions (113 coal, 224 sandstone, 59 coal and sandstone) and 52 indeterminate (no log or poor log) but probable Fruitland completions. In addition, recent Petroleum Information reports were searched and initial potentials for 71 new coalbed methane completions were recorded. There were many Meridian Oil completions that were reported as shut-in gas wells with no test data available.

Statistics

To better compare productivity among wells with long and short productive lives, minimizing the time variable inherent in cumulative production data, we plotted initial potential (IP) and maximum annual production (MAP) normalized to Mcf/d, where MAP is a well's highest annual production to date or during its productive life. In other words, one can better compare wells that have produced for a long time with those of short production times. However, there is no way to account for negative decline in the early years of a coalbed methane well's production. Commonly, IP's were run for 3 hours on 3/4-inch choke and are from stimulated and unstimulated wells. There are more IP's available than MAP's because many completions are recent, and in dually completed wells, IP's usually are conducted separately for each formation, whereas production is commingled.

Histograms of IP and MAP for coal and sandstone completions shows them to be log normally distributed (fig. 59); a cross plot of IP and MAP shows no relation. On initial testing,

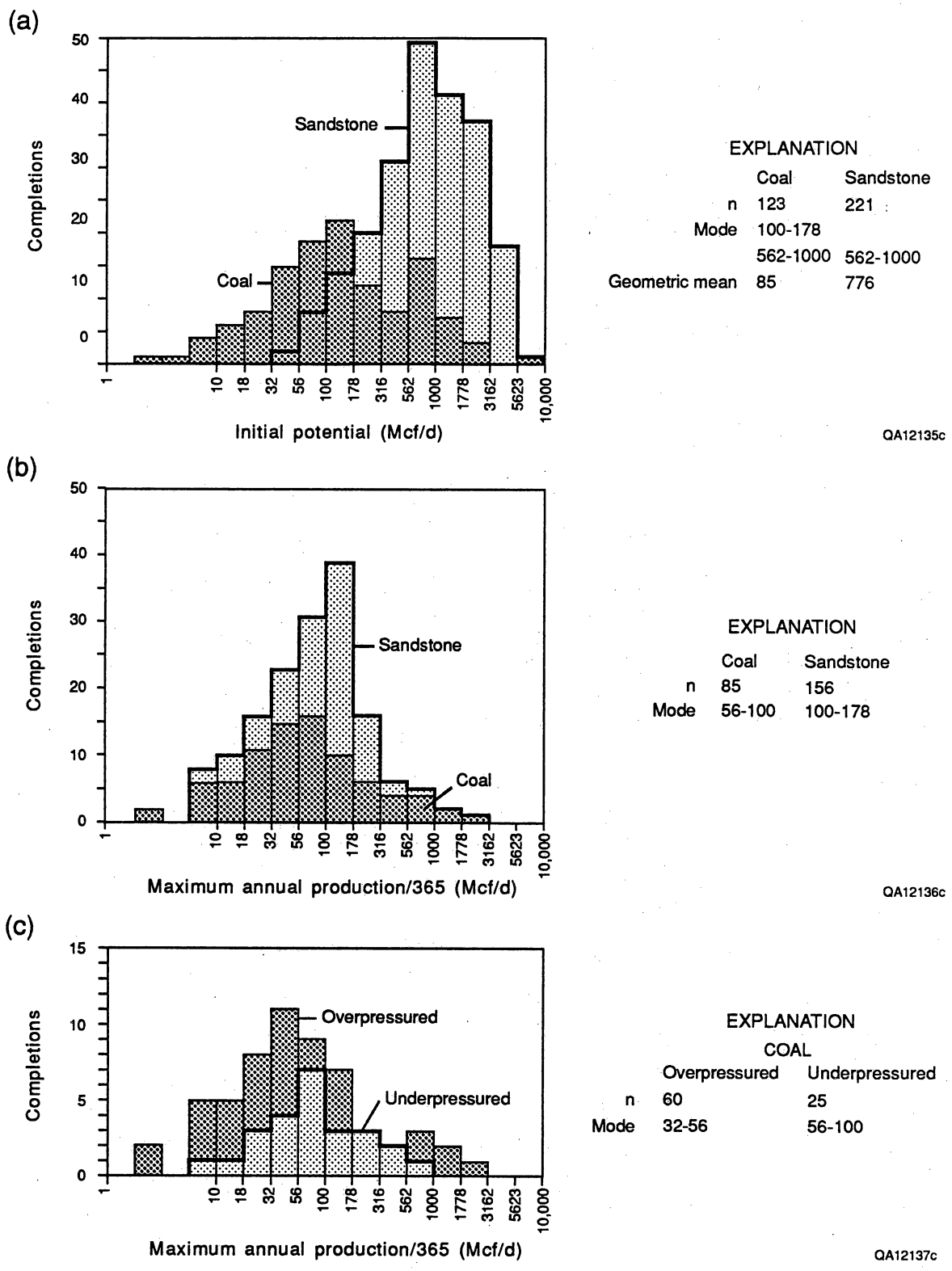

Figure 59. Nested histograms of Fruitland Formation initial potential and maximum-annual production.

coalbed methane production is bimodal; the second mode coincides with the sandstone production mode (fig. 59a), indicating the presence of some coal seams with free gas (significant fracture porosity) and/or fluid pressure below desorption pressure. On the other hand, low IP's may signal the presence of mainly adsorbed gas (fluid pressure above desorption pressure). The geometric mean for coal is much less than that of sandstone and undoubtedly reflects the typical early production behavior of coal reservoirs, when fluid pressure and water saturation are high.

Histograms of MAP from coal and sandstone completions have similar modes and identical geometric means (fig. 59b), suggesting that coal reservoirs have production rates similar to sandstone reservoirs after initial depressurization and the onset of desorption. In other words, the two reservoir types have similar production rates after negative decline in coal reservoirs is completed. Moreover, on the basis of similar production rates, fracture permeability of similar magnitude is inferred for coal and sandstone reservoirs. As expected, the sandstone MAP mode (100 to 178 Mcf/d) is much less than its IP mode (562 to 1,000 Mcf/d). A coal MAP mode (56 to 100 Mcf/d) less than its IP mode (100 to 178 Mcf/d) was unexpected and is not readily explained. A partial explanation may be that MAP modes are normalized to 365 d/yr and thus are minimum values. Negative decline is also a probable factor. In a plot of MAP for coal by pressure regime, the mode for overpressured coal seams is less than that for underpressured seams (fig. 59c). This probably reflects negative decline and the fact that many overpressured wells have not reached maximum production; only 8 and 3 wells, respectively, have greater than 5 yr and 10 yr of production. A secondary mode for overpressured coal seams (562 to 1,000 Mcf/d) reflects high MAP's in Meridian 400 and Cedar Hill areas, recorded in production times as short as 3 yr. Here, the presence of free gas and extraordinarily high fracture porosity is suspected. Alternatively, fluid pressure may be close to desorption pressure, allowing gas to desorb upon only slight depressurization.

Reservoir behavior is also evident in cumulative relative frequency plots of MAP by lithology and pressure regime (fig. 60). The low-value tail on the coal-overpressured curve is

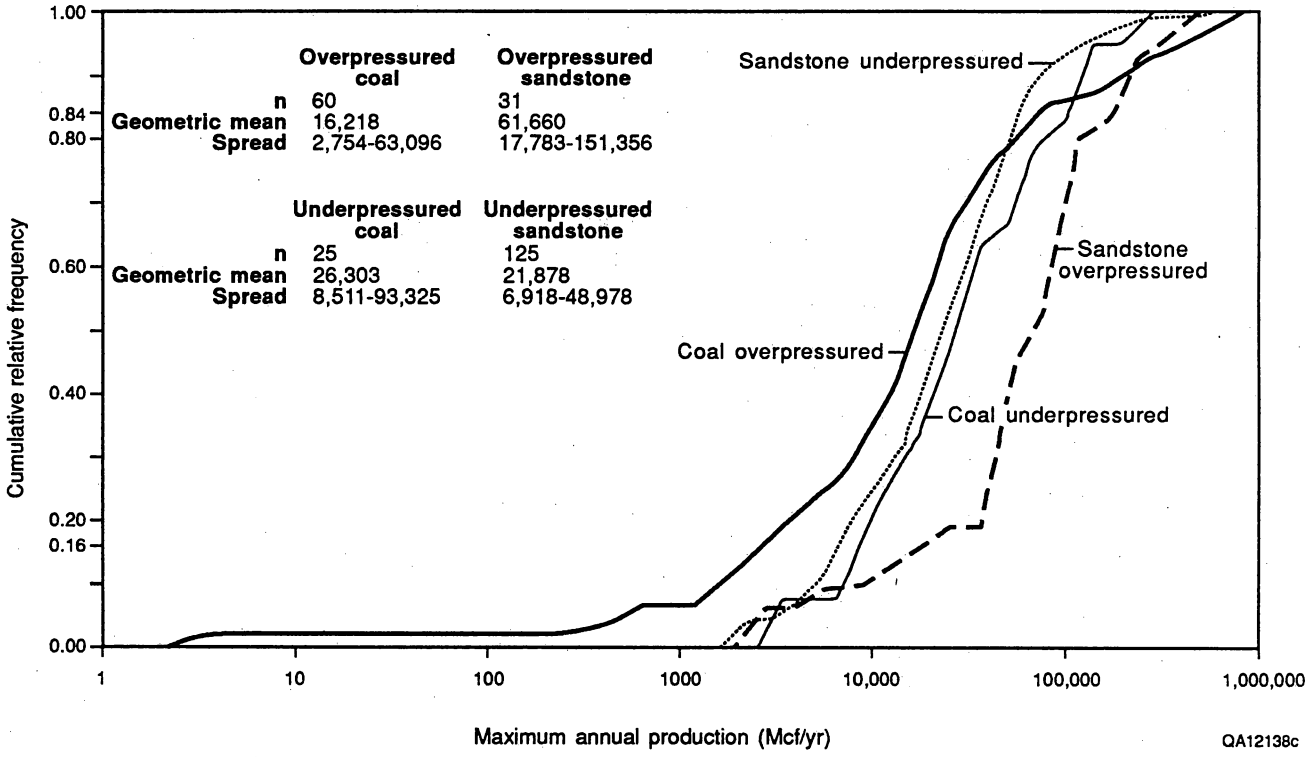

Figure 60. Cumulative relative frequency plots of Fruitland Formation maximum-annual production by lithology and pressure regime.

thought to reflect negative decline. The frequency curves for underpressured coal and sandstone are similar over the central 68 percent of the distribution, or spread between 16 and 84 percent, showing that they have similar production rates. Furthermore, it is thought to indicate that the underpressured coal seams contain free gas and possibly are below desorption pressure. High productivities from overpressured sandstones reflect the better deliverabilities expected from high-pressure conventional reservoirs. Note that this is not the case for high-pressure coal reservoirs.

Decline Behavior

We evaluated decline behavior by comparing production histories of coal and sandstone completions using decline curves and Q plots. The Q plot was developed by Research & Engineering Consultants, Inc. (REC, 1989a, 1989b). First year production (Q_1) divided by cumulative production to date (Q_{total}) is plotted against years of production, allowing comparison of decline behavior of wells individually, by reservoir, and by stratigraphic interval. To facilitate analysis, type decline curves were generated for selected decline rate factors of 5, 10, 20, 30, 50, and 75 percent per year, assuming exponential decline. With time, the curves asymptotically approach the selected rate factor.

Because long production histories are required to establish decline rates and there are many such sandstone wells, a basinwide plot of sandstone completions is used to introduce Q plots. Sandstones commonly show steep decline (20 to 50 percent) early in their production and typically less than 20 percent decline later, beyond 15 yr of production (fig. 61). Low decline rates are expected in the oldest wells as they should be little affected by depletion in offset wells. Newer wells (less than 15 yr production) showing steep decline probably are experiencing depletion due to production from older offset wells, whereas those with little decline (less than 10 percent) probably represent completions in new reservoirs. Scatter over the entire range of the Q plot reflects completions in a great number of different reservoirs.

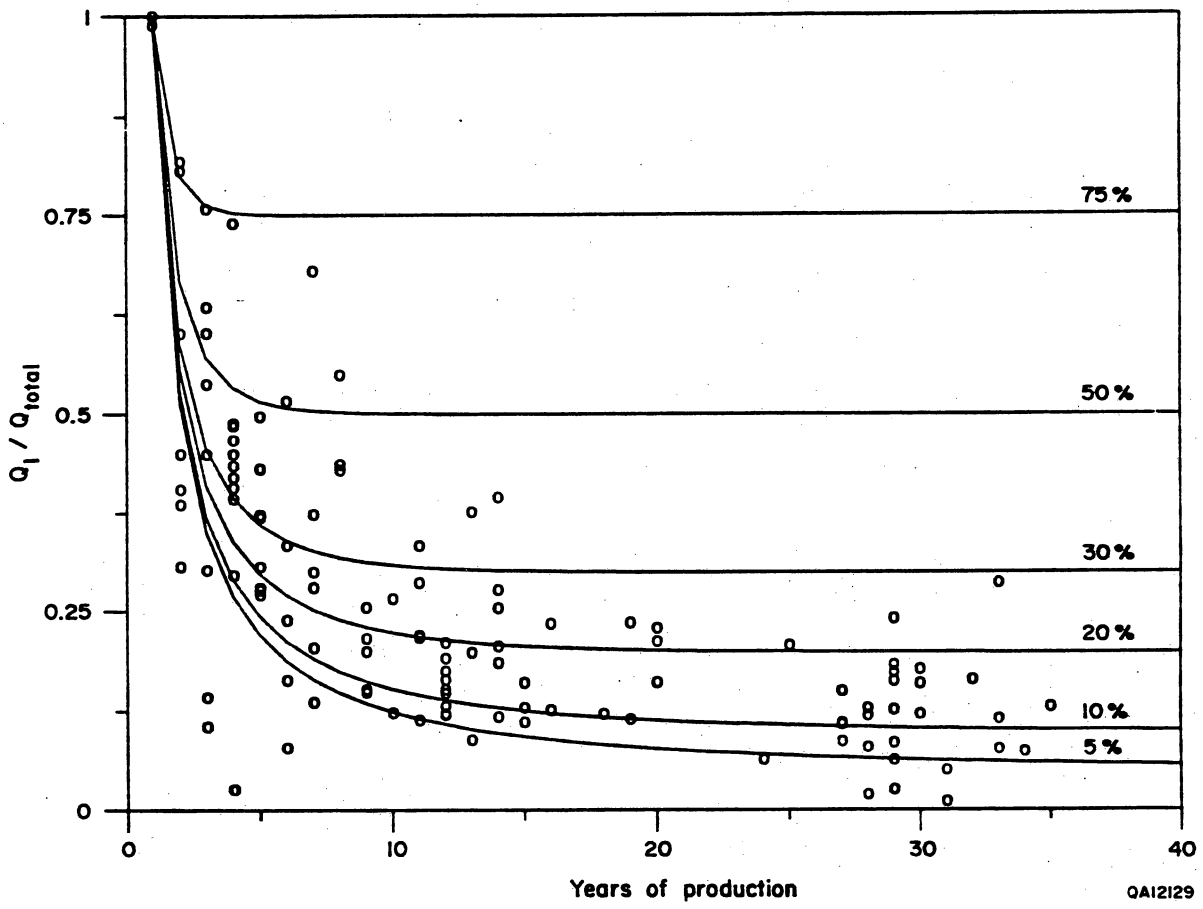

Figure 61. Q plot, Fruitland Formation sandstone wells.

Such a plot for a single reservoir would indicate a highly compartmentalized reservoir. Although the Q plot was designed to evaluate sandstone reservoirs, it can be used to analyze coal reservoirs. Because many coal reservoirs show negative decline, or increased production with time in the early years, there will be an obvious affect on the Q plot, giving the well a decline rate in its late history much lower than that for sandstone. To investigate coal and sandstone decline behavior we made Q plots for 40 selected wells—7 completed in coal and 33 in sandstone.

Q plots for coal wells show that coal reservoirs decline exponentially at rates of less 5 percent per year (fig. 62). The San Juan 32-7 unit 6 well (Phillips 6-17) has a decline rate of 2.5 percent over 32 yr. Coal reservoirs in the Black Warrior Basin also display exponential decline (David Bolin, personal communication, 1989). Wells exhibiting classic negative decline (Cahn and Knauff wells) fall well below the exponential curve early (sharply curved), whereas others (Clay and Western Federal wells) exhibit no negative decline and closely follow the type curve. The latter two wells are in the underpressured west-central part of the basin, and they produce little or no water. Sandstone wells commonly have decline curves that cross the type exponential-decline curves in the early years (gently curved) and then flatten in the late years to parallel the type curves at decline rates of 10 to 20 percent per year (fig. 63). From the Q plots, we conclude that sandstones exhibit exponential decline late as reported by operators and hyperbolic decline early in their production. Sandstone Q plots by pressure regime show that overpressured wells have decline rates greater than 10 percent and little scatter, whereas underpressured wells show great scatter and have lower decline rates (less than 10 percent). In fact, several wells in the underpressured west-central part of the basin, carried as sandstone completions, have anomalously low decline rates of less than 10 percent per year (fig. 61). These wells display coal decline behavior (negative decline and very low decline rates) and probably are producing coalbed methane indirectly from juxtaposed coal seams (fig. 64). The Scott 21 is located in such a setting at Cedar Hill. Sandstone wells that show greater decline (hyperbolic) early (gently curved Q plot) and exponential decline later (e.g., Schultz Com F 11)

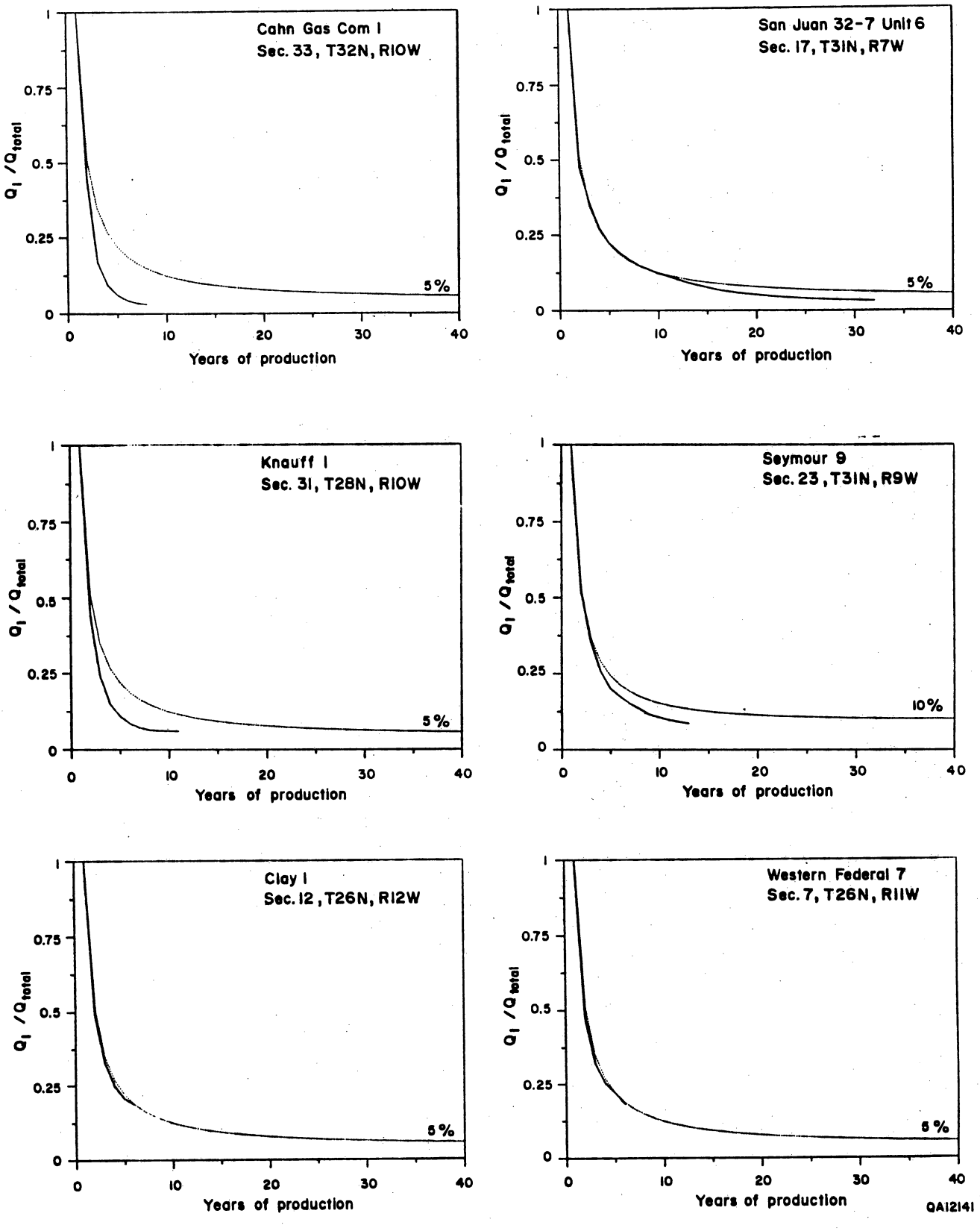

Figure 62. Q plots, individual Fruitland Formation coal wells.

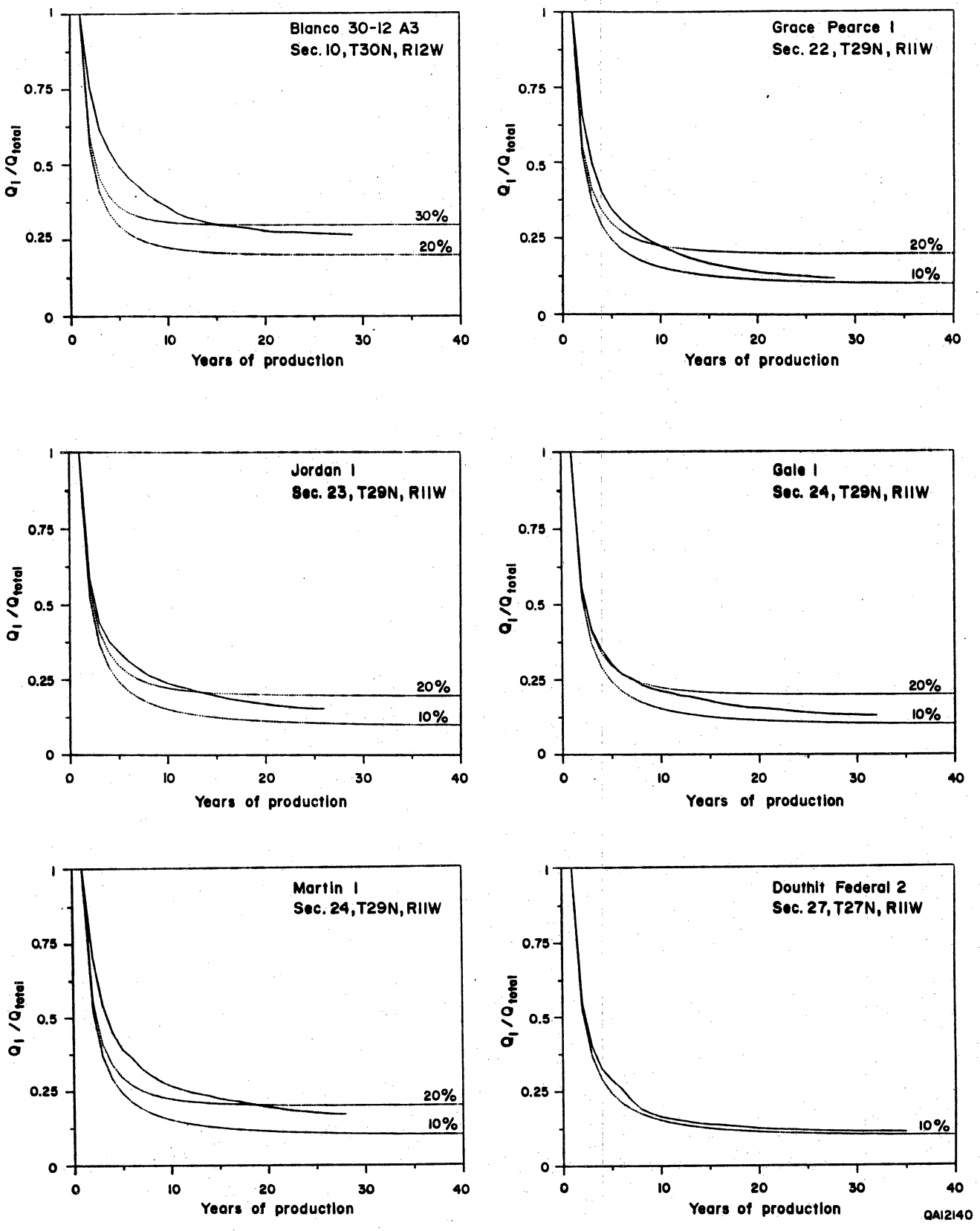

Figure 63. Q plots, individual Fruitland Formation sandstone wells.

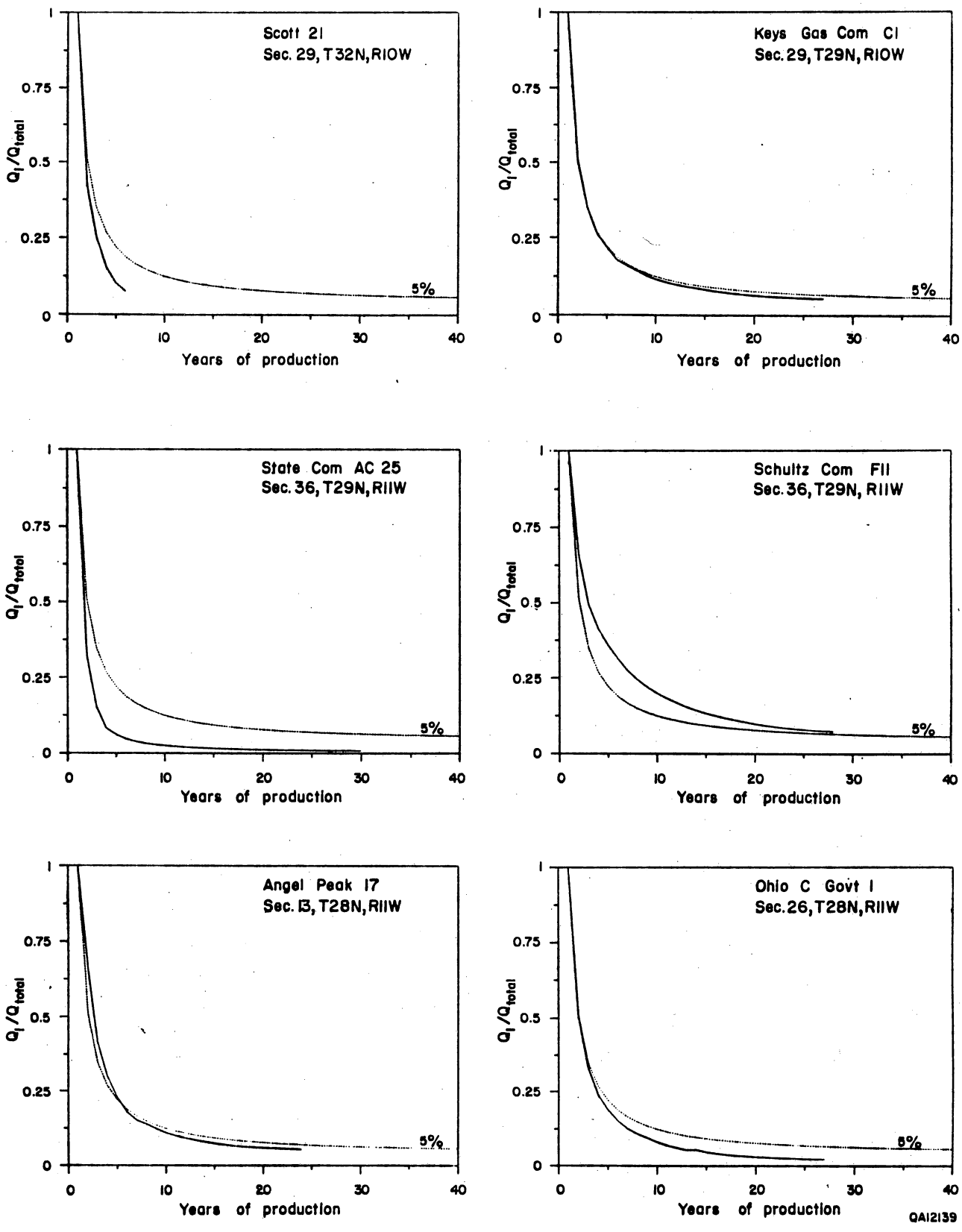

Figure 64. Q plots, individual Fruitland Formation sandstone wells that exhibit coal-decline behavior.

may reflect initial production directly from a conventional sandstone reservoir and later production indirectly from coal seams (fig. 64). This may be case for the San Juan 32-7 unit 6 well (fig. 62), which is completed open hole in interbedded sandstones and coal seams. Sandstone wells that show exponential decline throughout their productive histories may have been in early communication with coals.

In summary, three distinct Fruitland Q plots, exhibiting decline behavior characteristic of production from coal seams, sandstone beds, and sandstone beds in communication with coal seams, are recognized (fig. 65). The representative coalbed Q plots drops quickly (sharply curved early) to exponential decline rates of less than 5 percent per year, whereas the sandstone Q plot is gently curved early and exhibits decline rates of 10 to 20 percent. The Q plot of a sandstone completion with coalbed behavior has features of both curves, gentle curvature early and low exponential decline (less than 5 percent) later in its production history.

PRODUCIBILITY OF COALBED METHANE

Established Production

Through 1987, cumulative production of Fruitland methane was 41 Bcf from sandstone beds and 13 Bcf from coal beds. However, 6 Bcf of the 13 Bcf was produced in 1987. In 1988, coalbed methane production from the Fruitland Formation in the San Juan Basin was approximately 20 Bcf from more than 100 wells, illustrating a dramatic increase in production from coal beds. Meridian 400 and Cedar Hill areas and Ignacio Blanco field accounted for approximately 90 percent of the basinwide production in 1988. The most prolific coalbed methane wells are in Meridian 400 area (fig. 66), where in 1988 average daily production rates exceeded 2,000 Mcf/d (773 MMcf/yr). Wells in Cedar Hill area produce at rates of 500 to 1,200 Mcf/d (183 to 438 MMcf/yr). Those in Ignacio Blanco field are far less productive at 50 to 100

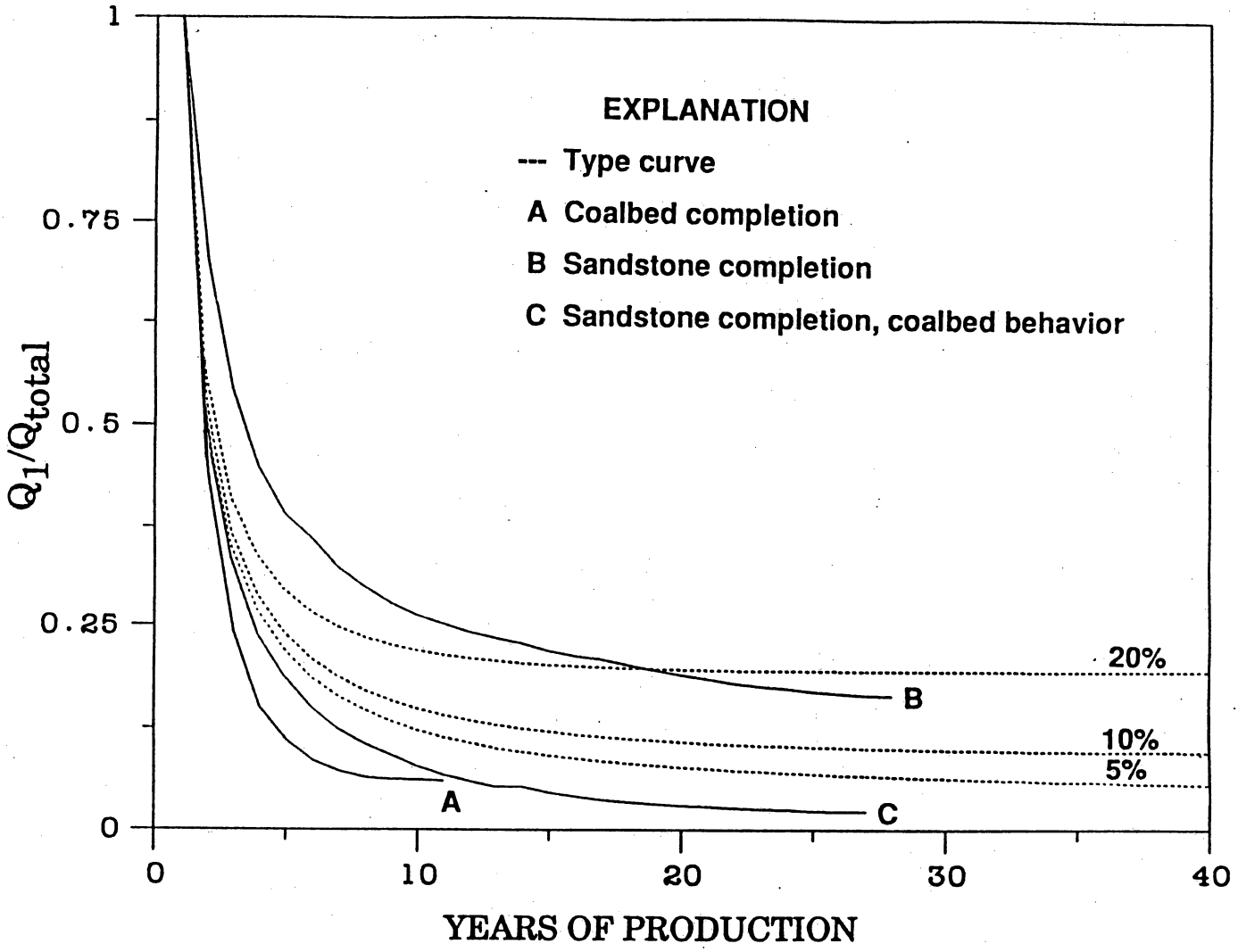

Figure 65. Q plots representative of gas production from coalbeds, sandstones, and sandstones in communication with coalbeds.

Mcf/d (18 to 37 MMcf/yr). Limited production has been established in the southern part of the basin as well as in new areas in the northern and western parts of the basin (fig. 67). There are two major areas of new development, one in south-central La Plata County, Colorado, (T32N, R9W, see fig. 38 for township and range grid) and the other in northwest Rio Arriba County, New Mexico (T32N, R4W and R5W). Some wells in the former area are reported to be producing at approximately 2,000 Mcf/d. A cluster of shut-in coalbed methane wells in T30N, R6W lies east of Meridian 400 area; no test data are available for these wells.

Because of recent orders by the New Mexico Oil Conservation Division R-8768 and R-8769, designating a Basin-Fruitland Coal Gas Pool, this report refers to productive areas in New Mexico by geographical area or by the name of the operator most active in the area (figs. 66 and 67). Order No. R-8768 established the Coal Gas Pool, and order No. R-8769 contracted the vertical limits of 26 existing Fruitland and Fruitland/Pictured Cliffs Gas Pools to include only the sandstone intervals. In Colorado, Ignacio Blanco field is the only Fruitland field, and it includes production from both coal and sandstone beds (fig. 68).

Hydrologic and Geologic Parameters

Hydrologic Parameters

Coalbed methane is produced in a variety of hydrologic settings—areas of upward and downward flow, overpressured and underpressured areas, and areas associated with potentiometric anomalies. The basin's most productive wells are in Meridian 400 area and occur in an area with strong potential for upward flow (fig. 46). Moreover, numerous Fruitland sandstone gas fields dot the southwest part of the basin, centered on the regional discharge area (fig. 68). Tóth (1980) argued that hydrocarbon accumulation is favored in regional discharge areas, which are areas of converging and ascending flow. Production of coalbed methane in the San Juan basin appears to be favored in areas of upward flow. Downward flow dominates in

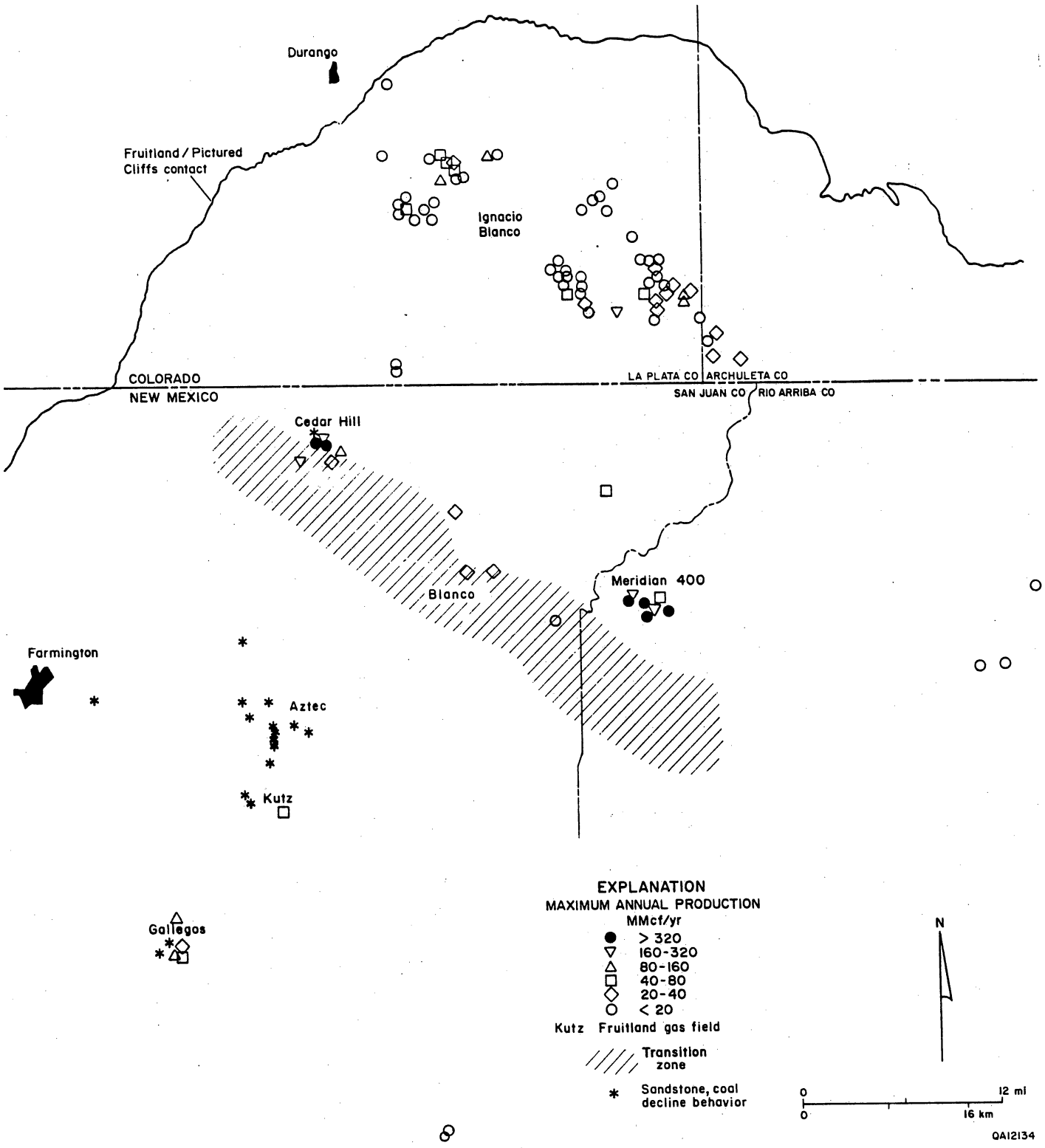

Figure 66. Fruitland Formation maximum-annual-production map of coalbed methane. Production through 1987.

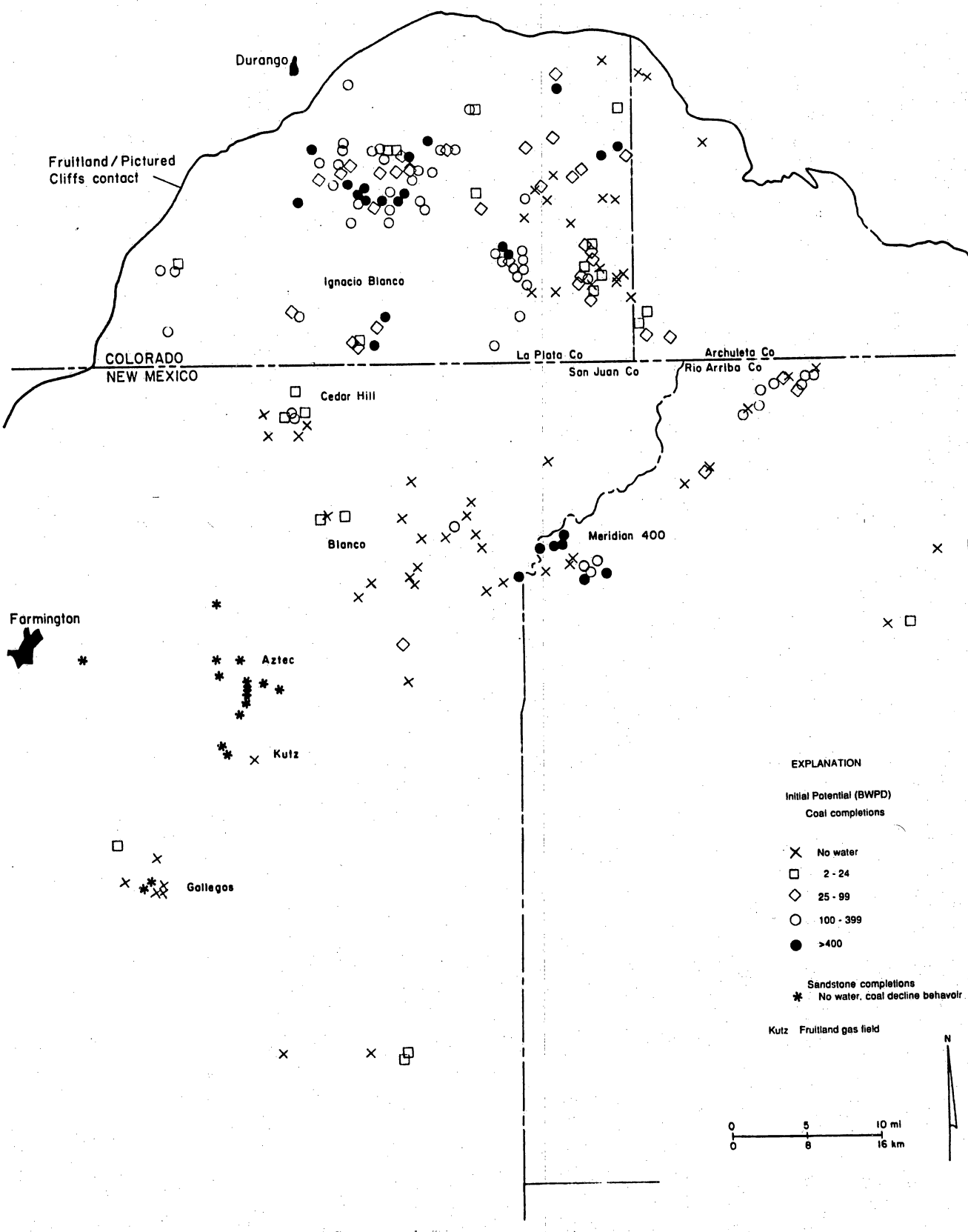

Figure 67. Fruitland Formation initial-potential map of water from coalbed methane wells. Initial potentials available through September 1989.

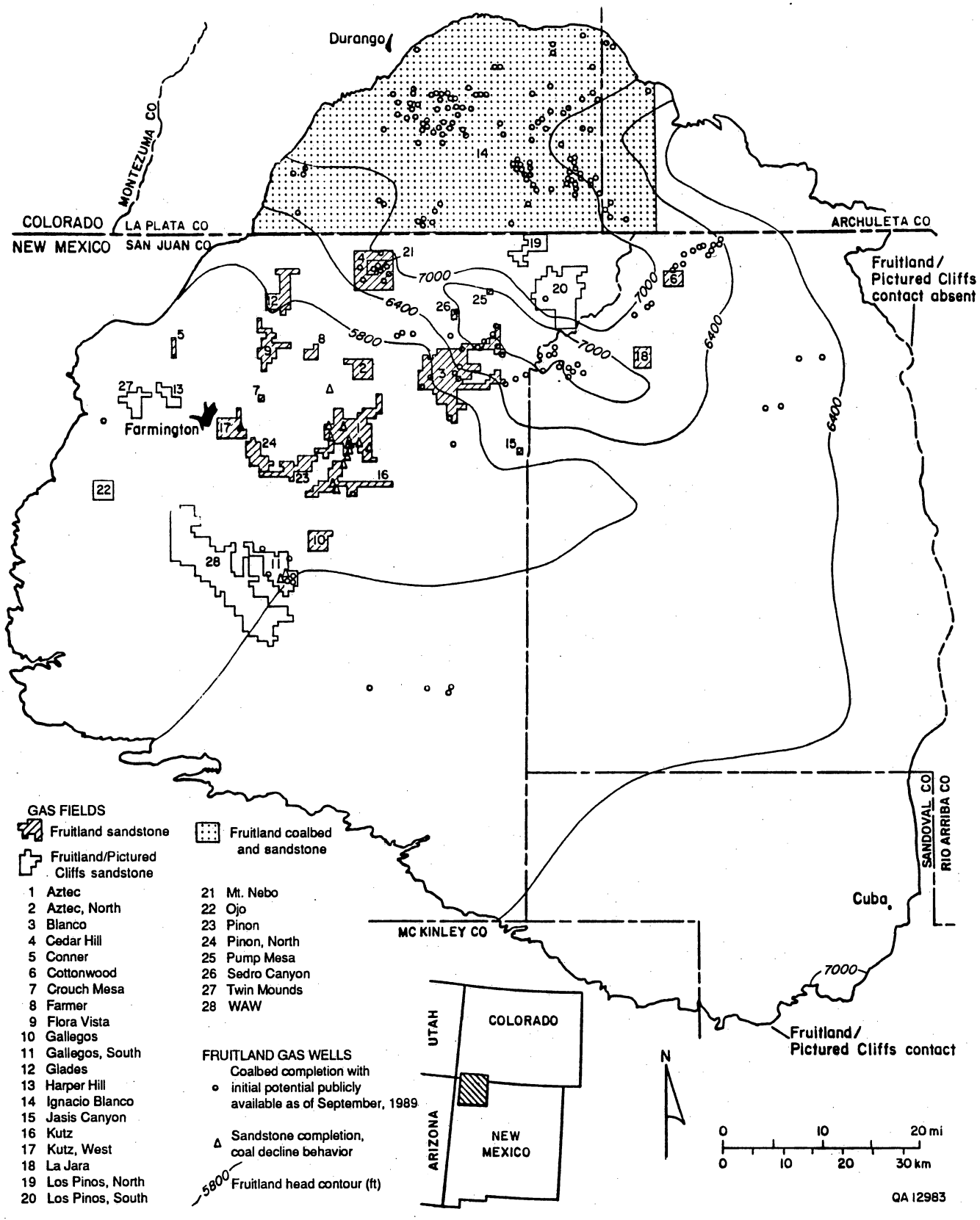

Figure 68. Fruitland Formation potentiometric-surface map (fresh-water head, in ft) and the distribution of Fruitland and Fruitland/Pictured Cliffs gas fields and tested Fruitland coalbed methane wells.

Ignacio Blanco field, where well productivities are less than those in other parts of the basin. Numerous wells produce less than 20 MMcf/yr (fig. 66) and have high water productivities (several 100 BWPD on IP, fig. 67), indicative of enhanced permeability. Those wells close to the basin margin, or recharge area, may be difficult to dewater (depressurize) and consequently may never produce gas at high rates.

Because more methane is adsorbed onto coal at higher pressure, overpressuring enhances production of coalbed methane. Certainly, wells in the overpressured area (figs. 49 and 66) are the basin's most productive. The highest MAP's correlate with high BHP's (fig. 69), reflecting greater volumes of adsorbed gas at higher pressures. In figure 69, two distinct populations are evident, reflecting the overpressured north-central part of the basin and underpressured west-central part of the basin. BHP's of coal wells in the west-central part of the basin are as low as 300 psi; yet these wells have MAP's comparable to several coal wells in the north-central part of the basin having BHP's of approximately 1,400 psi. Clearly, overpressuring in not a requirement for production of coalbed methane, as sustained production is evident from underpressured coals (figs. 59c and 69). Because the desorption curve flattens above 900 to 1,300 psi, pressure must be lowered considerably to release a small amount of gas, whereas at low pressure adsorbed gas volume is small (Koenig and others, 1989). They suggest that at reservoir pressures greater than 1,000 psi significant dewatering may be needed. Therefore, reservoir pressure that is either too high or too low is probably detrimental to the producibility of coalbed methane. The optimum pressure range is unknown but thought to be large. Commercial production in the San Juan Basin has been established in coal seams having BHP's as high as 1,900 psi and as low as 120 psi.

The most productive coalbed methane wells in the San Juan Basin are associated with potentiometric anomalies. Cedar Hill and Meridian 400 areas lie at the transition between a flattened potentiometric surface to the northeast and a steepened one to the southwest (figs. 45 and 66). Highly productive ARCO wells in T32N, R9W are in the flattened area between

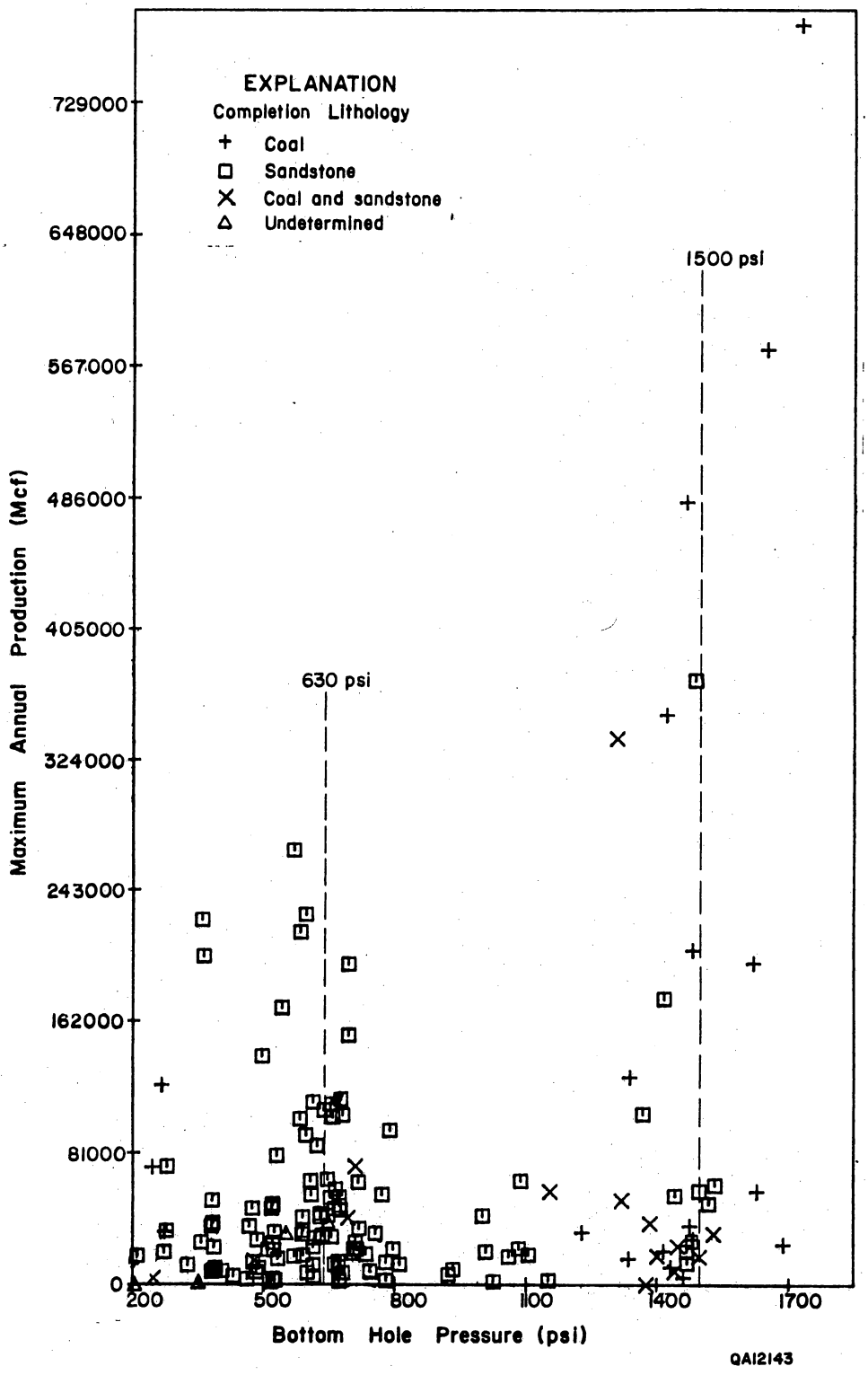

Figure 69. Cross plot of bottom-hole pressure versus maximum-annual production by producing lithology.

Cedar Hill and Ignacio Blanco. Numerous sandstone wells with coal-decline behavior are located at Kutz and Aztec fields within potentiometric mounds.

The steepened potentiometric surface southwest of Cedar Hill and Meridian 400 areas coincides with southwestwardly pinch-out of thick aquifer coals (fig. 4) (Kaiser and Swartz, 1988, 1989), the transition from overpressuring to underpressuring (fig. 49), and a chemical facies change from low-chloride, high-alkalinity formation waters to saline Na-Cl waters (fig. 50). On the assumption of continuity (flow in equals flow out), a region of reduced permeability is inferred from the steepened surface, and a region of enhanced permeability is inferred from the flattened surface (fig. 45). Numerous wells in the Blanco area produced no water on IP and are located in an area of steepened potentiometric surface (hydraulic gradient ~ 0.045) and at the transition from overpressured to underpressured conditions (figs. 49 and 67). Similarly, low permeability is inferred in the cluster of wells in eastern La Plata County (T32N, R6W), which lie in an area of steepened potentiometric surface and at the pressure transition.

Overpressuring, assuming an artesian origin, and low-chloride formation waters are also indicators of enhanced permeability. Strata too tight to accept and transmit measurable recharge remain underpressured. An example is the Pictured Cliffs Sandstone in the north-central part of the basin. Furthermore, because permeability in coal seams is stress dependent, higher permeability is predicted in overpressured coals, where overpressuring lowers the effective stress gradient (McKee and others, 1987). Permeable pathways are further indicated by the presence of low-chloride Fruitland formation waters, which imply an active, dynamic flow system. In contrast, the low-permeability Pictured Cliffs Sandstone contains Na-Cl type waters; it is too tight to receive meteoric recharge and is thus less well flushed. The existence of connate marine water, as inferred for parts of the southern basin, implies negligible permeability because connate waters can be preserved only where permeability is negligible.

Geologic Parameters

The producibility of coalbed methane is ultimately controlled by the permeability and thickness of the coal reservoirs. Thick coal seams lie landward (southwest) of and parallel to the pinch-out of northwest-trending upper Pictured Cliffs tongues and northeast of the southern hinge line of the basin floor (fig. 25). Accumulation and preservation of peat was favored northeast of the basin hinge line by temporal stability (aggradation) and differential subsidence. Southwest of the hinge line, coal seams are thinner and are oriented northeast-southwest (fig. 25). The transition from strike-elongate (shoreline) to dip-elongate (alluvial) depositional facies along coal-belt E and the updip limit (southwest) limit of UP1 is a regional facies boundary that coincides with the potentiometric, pressure, and chemical facies boundaries noted above (fig. 66, transition zone).

Coalbed wells clearly are associated with thick coal seams, as delineated by the maximum coal map (fig. 27). This is especially true of Meridian 400 and Cedar Hill areas and of clustered wells southeast of Durango (T34N, R8W and R9W), in south-central La Plata County (T32N, R9W), and in northwest Rio Arriba County (T32N, R4W, and R5W)(fig. 67). Fields and clusters of wells lie landward of the pinch-outs of UP1, UP2, and UP3. Thus, the coal seams were ideally positioned for possible compaction induced fracturing and permeability enhancement as their sandstone platforms pinched out to the southwest (fig. 33). Sandstone completions predominate in Aztec, Kutz, and Gallegos South fields, and as predicted, they occur in association with northeast-trending Fruitland sandstone belts (low-coal areas) lying between belts of northeast-trending thick coal (coal belts 2 and 3 of fig. 25; also, see figs. 27 and 29).

In contrast to maximum coal, the correlation of productive areas and net coal as defined by the 50-ft isopach is less evident (fig. 26), suggesting that maximum coal thickest is a critical production parameter. Assuming equal permeability and overpressuring, gas productivity will be greater in a thicker seam because a larger cone of depression is induced upon dewatering,

freeing a larger volume of gas. Several productive areas are outside the 50-ft net-coal isopach but within the 20-ft maximum-coal isopach. Cedar Hill area is cut by the 50-ft net-coal isopach and Meridian 400 area is well within it.

The relation of coalbed methane production to major structural elements is unclear. For example, coal completions are just as abundant off the Ignacio Anticline as on it (fig. 9), suggesting no structural control. Thinner coal seams on the Bondad Anticline in T33N, R9W (figs. 9, 26, and 27) may account for an absence of completions on it. New wells in northwest Rio Arriba County have been drilled at the structurally lowest part of the basin. In this area there is an abrupt change in dip and a subtle structural nose (inferred enhanced permeability) as well as potential for upward flow (fig. 45). Wells clustered just southeast of Durango occur in an area of abrupt change in dip, and fracture-enhanced permeability is possible (figs. 9 and 67). Gallegos South lies within an extensive homoclinal area in which strata dip northeast at less than 1 degree (~ 80 ft/mi). This does not imply that major structural elements play no role in the producibility of coalbed methane; just that small, subtle structural features, not recognizable at the regional scale, may be more important to the production of coalbed methane. The San Juan 32-7 unit 6 well has produced essentially water free since 1955 and is in pressure communication and structurally high to a well 1/4 mi away (NEBU 218) that produces water at the rate of 50 bbl/d. A gas-saturated seam and structural trapping are implied for the San Juan 32-7 well. The Seymour 9 has produced water free since 1978 and is located at Sedro Canyon, which was drilled on an anticline mapped on the top of the Pictured Cliffs Sandstone. Likewise, the Ross 1 well (Sec.18, T32N, R5W), structurally high to the Glover 1 well, blew out and flowed gas during completion, whereas the Glover behaved as a well completed in a water-saturated coal seam. Water-free production in coalbed wells may also imply lower permeability.

Fracture permeability dominates in coal seams and is controlled by the cleats, an orthogonal set of fractures oriented northeast and northwest in much of the San Juan Basin (fig. 36). Correlation between the cleat system and productive trends is tentative, but two associations are noteworthy. Coalbed wells in Meridian 400 area parallel a prominent northeast-

trending segment of the San Juan River (lineament) whose northeastward projection in turn parallels the trend of wells in northwest Rio Arriba County (fig. 67). Northeast-trending productive trends are consistent with the northeast-trending face cleat orientation reported in the NEBU 403 well (fig. 36). Inferred permeability anisotropy would favor fluid flow in the northeast direction. Finally, in the area southeast of Durango, highly water-productive wells are orthogonally oriented (fig. 67, solid and open circles) consistent with the cleat system.

HYDROGEOLOGIC CHARACTERIZATION

On the basis of hydrodynamics and geology, the San Juan Basin can be divided into three regions having similar reservoir characteristics. These are the (1) overpressured north-central part of the basin, (2) underpressured regional discharge area in the west-central part of the basin, and (3) underpressured eastern part of the basin (fig. 70). Except for the Hogback Monocline, fracture permeability, regional jointing, and compaction-induced fractures are not addressed.

The north-central part of the basin is regionally overpressured (simple pressure gradients of 0.50 to 0.60 psi/ft and BHP's greater than 1,200 psi). Fruitland produced waters typically contain less than 800 mg/L chloride and have total alkalinities of thousands of mg/L. The maximum coal is commonly 10 ft thick or more, although several northwest-trending and minor, northeast-trending belts of 20 ft or more of maximum coal are developed in this area (fig. 27).

Within the overpressured area, three subregions are identified (fig. 70). Area A at the south exhibits high BHP's (greater than 1,800 psi), high alkalinity waters (up to 25,000 mg/L), and high potential for upward flow (vertical pressure gradient ~ 0.80 psi/ft). Area B is an area of recharge along the north and northwest margins of the basin and because of tight folding, fracture permeability may be high. Area C at the center is defined by conspicuous flattening of the potentiometric surface, which is thought to indicate enhanced permeability. Vertical flow is potentially downward in area C.

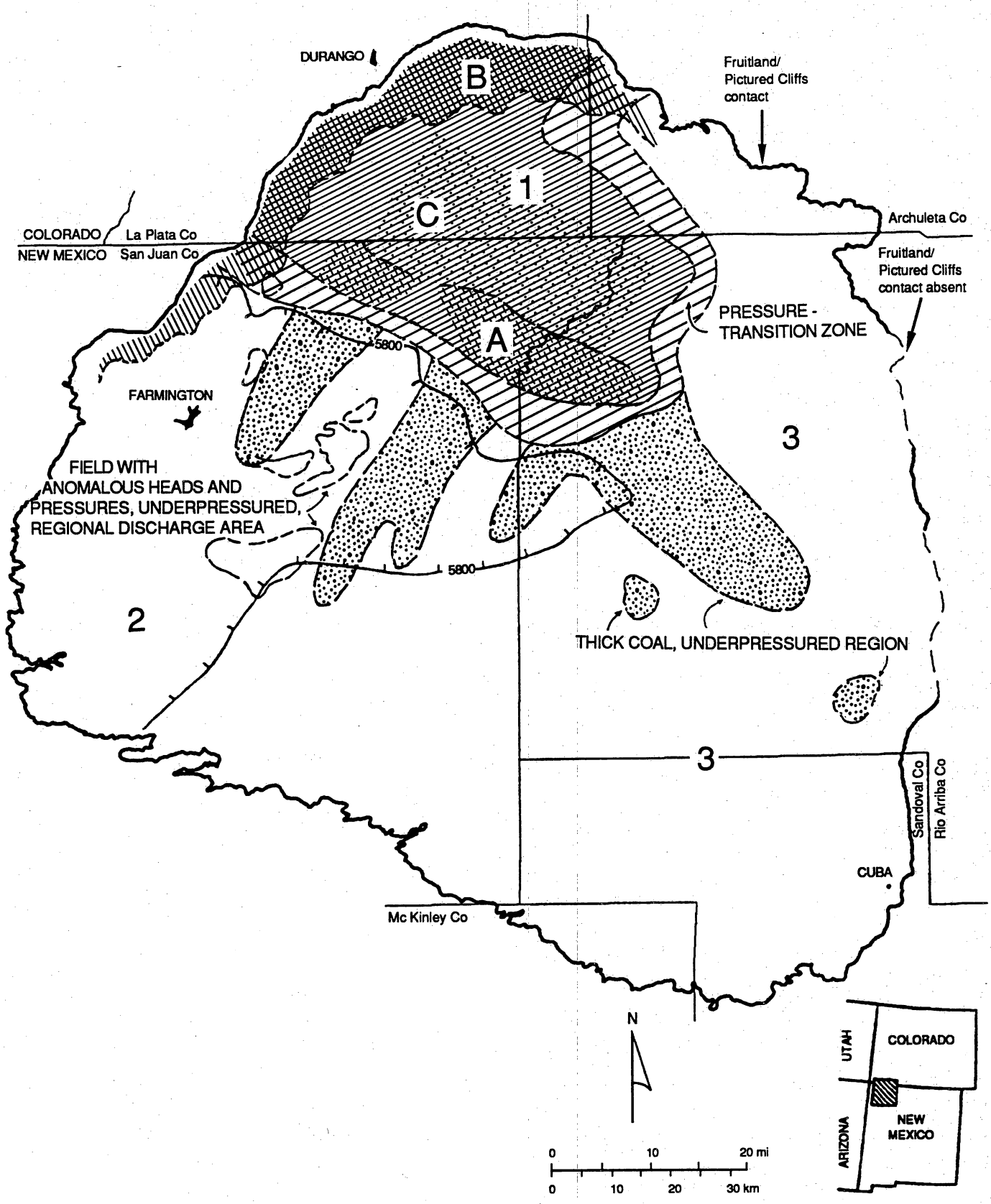

Figure 70. Hydrogeologic regions in the Fruitland Formation, San Juan Basin. Numbers refer to major regions and letters refer to subregions discussed in the text. Major regions are the (1) overpressured north-central area, (2) underpressured regional discharge area, and (3) underpressured area, outside the regional discharge area.

In the north-central part of the basin, maximum annual production (MAP) ranges from less than 20 to greater than 320 MMcf (fig. 66). All wells producing less than 20 MMcf/yr are in areas B and C and most are water productive. Many of these wells had IP's of several hundred BWPD (fig. 67). Good examples are the McKenzie Methane Southern Ute—Mobil 36-1 and ARCO's wells in south-central La Plata County, which lie in the area of flattened potentiometric surface and inferred high permeability. Coal seams of the 36-1 well have natural permeabilities of approximately 50 md and when stimulated produced low-chloride water at rates greater than 2,000 bbl/d. Some ARCO wells produce water at rates of 1,000 bbl/d. Wells positioned to receive direct recharge from the basin margin may be difficult to dewater (depressurize) and may never produce coalbed methane at high rates.

Although most wells in area 1 produce water, some produced little or no water on initial testing (fig. 67). Examples are clustered wells (e.g., eastern La Plata County), isolated individual wells (e.g., San Juan 32-7 unit 6 and Seymour 9), and individual wells within clusters of water producers (e.g., San Juan 30-6 unit 402). The San Juan 32-7 and Seymour 9 are thought to be associated with structural anomalies. Other wells at the northern and western margins of the basin may receive little direct recharge from the outcrop or have low permeability or both and thus produce water free. For example, the Fortyfour Canyon 22-2 (Sec. 22, T33N, R11W) initially produced too little gas to gauge and no water. When stimulated, it produced 281 Mcf/d and 17.5 BWPD. Meridian Oil's San Juan 30-6 unit 402 upon initial testing produced no water but subsequently produced water at an average annual rate of 108,780 bbl. This behavior, coupled with a high gas IP (2,460 Mcf/d), suggests the initial production of free gas and a coal seam with high fracture permeability (secondary porosity). The phenomenon of either isolated wells of low water (less than 20 BWPD) or high water potential (hundreds of BWPD) probably reflects a high degree of reservoir heterogeneity or compartmentalization in the coal seams.

The most productive wells in the San Juan Basin are in the north-central part of the basin in area A (figs. 66 and 70), corresponding to shoreline coals of coal-belt E (fig. 25), a prominent belt of thick coal seams evident on all coal maps (figs. 26 through 29). They are located in

Meridian 400 and Cedar Hill areas and have MAP's of over 1 Bcf. Wells in these fields are also prolific producers of water (cumulative productions of several hundred thousand barrels), whereas wells between these fields have MAP's of 20 to 40 MMcf and cumulative water productions of less than 1,000 barrels.

The west-central part of the basin is regionally underpressured (simple pressure gradients of 0.30 to 0.40 psi/ft and BHP's less than 1,000 psi), except for local pressure anomalies, and is a regional discharge area, as defined by the 5,800-ft head contour (fig. 70, area 2). No analyses of Fruitland produced waters are available for this area because most of these wells produce water free. Thick coal seams exceed 10 ft in thickness and occur in belts oriented northeast-southwest (figs. 27 and 29). Perhaps, these seams served as pathways for gas that migrated out of the north-central part of the basin entrained or dissolved in ground water or that diffused outward in response to the concentration gradient.

Water-free production in a regional discharge area seems counter intuitive but can be explained in terms of the hydrostratigraphy, trapping mechanism, and coal wettability. Most of the Fruitland wells in the west-central part of the basin are completed above the wet, basal coal seam that rests directly on the Pictured Cliffs Sandstone and thus may actually be completed in the Kirtland/Fruitland confining unit. Conventional trapping and low gas permeability relative to water are important factors. Stratigraphic trapping is postulated to be more important than structural trapping on the basis of gentle, structurally monotonous, northeast homoclinal dip and associated updip (southwest) pinch-out of reservoir coal seams (fig. 4). Coal seams in the southern part of the basin are low rank (high-volatile C to high-volatile B bituminous) and may be water wet; hence relative to gas, water is the less mobile fluid.

In the west-central part of the basin, most of the Fruitland wells are completed in sandstones. Only five definite coal completions had been identified through 1987 (fig. 66). These wells have MAP's ranging from 40 to 120 MMcf, exceeding MAP's of many wells in the north-central part of the basin in areas B and C, and have cumulative productions of up to 1 Bcf (e.g., Clay 1, Gallegos South area, 1 Bcf in 13 yr). Most wells in the southwest have cumulative

productions of a few hundred million Mcf, and some have produced small volumes of oil. Analysis of production decline has shown that many wells carried as sandstone completions actually have coal-decline behavior and probably are producing coalbed methane indirectly from coal seams (fig. 64). In some cases, sandstone volumetrics require gas production from the associated coals. Operationally, it may be advantageous to complete in sandstones interbedded with coals. Some wells are dually completed in Fruitland coal seams and Pictured Cliffs Sandstone or Mesaverde Group sandstones, and the production is commingled. Consequently, the contribution of Fruitland coalbed methane to total gas production in the west-central part of the basin is substantial but unquantifiable.

Little is known about the hydrogeology of the eastern part of the basin, which is regionally underpressured, and because of few data, appears to be hydrologically featureless (fig. 70, area 3). Widely spaced head contours suggest sluggish ground-water flow (fig. 45). Fruitland produced waters are Na-Cl type, closely resembling connate seawater. Coal thickness exceeds 10 ft in a northwest-trending area in Rio Arriba County, parallel to depositional strike, corresponding to shoreline coals of belt E (fig. 25). There are only five producing Fruitland wells (coal and/or sandstone completions) in the area. After 1 or 2 years of production, they have average annual productions of less than 1 to 3 MMcf, accompanied by little or no water.

CONCLUSIONS

1. Coalbed methane production in the Fruitland Formation is log normally distributed. Statistical analysis suggests that coal seams having free gas may be more common than previously thought. Surprisingly, production from underpressured coal seams was superior to that from overpressured seams (as of 1987). Decline behaviors of coalbed and sandstone reservoirs are unique. Coalbed wells have negative decline early in their production history, followed by exponential decline at less than 5 percent per year. Numerous sandstone wells

exhibit coal-decline behavior and probably are producing coalbed methane indirectly from interbedded coal seams.

2. Approximately 90 percent of the Fruitland coalbed methane production is from Meridian 400 and Cedar Hill areas and Ignacio Blanco field. Wells in Meridian 400 area are the most productive (more than 1,000 MMcf/yr), and those in Ignacio Blanco field are the least productive (~ 30 MMcf/yr). Coal wells in the west-central part of the basin are at least as productive as those in Ignacio Blanco field.

3. Coalbed methane is produced in a variety of hydrologic settings but is favored in areas of upward flow and hydrogeologic transitions. Hydrologic elements define an aquifer's ability to accept and transmit fluid; hence, they are indicators of permeability. Permeability is the most critical parameter for the production of coalbed methane. Enhanced permeability is inferred from potentiometric anomalies, overpressuring, and fresh, low-chloride formation waters. Enhanced permeability is inferred from a flattened potentiometric surface and reduced permeability from a steepened surface. Overpressuring is not required for the production of coalbed methane; it signifies enhanced permeability. Commercial production of coalbed methane is possible over a very wide pressure range. The presence of fresh water in the Fruitland Formation implies an active, dynamic flow system and permeable pathways, whereas connate water implies negligible permeability.

Maximum coal thickness is a critical parameter for the production of coalbed methane and is thought to be an indicator of productivity, whereas net-coal thickness indicates gas resources. Correlation of production with regional and local structural elements is evident but inconclusive without additional production data. These structural features may be sites of fracture-enhanced permeability. Northeast-oriented productive trends may reflect the trend of face cleats.

4. The north-central part of the basin is the most productive coalbed-methane region in the San Juan Basin. However, anomalously low or high water production reflects reservoir compartmentalization, or heterogeneity, in reservoir coals. Production of coalbed-methane directly or indirectly from underpressured coal seams in the west-central part of the basin is

substantial; coal seams in this part of the basin are viable exploration targets. The eastern part of the basin is largely unexplored but probably has low potential for coalbed methane production. Low permeability and general absence of thick coal seams, except in west-central Rio Arriba County, limit its potential.

ACKNOWLEDGMENTS

This research was funded by the Gas Research Institute under contract no. 5087-214-1544. Production data were collected by Nancy Oltmanns, A. H. Scanlon, and C. M. Tremain. We thank Craig Wandrey, Steve Condon, and Dan Knepper of the U.S. Geological Survey, Denver, Colorado; Charles Byrer of the Morgantown Energy Technology Center, Morgantown, West Virginia; Tom Erwin and Jay Close of Resource Enterprises, Inc., Grand Junction, Colorado; the proprietors of the Chimney Rock Strip Mine; the Colorado Division of Mines; the Colorado Oil and Gas Conservation Commission; the U.S. Geological Survey Core Library; and the staffs of the Colorado Geological Survey and the Texas Bureau of Economic Geology for their assistance. We also thank David Allen, U.S. Bureau of Reclamation, Denver; Art Ireland, National Park Service, Santa Fe; Dale Jackson and Iris Bryant, U.S. Bureau of Reclamation, Farmington; Carl Yost, U.S. Bureau of Land Management, Farmington; Grayson Heard, Consolidation Coal Company, St. Louis; and Ken Skipper, U.S. Bureau of Reclamation, Salt Lake City, Utah.

Drafting was by D. R. Grote and by the cartographic staff of the Bureau of Economic Geology under the direction of R. L. Dillon. Word processing was by Melissa Snell, and pasteup was by J. H. Coggin. The manuscript was edited by Amanda Masterson, and its production was coordinated by Maris Strautmanis.

REFERENCES

Aldrich, M. J., Jr., Chapin, C. E., and Laughlin, A. W., 1986, Stress history and tectonic development of the Rio Grande Rift, New Mexico: Journal of Geophysical Research, v. 91, no. B6, p. 6199–6211.

Aldrich, M. J., Jr., and Laughlin, A. W., 1982, Orientation of least-principle horizontal stress: Arizona, New Mexico, and the Trans-Pecos area of West Texas (stress data and references): Los Alamos National Laboratory, LA-9158-Map, scale 1:1,000,000.

Aldrich, M. J., Jr., and Laughlin, A. W., 1984, A model for the tectonic development of the southeastern Colorado Plateau boundary: Journal of Geophysical Research, v. 89, p. 10207–10218.

Anonymous, 1966, Final construction geologic report, Tunnel No. 1, Navajo Indian Irrigation Project: Bureau of Reclamation report, available for inspection at the Bureau of Reclamation, Navajo Indian Irrigation Project Office, Farmington, New Mexico.

Anonymous, 1967, Final construction geologic report, Tunnel No. 2, Navajo Indian Irrigation Project: Bureau of Reclamation report, available for inspection at the Bureau of Reclamation, Navajo Indian Irrigation Project Office, Farmington, New Mexico.

Armstrong, R. L., 1968, Sevier orogenic belt in Nevada and Utah: Geological Society of America Bulletin, v. 79, p. 429–458.

Ayers, W. B., Jr., and Kaiser, W. R., 1984, Lacustrine interdeltaic coal in the Fort Union Formation (Palaeocene), Powder River Basin, Wyoming and Montana, U.S.A., *in* Rahmani, R. A., and Flores, R. M., eds., Sedimentology of coal and coal-bearing sequences: International Association of Sedimentologists Special Publication No. 7, p. 61–84.

Ayers, W. B., Jr., Kaiser, W. R., Swartz, T. E., Zellers, S. D., and Scanlon, A. H., 1988, Geologic evaluation of critical production parameters for coalbed methane resources, part 1, San Juan Basin: The University of Texas at Austin, Bureau of Economic Geology annual report prepared for the Gas Research Institute under contract no. 5087-214-1544, 100 p.

Ayers, W. B., Jr., and Zellers, S. D., 1988, Sedimentologic and structural controls on the occurrence and producibility of coalbed methane, Fruitland Formation, northern San Juan and Rio Arriba Counties, New Mexico; in Ayers, W. B., Jr., and others, Geologic evaluation of critical production parameters for coalbed methane resources, Part I: San Juan Basin: Gas Research Institute, contract no. 5087-214-1544 (GRI- 88/0332.1), p. 3-59.

———— 1989, Geologic controls on occurrence and producibility of coalbed methane, Fruitland Formation, north-central San Juan Basin, New Nexico: The University of Alabama, School of Mines and Energy Development, Proceedings of the 1989 Coalbed Methane Symposium, p. 75–86.

Baltz, E. H., 1967, Stratigraphy and regional tectonic implications of part of Upper Cretaceous and Tertiary rocks in east-central San Juan Basin, New Mexico: U.S. Geological Survey Professional Paper 552, 101 p.

Bond, W. A., 1984, Application of Lopatin's method to determine burial history, evolution of the geothermal gradient, and timing of hydrocarbon generation in Cretaceous source rocks

in the San Juan Basin, northwestern New Mexico and southwestern Colorado, *in* Woodward, J., and others, eds., Hydrocarbon source rocks of the greater Rocky Mountain region: Denver, Rocky Mountain Association of Geologists, p. 433–447.

Bradley, W. C., 1963, Large-scale exfoliation in massive sandstones of the Colorado Plateau: Geological Society of America Bulletin, v. 74, p. 519–528.

Britten, R. A., Smyth, M., Bennett, A. J. R., and Shibaoka, M., 1975, Environmental interpretations of Gondwana coal measure sequence in the Sydney Basin of New South Wales, *in* Campbell, K. S. W., ed, Gondwana Geology: Australian National University Press, Canberra, p. 233–247.

Burchfiel, B. C., and Davis, G. A., 1975, Nature and controls of Cordilleran orogenesis, western United States: Extensions of an earlier synthesis: American Journal of Science, v. 275 A, p. 363–396.

Campbell, F. W., 1985, Chemical characteristics of the coals, *in* Roybal, G. H., Campbell, F. W., Beaumont, E. C., Cohen, A. D., Kuellmer, F. J., and Kottlowski, F. E., Quality assessment of strippable coals in the San Juan Basin of northwestern New Mexico: New Mexico Bureau of Mines and Mineral Resources division of New Mexico Energy Research and Development Institute Report No. 2-73-4304, 89 p.

Carothers, W. W., and Kharaka, Y. K., 1978, Aliphatic acid anions in oil field waters—implications for origin of natural gas: American Association of Petroleum Geologists Bulletin, v. 62, p. 2441–2453.

Chapin, C. E., and Cather, S. M., 1981, Eocene tectonics and sedimentation in the Colorado Plateau–Rocky Mountain area, *in* Dickinson, W. R., and Payne, M. D., eds., Relations of tectonics to ore deposits in the southern Cordillera: Arizona Geological Society Digest, v. 14, p. 173–198; *also in* Lowell, J. D., ed., Rocky Mountain foreland basins and uplifts: Rocky Mountain Association of Geologists, Guidebook, 1983 Field Conference, p. 33–56.

Choate, Raoul, Lent, J., and Rightmire, C. T., 1984, Upper Cretaceous geology, coal, and the potential for methane recovery from coalbeds in San Juan Basin–Colorado and New Mexico, *in* Rightmire, C. T., Eddy, G. E., and Kirr, J. N., eds., Coalbed methane resources of the United States: American Association of Petroleum Geologists Studies in Geology Series No. 17, p. 185–222.

Choate, Raoul, and Rightmire, C. T., 1982, Influence of the San Juan Mountain geothermal anomaly and other Tertiary igneous events on the coalbed methane potential in the Piceance, San Juan and Raton Basins, Colorado and New Mexico: SPE 10805, *in* Proceedings of the Unconventional Gas Recovery Symposium, May 16–18, 1982, Pittsburgh, Pennsylvania, Society of Petroleum Engineers/U.S. Department of Energy, p. 151–164.

Clarkson, Gerry, and Reiter, Marshall, 1988, An overview of geothermal studies in the San Juan Basin, New Mexico and Colorado, *in* Fassett, J. E., ed., Geology and coalbed methane resources of the northern San Juan Basin, Colorado and New Mexico: Rocky Mountain Association of Geologists, p. 285–291.

Condon, S. M., 1988, Joint patterns on the northwest side of the San Juan Basin (Southern Ute Indian Reservation), southwest Colorado, in Geology and coalbed methane resources of

the San Juan Basin, Colorado and New Mexico: Rocky Mountain Association of Geologists, p. 61–68.

Cooper, K. R., no date, Final construction geology report of Tunnels No. 3 and 3A, Navajo Indian Irrigation Project: Bureau of Reclamation report, available for public inspection at the Bureau of Reclamation, Navajo Indian Irrigation Project Office, Farmington, New Mexico.

Cooper, K. R., 1975, Final construction geologic report of Tunnel No. 4, Navajo Indian Irrigation Project: Bureau of Reclamation [mimeographed report, available for public inspection at the Bureau of Reclamation, Navajo Indian Irrigation Project Office, Farmington, New Mexico.

Cordell, Lindrith, 1983, Composite residual total intensity aeromagnetic map of New Mexico: New Mexico State University Energy Institute, scale 1:500,000.

Cordell, Lindrith, and Grauch, V. J. S., 1985, Mapping basement magnetization zones from aeromagnetic data in the San Juan Basin, New Mexico, *in* Hinze, W. J., ed., The utility of regional gravity and magnetic anomaly maps: Society of Exploration Geophysicists, p. 181–197.

Crist, T. E., Boyer, C. M., and Kelso, B. S., 1989, A geologic and coalbed methane resource analysis of the Menefee Formation in the San Juan Basin, southwestern Colorado and northwestern New Mexico: SPE Paper 18945, Proceedings 1989 SPE Joint Rocky Mountain Regional/Low Permeability Reservoirs Symposium and Exhibition, March 6-8, 1989, p. 153–160.

Cumella, S. P., 1981, Sedimentary history and diagenesis of the Pictured Cliffs Sandstone, San Juan Basin, New Mexico and Colorado: The University of Texas at Austin, Texas Petroleum Research Committee Report No. UT 81-1, 219 p.

Dane, C. H., 1936, The La Ventana - Chacra Mesa coal field, pt. 3A, Geology and fuel resources of the southern part of the San Juan Basin, New Mexico: U.S. Geological Survey Bulletin 860-C, p. 81–161.

Davis, G. H., 1984, Chapter 10, Joints, *in* Structural geology of rocks and regions: New York, John Wiley and Sons, p. 325–353.

Decker, A. D., Close, J. C., and McBane, R. A., 1989, The use of remote sensing, curvature analysis, and coal petrology as indicators of higher coal reservoir permeability: Proceedings, 1989 Coalbed Methane Symposium, the University of Alabama, Tuscaloosa, p. 325–340.

Devine, P. E., 1980, Depositional patterns in the Point Lookout Sandstone, northwest San Juan Basin, New Mexico: The University of Texas at Austin, Master's thesis, 238 p.

Dickinson, W. R., Klute, M. A., Hayes, M. J., Janecke, S. U., Lundin, E. R., McKittrick, M. A., and Olivares, M. D., 1988, Paleogeographic and paleotectonic setting of Laramide sedimentary basins in the central Rocky Mountain region: Geological Society of America Bulletin, v. 100, p. 1023–1039.

Dilworth, O. L., 1960, Upper Cretaceous Farmington Sandstone of northeastern San Juan County, New Mexico: New Mexico University, Master's thesis.

Donaldson, A. C., 1979, Origin of coal seam discontinuities, *in* Donaldson, A. C., Presley, M. W., and Renton, J. J., eds., Carboniferous coal guidebook: West Virginia Geological and Economic Survey Bulletin B-37-1, p. 102–132.

Donaldson, A. C., Presley, M. W., and Renton, J. J., eds., 1979, Carboniferous coal guidebook: West Virginia Geological and Economic Survey Bulletin B-37-1, 301 p.

Emmendorfer, Alan, 1989, Fracture orientation: use in the dipmeter type fracture log: The Mountain Geologist, v. 26, p. 63–67.

Engelder, Terry, 1985, Loading paths to joint propagation during a tectonic cycle: an example from the Appalachian Plateau, U.S.A.: Journal of Structural Geology, v. 7, nos. 3 and 4, p. 459–477.

Epis, R. C., and Chapin, C. E., 1975, Geomorphic and tectonic implications of the post-Laramide, late Eocene erosion surface in the southern Rocky Mountains, *in* Curtis, B. F., ed., Cenozoic history of the southern Rocky Mountains: Geological Society of America, Memoir 144, p. 45–74.

Erpenbeck, M. F., 1979, Stratigraphic relationships and depositional environments of the Upper Cretaceous Pictured Cliffs Sandstone and Fruitland Formation, southwestern San Juan Basin, New Mexico: Texas Tech University, Master's thesis, 78 p.

Fassett, J. E., 1985, Early Tertiary paleogeography and paleotectonics of the San Juan Basin area, New Mexico and Colorado, *in* Flores, R. M., and Kaplan, S. S., eds., Cenozoic paleogeography of the west-central United States: Society of Economic Paleontologists and

Mineralogists, Rocky Mountain Section, Rocky Mountain Paleogeography Symposium 3, p. 317–334.

———— 1986, The non-transferability of a Cretaceous coal model in the San Juan Basin of New Mexico and Colorado, *in* Lyons, P. C. and Rice, C. L., eds., Paleoenvironmental and tectonic controls in coal-forming basins in the United States: Geological Society of America Special Paper 210, p. 155–171.

———— 1987, Geometry and depositional environments of Fruitland Formation coalbeds, San Juan Basin, New Mexico and Colorado: anatomy of a giant coal-bed methane deposit: The University of Alabama, School of Mines and Energy Development, Proceedings, The 1987 Coalbed Methane Symposium, p. 19–35.

———— 1988, Geometry and depositional environment of Fruitland Formation coal beds, San Juan Basin, New Mexico and Colorado: anatomy of a giant coal-bed methane deposit, *in* Fassett, J. E., eds., Geology and coal-bed methane resources of the northern San Juan Basin, Colorado and New Mexico: Rocky Mountain Association of Geologists, p. 23–38.

Fassett, J. E., and Hinds, J. S., 1971, Geology and fuel resources of the Fruitland Formation and Kirtland Shale of the San Juan Basin, New Mexico and Colorado: U.S. Geological Survey Professional Paper 676, 76 p.

Fisher, W. L., Brown, L. F., Scott, A. J., and McGowen, J. H., 1969, Delta systems in the exploration for oil and gas: the University of Texas at Austin, Bureau of Economic Geology Research Colloquium, 212 p.

Flores, R. M., and Erpenbeck, M. F., 1981, Differentiation of delta front and barrier lithofacies of the Upper Cretaceous Pictured Cliffs Sandstone, southwestern San Juan Basin, New Mexico: The Mountain Geologist, v. 18, no. 2, p. 23–34.

Garven, G., 1986, The role of regional fluid flow in the genesis of the Pine Point deposit, western Canada sedimentary basin—a reply: Economic Geology, v. 81, p. 1015–1020.

Gorham, F .D., Woodward, L. A., Callender, J. F., and Greer, A. R., 1979, Fractures in Cretaceous rocks from selected areas of San Juan Basin, New Mexico—exploration implications: American Association of Petroleum Geologists Bulletin, v. 63, p. 598–607.

Hamilton, Warren, 1978, Mesozoic tectonics of the western United States, *in* Howell, D. G., and others, eds., Mesozoic paleogeography of the western United States: Society of Economic Paleontologists and Mineralogists, Pacific Coast Paleogeography Symposium No. 2, p. 33–70.

Hattin, D. E., 1965, Stratigraphy of the Graneros Shale (Upper Cretaceous) in central Kansas: Kansas Geological Survey, Bulletin 178, 83 p.

Heller, P. L., Bowdler, S. S., Chambers, H. P., Coogan, J. C., Hagen, E. S., Shuster, M. W., and Winslow, N. S., 1986, Time of initial thrusting in the Sevier orogenic belt, Idaho–Wyoming and Utah: Geology, v. 14, p. 388–391.

Horne, J. C., Ferm, J. C., Caruccio, F. T., and Baganz, B. P., 1978, Depositional models in coal exploration and mine planning in Appalachian region: American Association of Petroleum Geologists Bulletin, v. 62, p. 2379–2411.

Houseknecht, D. W., and Iannacchione, A. T., 1982, Anticipating facies-related coal mining problems on Hartshorne Formation, Arkoma Basin: American Association of Petroleum Geologists Bulletin, v. 66, no. 7, p. 923–946.

Hugman, R. H., Vidas, E. H., and Woods, T. J., 1989, Potential infill reserve additions by interval—San Juan Basin: Bulletin American Association of Petroleum Geologists, v. 73, p. 365–366.

Irving, E., 1979, Paleopoles and paleolatitudes of North America and speculations about displacement terrains: Canadian Journal Earth Sciences, v. 16, p. 669–694.

Jordan, T. E., 1981, Thrust loads and foreland basin evolution, Cretaceous, western United States: American Association of Petroleum Geologists Bulletin, v. 65, p. 2506–2520.

Kaiser, W. R., Johnston, J. E., and Bach, W. N., 1978, Sand-body geometry and the occurrence of lignite in the Eocene of Texas: The University of Texas at Austin, Bureau of Economic Geology Circular 78-4, 19 p.

Kaiser, W. R., and Swartz, T. E., 1988, Hydrology of the Fruitland Formation and coalbed methane producibility, *in* Ayers, W. B., Jr., and others, Geologic evaluation of critical production parameters for coalbed methane resources, part 1: San Juan Basin: Gas Research Institute, contract no. 5087-214-1544 (GRI-88/0332.1), p. 61–81.

———— 1989, Fruitland Formation hydrology and producibility of coalbed methane in the San Juan Basin, New Mexico and Colorado: The University of Alabama, School of Mines and Energy Development, Proceedings of the 1989 Coalbed Methane Symposium, p. 87–97.

Kauffman, E. G., 1977, Geological and biological overview—Western Interior Cretaceous basin, *in* Kauffman, E. G., ed., Cretaceous facies, faunas, and paleoenvironments across the Western Interior basin: The Mountain Geologist, v. 6, p. 227–245.

Kelley, V. C., 1951, Tectonics of the San Juan Basin: New Mexico Geological Society Guidebook of the south and west sides of the San Juan Basin, New Mexico and Arizona, Second Field Conference, p. 124–131.

Kelley, V. C., and Clinton, N. J., 1960, Fracture systems and tectonic elements of the Colorado Plateau: University of New Mexico Publications in Geology, no. 6, 104 p.

Kelso, B. S., Decker, A. D., Wicks, D. E., and Horner, D. M., 1987, GRI geologic and economic appraisal of coalbed methane in the San Juan Basin: The University of Alabama, School of Mines and Energy Development, Proceedings, The 1987 Coalbed Methane Symposium, p. 119–125.

Kelso, B. S., Goolsby, S. M., and Tremain, C. M., 1980, Deep coalbed methane potential of the San Juan River coal region, southwestern Colorado: Colorado Geological Survey Open-File Report 80-2, 56 p.

Kelso, B. S., Wicks, D. E., and Kuuskraa, V. A., 1988, A geologic assessment of natural gas from coal seams in the Fruitland Formation, San Juan Basin: Chicago, Gas Research Institute Topical Report GRI 88/034, 54 p.

Keystone, 1986, 1986 Keystone coal industry manual: New York, McGraw-Hill, Colorado—description of seams, p. 431–452; New Mexico—description of seams, p. 514–523.

Kharaka, Y. K., Hull, R. W., and Carothers, W. W., 1985, Water-rock interactions in sedimentary basins, *in* Gautier, D. L., and others, eds., Relationship of organic matter and mineral diagenesis: Society of Economic Paleontologists and Mineralogists, SEPM Short Course No. 17, p. 79–176.

Kharaka, Y. K., Law, L. M., Carothers, W. W., and Goerlitz, D. F., 1986, Role of organic species dissolved in formation waters from sedimentary basins in mineral diagenesis, *in* Gautier, D. L., ed., Roles of organic matter in sedimentary diagenesis: Society of Economic Paleontologists and Mineralogists, Special Publication No. 38, p. 111–122.

Kluth, C. F., and Coney, P. J., 1981, Plate tectonics of the Ancestral Rocky Mountains: Geology, v. 9, p. 10–15.

Knepper, D. H., Jr., 1982, Lineaments derived from analysis of linear features mapped from LANDSAT images of the Four Corners region of the southwestern United States: U.S. Geological Survey Open-File Report 82-849, 79 p.

Koenig, R. A., Bumb, A. C., McKee, C. R., Murphy, C. L., Ramesh, M. S., Reverand, J. M., and Way, S. C., 1989, Application of hydrology to evaluation of coalbed methane reservoirs: Gas Research Institute, contract no. 5087-214-1489 (GRI-89/0031), 114 p.

Kulander, B. R., Barton, C. C., and Dean, S. L., 1979, The application of fractography to core and outcrop fracture investigations: U.S. Department of Energy, METC/SP-79/3, 174 p.

Laubach, S. E., Reynolds, S. J., Spencer, J. E., and Marshak, Stephen, 1989, Progressive deformation and superposed fabrics related to Cretaceous crustal underthrusting in western Arizona, U.S.A.: Journal of Structural Geology. v. 11, no. 6, p. 735–749.

Lipman, P. W., Doe, B. R., Hedge, C. E., and Steven, T. A., 1978, Petrologic evolution of the San Juan volcanic field, southwestern Colorado: Pb and Sr isotope evidence: Geological Society of America Bulletin, v. 89, p. 59–82.

Lundegard, P. D., and Land, L. S., 1986, Carbon dioxide and organic acids: their origin and role in diagenesis, the Texas Gulf Coast Tertiary, *in* Gautier, D. L., ed., Roles of organic matter in sedimentary diagenesis: Society of Economic Palentologists and Mineralogists, Special Publication No. 38, p. 129–146.

Mallory, W. W., 1977, Oil and gas from fractured shale reservoirs in Colorado and northwestern New Mexico: Rocky Mountain Association Geologists Special Publication 1, 38 p.

Manfrino, Carrie, 1984, Stratigraphy and palynology of the upper Lewis Shale, Pictured Cliffs Sandstone, and lower Fruitland Formation (Upper Cretaceous) near Durango, Colorado: The Mountain Geologist, v. 21, no. 4, p. 115–132.

McCord, J. P., 1988, Hydrogeology of a Fruitland Formation aquifer, San Juan Basin—New Mexico and Colorado, with emphasis on using temperature distribution data to estimate lateral groundwater velocity: New Mexico Institute of Mining and Technology, Master's thesis, 121 p.

McGowen, J. H., 1968, Utilization of depositional models in exploration from nonmetallic minerals, *in* Brown, L. F., Jr., ed., Proceedings, Fourth forum on geology of industrial minerals: The University of Texas at Austin, Bureau of Economic Geology, p. 157–174.

McKee, C. R., Bumb, A. C., and Koenig, R. A., 1987, Stress-dependent permeability and porosity in coal: The University of Alabama, School of Mines and Energy Development, Proceedings of the 1987 Coalbed Methane Symposium, p. 183–193.

Meissner, F. F., 1984, Cretaceous and Lower Tertiary coals as sources for gas accumulations in the Rocky Mountain area, *in* Woodward, J., Meissner, F. F., and Clayton, J. L., eds., Hydrocarbon source rocks of the greater Rocky Mountain region: Rocky Mountain Association of Geologists, p. 401–431.

Merewether, E. A., and Cobban, W. A., 1986, Biostratigraphic units and tectonism in the Mid-Cretaceous foreland of Wyoming, Colorado, and adjoining areas, *in* Peterson, J. A., ed., Paleotectonics and sedimentation in the Rocky Mountain region, United States: American Association of Petroleum Geologists, Memoir 41, p. 443–468.

Molenaar, C. M., and Baird, J. K., 1989, North-south stratigraphic cross- sections of Upper Cretaceous rocks, northern San Juan Basin, Colorado: U.S. Geological Survey Miscellaneous Field Studies Map MF-2068, 3 sheets.

Morton, R. A., and Land, L. S., 1987, Regional variations in formation water chemistry, Frio Formation (Oligocene), Texas Gulf Coast: American Association of Petroleum Geologists Bulletin, v. 71, no. 2, p. 191–206.

Mytton, J. W., and Schneider, G. B., 1987, Interpretive geology of the Chaco area, northwestern New Mexico: U.S. Geological Survey, Miscellaneous Investigation Series, Map I-1777, scale 1:24,000.

Nelson, R. A., 1985, Geologic analysis of naturally fractured reservoirs: Houston, Gulf Publishing Company, 335 p.

Newman, K. R., and McCord, J. P., 1980, Detailed site investigation northern San Juan Basin: unpublished report to TRW for U.S. DOE, available for inspection at the Colorado Geological Survey, Denver, Colorado, variously paginated.

Novak, S. A., and Eckstein, Y., 1988, Hydrochemical characterization of brines and identification of brine contamination in aquifers: Ground Water, v. 26, no. 3, p. 317–324.

O'Leary, D. W., Friedman, J. D., and Pohn, H. A., 1976, Lineament and linear, a terminological reappraisal, *in* Podwysocki, M. H., and Earle, J. L., eds., Proceedings, 2nd International Conference on Basement Tectonics: Denver, Basement Tectonics Committee, p. 571–577.

Owen, L. B., 1988, Strain recovery measurements, Resource Enterprises, Inc. well: Blanco unit No. 403: Salt Lake City, TerraTek Inc., unpaginated.

———— 1989, ASR measurements, Resource Enterprises, Inc. project number 5265, well: Colorado 32-7 #9: Salt Lake City, TerraTek, Inc., unpaginated.

Palmer, J. J., and Scott, A. J., 1984, Stacked shoreline and shelf sandstone of La Ventana Tongue (Campanian), northwestern New Mexico: American Association of Petroleum Geologists Bulletin, v. 68, no. 1, p. 74–91.

Phillips, F. M., Peeters, L. A., Tansey, M. K., and Davis, S. N., 1986, Paleoclimatic inferences from an isotopic investigation of groundwater in the central San Juan Basin, New Mexico: Quaternary Research, v. 26, p. 179–193.

Phillips, F. M., Tansey, M. K., Peeters, L. A., Cheng, S., and Long, A., 1989, An isotopic investigation of groundwater in the central San Juan Basin, New Mexico: carbon 14 dating as a basis for numerical flow modeling: Water Resources Research, v. 25, no. 10, p. 2259–2273.

Pitman, J. K., and Sprunt, E. S., 1986, Origin and distribution of fractures in Lower Tertiary and Upper Cretaceous rocks, Piceance Basin, Colorado, and their relation to the occurrence of hydrocarbons, *in* Geology of Tight Gas Reservoirs: AAPG Studies in Geology No. 24, p. 221–233.

REC, 1989a, Stratton field, preliminary engineering assessment: Englewood, Colorado, Research & Engineering Consultants, Inc., prepared for the Bureau of Economic Geology, The University of Texas at Austin, report no. REC-SGR 89.1, 31 p.

———— 1989b, McAllen Ranch field, preliminary engineering assessment: Englewood, Colorado, Research & Engineering Consultants, Inc., prepared for the Bureau of Economic Geology, The University of Texas at Austin, report no. REC-SGR 89.2, 65 p.

Rice, D. D., Threlkeld, C. N., Vuletich, A. K., and Pawlewicz, M. J., 1988, Identification and significance of coal-bed gas, San Juan Basin, northwestern New Mexico and southwestern Colorado, *in* Fassett, J. E., ed., Geology and coal-bed methane resources of the northern San Juan Basin, Colorado and New Mexico: Denver, Rocky Mountain Association of Geologists, p. 51–59.

Ross, C. A., and Ross, J. R. P., 1986, Paleozoic paleotectonics and sedimentation in Arizona and New Mexico, *in* Peterson, J. A., ed., Paleotectonics and sedimentation in the Rocky Mountain region: American Association of Petroleum Geologists Memoir 41, p. 653–668.

Royse, F., Jr., Warner, M. A., and Reese, D. L., 1975, Thrust belt structural geometry and related stratigraphic problems, Wyoming–Idaho–northern Utah, *in* Bolyard, D. W., ed., Deep drilling frontiers of the central Rocky Mountains: Rocky Mountain Association of Geologists, p. 41–54.

Sandberg, D. T., 1988, Coal resources and coal-bed geometry, Fruitland Formation, Southern Ute Indian Reservation, Archuleta and La Plata Counties, Colorado, *in* Fassett, J. E., ed., Geology and coal-bed methane resources of the northern San Juan Basin, Colorado and New Mexico: Rocky Mountain Association of Geologists, p. 39–50.

Scruton, P. C., 1961, Rocky Mountain Cretaceous stratigraphy and regressive sandstones: Wyoming Geological Association Guidebook, 16th Annual Field Conference, p. 242–249.

Sears, J. D., Hunt, C. B., and Hendricks, T. A., 1941, Transgressive and regressive Cretaceous deposits in southern San Juan Basin, New Mexico: U.S. Geological Survey Professional Paper 193-F, p. 101–121.

Shock, E. L., 1988, Organic acid metastability in sedimentary basins: Geology, v. 16, p. 886–890.

Sikkink, P. G. L., 1987, Lithofacies relationships and depositional environment of the Tertiary Ojo Alamo Sandstone and related strata, San Juan Basin, New Mexico and Colorado, *in* Fassett, J. E., and Rigby, J. K., Jr., eds., The Cretaceous-Tertiary boundary in the San Juan and Raton Basins, New Mexico and Colorado: Geological Society of America Special Publication 209, p. 81–104.

Silver, Caswell, 1951, Cretaceous stratigraphy of the San Juan Basin: New Mexico Geological Society, Guidebook of the south and west sides of the San Juan Basin, New Mexico and Arizona, Second Field Conference, p. 104–118.

———— 1957, Relation of coastal and submarine topography to Cretaceous stratigraphy (N. Mexico): Four Corners Geological Society Guidebook, Geology of southwestern San Juan Basin, Second Field Conference, p. 128–137.

Steven, T. A., 1975, Middle Tertiary volcanic field in the southern Rocky Mountains, *in* Curtis, B. F., ed., Cenozoic history of the southern Rocky Mountains: Geological Society of America, Memoir 144, p. 75–94.

Stone, W. J., Lyford, F. P., Frenzel, P. F., Mizell, N. H., and Padgett, E. T., 1983, Hydrogeology and water resources of San Juan Basin, New Mexico: Socorro, New Mexico, New Mexico Bureau of Mines and Mineral Resources, Hydrologic Report 6, 70 p.

Surdam, R. C., Crossey, L. J., Hagen, E. S., and Heasler, H. P., 1989, Organic-inorganic interactions and sandstone diagenesis: American Association of Petroleum Geologists, v. 73, no. 1, p. 1–23.

Thaden, R. E., and Zech, R. S., 1984, Preliminary structure contour map on base of the Cretaceous Dakota Sandstone in the San Juan Basin and vicinity, New Mexico, Arizona, Colorado and Utah: U.S. Geological Survey Map MF-1673, scale 1:500,000.

Thompson, G. A., and Zoback, M. L., 1979, Regional geophysics of the Colorado Plateau: Tectonophysics, v. 61, p. 149–181.

Tóth, J., 1980, Cross-formational gravity-flow of ground-water: a mechanism of the transport and accumulation of petroleum (the generalized hydraulic theory of petroleum migration), *in* Roberts, W. H., III, and Cordell, R. J., eds., Problems of petroleum migration: American Association of Petroleum Geologists, Studies in Geology No. 10, p. 121–167.

Wandrey, C. J., 1989, Lineament map of part of the Southern Ute Reservation, San Juan Basin, Southwestern Colorado: U.S. Geological Survey Open File Report No. 89-112, scale 1:100,000.

Weimer, R. J., 1986, Relationship of unconformities, tectonics, and sea level changes in the Cretaceous of the Western Interior, United States, *in* Peterson, J. A., ed., Paleotectonics and sedimentation in the Rocky Mountain region, United States: American Association of Petroleum Geologists, Memoir 41, p. 397–422.

Williams, G. D., and Stelck, C. R., 1975, Speculations on the Cretaceous paleogeography of North America, *in* Caldwell, W. G. E., ed., The Cretaceous system in the Western Interior of North America: Geological Association of Canada Special Paper 13, p. 1–20.

Wong, I. G., and Humphrey, J. R., 1989, Contemporary seismicity, faulting and the state of stress in the Colorado Plateau: Geological Society of America Bulletin, v. 101, p. 1127–1146.

Wright, Robyn, 1986, Cycle stratigraphy as a paleogeographic tool: Point Lookout Sandstone, southeastern San Juan Basin, New Mexico: Geological Society of America Bulletin, v. 96, p. 661–673.

Zoback, M. L., 1988, State of stress in the Rocky Mountain region (abs.): Geological Society of America, Abstracts with Programs, v. 20, p. A12.

Zoback, M. L., and Zoback, M. D., 1980, State of stress in the conterminous United States: Journal of Geophysical Research, v. 85, p. 6113–6156.

———— in press, Tectonic stress field of the continental United States, *in* Pakiser, L., and Mooney, W., eds., Geophysical framework of the continental United States: Geological Society of America Memoir.